Direct Method of Generating Floor Response Spectra

by

Wei Jiang

A thesis
presented to the University of Waterloo
in fulfilment of the
thesis requirement for the degree of
Doctor of Philosophy
in
Civil Engineering

Waterloo, Ontario, Canada, 2016

Author's Declaration

I hereby declare that I am the sole author of this thesis. This is a true copy of the thesis, including any required final revisions, as accepted by my examiners.

I understand that my thesis may be made electronically available to the public.

Abstract

Floor Response Spectra (FRS), also called In-structure Response Spectra (IRS) in some standards and literature, are extensively used as seismic input in safety assessment for Systems, Structures, and Components (SSCs) in nuclear power plants. Efficient and accurate determination of FRS is crucial in Seismic Probabilistic Risk Analysis (SPRA) and design of nuclear power facilities. Time history method has been commonly used for generating FRS in practice. However, it has been demonstrated that time history analyses produce large variability in the resultant FRS, especially at FRS peaks, which are of main interest to engineers. Therefore, results from only a single, or a few, time history analysis cannot yield reliable FRS; a large number of time history analyses are needed to achieve sufficient accuracy in FRS. Nevertheless, this procedure is time-consuming and cumbersome from a practical point of view.

The purpose of this study is to develop a method of generating FRS that overcomes the deficiencies of the time history method and preserves the advantages of conventional response spectrum analysis for structures. A direct spectra-to-spectra method is analytically developed for the generation of FRS without introducing spectrum-compatible time histories as intermediate seismic input or performing time history analyses. Only the information required in a conventional response spectrum analysis for structural responses, including prescribed GRS and basic modal information of the structure (modal frequencies, mode shapes, and participation factors) is needed. The concept of t-response spectrum is proposed to determine the responses in the tuning case when the secondary system is resonant with the supporting structure. Furthermore, a new modal combination rule (called FRS-CQC), which fully considers the correlation between the responses of the secondary system and the supporting structure, and the correlation between modal responses of the structure, is derived based on random vibration theory.

A scaling method, based on the proposed direct spectra-to-spectra method, is further developed for generating FRS in a situation when the modal information of structure is not available. A system identification technique is carried out to recover the modal information of equivalent significant modes of the structure from existing GRS-I and FRS-I. Scaling

factors are then determined in terms of the equivalent modal information along with the GRS-I and GRS-II. The proposed scaling method can scale FRS to various damping ratios when the interpolation method recommended in standards are not applicable, and can also consider the large variations in the spectral shapes between GRS-I and GRS-II.

The proposed direct spectra-to-spectra method is further extended to generate FRS considering the effect of soil-structure interaction in conjunction with the substructure method. A methodology is presented to develop a vector of modification factors for the tri-directional Foundation Input Response Spectra (FIRS) obtained from a free-field site response analysis using the properties of the structure and underlying soil. The modified response spectra, called Foundation Level Input Response Spectra (FLIRS), are then used as input in the direct method to a fixed-base model for generating FRS.

The proposed methods are both efficient and accurate, giving a complete probabilistic description of FRS peaks, and accurate FRS comparable to those obtained from time history analysis using a large number of spectrum-compatible time histories.

Acknowledgement

I would like to express my special gratitude to my supervisors, Professor Wei-Chau Xie and Professor Mahesh D. Pandey, who have been tremendous mentors for me. I would like to thank them for encouraging my research and for allowing me to grow in all aspects of life. Their advice on both research as well as on my career have been invaluable.

I would like to extend my gratitude to Professors N. Sri Namachchivaya, Stanislav Potapenko, Lei Xu, Xinzhi Liu for the serving as my thesis committee members, and for their insightful comments and cares for my research.

I was delighted to interact with Dr. Binh-Le Ly, Mr. Wei Liu, Mr. Ming Han, Dr. Shun-Hao Ni, Dr. Zhi-Hua Chen, Dr. Yu-Xin Liu, Ms. Yi-Ming Jiang, Mr. Sudip Adhikari, and Dr. Ying An, of Candu Energy Inc., by sharing conversations to nuclear industry. Their engineering experiences and valuable suggestions have had a remarkable influence on this research.

Thanks also go to my friends and colleagues, Dr. Bo li, Zhen Cai, Yang Zhou, Dr. Donghui Lu, Xiaojun Yu, Sigong Zhang, Shijun Yang, Dr. Kexue Zhang, Chao Wu, Dr. George Balomenos, Dainy Manzana and other graduate students in the Department of Civil and Environmental Engineering.

The financial support by the Natural Sciences and Engineering Research Council of Canada (NSERC) and the University Network of Excellence in Nuclear Engineering (UNENE) in the form of a Research Assistantship is greatly appreciated.

Last but not least, without the unflagging love, support, and encouragement from my parents, my girlfriend, Nancy Sun, and her parents throughout these years, this thesis would not be possible.

TO

My Family

Contents

List of Figures

Nomenclature

AF	Amplification Factor
BE	Best Estimate
CENA	Central and Eastern North America ε
CQC	Complete Quadratic Combination
DBE	Design Basis Earthquake
DCF	Damping Correction Factors
DMF	Dynamic Magnification Factors
FIRS	Foundation Input Response Spectrum
FLIRS	Foundation Level Input Response Spectrum
FRS	Floor Response Spectrum
FRS-CQC	Complete Quadratic Combination for Floor Response Spectrum
GMRS	Ground Motion Response Spectra
GRS	Ground Response Spectrum
LB	Lower Bound
NEP	Non-Exceedance Probability
PEER	Pacific Earthquake Engineering Research
PGA	Peak Ground Acceleration
PSDF	Power Spectral Density Function
RLE	Review-Level Earthquake
SDOF	Single Degree-of-Freedom
SPRA	Seismic Probability Risk Assessment
SRSS	Square-Root-of-Sum-of-Squares

SSCs	Structures, Systems and Components
SSI	Soil-Structure Interaction
tRS	t-response spectrum
UB	Upper Bound
UHS	Uniform Hazard Spectrum
ZPA	Zero-Period Acceleration

CHAPTER 1

Introduction

Secondary systems are structures, systems and components (SSCs) that are attached to or supported by the traditional civil engineering structure, such as building, dam, nuclear power structure and so on, which are categorized as primary systems. For instance, in a nuclear power plant as shown in Figure 1.1, the primary systems consist of a reactor building, a service building and a turbine building. Secondary systems comprise various equipment including electrical systems, mechanical systems, control systems, etc. Secondary systems, however, are far from being of secondary importance in spite of the name. The fact is that secondary systems play various function to maintain operational process in the primary system and support human activities. Moreover, the cost of secondary systems may be considerably higher than that of the main structure.

During the past decades, it was demonstrated that secondary systems were vulnerable in earthquake events (Figure 1.2). The failure of secondary systems not only cause tremendous economic loss, but also threat to safety of life. In the 1994 Northridge earthquake in Los Angeles, several major hospitals were forced to be evacuated, not because of the damage of the main structures, but due to the failure of some crucial secondary systems, such as emergency power systems, control systems of medical equipment, water supply piping systems (Villaverde, 2009).

For seismic analysis of primary structure, the seismic input are usually given in terms of site-specific ground response spectra, which are provided by seismologists or specified

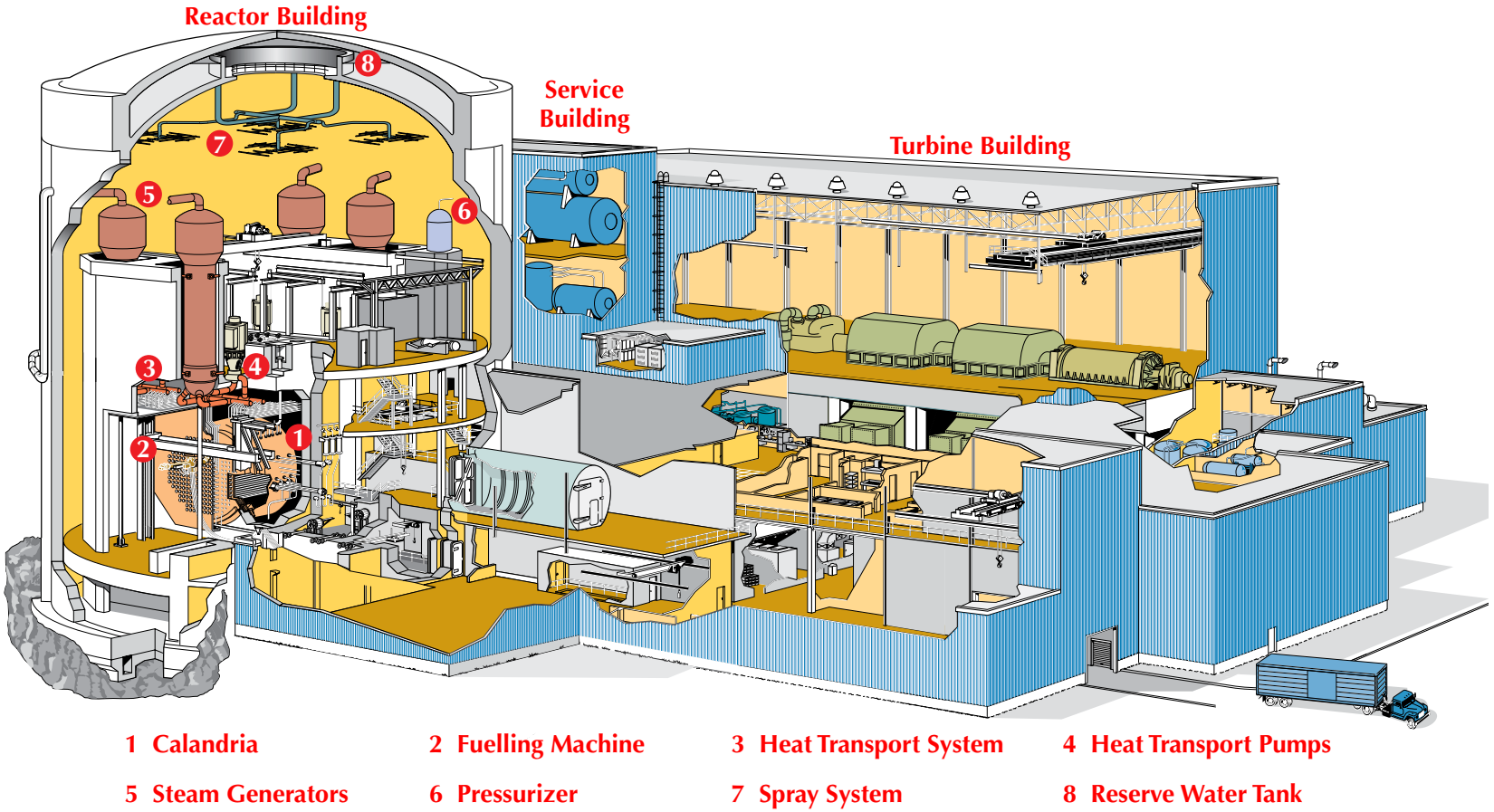

Figure 1.1 Primary and secondary systems in a nuclear power plant

Figure 1.2 Damage of secondary systems in earthquake events

in design code. Structural responses can be obtained by performing dynamic analysis for the structure, the methods for structural analysis are well developed. Contrary to primary systems which are designed to resist forces caused by earthquake, the preliminary design of secondary systems is generally accomplished by different groups. Only the capacity of resisting regular operational load and accidental load may be considered in this procedure. Since secondary systems are usually attached to the floors or walls of primary systems, when an earthquake occurs, secondary systems are suffered from the vibration of the floor to which they are attached, rather than subject to ground motions at the base of primary system directly. However, the motions of floor which are transmitted through the supporting

structure are modified and its amplitude can be amplified significantly, thus cause severe damage to the secondary systems. Therefore, the seismic input for secondary systems is not only determined by ground excitations acting on the base of the primary structure, but is also highly depended on the dynamic characteristics of the supporting primary structure.

Seismic design and analysis are mandatory for safety-related secondary systems in nuclear power plants (ASCE, 1998; ASCE, 2005). Seismic analysis of secondary systems provides useful information to seismic probability risk assessment (SPRA) of nuclear facilities, which is now widely used for seismic safety evaluation of existing power stations, and design of new-built plants. Therefore, it is necessary to study the seismic behavior of secondary systems and develop reliable and practical approaches to determine the seismic responses of secondary systems.

1.1 Seismic Analysis Methods for Secondary Systems

Practically, seismic responses of secondary systems can be determined by two approaches: floor response spectrum approach and combined primary-secondary system approach. An overview of these two approaches is illustrated in Figure 1.3.

The floor response spectrum approach is a decoupled analysis method, which means the primary and secondary systems are analyzed separately. A dynamic analysis is performed for the primary structure at first without considering the effect of the secondary system. The input for the primary structure can be a set of time histories compatible with prescribed ground motion spectra. Responses of the primary structure at the locations to which the secondary systems are attached can be obtained, then are utilized as the input to a single degree-of-freedom oscillator to generate floor response spectra, which is a plot of the maximum responses of the oscillator versus the frequency of the oscillator. Therefore, engineers can estimate the maximum response of a secondary system readily from the floor response spectra.

In the combined primary-secondary system approach, the primary and secondary systems are modelled as an integral part. Both time history analysis and response spectrum analysis can be applied for determining the responses of the secondary systems. There is no

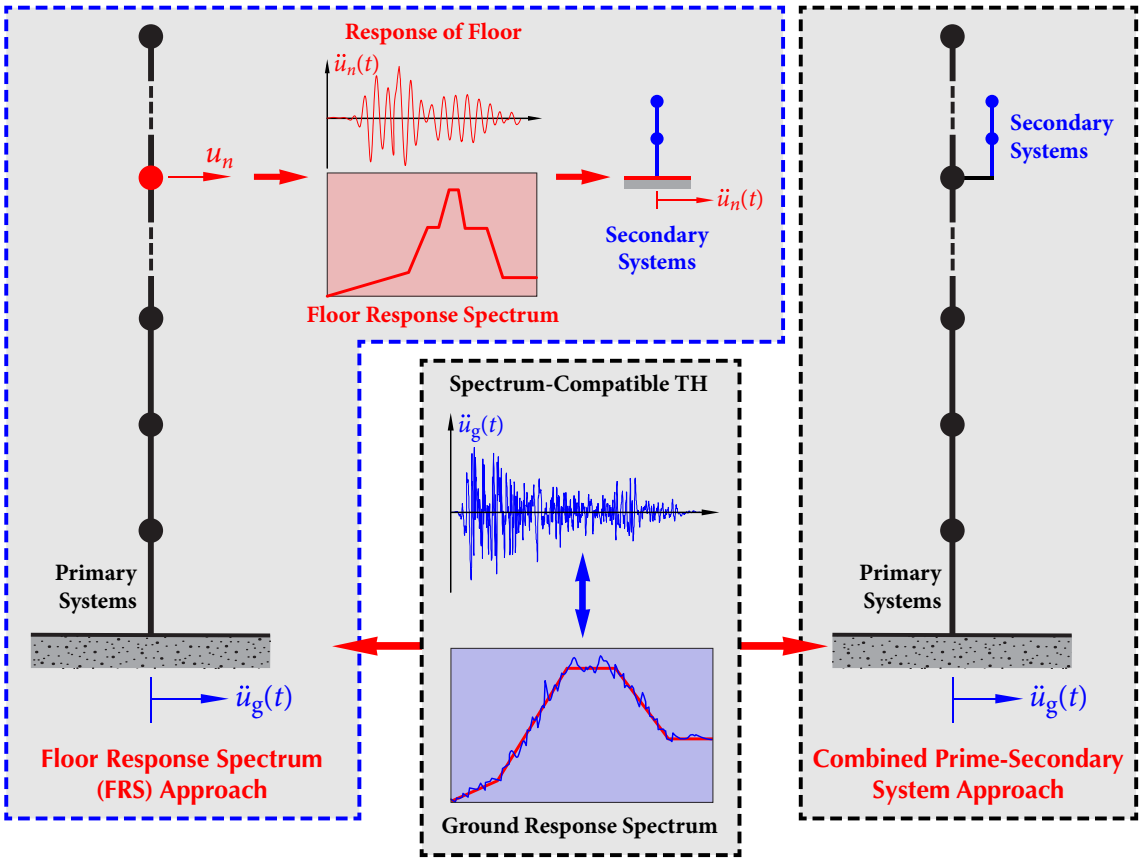

Figure 1.3 Seismic analysis methods for secondary systems

doubt that this approach can give an theoretically accurate responses of secondary systems, however, some challenges and difficulties exist. Large differences between the characteristics of primary systems and that of secondary systems, such as mass and stiffness, may cause serious numerical problems in a modal analysis or time history analysis, thus give inaccurate solutions. Also, there are usually excessive degrees-of-freedom in a combined primary-secondary system, dynamic analysis of the entire system is not efficient since only seismic responses of secondary systems are of interest. Moreover, although a combined primary-secondary system analysis can give seismic responses for a secondary system at a certain location. There may be a large number of secondary systems and the locations of secondary system may be varied, the calculation of each case is not feasible or desirable from a practical point of view. Consequently, the combined primary-secondary system approach is not widely used in practice. For secondary systems whose stiffness, mass, and result-

ing frequency range should be considered, a combined primary-secondary system will be established to account for possible dynamic interaction effects. Criteria to decoupled and coupled analyses are recommended in some studies (Gupta and Tembulkar, 1984; Hadjian and Ellison, 1986) and standards USNRC (2012); typical rules are shown in Figure 1.4. The blue line criteria is suggested in Hadjian's work based on performing parametric studies for two types of two degree-of-freedom models. It shows that the criteria of decoupling analysis mainly depends on the mass ratio and the frequency ratio between primary and secondary systems. The red line represents the criteria specified in the standard review plan of USNRC (2012).

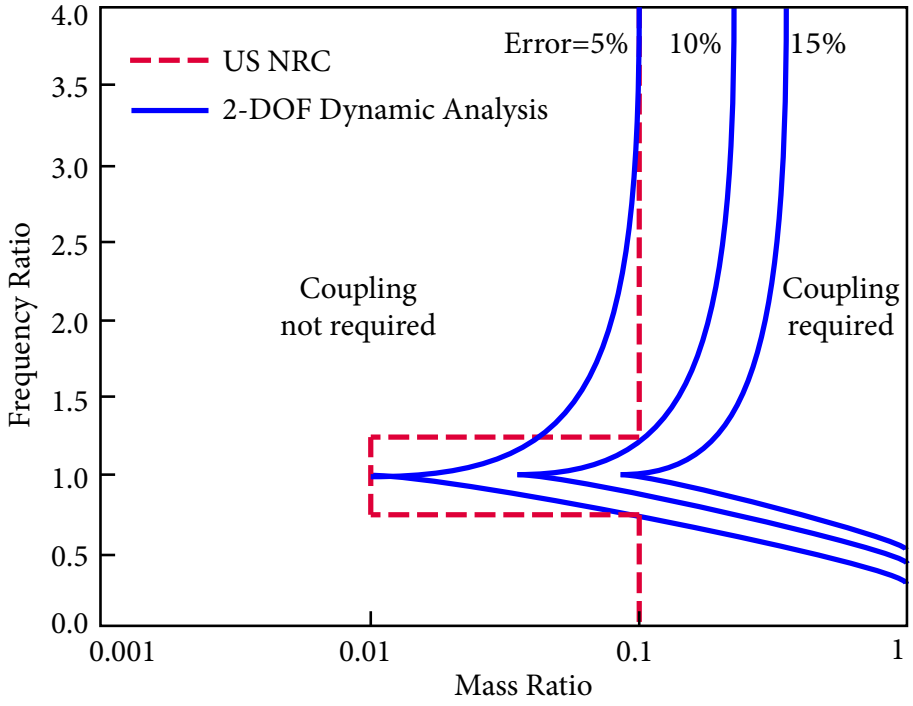

Figure 1.4 Decoupled and coupled analysis criteria

Although problems associated with the assumption of decoupled analysis may be encountered in some special applications, the floor response spectrum method with the decoupled assumption is widely accepted in practice since the majority of secondary systems have relative small mass compared to the mass of the supporting structure; the effect of interaction between the primary and secondary system can be negligible.

1.2 Floor Response Spectrum

ASCE (1998) proposes that floor response spectra shall be generated by time history analyses or a direct spectra-to-spectra method (Figure 1.5).

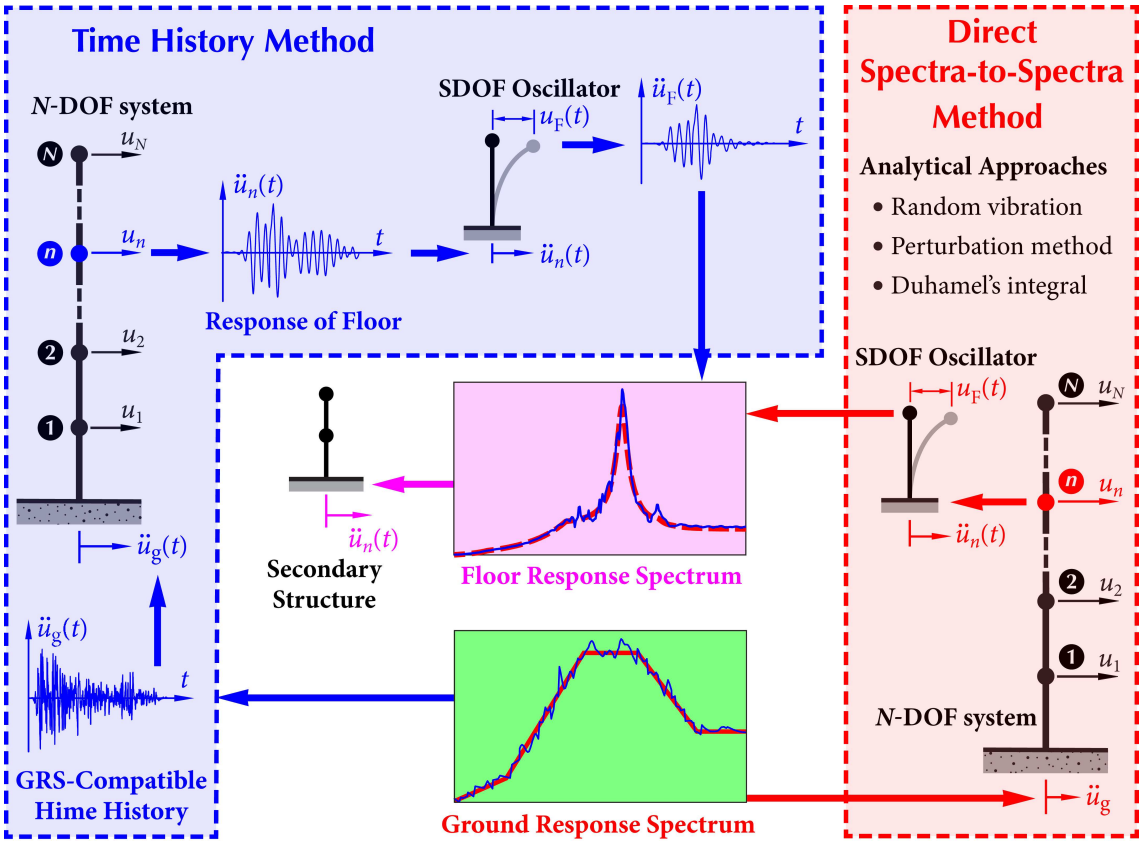

Figure 1.5 Two methods of generating floor response spectrum

1.2.1 Time History Method

For time history method, a dynamic analysis for primary structure is conduct by using modal superposition or direct time integration method. The time histories at the locations to which secondary systems are attached are obtained and sequently are used to generate floor response spectra. Conceptually, a time history analysis can give accurate responses for a given ground motion record. However, recorded ground motion time histories repre-

sentative of the site of interest are generally not available, therefore, artificial time histories compatible with a target ground response spectrum are usually generated as intermediate input to the primary structure. However, it has been recognized that there are significant variabilities in FRS generated by the time history method (Chen and Soong, 1988; Singh, 1988; Villaverde, 1997), in the sense that two spectrum-compatible time histories may give significantly different FRS. Hence, if only a single set of tri-directional earthquake time histories, or even a small number of sets of tri-directional earthquake time histories, is used in the time history analysis to calculate FRS, the FRS obtained is not reliable. Consequently, a large number of sets of tri-directional earthquake time histories may be required to obtain an reliable probabilistic description of FRS; but this procedure is not only cumbersome but also computationally expensive.

1.2.2 Direct Spectra-to-Spectra Method

Various direct spectra-to-spectra methods have been developed to avoid the deficiencies of time history methods. The "direct" means that ground response spectrum is used at input directly without generating any intermediate input such as spectrum-compatible time histories or spectrum-compatible power spectral density functions. In the direct methods, floor response spectra are analytically expressed in terms of ground motion spectra and some basic modal information of the primary structure, including modal frequencies and damping ratios, mode shapes, and modal participation factors, which can be obtained from a modal analysis.

1.3 Previous Research on Floor Response Spectra

Some research work on developing direct spectra-to-spectra method for generation of floor response spectra has been conducted during the past decades.

Biggs and Roesset (1970) first proposed a simple semi-empirical method to generate floor response spectra without performing time history analyses. Seismic response of secondary systems is considered as a combination of amplification of ground motion and amplification of structure motion. Amplification curves for the two types of amplification, which were

plotted versus the ratio between equipment period (T_e) and structure period (T_s) as shown in Figure 1.6, were developed empirically based on an analysis for a model subjected to four actual earthquake records. Maximum response of secondary system is calculated by combining the responses of all structural modes through the square root of the sum of the squares (SRSS) rule. Similar approaches were carried out later by Kapur and Shao (1970), Duff (1975).

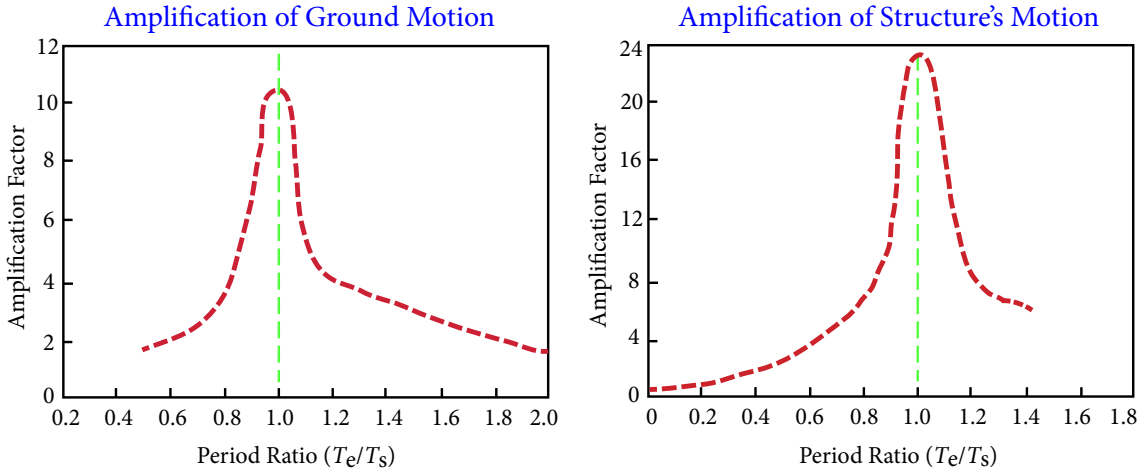

Figure 1.6 Empirical amplification curves in Biggs and Roesset's study

Singh (1975) develop a method to generate floor response spectra based on random vibration theory which incorporates a probabilistic concept. This approach is further extended by Singh (1980) considering resonance cases when the frequency of secondary systems is closed to one of the natural frequencies of the primary structure. In this method, the primary structure is assumed to be subject to a stochastic ground excitation characterized by power spectral density function (PSDF). The PSDF of structural responses, which are associated with the mean squared responses of secondary system, are obtained in terms of modal information of primary structure, complex frequency response functions, and PSDF of the prescribed ground motion. The mean square responses of secondary systems is then connected to its maximum response by multiplied with a peak factor as shown in Figure 1.7. A similar method on the basis random vibration principles in conjunction with mode acceleration formulation was also presented by Singh and Sharma (1985).

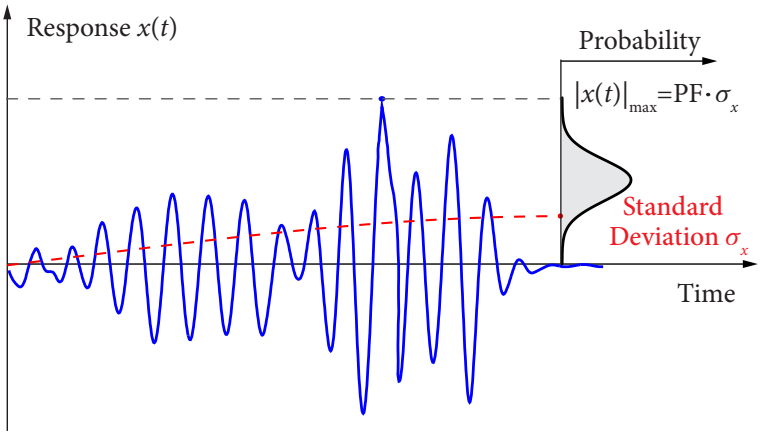

Figure 1.7 Relationship between maximum and mean responses in random process

Some direct approaches of generating FRS involving frequency domain analyses were developed. Scanlan (1974), Jeanpierre and Livolant (1977) present direct calculation methods of floor response spectra by taking the Fourier transform of ground motion. Peters *et al.* (1977) conducted a modal analysis for a structure with interaction-free, a single degree-of-freedom system attached, to produce approximate modal information of the structure-equipment system. An analytical expression of equipment response in non-resonance cases was derived and an approximation for secondary system response in a resonance case was recommended. The total responses of secondary system are determined through the SRSS modal combination rule.

It was pointed out by Kelly and Sackman (1978) that neglecting the dynamic interaction between primary and secondary systems yields conservative results in FRS when the mass ratio between secondary system and primary system is not small and resonance between primary and secondary system occurs. Sackman and Kelly (1978, 1979, 1980) employed a perturbation technique to solve eigenvalues of the combined primary-secondary system in which the equipment frequency is close to one of the natural frequencies of the supporting structure. Modal responses for non-tuning and tuning cases are given in closed-form, and the modal responses are sequently combined using the SRSS modal combination rule. Similar perturbation-based approaches were also utilized and improved by Sackman *et al.* (1983), Igusa and Kiureghian (1985), Gupta and Jaw (1986A), Singh and Suarez (1986), Suarez and Singh (1987A) to express the modal properties of the combined primary-secondary

system in term of that of each individual subsystem. Kiureghian *et al.* (1983), Igusa and Kiureghian (1985) investigated the responses of secondary system under stochastic seismic input using the modal properties of the combined primary-secondary system. Besides, a mode synthesis method was used by Suarez and Singh (1987B, 1987C) to consider the interaction between primary and secondary systems. A simple Newton-Raphson algorithm is employed to solve a nonlinear characteristic equation for the eigenvalues of the combined system. Since the approach is not derived on the basis of the perturbation theory, it is also applicable for relatively heavy secondary systems. Using this method, the interaction between two secondary systems and structure is considered by Suarez and Singh (1989) as well.

Generally, due to the difference between the damping of structure and equipment, the combined primary-secondary system possesses non-classical damping even though the primary system itself is classically damped. Therefore, the damping matrix of the system cannot be diagonalized by the eigenvectors of the undamped primary system. Igusa *et al.* (1987) derived a modal combination method to combine the spectral moments of the responses for the non-classically damped system characterized by complex eigenvalues and eigenfunctions. Singh and Sharma (1985) developed floor response spectra using equivalent modal frequencies and damping ratios which are transformed from the complex eigenvalues of a non-classical damping system. Gupta and Jaw (1986B) proposed a modal superposition method to deal with the non-classical damping problem. One complex eigenvector is replaced by two real eigenvectors, and modal equations can be obtained in the same form of classically damped system. Singh and Suarez (1987) expressed the characteristic equation of the combined primary-secondary system in terms of the exact dynamic properties of each subsystem, and solved the equation numerically to obtain the complex-valued eigenproperties, which are used for determining floor response spectra.

As some secondary systems such as piping system are multiply connected to the primary system, the spatial coupling effect on the response is also accounted in the generation of floor response spectra. Gupta (1984) evaluated the mode shapes and frequencies of a coupled model consists of a multiple degree-of-freedom secondary system and a multiple degree-of-freedom primary system using the perturbation theory. Floor response spectra at

the connecting degree-of-freedom are obtained deterministically alone with the correlation between the FRS. An improvement on this method was presented by Gupta and Jaw (1986c) with a better perturbation algorithm, the interaction and non-classical damping was also considered. Igusa and Kiureghian (1985) also extended their method which is on basis of modal synthesis, perturbation technique, and random vibration theory, to generate probabilistic FRS for multiply support secondary systems. Asfura and Kiureghian (1986) introduced a concept of cross-cross floor spectrum (CCFS), which is defined in terms of covariance of the responses of two oscillators mounted on two locations of the supporting structure, to consider the correlation between modal responses and between motions at supporting nodes. Burdisso and Singh (1987) developed a response spectrum method for seismic analysis of multiply support secondary systems. The response of the secondary system is divided into the inertia and the pseudo-static components. Maximum response of each component as well as the correlation between these two component, which is called cross response component, can be calculated by a response spectrum method. Since pseudo-acceleration floor response spectra, relative velocity floor response spectra and cross floor response spectra are required as input in the proposed response spectrum method, Singh and Burdisso (1987) also present a method to determine these spectra from ground response spectra directly.

The effect of nonlinear behavior of primary structure on floor response spectra was addressed by some researchers. Viti *et al.* (1981) studied the response of a single degree-of-freedom with elasto-plastic stiffness under seismic load. Peak reduction coefficients between Linear and non-linear floor response spectra which can reflect the effect of non-linearity are obtained for various damping ratios and ductility factors in numerical examples. Sewell (1986) performed a comprehensive parametric study on a multiple degree-of-freedom system, effect of various factors on linear and nonlinear floor response spectra was investigated. Igusa (1990) employed an equivalent linearization technique to investigate the dynamic behavior of an inelastic two degree-of-freedom primary-secondary system. The seismic response of the secondary system is derived analytically, and the effect of the non-linearities on the response is examined. Politopoulos and Feau (2007) proposed a design floor response spectrum through developing equivalent linear models for a single degree-

of-freedom primary structure with different types of nonlinearity. An extensive parametric study was also carried out by Chaudhuri and Villaverde (2008) to understand the effect of structure nonlinearity on seismic responses of secondary systems. The results indicated that the responses of secondary system may be amplified in special situations considering the nonlinearity of the primary structure.

In current practice, FRS is generally generated without considering the effect interaction. For the tuning cases, one of the terms becomes the first-order derivative of the relative velocity with respect to damping (see equation (2.2.27)), which cannot be determined analytically in terms of the input GRS. Singh (1980), Kiureghian *et al.* (1983), Igusa and Kiureghian (1985) studied the response of a tuned primary-secondary system under a wide-band stochastic input which can be approximated as a white noise in this case. Yasui *et al.* (1993), An *et al.* (2013) considered the phase differences between the primary and secondary system in time domain to obtain an approximate value of this tuning term.

Although there have been a number of direct spectra-to-spectra methods available for generating FRS since 1970s, they have not been widely used in nuclear industry. Some methods give conservative results in some frequency ranges but unconservative results in other frequency ranges due to the various approximations used. Furthermore, it is unknown when and by how much the FRS obtained is conservative or unconservative. If the results are scaled so that the resulting FRS are conservative over the entire frequency range, FRS in some frequency ranges become excessively conservative. The results of FRS should be conservative but not too conservative; otherwise, the cost of seismic qualification of systems, structures, and components (SSC) of nuclear power plants will be significantly increased. Some methods are derived based on pronounced theories, the implementation of these methods are, however, not free of complication and difficulties. For instance, the direct method developed by Singh (1975, 1980) is recommended in standard ASCE (1998). Although FRS is defined analytically in terms of the modal information of the primary structure and ground response spectra, some coefficients are not given explicitly. These coefficients which lack for physical meaning to engineers have to be obtained by solving systems of equations. Moreover, numerical difficulties may be encountered in solving the equations, particularly, for large complex structure.

1.4 Objectives of This Study

The objective of this study is to develop an accurate and efficient direct spectra-to-spectra method for generating floor response spectra:

- This method should provide accurate FRS peaks, where large variability exhibits if the time history method is used.
- The method should preserve the conventional form of spectrum analysis to which engineers are accustomed.
- No additional information is required except that needed in a traditional response spectrum analysis of structural responses.
- All the coefficients and parameters in this method should be given explicitly so that the formulations are convenient to implement.
- This method should be applicable to large three-dimensional complex structures with closely-spaced modes.

1.5 Organization of This Study

In Chapter 2, a direct spectra-to-spectra method for generating floor response spectra (FRS) of large three-dimensional structure is developed. Starting with the fundamentals of structural dynamics, seismic response of a SDOF oscillator mounted on a SDOF primary structure is studied first. The response of the oscillator is derived analytically based on Duhamel's integral. For the tuning case when the oscillator is resonant with the SDOF primary structure, the concept of t-response spectrum (tRS) is introduced, along with the statistical relationships between tRS and GRS developed through extensive numerical simulations, to give an accurate and complete probabilistic description of FRS, since large variabilities exist in this important case. The formulation is then extended to a SDOF oscillator mounted on a multiple DOF primary structure. A new modal combination method for generating FRS, called FRS-CQC, is developed based on random vibration theory. FRS-CQC can fully account for the correlation of responses between equipment and its supporting structure with closely-spaced modes. FRS is formulated in terms of input

GRS and the basic modal information of structure which is needed in the conventional spectrum analysis of structural responses.

In Chapter 3, the direct method proposed in Chapter 2 prompted the development of a scaling method of generating FRS. The challenge and difficulties of two typical scaling problems are introduced first. Based on the analytical formulation of the direct method which provides a strong physical insights into the essential characteristics of FRS, a system identification technique is presented to recover the dynamical information of significant equivalent modes of the underlying structure from the GRS and available FRS. A large number of numerical simulations are performed to quantify the relationship between tRS and different equipment damping ratios. Scaling factors are then determined in terms of the equivalent dynamical information (modal frequencies, modal damping ratios, and modal contribution factors) and input GRS. The effect of higher equipment damping ratio and variations of GRS spectral shapes can be fully accounted.

In Chapter 4, a methodology is developed for generating FRS considering the effect of dynamic soil-structure interaction based on the substructure technique and the proposed direct spectra-to-spectra method. Dynamic stiffness matrix of a three-dimensional structure with rigid foundation under three translational and three rotational base excitations is derived, and is expressed in terms of the modal information of the structure. A transfer matrix which is dependent on the dynamic stiffness matrix of the structure-foundation system and that of generalized soil springs is developed to modify the tri-directional response spectra at the foundation level of the free-field (FIRS). The modified response spectra, called foundation level input response spectra (FLIRS), are then used as the input to the fixed-base structure to generate FRS using the direct spectra-to-spectra method. The effect of soil-structure interaction on FRS is studied, the physical meaning and advantages of the proposed method are highlighted.

Chapter 5 presents some conclusions from this study and proposes directions for future research.

CHAPTER 2

Generating Floor Response Spectra: Direct Spectra-to-Spectra Method

Theoretically, time history analyses can give accurate structural responses for a real earthquake event, the ground motion time histories of the next earthquake event are, however, unpredictable. Therefore, response spectrum analysis which incorporates a probabilistic concept into the seismic input are commonly used by engineers in seismic design and analysis. A modal analysis of the structure is performed prior to a response spectrum analysis to identify the basic modal information of the structure including natural frequencies, modal damping ratios, mode shapes and modal participation factors. Maximum modal response of the structure can be estimated by reading the spectral value from the prescribed ground response spectrum for the corresponding frequency of the mode. An appropriate modal combination rule is then used to combine the maximum responses of all modes to determine the maximum total response of the structure.

Nevertheless, the maximum responses of structure are not adequate to determine floor response spectra (FRS). Spectrum-compatible time histories, as intermediate seismic input to the structure, have to be generated, and time history analyses are performed to obtain the time histories of the structural responses, which will be sequently used for generating FRS. However, as mentioned in Chapter 1, since time history analysis produces large variability in the resultant FRS due to the inherent randomness and uncertainties of the time histories,

a large number of time history analyses are needed to achieve reliable results which are time-consuming and cumbersome.

In this chapter, it is aimed to develop FRS analytically in time domain based on Duhamel's integral. Only the basic structural modal information required in a traditional response spectrum analysis of a structure, including natural frequencies, modal damping ratios, mode shapes and modal participation factors, is needed. Starting from the fundamentals of structure dynamics, responses of secondary system mounted on a structure are derived rigorously. A full probabilistic description on FRS peaks where large variability exhibits is implicitly incorporated into the formulation, and a new modal combination rule for FRS which is applicable for structure with closely-spaced modes is derived.

2.1 Response Spectra

2.1.1 Ground Response Spectra

In seismic design and assessment of nuclear power plants, seismic excitations in two orthogonal horizontal directions H_1 and H_2, and vertical direction V are usually applied. Suppose that $u_g^i(t)$, $i=1, 2, 3$, where $u_g^1(t)=u_g^{H_1}(t)$, $u_g^2(t)=u_g^{H_2}(t)$, and $u_g^3(t)=u_g^V(t)$, is the displacement of the ground motion in direction *i*. When a single degree-of-freedom (SDOF) oscillator with circular frequency ω_0 and damping coefficient ζ_0 is subjected to this ground motion, as shown in Figure 2.1, the equation of motion is

$$\ddot{x}_G^i + 2\zeta_0\omega_0\dot{x}_G^i + \omega_0^2 x_G^i = -\ddot{u}_g^i(t), \tag{2.1.1}$$

where $x_G^i(t)=u_G^i(t)-u_g^i(t)$ is the relative displacement of the oscillator and $u_G^i(t)$ is the absolute displacement. The subscript "G" denotes that the oscillator is mounted on the ground. The absolute acceleration is $\ddot{u}_G^i(t)=\ddot{x}_G^i(t)+\ddot{u}_g^i(t)=-(2\zeta_0\omega_0\dot{x}_G^i+\omega_0^2 x_G^i)$. The maximum absolute acceleration of the oscillator $\mathcal{S}_A^i(\omega_0,\zeta_0) = \max\left|\ddot{u}_G^i(t)\right|$ is the ground (acceleration) response spectrum (GRS) in direction *i*.

2.1.2 FRS of SDOF Primary Structure

For the special case when the primary structure is SDOF with circular frequency ω and damping coefficient ζ, $u(t)$ and $x(t)=u(t)-u_g(t)$ are the absolute and relative displace-

ments of the structure, respectively, satisfying

$$\ddot{x}(t) + 2\zeta\omega\dot{x}(t) + \omega^2 x(t) = -\ddot{u}_g(t), \tag{2.1.2}$$

$$\ddot{u}(t) = \ddot{x}(t) + \ddot{u}_g(t) = -2\zeta\omega\dot{x}(t) - \omega^2 x(t). \tag{2.1.3}$$

The motion of a SDOF oscillator with circular natural frequency ω_0 and damping coefficient ζ_0 mounted on the primary structure (Figure 2.2) is governed by

$$\ddot{x}_F + 2\zeta_0\omega_0\dot{x}_F + \omega_0^2 x_F = -\ddot{u}(t), \tag{2.1.4}$$

$$\ddot{u}_F(t) = \ddot{x}_F(t) + \ddot{u}(t) = -2\zeta_0\omega_0\dot{x}_F(t) - \omega_0^2 x_F(t), \tag{2.1.5}$$

where $x_F(t) = u_F(t) - u(t)$ and $u_F(t)$ are the relative and absolute displacements of the oscillator. The maximum absolute acceleration of the oscillator $\mathcal{S}_F(\omega_0, \zeta_0) = \max\left|\ddot{u}_F(t)\right|$ is the floor (acceleration) response spectrum (FRS) of the SDOF primary structure.

2.1.3 FRS of Multiple DOF Primary Structure

Consider a three-dimensional model of a structure with N nodes. A typical node n has six DOF: three translational DOF $u_{n,1}$, $u_{n,2}$, $u_{n,3}$, and three rotational DOF $u_{n,4}$, $u_{n,5}$, $u_{n,6}$. The structure is subjected to tri-directional seismic excitations (Figure 2.1). The relative displacement vector $\mathbf{x}$ of dimension $6N$ is governed by

$$\mathbf{M}\ddot{\mathbf{x}}(t) + \mathbf{C}\dot{\mathbf{x}}(t) + \mathbf{K}\mathbf{x}(t) = -\mathbf{M}\sum_{i=1}^{3} \boldsymbol{\mathcal{T}}^i \ddot{u}_g^i(t), \tag{2.1.6}$$

where

$$\mathbf{x} = \begin{Bmatrix} \mathbf{x}_1 \\ \mathbf{x}_2 \\ \vdots \\ \mathbf{x}_N \end{Bmatrix}, \quad \mathbf{x}_n = \begin{Bmatrix} x_{n,1} \\ x_{n,2} \\ \vdots \\ x_{n,6} \end{Bmatrix}, \quad \boldsymbol{\mathcal{T}}^i = \begin{Bmatrix} \mathbf{1}^i \\ \mathbf{1}^i \\ \vdots \\ \mathbf{1}^i \end{Bmatrix}, \quad \mathbf{1}^i = \begin{Bmatrix} \delta_{i1} \\ \delta_{i2} \\ \vdots \\ \delta_{i6} \end{Bmatrix},$$

$\mathbf{M}$, $\mathbf{C}$, $\mathbf{K}$ are, respectively, the mass, damping, and stiffness matrices of dimension $6N \times 6N$, $\mathbf{x}_n$ is the relative displacement vector of node n, $\boldsymbol{\mathcal{T}}^i$ is the influence vector of the seismic excitation in direction i, and δ_{ij} denotes the Kronecker delta function.

Let $\mathbf{x} = \mathbf{x}^1 + \mathbf{x}^2 + \mathbf{x}^3$, where $\mathbf{x}^i$ is the relative displacement vector due to the earthquake excitation $u_g^i(t)$ in direction i. Hence, $x_{n,j}^i = u_{n,j}^i - u_g^i \delta_{ij}$, where $x_{n,j}^i$ and $u_{n,j}^i$ are,

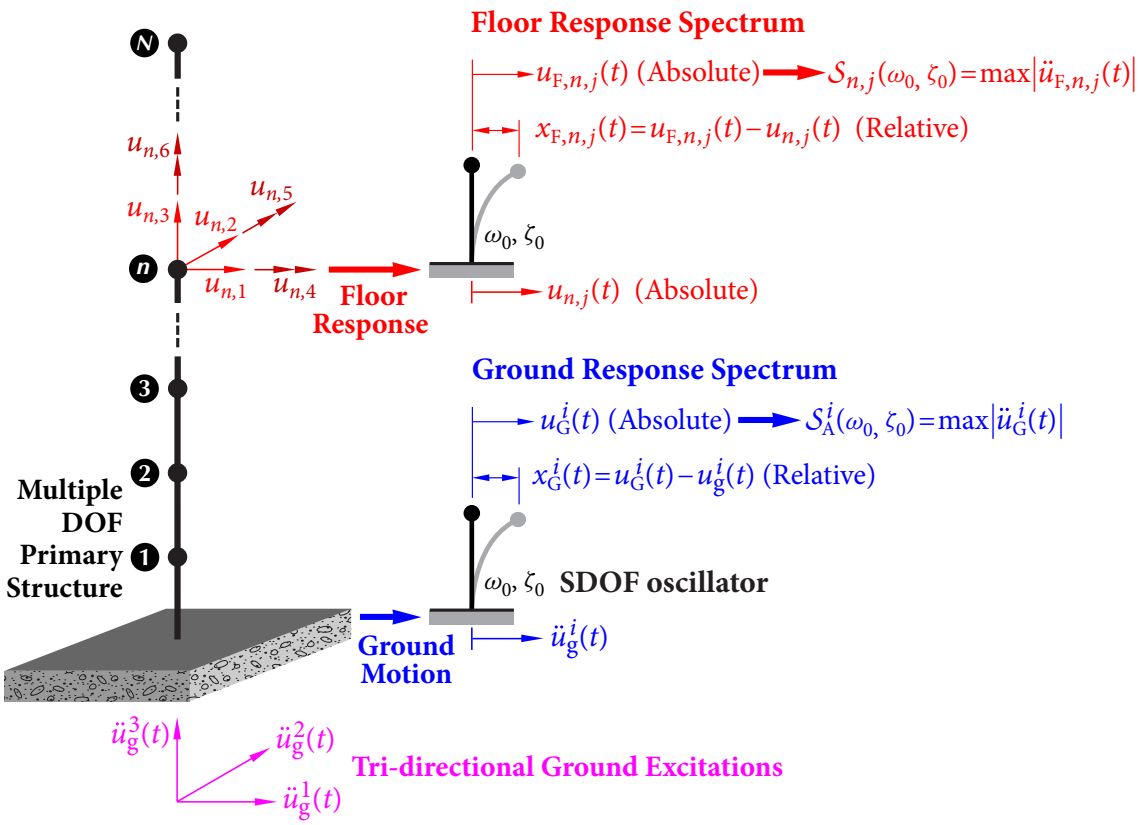

Figure 2.1 Response spectra.

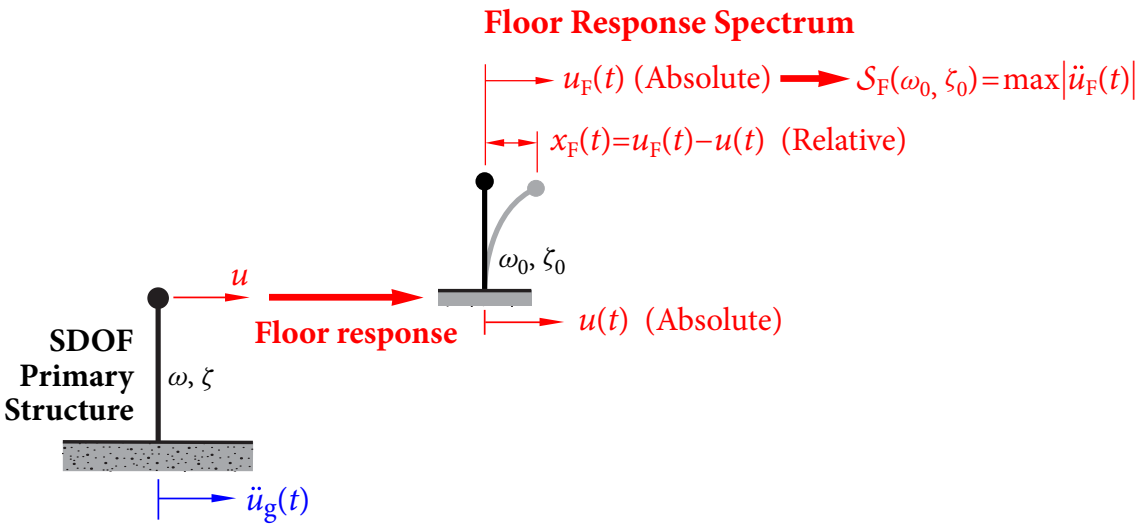

Figure 2.2 FRS of SDOF primary structure.

respectively, the relative and absolute displacements of node n in direction j due to the earthquake excitation in direction i. Since the system is linear, from equation (2.1.6), $\mathbf{x}^i$ is governed by

$$\mathbf{M}\ddot{\mathbf{x}}^i(t) + \mathbf{C}\dot{\mathbf{x}}^i(t) + \mathbf{K}\mathbf{x}^i(t) = -\mathbf{M}\,\boldsymbol{\mathcal{T}}^i\,\ddot{u}_{\mathrm{g}}^i(t), \quad i = 1, 2, 3. \tag{2.1.7}$$

Free Vibration

Consider the undamped free vibration of the structure $\mathbf{M}\ddot{\mathbf{x}}(t) + \mathbf{K}\mathbf{x}(t) = \mathbf{0}$. Let ω_1, ω_2, …, ω_{6N} be the $6N$ natural frequencies and $\boldsymbol{\Phi} = [\boldsymbol{\varphi}_1, \boldsymbol{\varphi}_2, \ldots, \boldsymbol{\varphi}_{6N}]$ be the modal matrix, where $\boldsymbol{\varphi}_k = \{\boldsymbol{\varphi}_{1,k}^T, \boldsymbol{\varphi}_{2,k}^T, \ldots, \boldsymbol{\varphi}_{N,k}^T\}^T$ is the mode shape of the kth mode, with $\boldsymbol{\varphi}_{n,k} = \{\varphi_{n,1;k}, \varphi_{n,2;k}, \ldots, \varphi_{n,6;k}\}^T$. In element $\varphi_{n,j;k}$, the first subscript n refers to the node number, the second subscript j indicates the direction of response, and the third subscript k refers to the mode number.

The modal matrix $\boldsymbol{\Phi}$ has the following orthogonal properties

$$\begin{aligned} \boldsymbol{\Phi}^T\mathbf{M}\boldsymbol{\Phi} &= \mathrm{diag}\{\bar{m}_1, \bar{m}_2, \ldots, \bar{m}_{6N}\}^T = \bar{\mathbf{m}}, \\ \boldsymbol{\Phi}^T\mathbf{K}\boldsymbol{\Phi} &= \bar{\mathbf{m}}\,\boldsymbol{\Omega}^2 = \mathrm{diag}\{\bar{m}_1\omega_1^2, \bar{m}_2\omega_2^2, \ldots, \bar{m}_{6N}\omega_{6N}^2\}^T, \\ \boldsymbol{\Omega} &= \mathrm{diag}\{\omega_1, \omega_2, \ldots, \omega_{6N}\}^T, \end{aligned} \tag{2.1.8}$$

where $\bar{m}_1$, $\bar{m}_2$, …, $\bar{m}_{6N}$ are the modal masses. Assume that the structure has classical damping so that the modal matrix $\boldsymbol{\Phi}$ can also diagonalize the damping matrix, i.e.,

$$\boldsymbol{\Phi}^T\mathbf{C}\boldsymbol{\Phi} = \mathrm{diag}\{\bar{c}_1, \bar{c}_2, \ldots, \bar{c}_{6N}\}^T, \qquad \bar{c}_k = \bar{m}_k \cdot 2\zeta_k\omega_k. \tag{2.1.9}$$

Forced Vibration

Apply the transformation

$$\mathbf{x}^i(t) = \boldsymbol{\Phi}\,\mathbf{Q}^i(t), \quad i = 1, 2, 3, \tag{2.1.10}$$

where

$$\mathbf{Q}^i = \begin{Bmatrix} \mathbf{Q}_1^i \\ \mathbf{Q}_2^i \\ \vdots \\ \mathbf{Q}_N^i \end{Bmatrix} = \begin{Bmatrix} \Gamma_1^i q_1^i \\ \Gamma_2^i q_2^i \\ \vdots \\ \Gamma_{6N}^i q_{6N}^i \end{Bmatrix}, \quad \mathbf{Q}_n^i = \begin{Bmatrix} \Gamma_{n,1}^i q_{n,1}^i \\ \Gamma_{n,2}^i q_{n,2}^i \\ \vdots \\ \Gamma_{n,6}^i q_{n,6}^i \end{Bmatrix}, \quad \mathbf{x}^i = \begin{Bmatrix} \mathbf{x}_1^i \\ \mathbf{x}_2^i \\ \vdots \\ \mathbf{x}_N^i \end{Bmatrix}, \quad \mathbf{x}_n^i = \begin{Bmatrix} x_{n,1}^i \\ x_{n,2}^i \\ \vdots \\ x_{n,6}^i \end{Bmatrix}, \tag{2.1.11}$$

$$x_{n,j}^{i} = \sum_{\nu=1}^{N}\sum_{\delta=1}^{6} \varphi_{n,j;6(\nu-1)+\delta}\,\Gamma_{\nu,\delta}^{i}\,q_{\nu,\delta}^{i} = \sum_{k=1}^{6N} \varphi_{n,j;k}\,\Gamma_{k}^{i} q_{k}^{i}, \tag{2.1.12}$$

$$L_{n,j}^{i} = \boldsymbol{\varphi}_{6(n-1)+j}^{T}\mathbf{M}\boldsymbol{\mathcal{T}}^{i}, \quad \text{or} \quad L_{k}^{i} = \boldsymbol{\varphi}_{k}^{T}\mathbf{M}\boldsymbol{\mathcal{T}}^{i}, \tag{2.1.13}$$

$$\Gamma_{n,j}^{i} = \frac{L_{n,j}^{i}}{\bar{m}_{6(n-1)+j}}, \quad \text{or} \quad \Gamma_{k}^{i} = \frac{L_{k}^{i}}{\bar{m}_{k}} = \frac{\boldsymbol{\varphi}_{k}^{T}\mathbf{M}\boldsymbol{\mathcal{T}}^{i}}{\boldsymbol{\varphi}_{k}^{T}\mathbf{M}\boldsymbol{\varphi}_{k}}. \tag{2.1.14}$$

For ease of presentation, the two-subscript-notation n, j (node, direction) and the one-subscript-notation $k=6(n-1)+j$ are used interchangeably; the former is advantageous in describing the meaning of the quantity in terms of node and direction, and the latter gives the position of the quantity in the corresponding vector. $L_{n,j}^{i}$ is the *earthquake excitation factor*, quantifying the contribution of earthquake excitation in the ith direction to the modal response $q_{n,j}^{i}$. Γ_{k}^{i} is the *modal participation factors*; if Γ_{k}^{i} is small, then the contribution of mode $\boldsymbol{\varphi}_{k}$ to the structural response due to excitation in the ith direction is small.

Substituting equation (2.1.10) into (2.1.7) and multiplying $\boldsymbol{\Phi}^{T}$ from the left yield

$$(\boldsymbol{\Phi}^{T}\mathbf{M}\boldsymbol{\Phi})\ddot{\mathbf{Q}}^{i}(t) + (\boldsymbol{\Phi}^{T}\mathbf{C}\boldsymbol{\Phi})\dot{\mathbf{Q}}^{i}(t) + (\boldsymbol{\Phi}^{T}\mathbf{K}\boldsymbol{\Phi})\mathbf{Q}^{i}(t) = -\boldsymbol{\Phi}^{T}\mathbf{M}\boldsymbol{\mathcal{T}}^{i}\ddot{u}_{\mathrm{g}}^{i}(t).$$

Using relations (2.1.8), (2.1.9), (2.1.13), and (2.1.14) gives

$$\ddot{q}_{k}^{i}(t) + 2\zeta_{k}\omega_{k}\dot{q}_{k}^{i}(t) + \omega_{k}^{2}q_{k}^{i}(t) = -\ddot{u}_{\mathrm{g}}^{i}(t), \quad k=1, 2, \ldots, 6N, \quad i=1, 2, 3. \tag{2.1.15}$$

The absolute acceleration of the nth node in direction j due to the earthquake excitation in direction i can be obtained using equations (2.1.12) and (2.1.15)

$$\begin{aligned}
\ddot{u}_{n,j}^{i}(t) &= \ddot{x}_{n,j}^{i}(t) + \ddot{u}_{\mathrm{g}}^{i}(t)\,\delta_{ij} = \sum_{k=1}^{6N} \varphi_{n,j;k}\,\Gamma_{k}^{i}\ddot{q}_{k}^{i}(t) + \ddot{u}_{\mathrm{g}}^{i}(t)\,\delta_{ij} \\
&= \sum_{k=1}^{6N} \varphi_{n,j;k}\,\Gamma_{k}^{i}\Big[-\ddot{u}_{\mathrm{g}}^{i}(t) - (2\zeta_{k}\omega_{k}\dot{q}_{k}^{i} + \omega_{k}^{2}q_{k}^{i})\Big] + \ddot{u}_{\mathrm{g}}^{i}(t)\,\delta_{ij}, \quad \sum_{k=1}^{6N} \varphi_{n,j;k}\Gamma_{k}^{i} = \delta_{ij}, \\
&= -\sum_{k=1}^{6N} \varphi_{n,j;k}\,\Gamma_{k}^{i}\,(2\zeta_{k}\omega_{k}\dot{q}_{k}^{i} + \omega_{k}^{2}q_{k}^{i}) \\
&= -\sum_{k=1}^{6N} \ddot{u}_{n,j;k}^{i}, \qquad \ddot{u}_{n,j;k}^{i} = \varphi_{n,j;k}\,\Gamma_{k}^{i}\,(2\zeta_{k}\omega_{k}\dot{q}_{k}^{i} + \omega_{k}^{2}q_{k}^{i}),
\end{aligned} \tag{2.1.16}$$

in which $\ddot{u}^i_{n,j;k}$ is the contribution from the kth mode and $\varphi_{n,j;k}\Gamma^i_k$ is the contribution factor.

Floor Response Spectrum

If the absolute response $u^i_{n,j}(t)$ of the nth node in direction j due to earthquake excitation in direction i is input to a SDOF oscillator with circular frequency ω_0 and damping coefficient ζ_0, as shown in Figure 2.1, the governing equation of motion is

$$\ddot{x}^i_{\mathrm{F},n,j} + 2\zeta_0\omega_0\dot{x}^i_{\mathrm{F},n,j} + \omega_0^2 x^i_{\mathrm{F},n,j} = -\ddot{u}^i_{n,j}(t), \tag{2.1.17}$$

$$\ddot{u}^i_{\mathrm{F},n,j}(t) = \ddot{x}^i_{\mathrm{F},n,j}(t) + \ddot{u}^i_{n,j}(t) = -2\zeta_0\omega_0\dot{x}^i_{\mathrm{F},n,j} - \omega_0^2 x^i_{\mathrm{F},n,j}, \tag{2.1.18}$$

where $x^i_{\mathrm{F},n,j}(t) = u^i_{\mathrm{F},n,j}(t) - u^i_{n,j}(t)$ is the displacement of the oscillator relative to the nth node in direction j, and $u^i_{\mathrm{F},n,j}(t)$ is the absolute displacement of the oscillator. The subscript "F" denotes that the oscillator is mounted on the floor. The maximum absolute acceleration of the oscillator

$$\mathcal{S}^i_{n,j}(\omega_0,\zeta_0) = \left|\ddot{u}^i_{\mathrm{F},n,j}(t)\right|_{\max} \tag{2.1.19}$$

is the floor (acceleration) response spectrum (FRS) of the nth node (floor) in direction j subjected to earthquake excitation in direction i.

It is specified in ASCE 4-98 (ASCE, 1998) that, for direct spectra-to-spectra methods, when the response spectrum of a given direction at a given location has contributions from more than one spatial component of earthquakes, these contributions shall be combined by the SRSS rule. Hence, combining contributions from tri-directional earthquake excitations, FRS of the nth node in direction j is given by

$$\mathcal{S}_{n,j}(\omega_0,\zeta_0) = \sqrt{\sum_{i=1}^{3}\left[\mathcal{S}^i_{n,j}(\omega_0,\zeta_0)\right]^2}. \tag{2.1.20}$$

2.2 Direct Method for Generating FRS

In this section, a direct spectra-to-spectra method for generating FRS is developed based on Duhamel's integral.

2.2.1 SDOF Oscillator Mounted on SDOF Structure

Consider a SDOF oscillator mounted on a SDOF structure, as shown in Figure 2.2. Adopt the notations

$$h(t) = \mathrm{e}^{-\zeta\omega t}\frac{\sin\omega_{\mathrm{d}}t}{\omega_{\mathrm{d}}}, \qquad h^{\mathrm{c}}(t) = \mathrm{e}^{-\zeta\omega t}\frac{\cos\omega_{\mathrm{d}}t}{\omega_{\mathrm{d}}}, \qquad \omega_{\mathrm{d}} = \omega\sqrt{1-\zeta^2}, \tag{2.2.1}$$

$$h_0(t) = \mathrm{e}^{-\zeta_0\omega_0 t}\frac{\sin\omega_{0,\mathrm{d}}t}{\omega_{0,\mathrm{d}}}, \quad h_0^{\mathrm{c}}(t) = \mathrm{e}^{-\zeta_0\omega_0 t}\frac{\cos\omega_{0,\mathrm{d}}t}{\omega_{0,\mathrm{d}}}, \quad \omega_{0,\mathrm{d}} = \omega_0\sqrt{1-\zeta_0^2}. \tag{2.2.2}$$

Motion of Structure

For a SDOF system governed by equation (2.1.2) with zero initial conditions, using Duhamel's integral (Clough and Penzien, 2003), the relative displacement $x(t)$ and the relative velocity $\dot{x}(t)$ of the structure can be given the convolutions as follows

$$x(t) = h(t) * \ddot{u}_{\mathrm{g}}(t), \qquad \dot{x}(t) = \dot{h}(t) * \ddot{u}_{\mathrm{g}}(t), \tag{2.2.3}$$

where $h(t)$ is the unit impulse response function of the structure and ω_{d} is the damped circular frequency defined by equation (2.2.1). The derivative of $h(t)$ is

$$\dot{h}(t) = -\frac{\zeta}{\sqrt{1-\zeta^2}}\mathrm{e}^{-\zeta\omega t}\sin\omega_{\mathrm{d}}t + \mathrm{e}^{-\zeta\omega t}\cos\omega_{\mathrm{d}}t = -\zeta\omega h(t) + \mathrm{e}^{-\zeta\omega t}\cos\omega_{\mathrm{d}}t. \tag{2.2.4}$$

Substituting equation (2.2.3) into (2.1.3), the absolute acceleration of the structure is given by

$$\ddot{u}(t) = -2\zeta\omega\dot{h}(t) * \ddot{u}_{\mathrm{g}}(t) - \omega^2 h(t) * \ddot{u}_{\mathrm{g}}(t). \tag{2.2.5}$$

Motion of Oscillator

The motion of the structure, to which the oscillator is attached, defines the input to the SDOF oscillator with circular natural frequency ω_0 and damping coefficient ζ_0; the relative and absolute motions of the oscillator are governed by equations (2.1.4) and (2.1.5), respectively. Substituting equation (2.2.5) into Duhamel's integral and using the associativity of convolutions, the relative displacement $x_{\mathrm{F}}(t)$ and velocity $\dot{x}_{\mathrm{F}}(t)$ between the structure

and the oscillator are

$$\begin{aligned} x_{\mathrm{F}}(t) &= h_0(t) * \ddot{u}(t) = -2\zeta\omega h_0(t) * \dot{h}(t) * \ddot{u}_{\mathrm{g}}(t) - \omega^2 h_0(t) * h(t) * \ddot{u}_{\mathrm{g}}(t), \\ \dot{x}_{\mathrm{F}}(t) &= \dot{h}_0(t) * \ddot{u}(t) = -2\zeta\omega \dot{h}_0(t) * \dot{h}(t) * \ddot{u}_{\mathrm{g}}(t) - \omega^2 \dot{h}_0(t) * h(t) * \ddot{u}_{\mathrm{g}}(t), \end{aligned} \tag{2.2.6}$$

where the unit impulse response function $h_0(t)$ is defined by equation (2.2.2).

Substituting equation (2.2.6) into (2.1.5) and applying the distributivity of convolutions, the absolute acceleration of the oscillator is expressed as

$$\begin{aligned} \ddot{u}_{\mathrm{F}}(t) &= -2\zeta_0\omega_0\dot{x}_{\mathrm{F}}(t) - \omega_0^2 x_{\mathrm{F}}(t) \\ &= \big[4\zeta_0\zeta\omega_0\omega \cdot \dot{h}_0(t) * \dot{h}(t) + 2\zeta_0\omega_0\omega^2 \cdot \dot{h}_0(t) * h(t) \\ &\quad + 2\zeta\omega_0^2\omega \cdot h_0(t) * \dot{h}(t) + \omega_0^2\omega^2 \cdot h_0(t) * h(t) \big] * \ddot{u}_{\mathrm{g}}(t) \\ &= \big[(1-2\zeta_0^2-2\zeta^2+4\zeta_0^2\zeta^2)\omega_0^2\omega^2 \cdot h_0(t) * h(t) \\ &\quad + 4\zeta_0\zeta\sqrt{(1-\zeta^2)(1-\zeta_0^2)}\,\omega_0^2\omega^2 \cdot h_0^{\mathrm{c}}(t) * h^{\mathrm{c}}(t) \\ &\quad + 2\zeta_0\sqrt{1-\zeta_0^2}\,(1-2\zeta^2)\omega_0^2\omega^2 \cdot h(t) * h_0^{\mathrm{c}}(t) \\ &\quad + 2(1-2\zeta_0^2)\zeta\sqrt{1-\zeta^2}\,\omega_0^2\omega^2 \cdot h_0(t) * h^{\mathrm{c}}(t) \big] * \ddot{u}_{\mathrm{g}}(t), \end{aligned} \tag{2.2.7}$$

where $h^{\mathrm{c}}(t)$ and $h_0^{\mathrm{c}}(t)$ are defined in equations (2.2.1) and (2.2.2).

For most SSCs in nuclear power plants, the damping coefficients ζ, $\zeta_0 < 0.2$ (EPRI, 1994). When the duration of the excitation t is sufficiently long, it is reasonable to assume that

$$\begin{aligned} &\left|h_0(t) * h(t) * \ddot{u}_{\mathrm{g}}(t)\right|_{\max} \approx \left|h_0^{\mathrm{c}}(t) * h^{\mathrm{c}}(t) * \ddot{u}_{\mathrm{g}}(t)\right|_{\max} \\ &\quad \approx \left|h(t) * h_0^{\mathrm{c}}(t) * \ddot{u}_{\mathrm{g}}(t)\right|_{\max} \approx \left|h_0(t) * h^{\mathrm{c}}(t) * \ddot{u}_{\mathrm{g}}(t)\right|_{\max}. \end{aligned} \tag{2.2.8}$$

In principle, the maximum values of the convolution terms in equation (2.2.7) do not occur simultaneously because of the phase differences between the sine and cosine terms. For lightly-damped systems, the values of the higher order terms ζ^2, ζ_0^2, and $\zeta_0\zeta$ are very small compared to 1, so that the corresponding terms are negligible. The maximum response of the oscillator is then reduced to

$$\left|\ddot{u}_{\mathrm{F}}(t)\right|_{\max} \approx \omega_0^2\omega^2 \left|h_0(t) * h(t) * \ddot{u}_{\mathrm{g}}(t)\right|_{\max}, \tag{2.2.9}$$

which is expressed analytically as a double convolution. Note that, if the SDOF oscillator is mounted directly on the ground, the term $\omega^2 h(t)$ is removed from equation (2.2.9) and

FRS reduces to GRS, i.e.,

$$\mathcal{S}_{\mathrm{A}}(\omega_0,\zeta_0)=\omega_0^2\left|h_0(t)*\ddot{u}_{\mathrm{g}}(t)\right|_{\max}=\left|\omega_0\mathrm{e}^{-\zeta_0\omega t}\sin\omega_0 t*\ddot{u}_{\mathrm{g}}(t)\right|_{\max}. \tag{2.2.10}$$

Denote $C(t)=h_0(t)*h(t)$. From the definition of Duhamel's integral, it is obvious that $C(t)$ is the response of an oscillator with the circular frequency ω_0 and damping coefficient ζ_0 under the excitation of $h(t)$. The equation of motion is written as

$$\ddot{C}(t)+2\zeta_0\omega_0\dot{C}(t)+\omega_0^2C(t)=h(t)=\frac{1}{\omega_{\mathrm{d}}}\mathrm{e}^{-\zeta\omega}\sin\omega_{\mathrm{d}}t. \tag{2.2.11}$$

The general solution for this differential equation consists of the complementary solution and a particular solution $C(t)=C_{\mathrm{C}}(t)+C_{\mathrm{P}}(t)$, where

$$C_{\mathrm{C}}(t)=\mathrm{e}^{-\zeta_0\omega_0 t}\left(C_1\cos\omega_{0,\mathrm{d}}t+C_2\sin\omega_{0,\mathrm{d}}t\right),\quad \text{for}\ \ \zeta_0<1, \tag{2.2.12}$$

is the complementary solution with coefficients C_1 and C_2 determined by the initial conditions, and $C_{\mathrm{P}}(t)$ is a particular solution determined in the following.

2.2.2 Non-tuning Case

If $\omega\neq\omega_0$ and $\zeta\neq\zeta_0$, a particular solution $C_{\mathrm{P}}(t)$ is given by

$$C_{\mathrm{P}}(t)=\mathrm{e}^{-\zeta\omega t}\left(P_1\cos\omega_{\mathrm{d}}t+P_2\sin\omega_{\mathrm{d}}t\right), \tag{2.2.13}$$

where

$$P_1=-\frac{r\sqrt{1-\zeta^2}\cdot A}{\omega_0^2\omega_{\mathrm{d}}\cdot\Delta},\quad P_2=\frac{(1-\zeta^2)\cdot B}{\omega_0^2\omega_{\mathrm{d}}\cdot\Delta},\quad r=\frac{\omega}{\omega_0}, \tag{2.2.14}$$

and $A=2(\zeta_0-\zeta r)$, $B=1-r^2-\zeta r\cdot A$, $\Delta=r^2\cdot A+(1-\zeta^2)\cdot B^2$. For zero initial conditions $y(0)=0$ and $\dot{y}(0)=0$, the coefficients C_1 and C_2 of the complementary solution are given by

$$C_1=-P_1,\quad C_2=-\frac{A\cdot P_1}{2\sqrt{1-\zeta_0^2}}-\frac{r\sqrt{1-\zeta^2}\cdot P_2}{\sqrt{1-\zeta_0^2}}. \tag{2.2.15}$$

Having obtained $C(t)=h_0(t)*h(t)$, the maximum absolute acceleration of the oscillator given by equation (2.2.9) is

$$\begin{aligned}\left|\ddot{u}_{\mathrm{F}}(t)\right|_{\max}=\Big|&\left(C_1\omega_0^2\omega^2\mathrm{e}^{-\zeta_0\omega_0 t}\cos\omega_{0,\mathrm{d}}t+C_2\omega_0^2\omega^2\mathrm{e}^{-\zeta_0\omega_0 t}\sin\omega_{0,\mathrm{d}}t\right.\\&\left.+P_1\omega_0^2\omega^2\mathrm{e}^{-\zeta\omega t}\cos\omega_{\mathrm{d}}t+P_2\omega_0^2\omega^2\mathrm{e}^{-\zeta\omega t}\sin\omega_{\mathrm{d}}t\right)*\ddot{u}_{\mathrm{g}}(t)\Big|_{\max}.\end{aligned} \tag{2.2.16}$$

Floor Response Spectra

For lightly damped systems (say, ζ, $\zeta_0 < 0.2$), $\omega_{0,\mathrm{d}} \approx \omega_0$ and $\omega_{\mathrm{d}} \approx \omega$. Equation (2.2.16) reduces to

$$\begin{aligned}\left|\ddot{u}_{\mathrm{F}}(t)\right|_{\max} &= \Big|\big(C_1\omega_0^2\omega^2 \mathrm{e}^{-\zeta_0\omega_0 t}\cos\omega_0 t + C_2\omega_0^2\omega^2\mathrm{e}^{-\zeta_0\omega_0 t}\sin\omega_0 t \\ &\quad + P_1\omega_0^2\omega^2\mathrm{e}^{-\zeta\omega t}\cos\omega t + P_2\omega_0^2\omega^2\mathrm{e}^{-\zeta\omega t}\sin\omega t\big) * \ddot{u}_{\mathrm{g}}(t)\Big|_{\max} \\ &= \Big|C_1\omega_0\omega^2\cdot\left[\omega_0\dot{h}_0(t) * \ddot{u}_{\mathrm{g}}(t)\right] + C_2\omega_0\omega^2\cdot\left[\omega_0^2 h_0(t) * \ddot{u}_{\mathrm{g}}(t)\right] \\ &\quad + P_1\omega_0^2\omega\cdot\left[\omega\dot{h}(t) * \ddot{u}_{\mathrm{g}}(t)\right] + P_2\omega_0^2\omega\cdot\left[\omega^2 h(t) * \ddot{u}_{\mathrm{g}}(t)\right]\Big|_{\max}. \end{aligned} \tag{2.2.17}$$

The maximum response $\left|\ddot{u}_{\mathrm{F}}(t)\right|_{\max}$ may be over-estimated if it is calculated by the sum of the maximum values of each term in equation (2.2.17), since the maximum values of $\left|\omega^2 h(t) * \ddot{u}_{\mathrm{g}}(t)\right|_{\max}$ and $\left|\omega\dot{h}(t) * \ddot{u}_{\mathrm{g}}(t)\right|_{\max}$, or $\left|\omega_0^2 h_0(t) * \ddot{u}_{\mathrm{g}}(t)\right|_{\max}$ and $\left|\omega_0\dot{h}_0(t) * \ddot{u}_{\mathrm{g}}(t)\right|_{\max}$, do not occur simultaneously.

Since there is a $\pi/2$ phase difference between the sine and cosine functions, it is appropriate to employ the SRSS combination rule to calculate the maximum absolute acceleration. Therefore, in non-tuning cases (when the frequencies of the structure and equipment are well separated), the FRS is obtained from equation (2.2.17) as

$$\mathcal{S}_{\mathrm{F}}^2(\omega_0,\zeta_0) = \mathit{AF}_0^2\cdot\mathcal{S}_{\mathrm{A}}^2(\omega_0,\zeta_0) + \mathit{AF}^2\cdot\mathcal{S}_{\mathrm{A}}^2(\omega,\zeta), \tag{2.2.18}$$

in which $\mathcal{S}_{\mathrm{F}}(\omega_0,\zeta_0) = \left|\ddot{u}_{\mathrm{F}}(t)\right|_{\max}$ is the FRS or the spectral acceleration of a SDOF oscillator (with circular frequency ω_0 and damping ratio ζ_0) mounted on the SDOF structure (with circular frequency ω and damping ratio ζ), $\mathcal{S}_{\mathrm{A}}(\omega_0,\zeta_0)$ is the GRS or the spectral acceleration of the oscillator mounted on the ground, and AF and AF_0 are the amplification factors discussed in the following subsection.

2.2.3 Amplification Factors

For non-tuning cases, the amplification factors AF_0 and AF are given by

$$\begin{aligned}\mathit{AF}_0 &= \frac{r^2}{\sqrt{(1-r^2)^2+4(\zeta_0^2+\zeta^2)r^2-4\zeta_0\zeta r(1+r^2)}}, \\ \mathit{AF} &= \frac{1}{\sqrt{(1-r^2)^2+4(\zeta_0^2+\zeta^2)r^2-4\zeta_0\zeta r(1+r^2)}}.\end{aligned} \tag{2.2.19}$$

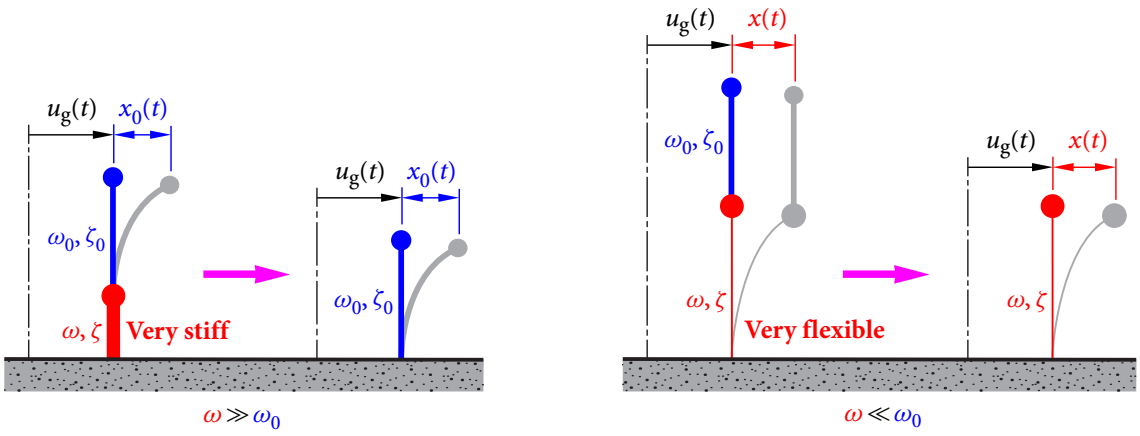

Figure 2.3 Two extreme cases of motion amplification

If damping is light and the effect of damping is neglected, the amplification factors are approximately

$$AF_0 \approx \frac{r^2}{1-r^2}, \quad AF \approx \frac{1}{1-r^2}, \quad r = \frac{\omega}{\omega_0}. \tag{2.2.20}$$

From equation (2.2.18), the FRS $\mathcal{S}_F(\omega_0, \zeta_0)$ can be interpreted as a combination of

- amplified spectral acceleration $AF_0 \cdot \mathcal{S}_A(\omega_0, \zeta_0)$ of the oscillator, and
- amplified spectral acceleration $AF \cdot \mathcal{S}_A(\omega, \zeta)$ of the structure.

To illustrate the physical meaning of equation (2.2.18), consider two extreme cases (Figure 2.3):

- **Frequency ratio** $r \to \infty$ ($\omega \gg \omega_0$): The structure is very stiff comparing to the oscillator, so that the structure and the ground can be considered as an integral rigid body. The frequency components of ground motions, to which the oscillator is sensitive, are transmitted by the structure without modification. Therefore, the equipment behaves as if it is directly mounted on the ground. When $r \to \infty$, the amplification factors $AF_0 = 1$ and $AF = 0$ agree with this case.
- **Frequency ratio** $r \to 0$ ($\omega \ll \omega_0$): The oscillator is very stiff comparing to the structure or the structure is very flexible comparing to the oscillator, so that the response of the oscillator is the same as that of the structure. When $r = 0$, the amplification factors

$AF_0 = 0$ and $AF = 1$, and the maximum response of the oscillator is equal to the spectral acceleration of the structure.

The amplification factors AF_0 and AF given by equations (2.2.19) and (2.2.20) are for non-tuning cases. To extend the concept of amplification factors to perfect-tuning and near-tuning cases, the behavior of the amplification factors given by equation (2.2.20) is investigated by plotting them in Figure 2.4(a):

- The amplification factor of ground motion AF_0 is similar to the Dynamic Magnification Factors (DMF) of a SDOF oscillator subjected to a harmonic loading

$$\mathrm{DMF}_0 = \frac{r^2}{\sqrt{(1-r^2)^2 + (2\zeta r)^2}}. \tag{2.2.21}$$

- The amplification factor of structure motion AF is similar to the DMF of a SDOF oscillator under harmonic base excitation

$$\mathrm{DMF} = \frac{1}{\sqrt{(1-r^2)^2 + (2\zeta r)^2}}. \tag{2.2.22}$$

DMF_0 and DMF given by equations (2.2.21) and (2.2.22) are shown in Figures 2.4(b) and (c). It is seen that damping has little effect on the response amplification in non-resonant or non-tuning cases (when r is not close to 1), but has a significant effect on the response in perfect-tuning or near-tuning cases (when r approaches 1).

Based on the expressions of DMF_0 and DMF given by equations (2.2.21) and (2.2.22), when the effect of damping is considered, it is appropriate to assume that the amplification factors AF_0 and AF are of the form, for both tuning and non-tuning cases,

$$AF_0 = \frac{r^2}{\sqrt{(1-r^2)^2 + (2\zeta_{0,\mathrm{e}} r)^2}}, \qquad AF = \frac{1}{\sqrt{(1-r^2)^2 + (2\zeta_{\mathrm{e}} r)^2}}, \tag{2.2.23}$$

in which $\zeta_{0,\mathrm{e}}$ and ζ_{e} are considered to be the *equivalent damping coefficients* for the amplification factors of ground motion and structure motion, respectively.

In the non-tuning cases, the amplification factors given by equations (2.2.19) and (2.2.20) can be used directly; it is not necessary to specify the equivalent damping coefficients $\zeta_{0,\mathrm{e}}$ and ζ_{e} in equation (2.2.23).

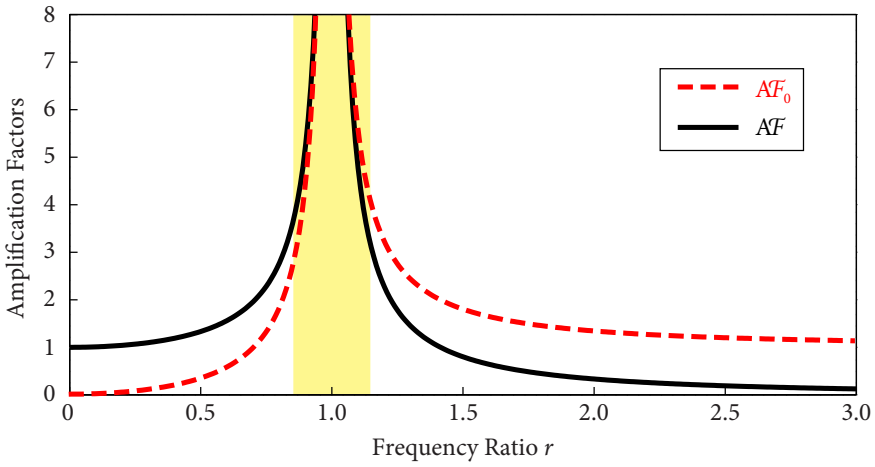

(a) Amplification Factors of FRS

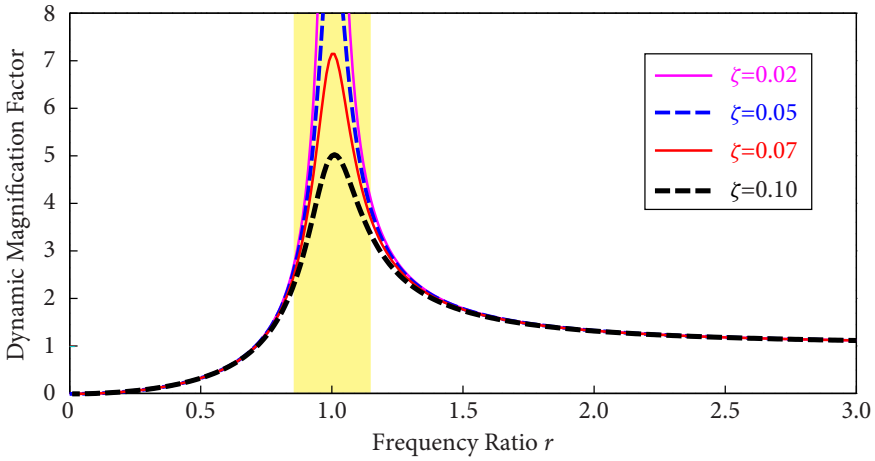

(b) Dynamic Magnification Factor DMF_0

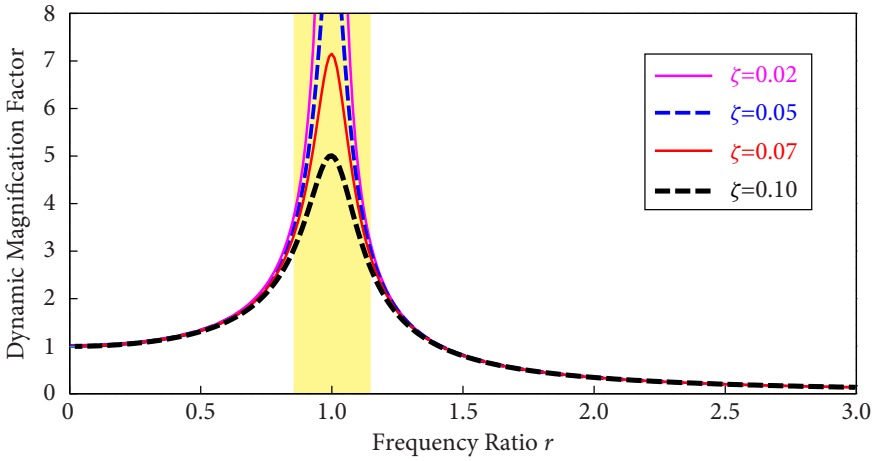

(c) Dynamic Magnification Factor DMF

Figure 2.4 Amplification Factors

In the following subsection, the tuning case is investigated to quantify the equivalent damping coefficients $\zeta_{0,e}$ and ζ_e.

2.2.4 Perfect-tuning Case

When $\omega_0 = \omega$ and for small damping $\zeta_0, \zeta < 0.2$, $C(t) = h_0(t) * h(t)$ becomes

$$\begin{aligned} h_0(t) * h(t) &= \int_0^t \frac{1}{\omega_0} \mathrm{e}^{-\zeta_0\omega_0(t-\tau)} \sin\omega_0(t-\tau) \cdot \frac{1}{\omega} \mathrm{e}^{-\zeta\omega\tau} \sin\omega\tau \,\mathrm{d}\tau \\ &= \frac{1}{\omega^3\left[4+(\zeta-\zeta_0)^2\right]} \left[\frac{2}{\zeta-\zeta_0} (\mathrm{e}^{-\zeta\omega t} - \mathrm{e}^{-\zeta_0\omega t}) \cos\omega t + (\mathrm{e}^{-\zeta\omega t} + \mathrm{e}^{-\zeta_0\omega t}) \sin\omega t \right], \end{aligned}$$

which can be simplified to, for small damping $(\zeta - \zeta_0) \to 0$,

$$\begin{aligned} h_0(t) * h(t) &= \frac{1}{2\omega^3(\zeta-\zeta_0)} (\mathrm{e}^{-\zeta\omega t} - \mathrm{e}^{-\zeta_0\omega t}) \cos\omega t + \frac{1}{4\omega^3} (\mathrm{e}^{-\zeta\omega t} + \mathrm{e}^{-\zeta_0\omega t}) \sin\omega t \\ &= \frac{\dot{h}(t) - \dot{h}_0(t)}{2\omega^3(\zeta-\zeta_0)} + \frac{h(t) + h_0(t)}{4\omega^2}. \end{aligned} \tag{2.2.24}$$

Substituting equation (2.2.24) into (2.2.9) yields the maximum response of the oscillator

$$\begin{aligned} \left|\ddot{u}_F(t)\right|_{\max} &= \left| \frac{\omega\dot{h}(t) * \ddot{u}_g(t) - \omega\dot{h}_0(t) * \ddot{u}_g(t)}{2(\zeta-\zeta_0)} + \frac{\omega^2 h(t) * \ddot{u}_g(t) + \omega^2 h_0(t) * \ddot{u}_g(t)}{4} \right|_{\max} \\ &= \left| \frac{\omega}{2} \cdot \frac{\dot{u}(t) - \dot{u}_0(t)}{\zeta-\zeta_0} + \frac{\ddot{u}(t) + \ddot{u}_0(t)}{4} \right|_{\max}, \end{aligned} \tag{2.2.25}$$

in which the following relationships have been used

$$u(t) = h(t) * \ddot{u}_g(t), \;\; \dot{u}(t) = \dot{h}(t) * \ddot{u}_g(t), \;\; \ddot{u}(t) = \omega^2 h(t) * \ddot{u}_g(t) = \omega\dot{h}(t) * \ddot{u}_g(t). \tag{2.2.26}$$

When $\zeta_0 = \zeta$, $\dot{u}(t) = \dot{u}_0(t)$ and $\ddot{u}(t) = \ddot{u}_0(t)$; the first term in equation (2.2.25), which is dominant, is undefined. For $(\zeta - \zeta_0) \to 0$, equation (2.2.25) becomes

$$\left|\ddot{u}_F(t)\right|_{\max} = \frac{1}{2} \left| \omega \frac{\partial\dot{u}(t)}{\partial\zeta} + \ddot{u}(t) \right|_{\max}. \tag{2.2.27}$$

Differentiating $\dot{u}(t) = \dot{h}(t) * \ddot{u}_g(t)$ with respect to ζ gives

$$\frac{\partial\dot{u}(t)}{\partial\zeta} = \frac{\partial\left[\dot{h}(t) * \ddot{u}_g(t)\right]}{\partial\zeta} = -\omega t \mathrm{e}^{-\zeta\omega t} \cos\omega t * \ddot{u}_g(t). \tag{2.2.28}$$

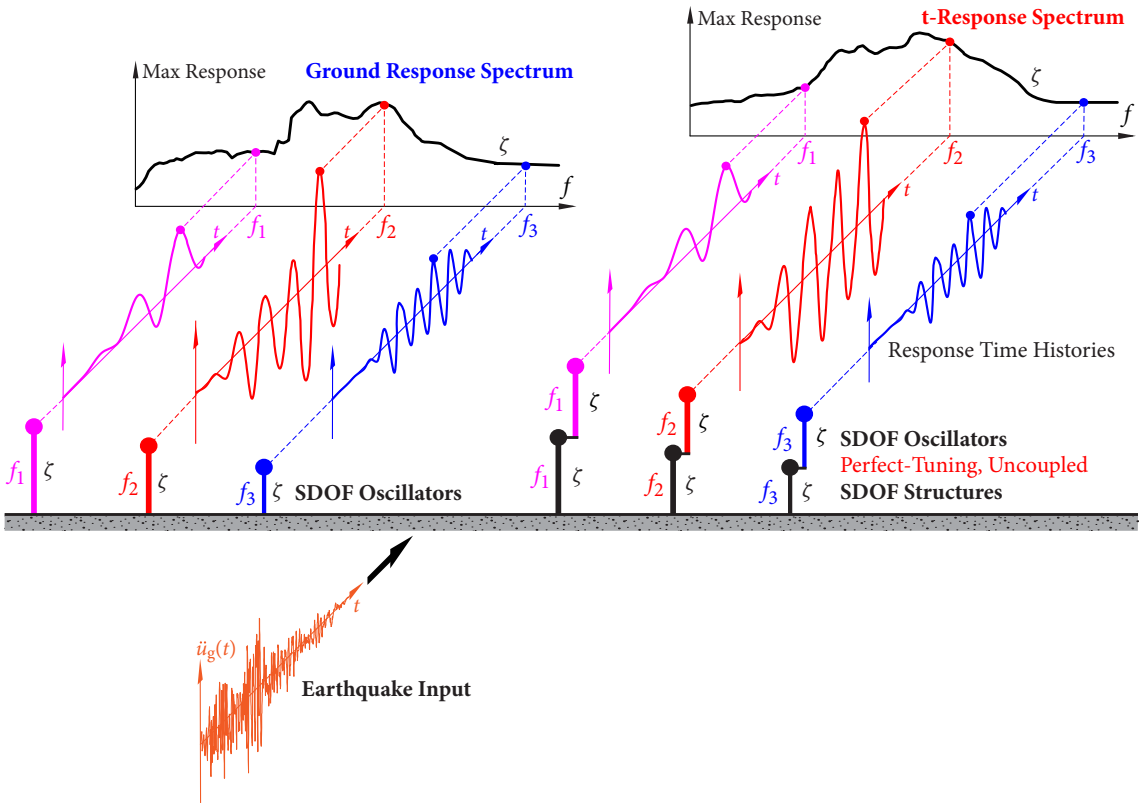

Figure 2.5 Illustration of GRS and tRS

Note that $\ddot{u}(t)$ can also be written as $\ddot{u}(t) = \omega^2 h(t) * \ddot{u}_g(t) = \omega e^{-\zeta\omega t} \sin \omega t * \ddot{u}_g(t)$.

Hence, in the perfect-tuning case with $\omega_0 = \omega$, $\zeta_0 = \zeta$, FRS given by equation (2.2.27) becomes

$$\begin{aligned} \mathcal{S}_F(\omega, \zeta) &= \frac{1}{2} \left| -\omega^2 t e^{-\zeta\omega t} \cos \omega t * \ddot{u}_g(t) + \omega e^{-\zeta\omega t} \sin \omega t * \ddot{u}_g(t) \right|_{\max} \\ &= \mathcal{S}_A^t(\omega, \zeta). \end{aligned} \tag{2.2.29}$$

Analogous to GRS defined in (2.2.10), equation (2.2.29) is defined as t-Response Spectrum (tRS), in which "t" indicates "tuning" or the extra "t" variable in the first convolution term as compared to GRS defined in equation (2.2.10) . The concepts of GRS and tRS are illustrated in Figure 2.5. Under an earthquake excitation $\ddot{u}_g(t)$,

- GRS $\mathcal{S}_A(f, \zeta)$ is the maximum acceleration response of a SDOF oscillator (with frequency f and damping ratio ζ) mounted directly on ground;

- tRS $\mathcal{S}_{\mathrm{A}}^{\mathrm{t}}(f,\zeta)$ is the maximum acceleration response of a SDOF oscillator (with frequency f and damping ratio ζ) mounted on top of a SDOF structure (with the same f and ζ) that is mounted on ground. The identical SDOF oscillator and SDOF structure are uncoupled and are in *resonance* or *tuning*.

FRS given by equation (2.2.29) can be expressed in the form of equation (2.2.18). Note that, in the perfect-tuning case, $\omega_0=\omega$, $r=1$, $\zeta_0=\zeta$, and $\mathcal{S}_{\mathrm{A}}(\omega_0,\zeta_0)=\mathcal{S}_{\mathrm{A}}(\omega,\zeta)$, $\mathit{AF}_0=\mathit{AF}$. Equation (2.2.18) reduces to

$$\mathcal{S}_{\mathrm{F}}(\omega_0,\zeta_0)=\sqrt{2}\cdot\mathit{AF}_0\cdot\mathcal{S}_{\mathrm{A}}(\omega_0,\zeta_0)=\mathcal{S}_{\mathrm{A}}^{\mathrm{t}}(\omega_0,\zeta_0), \tag{2.2.30}$$

which gives

$$\mathit{AF}_0=\mathit{AF}=\frac{1}{\sqrt{2}}\cdot\frac{\mathcal{S}_{\mathrm{A}}^{\mathrm{t}}(\omega_0,\zeta_0)}{\mathcal{S}_{\mathrm{A}}(\omega_0,\zeta_0)}. \tag{2.2.31}$$

From equation (2.2.23), when $r=1$, one has

$$\mathit{AF}_0=\left.\frac{r^2}{\sqrt{(1-r^2)^2+(2\zeta_{0,\mathrm{e}}r)^2}}\right|_{r=1}=\frac{r^2}{2\zeta_{0,\mathrm{e}}},\qquad \mathit{AF}=\frac{1}{2\zeta_{\mathrm{e}}}. \tag{2.2.32}$$

Hence, from equations (2.2.31) and (2.2.32), the equivalent damping coefficients for the perfect-tuning case are given by

$$\zeta_{0,\mathrm{e}}=\zeta_{\mathrm{e}}=\frac{1}{\sqrt{2}}\cdot\frac{\mathcal{S}_{\mathrm{A}}(\omega_0,\zeta_0)}{\mathcal{S}_{\mathrm{A}}^{\mathrm{t}}(\omega_0,\zeta_0)}. \tag{2.2.33}$$

A comprehensive study on the statistical relationship between GRS and tRS is conducted by Li *et al.* (2015). A large number of real horizontal and vertical ground motions, which are selected from the Pacific Earthquake Engineering Research Center Strong Motion Database (PEER, 2010) and the European Strong Motion Database, are employed to perform numerical simulations. Statistical relationships between tRS and GRS are constructed based on three different site conditions following the the site classification criteria (ASCE, 2010; IBC, 2012):

- 49 horizontal and 49 vertical ground motions of B sites;
- 154 horizontal and 154 vertical ground motions of C sites; and
- 220 horizontal and 220 vertical ground motions of D sites.

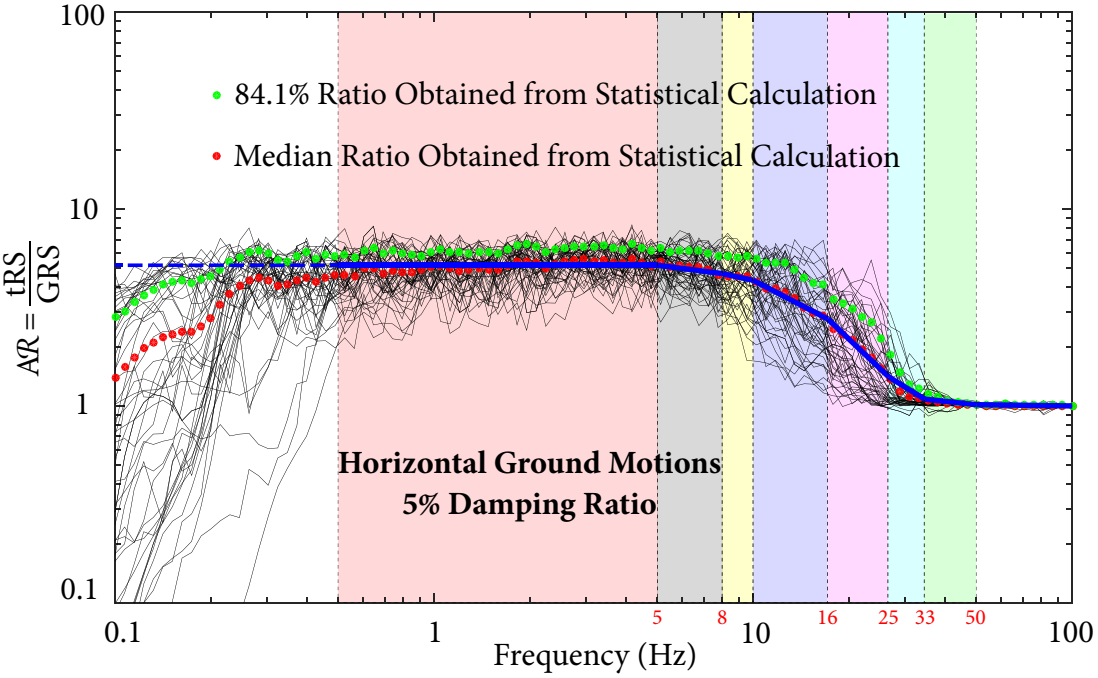

Figure 2.6 Ratio of tRS to GRS for the 49 horizontal ground motions at B sites

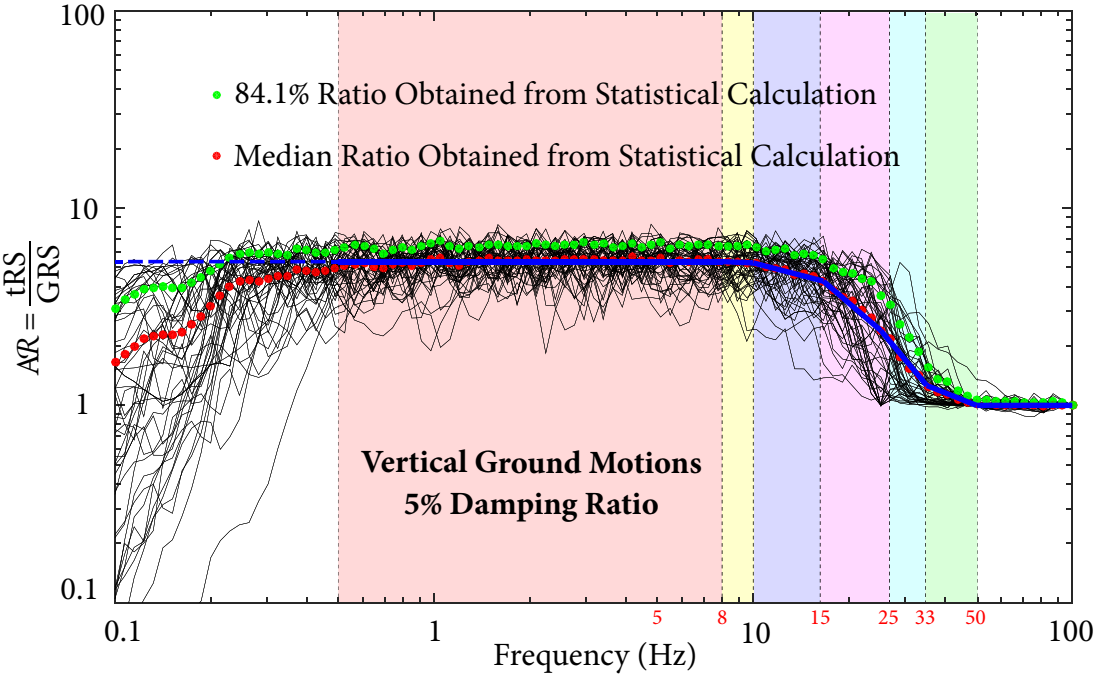

Figure 2.7 Ratio of tRS to GRS for the 49 vertical ground motions at B sites

Table 2.1 Coefficients of simplified horizontal statistical relationship for various damping ratios

f (Hz)	Damping Ratio ζ (%)																				
	1.0			3.0			5.0			7.0			10.0			15.0			20.0		
	c_1	c_2	$\sigma_{\ln \mathcal{S}_A^t}$	c_1	c_2	$\sigma_{\ln \mathcal{S}_A^t}$	c_1	c_2	$\sigma_{\ln \mathcal{S}_A^t}$	c_1	c_2	$\sigma_{\ln \mathcal{S}_A^t}$	c_1	c_2	$\sigma_{\ln \mathcal{S}_A^t}$	c_1	c_2	$\sigma_{\ln \mathcal{S}_A^t}$	c_1	c_2	$\sigma_{\ln \mathcal{S}_A^t}$
0.1∼5	3.00	1.12	0.30	2.11	1.07	0.24	1.70	1.07	0.21	1.44	1.07	0.20	1.18	1.09	0.19	0.93	1.14	0.18	0.80	1.21	0.19
8	3.00	1.33	0.27	2.14	1.45	0.25	1.76	1.51	0.24	1.54	1.55	0.23	1.34	1.61	0.21	1.20	1.69	0.16	1.09	1.69	0.14
10	2.99	1.45	0.29	2.19	1.65	0.28	1.88	1.77	0.28	1.70	1.84	0.26	1.52	1.89	0.22	1.30	1.85	0.18	1.16	1.80	0.13
16	3.31	2.21	0.43	2.72	2.57	0.40	2.39	2.58	0.33	2.15	2.52	0.27	1.86	2.38	0.21	1.48	2.14	0.15	1.30	2.01	0.11
25	6.42	5.67	0.62	5.07	5.02	0.35	3.66	3.95	0.22	2.80	3.27	0.16	2.20	2.80	0.10	1.72	2.42	0.06	1.52	2.25	0.04
33	7.35	6.68	0.49	3.77	4.02	0.21	2.32	2.88	0.11	1.67	2.36	0.07	1.30	2.06	0.04	1.20	1.98	0.03	1.18	1.97	0.02
50∼100	0.0	1.00	0.0	0.0	1.00	0.0	0.0	1.00	0.0	0.0	1.00	0.0	0.0	1.00	0.0	0.0	1.00	0.0	0.0	1.00	0.0

Table 2.2 Equations for coefficients and standard deviations of horizontal statistical relationship

Frequency (Hz)	Coefficient c_1	Coefficient c_2	Standard deviation $\sigma_{\ln \mathcal{S}_A^t}$
0.1∼5.0	$0.06(\ln\zeta)^2 - 0.92\ln\zeta + 3.03$	$0.02(\ln\zeta)^3 - 0.04(\ln\zeta)^2 - 0.02\ln\zeta + 1.12$	$-0.01(\ln\zeta)^2 - 0.05\ln\zeta + 0.30$
8.0	$0.10(\ln\zeta)^2 - 0.93\ln\zeta + 3.01$	$-0.01(\ln\zeta)^3 + 0.07(\ln\zeta)^2 + 0.03\ln\zeta + 1.35$	$-0.01(\ln\zeta)^3 + 0.02(\ln\zeta)^2 - 0.02\ln\zeta + 0.27$
10.0	$0.06(\ln\zeta)^2 - 0.80\ln\zeta + 2.99$	$-0.06(\ln\zeta)^3 + 0.21(\ln\zeta)^2 + 1.45$	$-0.01(\ln\zeta)^3 + 0.01(\ln\zeta)^2 + 0.28$
16.0	$-0.08(\ln\zeta)^2 - 0.45\ln\zeta + 3.32$	$-0.22(\ln\zeta)^2 + 0.58\ln\zeta + 2.24$	$0.02(\ln\zeta)^3 - 0.12(\ln\zeta)^2 + 0.07\ln\zeta + 0.43$
25.0	$0.39(\ln\zeta)^3 - 1.74(\ln\zeta)^2 + 0.16\ln\zeta + 6.33$	$0.35(\ln\zeta)^3 - 1.66(\ln\zeta)^2 + 0.77\ln\zeta + 5.58$	$0.02(\ln\zeta)^3 - 0.04(\ln\zeta)^2 - 0.21\ln\zeta + 0.60$
33.0	$0.21(\ln\zeta)^3 - 0.22(\ln\zeta)^2 - 3.16\ln\zeta + 7.23$	$0.20(\ln\zeta)^3 - 0.38(\ln\zeta)^2 - 2.15\ln\zeta + 6.58$	$0.04(\ln\zeta)^2 - 0.31\ln\zeta + 0.49$
50.0∼100.0	0	1	0

Table 2.3 Coefficients of simplified vertical statistical relationships for hard sites

f (Hz)	Damping Ratio ζ (%)																			
	1.0			3.0			5.0			7.0			10.0			15.0			20.0		
	c_1	c_2	$\sigma_{\ln S_A^t}$	c_1	c_2	$\sigma_{\ln S_A^t}$	c_1	c_2	$\sigma_{\ln S_A^t}$	c_1	c_2	$\sigma_{\ln S_A^t}$	c_1	c_2	$\sigma_{\ln S_A^t}$	c_1	c_2	$\sigma_{\ln S_A^t}$	c_1	c_2	$\sigma_{\ln S_A^t}$
0.1∼8.0	3.06	1.15	0.28	2.17	1.09	0.23	1.76	1.08	0.21	1.49	1.07	0.21	1.21	1.08	0.20	0.93	1.11	0.19	0.78	1.17	0.20
10.0	3.07	1.23	0.20	2.19	1.28	0.19	1.80	1.35	0.19	1.58	1.42	0.20	1.37	1.48	0.19	1.14	1.51	0.16	1.00	1.52	0.14
15.0	3.04	1.35	0.26	2.20	1.54	0.25	1.85	1.66	0.25	1.66	1.75	0.23	1.48	1.80	0.21	1.32	1.83	0.17	1.23	1.84	0.14
25.0	3.28	2.28	0.6	2.64	2.53	0.43	2.33	2.55	0.33	2.14	2.53	0.27	1.94	2.48	0.20	1.62	2.28	0.13	1.45	2.16	0.09
33.0	3.87	3.29	0.65	3.42	3.56	0.39	2.90	3.27	0.28	2.39	2.89	0.23	1.88	2.50	0.16	1.36	2.09	0.10	1.20	1.96	0.07
50.0∼100	0.0	1.00	0.0	0.0	1.00	0.0	0.0	1.00	0.0	0.0	1.00	0.0	0.0	1.00	0.0	0.0	1.00	0.0	0.0	1.00	0.0

Table 2.4 Coefficients of simplified vertical statistical relationships for soft sites

f (Hz)	Damping Ratio ζ (%)																			
	1.0			3.0			5.0			7.0			10.0			15.0			20.0		
	c_1	c_2	$\sigma_{\ln S_A^t}$	c_1	c_2	$\sigma_{\ln S_A^t}$	c_1	c_2	$\sigma_{\ln S_A^t}$	c_1	c_2	$\sigma_{\ln S_A^t}$	c_1	c_2	$\sigma_{\ln S_A^t}$	c_1	c_2	$\sigma_{\ln S_A^t}$	c_1	c_2	$\sigma_{\ln S_A^t}$
0.1∼8.0	3.1	1.17	0.32	2.22	1.11	0.28	1.8	1.10	0.27	1.53	1.10	0.26	1.26	1.11	0.26	0.98	1.14	0.25	0.84	1.20	0.24
10.0	3.06	1.24	0.22	2.18	1.32	0.18	1.78	1.35	0.18	1.53	1.38	0.18	1.28	1.39	0.18	1.06	1.42	0.16	0.88	1.37	0.14
15.0	3.02	1.40	0.24	2.15	1.47	0.27	1.75	1.51	0.28	1.53	1.55	0.25	1.31	1.57	0.23	1.11	1.60	0.18	1.01	1.64	0.15
25.0	3.20	2.62	0.73	2.70	2.84	0.48	2.51	2.88	0.34	2.34	2.82	0.27	2.12	2.68	0.22	1.81	2.45	0.17	1.59	2.28	0.12
33.0	3.17	2.62	0.58	3.05	3.19	0.39	2.79	3.15	0.28	2.45	2.93	0.22	2.15	2.73	0.15	1.80	2.46	0.11	1.58	2.29	0.08
50.0∼100	0.0	1.00	0.0	0.0	1.00	0.0	0.0	1.00	0.0	0.0	1.00	0.0	0.0	1.00	0.0	0.0	1.00	0.0	0.0	1.00	0.0

Table 2.5 Equations for coefficients and standard deviations of vertical statistical relationships for hard sites

Frequency (Hz)	Coefficient c_1	Coefficient c_2	Standard deviation $\sigma_{\ln \mathcal{S}_A^t}$
0.5∼8.0	$0.04(\ln\zeta)^2 - 0.89\ln\zeta + 3.09$	$0.01(\ln\zeta)^4 - 0.06(\ln\zeta)^3 + 0.12(\ln\zeta)^2 - 0.12\ln\zeta + 1.15$	$0.01(\ln\zeta)^2 - 0.06\ln\zeta + 0.28$
10.0	$0.07(\ln\zeta)^2 - 0.90\ln\zeta + 3.08$	$-0.04(\ln\zeta)^3 + 0.19(\ln\zeta)^2 - 0.13\ln\zeta + 1.24$	$-0.01(\ln\zeta)^3 + 0.05(\ln\zeta)^2 - 0.05\ln\zeta + 0.2$
15.0	$0.10(\ln\zeta)^2 - 0.90\ln\zeta + 3.06$	$-0.03(\ln\zeta)^3 + 0.13(\ln\zeta)^2 + 0.08\ln\zeta + 1.35$	$-0.01(\ln\zeta)^3 + 0.01(\ln\zeta)^2 + 0.25$
25.0	$-0.03(\ln\zeta)^2 - 0.52\ln\zeta + 3.25$	$-0.03(\ln\zeta)^3 - 0.02(\ln\zeta)^2 + 0.29\ln\zeta + 2.28$	$0.01(\ln\zeta)^3 - 0.05(\ln\zeta)^2 - 0.12\ln\zeta + 0.60$
33.0	$0.17(\ln\zeta)^3 - 0.98(\ln\zeta)^2 + 0.51\ln\zeta + 3.83$	$0.17(\ln\zeta)^3 - 1.10(\ln\zeta)^2 + 1.28\ln\zeta + 3.26$	$0.01(\ln\zeta)^2 - 0.26\ln\zeta + 0.65$
50.0∼100	0	1	0

Table 2.6 Equations for coefficients and standard deviations of vertical statistical relationships for soft sites

Frequency (Hz)	Coefficient c_1	Coefficient c_2	Standard deviation $\sigma_{\ln \mathcal{S}_A^t}$
0.5∼8.0	$0.04(\ln\zeta)^2 - 0.90\ln\zeta + 3.13$	$0.01(\ln\zeta)^3 - 0.03(\ln\zeta)^2 - 0.04\ln\zeta + 1.17$	$-0.04\ln\zeta + 0.32$
10.0	$0.05(\ln\zeta)^2 - 0.90\ln\zeta + 3.08$	$-0.02(\ln\zeta)^4 + 0.09(\ln\zeta)^3 - 0.14(\ln\zeta)^2 + 0.14\ln\zeta + 1.24$	$-0.01(\ln\zeta)^3 + 0.06(\ln\zeta)^2 - 0.09\ln\zeta + 0.22$
15.0	$0.09(\ln\zeta)^2 - 0.95\ln\zeta + 3.05$	$0.01(\ln\zeta)^4 - 0.07(\ln\zeta)^3 + 0.15(\ln\zeta)^2 - 0.03\ln\zeta + 1.40$	$-0.01(\ln\zeta)^3 - 0.01(\ln\zeta)^2 + 0.04\ln\zeta + 0.24$
25.0	$-0.08(\ln\zeta)^2 - 0.27\ln\zeta + 3.15$	$0.04(\ln\zeta)^4 - 0.25(\ln\zeta)^3 + 0.37(\ln\zeta)^2 + 0.06\ln\zeta + 2.63$	$0.01(\ln\zeta)^3 - 0.02(\ln\zeta)^2 - 0.24\ln\zeta + 0.74$
33.0	$-0.19(\ln\zeta)^2 + 3.21$	$0.07(\ln\zeta)^4 - 0.34(\ln\zeta)^3 + 0.17(\ln\zeta)^2 + 0.65\ln\zeta + 2.62$	$0.02(\ln\zeta)^3 - 0.07(\ln\zeta)^2 - 0.13\ln\zeta + 0.58$
50.0∼100.0	0	1	0

Figures 2.6 and 2.7 shows the statistical relationship between GRS and tRS for horizontal and vertical ground motions at B sites, respectively. It is found through regression analyses of the simulation results that site conditions affect the statistical relationship between tRS and GRS in vertical direction only, and the statistical relationship could be categorized by soil sites and rock sites. For a given GRS $\mathcal{S}_{\mathrm{A}}(f,\,\zeta)$, the corresponding tRS $\mathcal{S}_{\mathrm{A}}^{\mathrm{t},p}(f,\,\zeta)$ with any non-exceedance probability (NEP) can be estimated as

$$\ln \mathcal{S}_{\mathrm{A}}^{\mathrm{t},p}(f,\,\zeta) = c_1(f,\,\zeta) + c_2(f,\,\zeta)\cdot \ln \mathcal{S}_{\mathrm{A}}(f,\,\zeta) + \sigma_{\ln \mathcal{S}_{\mathrm{A}}^{\mathrm{t}}}(f,\,\zeta)\cdot \Phi^{-1}(p), \tag{2.2.34}$$

where the coefficients $c_1(f,\,\zeta)$ and $c_2(f,\,\zeta)$, and the standard deviation $\sigma_{\ln \mathcal{S}_{\mathrm{A}}^{\mathrm{t}}}(f,\,\zeta)$ are determined through the regression analyses. Table 2.2 and Tables 2.5 and 2.6 provide the values of the coefficients and the standard deviation for the horizontal and vertical tRS, respectively. Values for other frequencies can be obtained by linear interpolation in the logarithmic scale of frequency.

For the perfect tuning case, two equivalent damping ratios $\zeta_{0,\mathrm{e}}$ and ζ_{e} are used in formulating the amplification factors in equation (2.2.23), which depend on tRS that are employed to calculate the FRS in the tuning cases. In other words, the equivalent damping ratios affect FRS mainly in the tuning cases. There are two unknown parameters $\zeta_{0,\mathrm{e}}$ and ζ_{e} to be determined. However, it is not necessary to know the relationship between these two parameters since only the maximum value $\left|\ddot{u}_{\mathrm{F}}(t)\right|_{\max}$ is to be determined. Hence, one could manipulate and let $\zeta_{0,\mathrm{e}} = \zeta_{\mathrm{e}}$ which yields

$$\left|\ddot{u}_{\mathrm{F}}(t)\right|_{\max} = \frac{1}{2\,\zeta_{\mathrm{e}}}\sqrt{\left[\mathcal{S}_{\mathrm{A}}(\zeta_0)\right]^2 + \left[\mathcal{S}_{\mathrm{A}}(\zeta)\right]^2}. \tag{2.2.35}$$

As $\left|\ddot{u}_{\mathrm{F}}(t)\right|_{\max}$ is actually tRS in this case, for $\zeta_{0,\mathrm{e}} = \zeta_{\mathrm{e}}$, the only parameter ζ_{e} can be easily determined as

$$\zeta_{0,\mathrm{e}} = \zeta_{\mathrm{e}} = \frac{\mathcal{S}_{\mathrm{A}}(\omega_0,\zeta_0)}{\sqrt{2}\cdot \mathcal{S}_{\mathrm{A}}^{\mathrm{t}}(\omega_0,\zeta_0)}. \tag{2.2.36}$$

The validity and the accuracy of using only one equivalent damping ratio have been verified by a large number of simulations. Formulation of FRS with various equipment damping ratio for $\zeta_0 \neq \zeta$ will be discussed in Chapter 3.

Comments on Approximations of FRS

In equation (2.2.29), FRS is equal to tRS for the perfect-tuning case. However, due to the presence of a time variable t in the first convolution term, it is difficult to obtain an analytical expression for equation (2.2.29) in terms of GRS.

Over the past decades, researchers (Yasui *et al.*, 1993; An *et al.*, 2013) have made some approximations to evaluate equation (2.2.25).

The second term on the right-hand side of equation (2.2.25) may be neglected, since its contribution is far less than that of the dominant first term. Therefore, equation (2.2.25) becomes

$$\left|\ddot{u}_{\mathrm{F}}(t)\right|_{\max} \approx \left|\frac{\ddot{u}(t)-\ddot{u}_0(t)}{2(\zeta-\zeta_0)}\right|_{\max}. \tag{2.2.37}$$

A similar formula is derived in (Yasui *et al.*, 1993) through integration by parts

$$2\zeta\,\ddot{u}_{\mathrm{F}}(t) - 2\zeta_0\,\ddot{u}_{\mathrm{F}}(t+\Delta t) \approx \ddot{u}(t) - \ddot{u}_0(t). \tag{2.2.38}$$

It is assumed that the two terms on the left-hand side of equation (2.2.38) have different phase angles, and the maximum value of the left-hand side is obtained by summing the maximum absolute value of each term

$$2(\zeta+\zeta_0)\left|\ddot{u}_{\mathrm{F}}(t)\right|_{\max} = \left|\ddot{u}(t) - \ddot{u}_0(t)\right|_{\max}. \tag{2.2.39}$$

Since the maximum values $\left|\ddot{u}(t)\right|_{\max} = \mathcal{S}_{\mathrm{A}}(\omega,\zeta)$ and $\left|\ddot{u}_0(t)\right|_{\max} = \mathcal{S}_{\mathrm{A}}(\omega_0,\zeta_0)$ do not occur simultaneously, the SRSS combination rule is applied to evaluate the right-hand side of equation (2.2.39). Hence, the maximum response of the oscillator or FRS is given by

$$\mathcal{S}_{\mathrm{F}}(\omega_0,\zeta_0) = \left|\ddot{u}_{\mathrm{F}}(t)\right|_{\max} = \frac{\sqrt{\mathcal{S}_{\mathrm{A}}^2(\omega,\zeta)+\mathcal{S}_{\mathrm{A}}^2(\omega_0,\zeta_0)}}{2(\zeta+\zeta_0)}. \tag{2.2.40}$$

In the perfect-tuning case, $\omega_0=\omega$, $\zeta_0=\zeta$, $\mathcal{S}_{\mathrm{A}}(\omega_0,\zeta_0)=\mathcal{S}_{\mathrm{A}}(\omega,\zeta)$, it reduces to

$$\mathcal{S}_{\mathrm{F}}(\omega_0,\zeta_0) = \frac{1}{2\sqrt{2}\,\zeta_0}\cdot\mathcal{S}_{\mathrm{A}}(\omega_0,\zeta_0). \tag{2.2.41}$$

However, these approximations are reasonable only when the phase differences between the two terms on the left-hand side and right-hand side of equation (2.2.39) are π and $\pi/2$,

respectively. In this case, the maximum values of the two sides can be obtained by the sum of absolute values and the SRSS rules, respectively.

Otherwise, this assumption, which gives a constant amplification factor $1/(2\sqrt{2}\zeta_0)$, can be inaccurate. For example, considering an extreme case for $f_0 = f = 100$ Hz, the structure and equipment are both extremely stiff so that the maximum acceleration of the equipment should be close to the PGA of GRS, i.e., $\mathcal{S}_{\mathrm{F}}(\omega_0, \zeta_0) = \mathcal{S}_{\mathrm{A}}(\omega_0, \zeta_0)$. For a given damping coefficient ζ_0, the amplification factor for the perfect-tuning case should be dependent on the frequency instead of being a constant.

2.2.5 SDOF Oscillator Mounted on Multiple DOF Structure

Since almost all engineering structures have multiple DOF, the formulation for an oscillator mounted on a SDOF structure is extended to an oscillator mounted on a multiple DOF structure in this subsection.

Consider a three-dimensional model of a structure with N nodes, in which each node has six DOF, subjected to tri-directional earthquake excitations, as shown in Figure 2.1. The equation of motion in the matrix form is given by equation (2.1.6).

Applying modal analysis as presented in Section 2.1.3, the $6N$-DOF system (2.1.7) is reduced to a series of $6N$ SDOF systems, in which the modal displacement $q_k^i(t)$ of the kth mode (SDOF system) under the earthquake excitation in direction i is governed by equation (2.1.15). The absolute acceleration $\ddot{u}_{n,j}^i(t)$ of node n in direction j under the earthquake excitation in direction i is given by equation (2.1.16), which is a linear combination of all $6N$ modal responses and the contribution factor of the kth modal response q_k^i is $\varphi_{n,j;k}\Gamma_k^i$.

Maximum Modal Response Contribution

As derived in Section 2.2.3, for a SDOF oscillator mounted on a SDOF structure, the maximum response of the oscillator is given by equation (2.2.18). Therefore, from equations (2.1.15) to (2.1.19), for the maximum absolute acceleration $\mathcal{S}_{n,j}^i(\omega_0, \zeta_0)$ in direction j of an oscillator (with frequency ω_0 and damping ratio ζ_0) mounted at node n under the earthquake excitation in direction i, the maximum contribution by the kth mode, i.e., the maximum absolute acceleration of the oscillator under the excitation $\ddot{u}_{n,j;k}^i$ of equation

(2.1.16), is given by

$$R^i_{n,j;k} = \varphi_{n,j;k}\,\Gamma^i_k \sqrt{\left\{ \mathit{AF}^2_{0,k} \cdot \left[\mathcal{S}^i_{\mathrm{A}}(\omega_0,\zeta_0)\right]^2 + \mathit{AF}^2_k \cdot \left[\mathcal{S}^i_{\mathrm{A}}(\omega_k,\zeta_k)\right]^2 \right\}}, \tag{2.2.42}$$

where $\mathcal{S}^i_{\mathrm{A}}(\omega,\zeta)$ is GRS of the earthquake excitation in direction i, and $\mathit{AF}_{0,k}$ and AF_k are the amplification factors of the kth mode given by

$$\mathit{AF}_{0,k} = \frac{r_k^2}{\sqrt{(1-r_k^2)^2+(2\zeta_{k,\mathrm{e}} r_k)^2}}, \quad \mathit{AF}_k = \frac{1}{\sqrt{(1-r_k^2)^2+(2\zeta_{k,\mathrm{e}} r_k)^2}}, \quad r_k = \frac{\omega_k}{\omega_0}. \tag{2.2.43}$$

Modal Combination: FRS-CQC

Since the maximum responses $R^i_{n,j;k}$ of the oscillator contributed to $\mathcal{S}^i_{n,j}(\omega_0,\zeta_0)$ by each of the k modes ($k=1,2,\ldots,6N$) do no occur simultaneously, they have to be combined following an appropriate combination rule.

Comparing equations (2.1.2) to (2.1.5) with equations (2.1.15) to (2.1.18), and using equation (2.2.9), the contribution from the kth mode to the response of the oscillator (with frequency ω_0 and damping ratio ζ_0) mounted on the multiple DOF structure under the earthquake excitation in direction i is approximately given by

$$Q^i_k(t) = \omega_0^2\omega_k^2 \cdot h_0(t) * h_k(t) * \ddot{u}^i_{\mathrm{g}}(t) = \omega_0^2\omega_k^2 \cdot C_k(t) * \ddot{u}^i_{\mathrm{g}}(t), \tag{2.2.44}$$

where $C_k(t) = h_0(t) * h_k(t)$. The covariance between $Q^i_k(t)$ and $Q^i_\kappa(t)$ of modes k and κ is given by

$$\begin{aligned}
&\mathrm{E}\left[Q^i_k(t)\, Q^i_\kappa(t+\tau) \right] \\
&\quad = \omega_0^4\omega_k^2\omega_\kappa^2 \cdot \mathrm{E}\left[\int_{-\infty}^{\infty} C_k(\tau_1)\, \ddot{u}^i_{\mathrm{g}}(t-\tau_1)\, \mathrm{d}\tau_1 \int_{-\infty}^{\infty} C_\kappa(\tau_2)\, \ddot{u}^i_{\mathrm{g}}(t+\tau-\tau_2)\, \mathrm{d}\tau_2 \right] \\
&\quad = \omega_0^4\omega_k^2\omega_\kappa^2 \int_{-\infty}^{\infty}\int_{-\infty}^{\infty} C_k(\tau_1)\, C_\kappa(\tau_2)\, \mathrm{E}\left[\ddot{u}^i_{\mathrm{g}}(t-\tau_1)\, \ddot{u}^i_{\mathrm{g}}(t+\tau-\tau_2) \right] \mathrm{d}\tau_1 \mathrm{d}\tau_2 \\
&\quad = \omega_0^4\omega_k^2\omega_\kappa^2 \int_{-\infty}^{\infty}\int_{-\infty}^{\infty} C_k(\tau_1)\, C_\kappa(\tau_2)\, R_{\ddot{u}^i_{\mathrm{g}}\ddot{u}^i_{\mathrm{g}}}(\tau+\tau_1-\tau_2)\, \mathrm{d}\tau_1 \mathrm{d}\tau_2.
\end{aligned} \tag{2.2.45}$$

Taking Fourier transform of both sides yields

$$S_{Q^i_k Q^i_\kappa}(\omega) = \int_{-\infty}^{\infty} \mathrm{E}\left[Q^i_k(t)\, Q^i_\kappa(t+\tau) \right] \cdot \mathrm{e}^{-\mathrm{i}\omega\tau}\, \mathrm{d}\tau$$

$$= \omega_0^4 \omega_k^2 \omega_\kappa^2 \int_{-\infty}^{\infty}\int_{-\infty}^{\infty}\int_{-\infty}^{\infty} C_k(\tau_1)\, C_\kappa(\tau_2)\, R_{\ddot{u}_g^i \ddot{u}_g^i}(\tau+\tau_1-\tau_2)\cdot \mathrm{e}^{-\mathrm{i}\omega\tau}\,\mathrm{d}\tau_1\mathrm{d}\tau_2\mathrm{d}\tau. \tag{2.2.46}$$

Setting $\tau_3 = \tau+\tau_1-\tau_2$, equation (2.2.44) can be written as

$$\begin{aligned} S_{Q_k^i Q_\kappa^i}(\omega) &= \omega_0^4 \omega_k^2 \omega_\kappa^2 \int_{-\infty}^{\infty} C_k(\tau_1)\,\mathrm{e}^{\mathrm{i}\omega\tau_1}\mathrm{d}\tau_1 \int_{-\infty}^{\infty} C_\kappa(\tau_2)\,\mathrm{e}^{-\mathrm{i}\omega\tau_2}\mathrm{d}\tau_2 \int_{-\infty}^{\infty} R_{\ddot{u}_g^i \ddot{u}_g^i}(\tau_3)\,\mathrm{e}^{-\mathrm{i}\omega\tau_3}\mathrm{d}\tau \\ &= \omega_k^2 \omega_\kappa^2 \cdot \mathscr{C}_k^*(\omega)\cdot \mathscr{C}_\kappa(\omega)\cdot S_{\ddot{u}_g^i \ddot{u}_g^i}(\omega), \end{aligned} \tag{2.2.47}$$

where $\mathscr{C}_k(\omega) = H_0(\omega) H_k(\omega)$ is the Fourier transform of the convolution $C_k(t) = h_0(t) * h_k(t)$, $\mathscr{C}_k^*(\omega)$ is the complex conjugate of $\mathscr{C}_k(\omega)$, and $S_{\ddot{u}_g^i \ddot{u}_g^i}(\omega)$ is the power spectral density of the earthquake excitation $\ddot{u}_g^i(t)$.

Taking the inverse Fourier transform of equation (2.2.47) yields

$$\begin{aligned} \mathrm{E}\big[Q_k^i(t)\, Q_\kappa^i(t+\tau)\big] &= \frac{1}{2\pi}\int_{-\infty}^{\infty} S_{Q_k^i Q_\kappa^i}(\omega)\,\mathrm{e}^{\mathrm{i}\omega\tau}\,\mathrm{d}\omega \\ &= \frac{\omega_0^4 \omega_k^2 \omega_\kappa^2}{2\pi}\int_{-\infty}^{\infty} \mathscr{C}_k^*(\omega)\cdot \mathscr{C}_\kappa(\omega)\cdot S_{\ddot{u}_g^i \ddot{u}_g^i}(\omega)\,\mathrm{e}^{\mathrm{i}\omega\tau}\,\mathrm{d}\omega. \end{aligned} \tag{2.2.48}$$

Setting $\tau = 0$ results in

$$\begin{aligned} \mathrm{E}\big[Q_k^i(t)\, Q_\kappa^i(t)\big] &= \frac{\omega_0^4 \omega_k^2 \omega_\kappa^2}{2\pi}\int_{-\infty}^{\infty} \mathscr{C}_k^*(\omega)\cdot \mathscr{C}_\kappa(\omega)\cdot S_{\ddot{u}_g^i \ddot{u}_g^i}(\omega)\,\mathrm{d}\omega \\ &= \frac{\omega_0^4 \omega_k^2 \omega_\kappa^2}{2\pi}\int_{-\infty}^{\infty} H_0^*(\omega)\, H_k^*(\omega)\cdot H_0(\omega)\, H_\kappa(\omega)\cdot S_{\ddot{u}_g^i \ddot{u}_g^i}(\omega)\,\mathrm{d}\omega. \end{aligned} \tag{2.2.49}$$

Since ground motions can be generally modelled as wide-band noises, it is reasonable to assume the seismic input $\ddot{u}_g^i(t)$ as a white noise by letting the power spectral density $S_{\ddot{u}_g^i \ddot{u}_g^i}(\omega) = S^i$. Therefore, equation (2.2.49) can be written as

$$\mathrm{E}\big[Q_k^i(t)\, Q_\kappa^i(t)\big] = \frac{\omega_0^4 \omega_k^2 \omega_\kappa^2}{2\pi}\cdot S^i \cdot I_{k\kappa}, \tag{2.2.50}$$

where

$$I_{k\kappa} = \int_{-\infty}^{\infty} H_0^*(\omega)\, H_k^*(\omega)\cdot H_0(\omega)\, H_\kappa(\omega)\,\mathrm{d}\omega$$

$$= \int_{-\infty}^{\infty} \frac{1}{(\omega_0^2-\omega^2)^2+(2\zeta_0\omega_0\omega)^2} \cdot \frac{1}{(\omega_k^2-\omega^2)-\mathrm{i}2\zeta_k\omega_k\omega} \cdot \frac{1}{(\omega_\kappa^2-\omega^2)+\mathrm{i}2\zeta_\kappa\omega_\kappa\omega}\,\mathrm{d}\omega$$

$$= \int_{-\infty}^{\infty} \frac{\left[(\omega_k^2-\omega^2)+\mathrm{i}2\zeta_k\omega_k\omega\right]\cdot\left[(\omega_\kappa^2-\omega^2)-\mathrm{i}2\zeta_\kappa\omega_\kappa\omega\right]}{\Delta_{k\kappa}}\,\mathrm{d}\omega$$

$$= \mathcal{R}e(I_{k\kappa}) + \mathrm{i}\,\mathcal{I}m(I_{k\kappa}) \tag{2.2.51}$$

where

$$\Delta_{k\kappa} = \left[(\omega_0^2-\omega^2)^2+(2\zeta_0\omega_0\omega)^2\right]\cdot\left[(\omega_k^2-\omega^2)^2+(2\zeta_k\omega_k\omega)^2\right]\cdot\left[(\omega_\kappa^2-\omega^2)^2+(2\zeta_\kappa\omega_\kappa\omega)^2\right],$$

$\mathcal{R}e(I_{k\kappa})$ and $\mathcal{I}m(I_{k\kappa})$ are the real and imaginary parts of $I_{k\kappa}$, respectively, given by

$$\mathcal{R}e(I_{k\kappa}) = \int_{-\infty}^{\infty} \frac{(\omega_k^2-\omega^2)\cdot(\omega_\kappa^2-\omega^2) + (2\zeta_k\omega_k\omega)\cdot(2\zeta_\kappa\omega_\kappa\omega)}{\Delta_{k\kappa}}\mathrm{d}\omega,$$

$$\mathcal{I}m(I_{k\kappa}) = \int_{-\infty}^{\infty} \frac{2\zeta_k\omega_k\omega\cdot(\omega_\kappa^2-\omega^2) - 2\zeta_\kappa\omega_\kappa\omega\cdot(\omega_k^2-\omega^2)}{\Delta_{k\kappa}}\mathrm{d}\omega,$$

which can be evaluated by the method of residue to yield

$$\mathcal{R}e(I_{k\kappa}) = \frac{\pi\cdot\alpha_{k\kappa}}{2\zeta_0\omega_0^3\cdot\omega_0^4}, \qquad \mathcal{I}m(I_{k\kappa}) = 0, \tag{2.2.52}$$

in which

$$\alpha_{k\kappa} = \prod_{l=1}^{3} D_{k\kappa,l}^{-1}\cdot\sum_{l=0}^{4} C_{k\kappa,l}\,\zeta_0^l, \tag{2.2.53}$$

$C_{k\kappa,l}$ and $D_{k\kappa,l}$ are constants in terms of ζ_0, ζ_k, ζ_κ, $r_k=\omega_k/\omega_0$, and $r_\kappa=\omega_\kappa/\omega_0$, given by

$$D_{k\kappa,1} = 1 - 2r_\kappa^2 + r_\kappa^4 + 4\zeta_0\zeta_\kappa r_\kappa + 4\zeta_0\zeta_\kappa r_\kappa^3 + 4\zeta_0^2 r_\kappa^2 + 4\zeta_\kappa^2 r_\kappa^2,$$

$$D_{k\kappa,2} = 1 - 2r_k^2 + r_k^4 + 4\zeta_0\zeta_k r_k + 4\zeta_0\zeta_k r_k^3 + 4\zeta_0^2 r_k^2 + 4\zeta_k^2 r_k^2,$$

$$D_{k\kappa,3} = (r_k^2-r_\kappa^2)^2 + 4\zeta_k\zeta_\kappa r_k r_\kappa(r_k^2+r_\kappa^2) + 4r_k^2 r_\kappa^2(\zeta_k^2+\zeta_\kappa^2),$$

$$C_{k\kappa,0} = (1 - r_k^2 - r_\kappa^2 + r_k^2 r_\kappa^2 + 4\zeta_k\zeta_\kappa r_k r_\kappa)\cdot D_{k\kappa,3},$$

$$C_{k\kappa,1}/4 = 2\zeta_k r_k + 2\zeta_\kappa r_\kappa + 8\zeta_k\zeta_\kappa r_k r_\kappa(\zeta_k r_k+\zeta_\kappa r_\kappa) - 4(\zeta_k r_k^3+\zeta_\kappa r_\kappa^3) + 8\zeta_k^3 r_k^3 + 8\zeta_\kappa^3 r_\kappa^3$$
$$- 2r_k r_\kappa(\zeta_k r_\kappa^3+\zeta_\kappa r_k^3) + 8\zeta_k\zeta_\kappa r_k r_\kappa(\zeta_k r_k^3+\zeta_\kappa r_\kappa^3) + 4r_k^2 r_\kappa^2(\zeta_k r_k+\zeta_\kappa r_\kappa)$$

$$
\begin{aligned}
&- 8r_k^2r_\kappa^2(\zeta_k^3r_k+\zeta_\kappa^3r_\kappa) - 8\zeta_k\zeta_\kappa r_k^2r_\kappa^2(\zeta_kr_\kappa+\zeta_\kappa r_k) + 32\zeta_k^2\zeta_\kappa^2r_k^2r_\kappa^2(\zeta_kr_k+\zeta_\kappa r_\kappa)\\
&+ r_kr_\kappa(\zeta_kr_\kappa^5+\zeta_\kappa r_k^5) + r_k^2r_\kappa^2(\zeta_kr_k^3+\zeta_\kappa r_\kappa^3) + 4\zeta_k\zeta_\kappa r_k^2r_\kappa^2(\zeta_kr_\kappa^3+\zeta_\kappa r_k^3)\\
&- 2r_k^3r_\kappa^3(\zeta_kr_\kappa+\zeta_\kappa r_k) + 4r_k^3r_\kappa^3(\zeta_k^3r_\kappa+\zeta_\kappa^3r_k) + 8\zeta_k\zeta_\kappa r_k^3r_\kappa^3(\zeta_kr_k+\zeta_\kappa r_\kappa),
\end{aligned}
$$

$$
\begin{aligned}
C_{k\kappa,2}/4 &= 8\zeta_k^2r_k^2 + 8\zeta_\kappa^2r_\kappa^2 + 16\zeta_k\zeta_\kappa r_kr_\kappa + 64\zeta_k^2\zeta_\kappa^2r_k^2r_\kappa^2 - 4\zeta_k\zeta_\kappa r_kr_\kappa(r_k^2+r_\kappa^2)\\
&+ 32\zeta_k\zeta_\kappa r_kr_\kappa(\zeta_k^2r_k^2+\zeta_\kappa^2r_\kappa^2) + 6r_k^2r_\kappa^2 - 12r_k^2r_\kappa^2(\zeta_k^2+\zeta_\kappa^2) - 3(r_k^4+r_\kappa^4)\\
&+ 8\zeta_k\zeta_\kappa r_kr_\kappa(r_k^4+r_\kappa^4) - r_k^2r_\kappa^2(r_k^2+r_\kappa^2) + 8\zeta_k^2r_k^4 + 8\zeta_\kappa^2r_\kappa^4 + 4r_k^2r_\kappa^2(\zeta_k^2+\zeta_\kappa^2)(r_k^2+r_\kappa^2)\\
&+ 16\zeta_k^2\zeta_\kappa^2r_k^2r_\kappa^2(r_k^2+r_\kappa^2) + 16\zeta_k\zeta_\kappa r_k^3r_\kappa^3(\zeta_k^2+\zeta_\kappa^2) + r_k^6 + r_\kappa^6,
\end{aligned}
$$

$$
\begin{aligned}
C_{k\kappa,3}/16 &= 8\zeta_k\zeta_\kappa r_kr_\kappa(\zeta_kr_k+\zeta_\kappa r_\kappa) + 2\zeta_kr_k^3 + 2\zeta_\kappa r_\kappa^3 + r_kr_\kappa(\zeta_kr_\kappa^3+\zeta_\kappa r_k^3)\\
&+ 4\zeta_k\zeta_\kappa r_kr_\kappa(\zeta_kr_k^3+\zeta_\kappa r_\kappa^3) - 2r_k^2r_\kappa^2(\zeta_kr_k+\zeta_\kappa r_\kappa) + 4r_k^2r_\kappa^2(\zeta_k^3r_k+\zeta_\kappa^3r_\kappa)\\
&+ 8\zeta_k\zeta_\kappa r_k^2r_\kappa^2(\zeta_kr_\kappa+\zeta_\kappa r_k) + \zeta_kr_k^5 + \zeta_\kappa r_\kappa^5,
\end{aligned}
$$

$$C_{k\kappa,4}/16 = D_{k\kappa,3}.$$

Therefore, equation (2.2.50) can be expressed as

$$\mathrm{E}\big[Q_k^i(t)\,Q_\kappa^i(t)\big] = \frac{\omega_0^4\omega_k^2\omega_\kappa^2}{2\pi}\cdot S^i\cdot\frac{\pi\cdot\alpha_{k\kappa}}{2\zeta_0\omega_0^3\cdot\omega_0^4} = \frac{\omega_0 S^i}{4\zeta_0}\cdot\alpha_{k\kappa}\cdot r_k^2r_\kappa^2. \tag{2.2.54}$$

When $\kappa = k$, equation (2.2.54) becomes

$$\mathrm{E}\big[\{Q_k^i(t)\}^2\big] = \frac{\omega_0 S^i}{4\zeta_0}\cdot\beta_k\cdot r_k^4, \tag{2.2.55}$$

where

$$\beta_k = \frac{\zeta_0+4\zeta_0^2\zeta_kr_k+4\zeta_0\zeta_k^2r_k^2+\zeta_kr_k^3}{\zeta_kr_k^3\big(1-2r_k^2+r_k^4+4\zeta_0\zeta_kr_k+4\zeta_k^2r_k^2+4\zeta_0^2r_k^2+4\zeta_0\zeta_kr_k^3\big)}. \tag{2.2.56}$$

Hence, the correlation coefficient between the contributions to the response of an oscillation mounted on the structure under an earthquake excitation in direction i by kth and κth modes is obtained as

$$\rho_{k\kappa}^i = \frac{\mathrm{E}\big[Q_k^i(t)\,Q_\kappa^i(t)\big]}{\sqrt{\mathrm{E}\big[\{Q_k^i(t)\}^2\big]\cdot\mathrm{E}\big[\{Q_\kappa^i(t)\}^2\big]}} = \frac{\dfrac{\omega_0 S^i}{4\zeta_0}\cdot\alpha_{k\kappa}\cdot r_k^2r_\kappa^2}{\sqrt{\dfrac{\omega_0 S^i}{4\zeta_0}\cdot\beta_k\cdot r_k^4\times\dfrac{\omega_0 S^i}{4\zeta_0}\cdot\beta_\kappa\cdot r_\kappa^4}} = \frac{\alpha_{k\kappa}}{\sqrt{\beta_k\beta_\kappa}},$$

which is independent of the direction i of the earthquake excitation and can be written as

$$\rho_{k\kappa} = \frac{\alpha_{k\kappa}}{\sqrt{\beta_k \beta_\kappa}}. \tag{2.2.57}$$

Combining the maximum absolute acceleration $R^i_{n,j;k}$ of the oscillator contributed by mode k, given by equation (2.2.42), for all $6N$ modes gives the FRS of node n in direction j under the earthquake excitation in direction i defined by equation (2.1.19):

$$\mathcal{S}^i_{n,j}(\omega_0, \zeta_0) = \left|\ddot{u}^i_{\mathrm{F},n,j}(t)\right|_{\max} = \sqrt{\sum_{k=0}^{6N}\sum_{\kappa=0}^{6N} \rho_{k\kappa} R^i_k R^i_\kappa}\,. \tag{2.2.58}$$

FRS $\mathcal{S}_{n,j}(\omega_0, \zeta_0)$ of the nth node in direction j under tri-directional earthquake excitations is then obtained from FRS $\mathcal{S}^i_{n,j}(\omega_0, \zeta_0)$, $i = 1, 2, 3$, using the SRSS combination rule given by equation (2.1.20).

Comments on Modal Combination

Since the modal combination in equation (2.2.58) is a complete quadrature for maximum responses of the oscillator contributed by all $6N$ modes, it is therefore called FRS-CQC to differentiate it from CQC (Complete Quadratic Combination), which combines maximum responses of the $6N$ modes. To visualize the correlation coefficient of FRS-CQC, for given damping ratios ζ_0, ζ_k, and ζ_κ, the correlation coefficient $\rho_{k\kappa}$ is a function of frequency ratios r_k and r_κ and can be plotted as a surface. Figure 2.8 shows the plot of $\rho_{k\kappa}$ with $\zeta_0 = \zeta_k = \zeta_\kappa = 5\%$, r_k and r_κ ranging from 0 to 2.50. Some remarkable features of FRS-CQC can be observed:

- Similar to the correlation curve of the conventional CQC which is symmetric about $\omega_k = \omega_\kappa$, the correlation surface of FRS-CQC is symmetric about the plane $r_k = r_\kappa$ ($\omega_k = \omega_\kappa$). The correlation coefficient $\rho_{k\kappa} = 1$ for $r_k = r_\kappa$, meaning that responses of closely-spaced modes are fully correlated.
- Different from the correlation coefficient in conventional CQC, which is uniformly positive, the correlation coefficient of FRS-CQC is negative inside the areas approximately for $r_k < 1 < r_\kappa$ and $r_\kappa < 1 < r_k$ as shown in Figure 2.9. In other words, negative correlation generally occurs when the equipment frequency is located between the

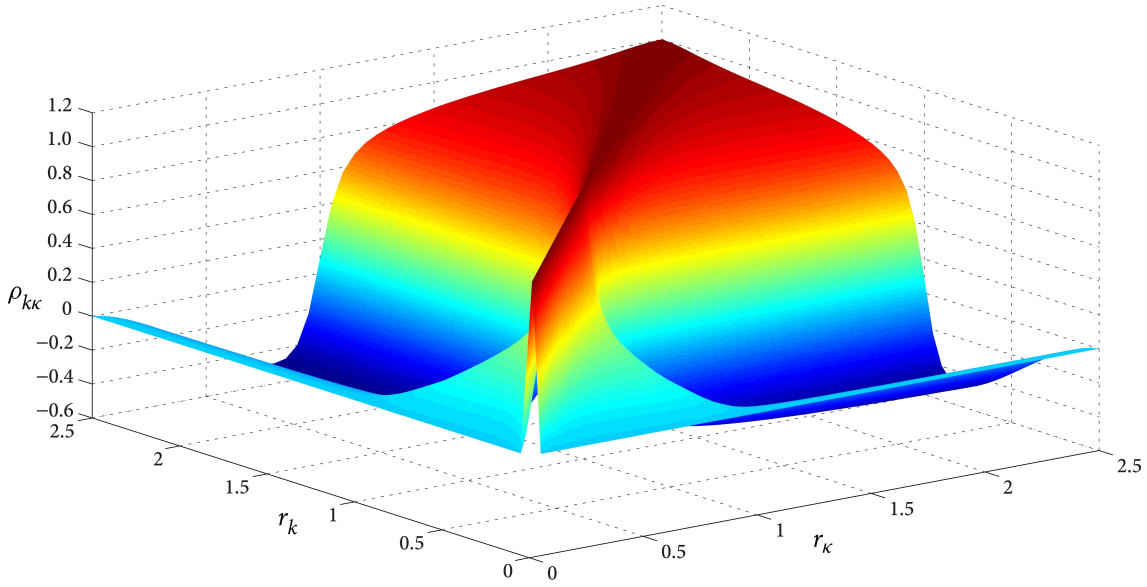

Figure 2.8 3D-view of FRS-CQC correlation coefficients with $0 \leqslant r \leqslant 2.5$

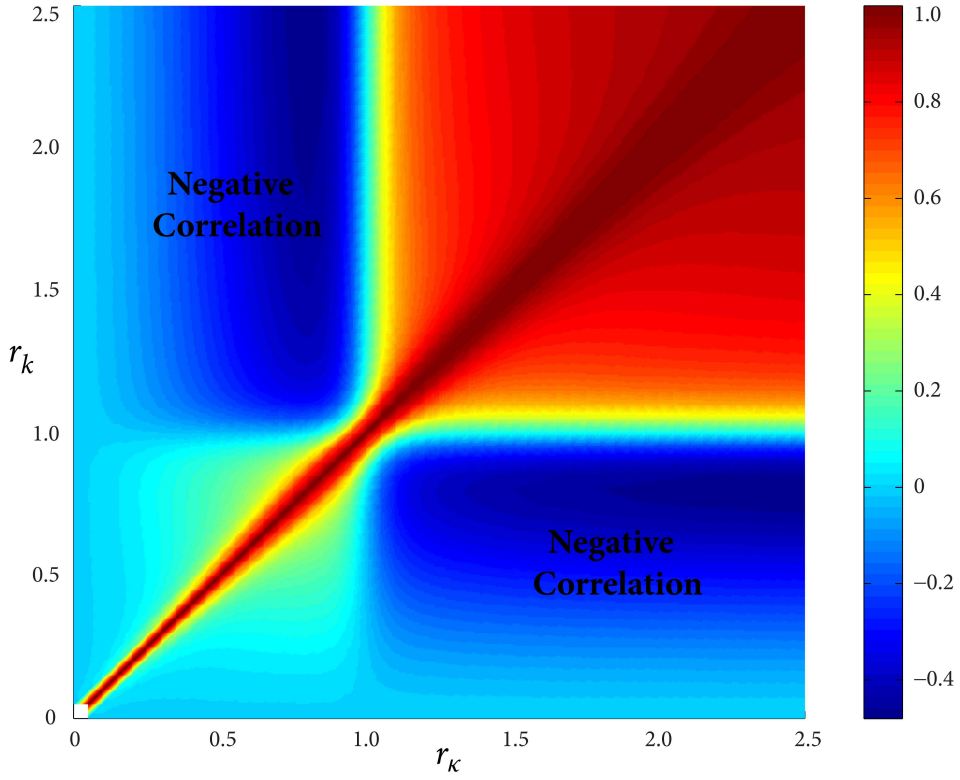

Figure 2.9 2D-view of FRS-CQC correlation coefficients with $0 \leqslant r \leqslant 2.5$

structural frequencies of two not-closely-spaced modes, which usually results in a valley between the FRS peaks.

- For the extreme case when the equipment frequency is significantly higher than the structural frequency with $r_k \to 0$ and $r_\kappa \to 0$, FRS-CQC is reduced to the conventional CQC. Figure 2.10 shows the correlation surface of FRC-CQC for r_k and r_κ ranging from 0 to 0.02, which is an enlarged view of the tiny portion of the surface close to the origin in Figure 2.8. The intersection between the surface and a plane defined by $r_k = a$ or $r_\kappa = a$ (a is an arbitrary positive value that approaches zero) can provide a correlation curve of the conventional CQC. For instance, the correlation surface is cut by a plane $r_k = 0.01$ as shown in Figure 2.11. It can be observed that the correlation coefficient $\rho_{k\kappa} = 1$ at $r_\kappa = 0.01$, when two structural frequencies are coincident $\omega_k = \omega_\kappa$. Furthermore, the correlation curve is positive and symmetric about $r_k = r_\kappa = 1$.
- To determine responses of multiple DOF structures under earthquake excitations using a response spectrum method, the correlation coefficient between two modal responses is determined for CQC (Kiureghian, 1980; Der Kiureghian, 1981), i.e.,

$$\rho_{k\kappa}^{\text{CQC}} = \frac{\mathrm{E}\left[q_k(t)\, q_\kappa(t)\right]}{\sqrt{\mathrm{E}\left[\left\{q_k(t)\right\}^2\right] \cdot \mathrm{E}\left[\left\{q_\kappa(t)\right\}^2\right]}}, \tag{2.2.59}$$

where $q_k(t) = h_k(\omega) * \ddot{u}_{\mathrm{g}}(t)$ is the response of the kth mode.

- To determine FRS, the response of an oscillator (with frequency ω_0 and damping ratio ζ_0) mounted on the multiple DOF structure is required. The correlation coefficient between the responses of the oscillator contributed by two modal responses is determined for FRS-CQC, i.e.,

$$\rho_{k\kappa}^{\text{FRS-CQC}} = \frac{\mathrm{E}\left[Q_k(t)\, Q_\kappa(t)\right]}{\sqrt{\mathrm{E}\left[\left\{Q_k(t)\right\}^2\right] \cdot \mathrm{E}\left[\left\{Q_\kappa(t)\right\}^2\right]}}, \tag{2.2.60}$$

where $Q_k(t) = \omega_0^2 \omega_k^2 h_0(t) * h_k(t) * \ddot{u}_{\mathrm{g}}(t)$ is the response of the oscillator contributed by the kth mode.

- When $\omega_0 \to \infty$, i.e., when the oscillator is very rigid, $Q_k(t) \to q_k(t)$. Therefore, $\rho_{k\kappa}^{\text{FRS-CQC}}$ includes

- the correlation between $Q_k(t)$ and $Q_\kappa(t)$,
- the correlation between $q_k(t)$ and $q_\kappa(t)$,
- the correlations between $Q_k(t)$ and $q_\kappa(t)$ and between $Q_\kappa(t)$ and $q_k(t)$.

☙ It is important to note that CQC was derived for responses of multiple DOF (Kiureghian, 1980; Der Kiureghian, 1981), considering only the correlation between two modal responses $q_k(t)$ and $q_\kappa(t)$. If CQC (with $\rho_{k\kappa}^{\mathrm{CQC}}$) or SRSS is used in modal combination to generate FRS, large errors may occur, especially for structures with closely-spaced modes.

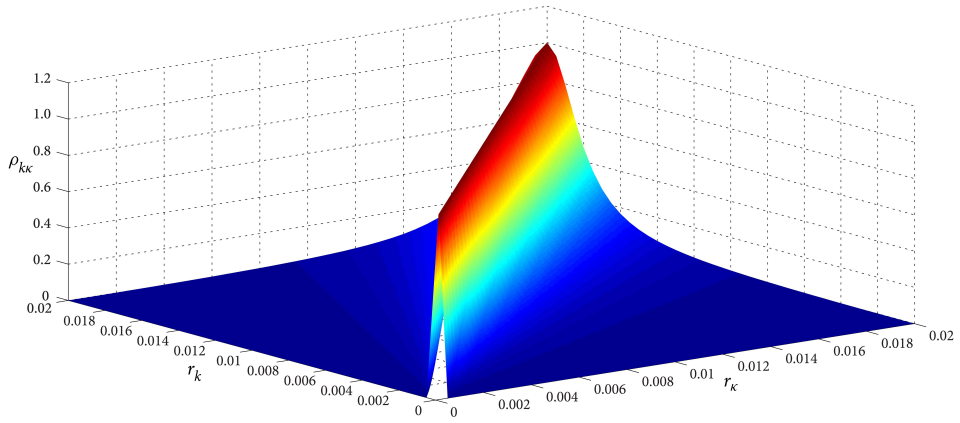

Figure 2.10 3D-view of FRS-CQC correlation coefficients with $0 \leqslant r \leqslant 0.02$

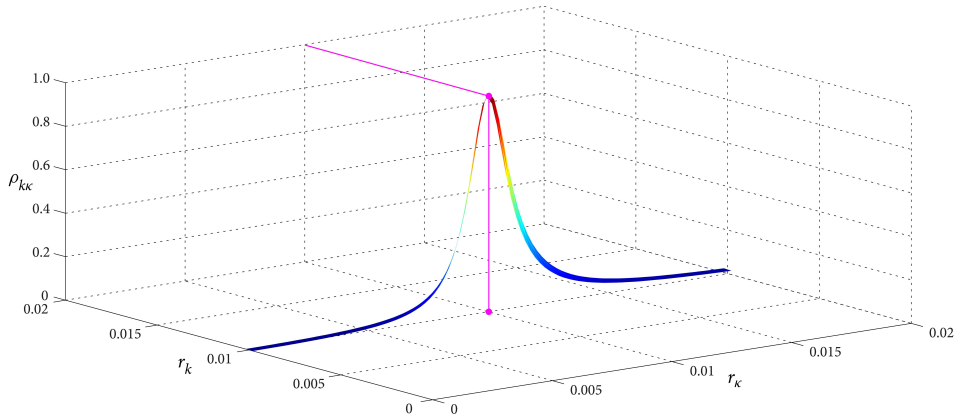

Figure 2.11 3D-view of FRS-CQC cut by $r_k = 0.01$

Generation of floor response spectra

Therefore, for a SDOF oscillator mounted on a multiple DOF structure, the procedure of the proposed direct spectra-to-spectra method of generating FRS is illustrated in Figure 2.12. A modal analysis is performed first to obtain the modal information of the structure. The amplification factors and FRS-CQC coefficients are determined from the modal information along with tRS that corresponds to the prescribed GRS. Multiplying the amplification factors to the target GRS results in the modal responses, which are sequently combined by FRS-CQC rule to generate FRS.

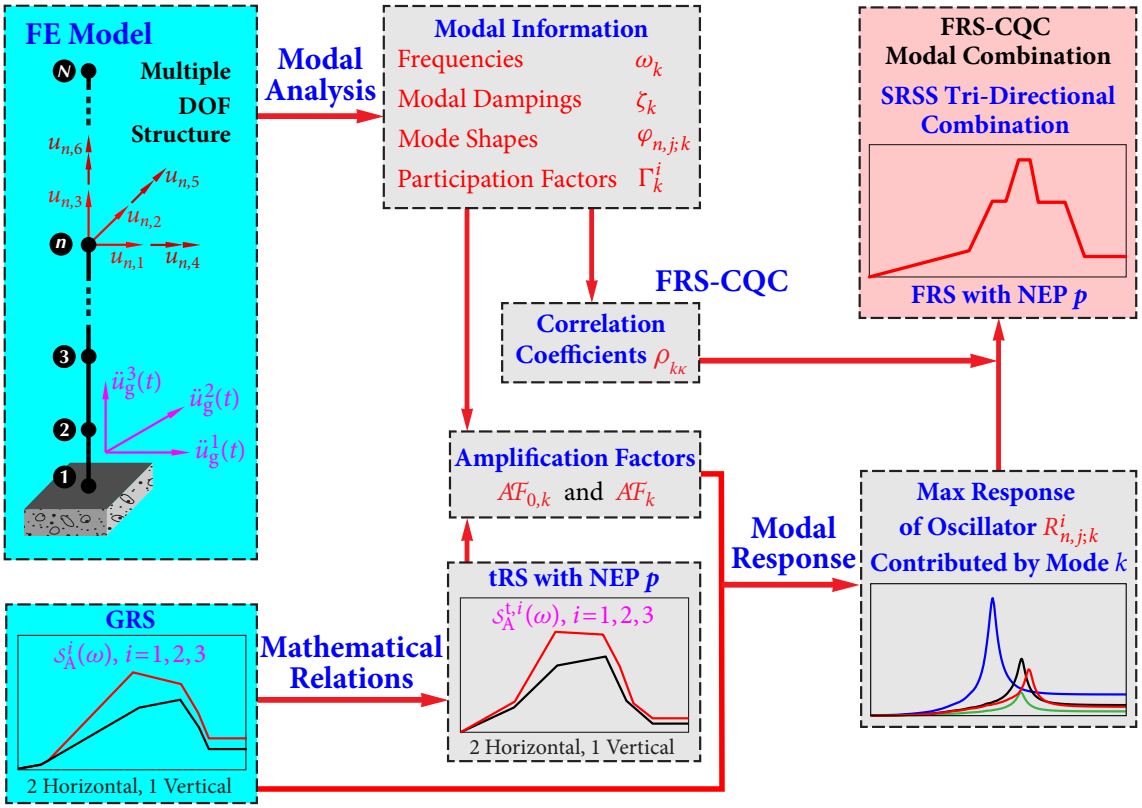

Figure 2.12 Procedure of proposed direct method for generating FRS

2.3 Numerical Examples

The accuracy and efficiency of the direct spectra-to-spectra method developed in this chapter for generating FRS is demonstrated through numerical examples by comparing results from the proposed direct method with those from time history analyses.

The primary source of variability in time history analysis stems from the inherent uncertainties and randomness of the time histories, reflected in the rugged spectral shapes of FRS. Although there are large variations in individual FRS as shown later in this section, the statistical results of FRS (such as mean FRS or FRS with 84.1% non-exceedance probability (NEP)) from a number of time histories converge to smooth spectra as the number of time histories increases.

In this study, the statistical results of FRS of a large number of time history analyses are considered as the "exact" FRS and used as benchmark for verifying the accuracy of the direct method.

2.3.1 Model Information

A service building of a nuclear power plant is selected as the primary structure. A three-dimensional finite element model of the building, as shown in Figure 2.13, is established using the commercial finite element analysis software STARDYNE.

The superstructure of the building consists of steel frames and concrete floor slabs, and the basement is constructed using concrete. The elevation of each floor and the dimensions of the building are shown in Figure 2.13. Some information of the finite element model is listed in Table 2.7.

A modal analysis is performed to obtain modal frequencies, modal participation factors, and modal shapes of the model. Modal information of 145 modes, in which the modal frequencies are less than 33 Hz, is extracted.

FRS at two nodes located on the second and third floors of the building are considered. Node 1 is on an edge of the second floor and Node 2 is on the third floor, as shown in Figure 2.13.

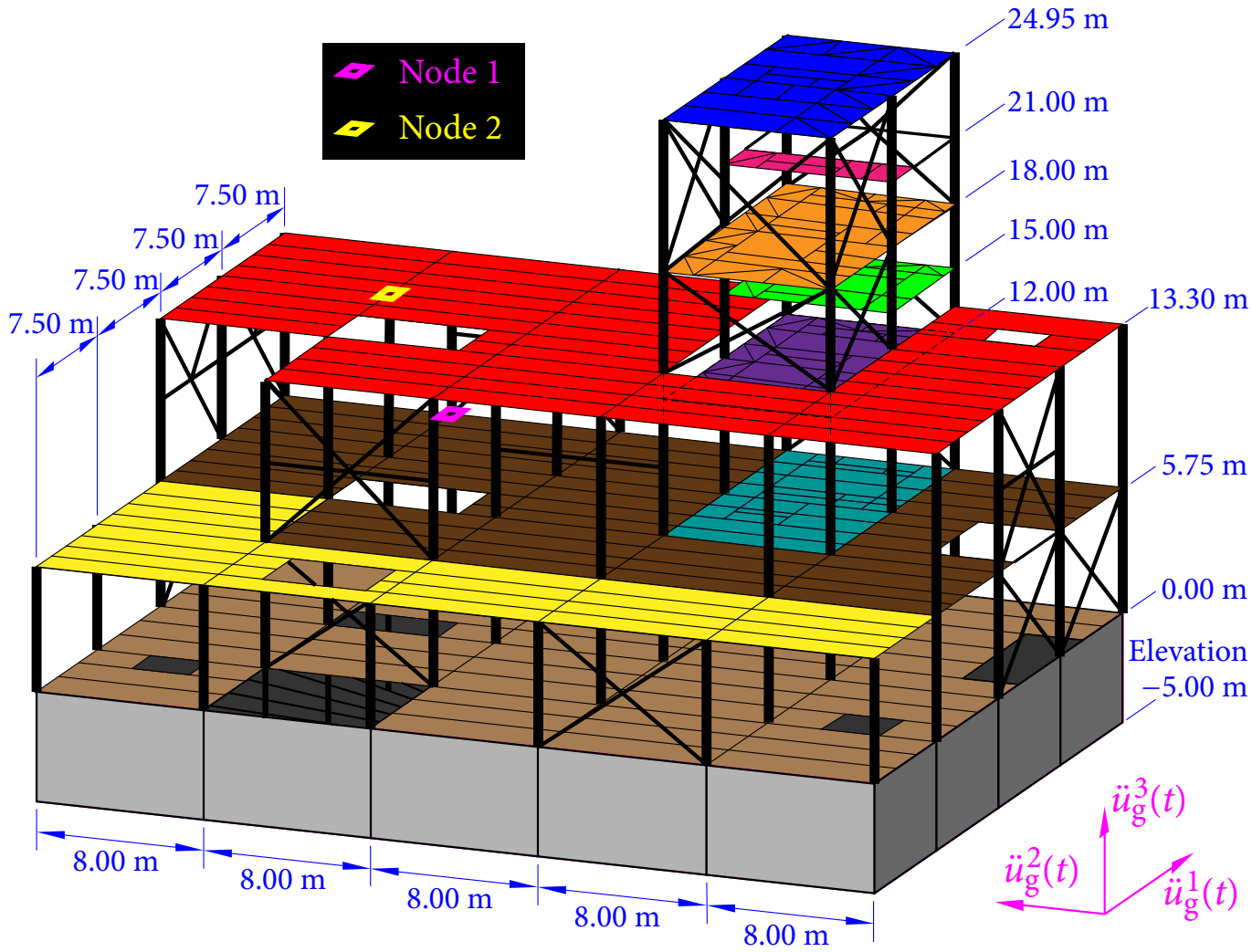

Figure 2.13 Primary and secondary systems in a nuclear power plant

Table 2.7 Information of finite element model

	Node	Lumped Mass	Beam		Shell	
			Element	Section	Element	Section
Number	1351	120	1740	31	830	8

Table 2.8 Modal information at Node 1

Mode	Frequency (Hz)	Participation factor	Modal shape	Contribution factor
2	2.676	−7.413	−0.05082	0.38
20	5.838	−2.945	−0.02603	0.08
21	5.918	2.943	0.06409	0.19
31	7.212	−8.883	−0.01942	0.17
103	22.95	−100.8	0.00088	−0.09
106	23.96	−337.3	0.00024	−0.08

Table 2.9 Modal information at Node 2

Mode	Frequency (Hz)	Participation factor	Modal shape	Contribution factor
2	2.676	−7.413	−0.14630	1.08
20	5.838	−2.945	−0.01904	0.06
21	5.918	2.943	0.04151	0.12
31	7.212	−8.883	0.03847	−0.34
105	23.34	−96.07	−0.00045	0.04
106	23.96	−337.3	−0.00011	0.04
107	23.98	−50.65	−0.00092	0.05

Modal information of the significant modes at these two typical nodes is listed in Tables 2.8 and 2.9. The participation factors and modal shapes in these two tables are for direction 2 shown in Figure 2.13. The contribution factor is the product of the participation factor and the modal shape, quantifying the contribution of the corresponding mode in the response of the node; all other modes that are not listed in Tables 2.8 and 2.9 have absolute values of the contribution factors less than 0.04. The summation of the 145 mode contribution factors at each node is close to 1. It is seen that there are closely-spaced modes with considerable contributions to the responses at both Nodes 1 and 2. For example, modes 20 and 21 are closely-spaced for Node 1; modes 20 and 21, modes 105 to 107 are closely-spaced for Node 2.

2.3.2 Input GRS

Two types of response spectra, GRS of USNRC R.G. 1.60 (1973) and Standard UHS for CENA (2007), are selected as input GRS in the numerical examples. These GRS are piecewise straight lines in log-log scale as shown in Figure 2.14. However, in nuclear industry practice, they are often plotted in the log-linear scale for better visualization in the range of engineering interest. In the log-linear scale, the spectra become piecewise curves as shown by dashed lines in Figure 2.15. For the ease of application, the critical (corner) points are commonly connected by straight lines as shown by the solid lines in Figure 2.15 for analysis and design. It can be seen that the GRS become smoother and conservative after the adjustment. Therefore, the spectral shapes consisting of piecewise straight lines in log-linear scale will be adopted in this study.

GRS of USNRC R.G. 1.60

The 5% horizontal and vertical design spectra in USNRC R.G. 1.60 (1973) are taken as GRS in this example. The horizontal GRS are anchored at $0.3g$ PGA, and the vertical PGA is taken as 2/3 of the horizontal PGA. To perform time history analyses, 30 sets of tri-directional time histories spectrum-compatible with GRS (two horizontal GRS and one vertical GRS) are generated following the Approach 2 of USNRC SRP 3.7.1, as shown in Figure 2.16.

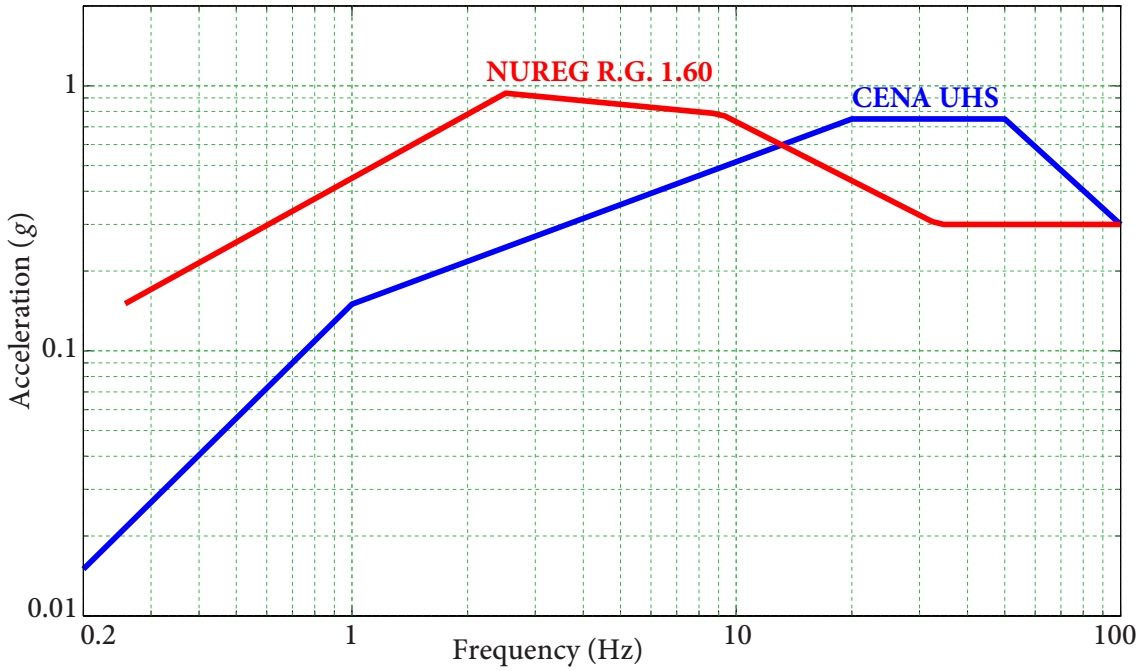

Figure 2.14 Input GRS in log-log scale

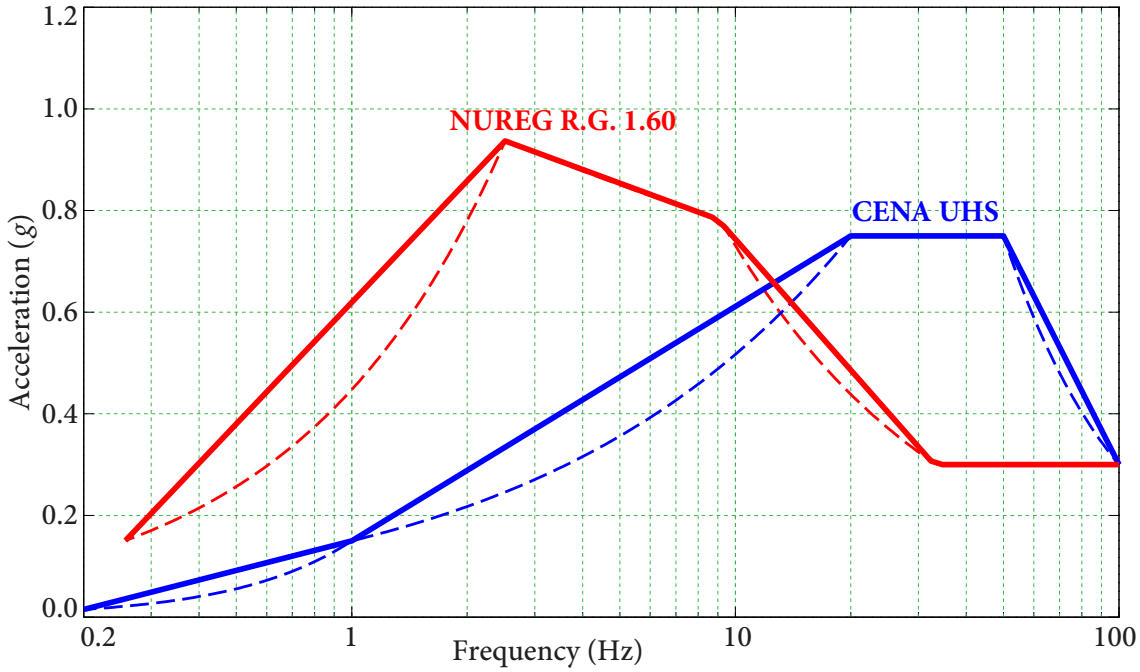

Figure 2.15 Input GRS in log-linear scale

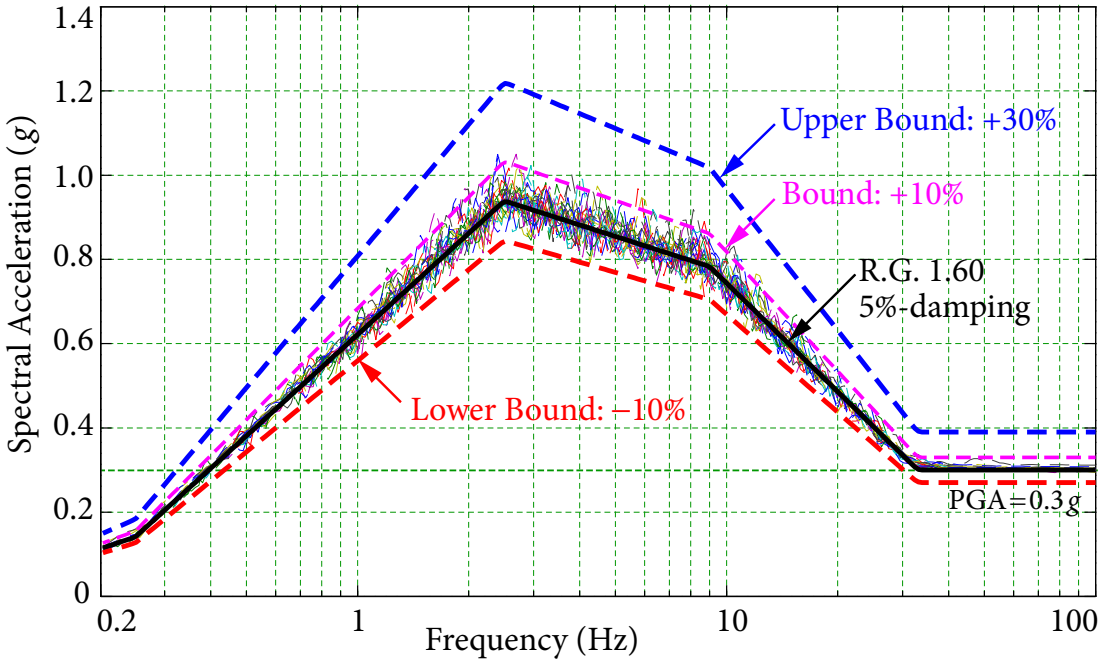

Figure 2.16 Ground response spectrum

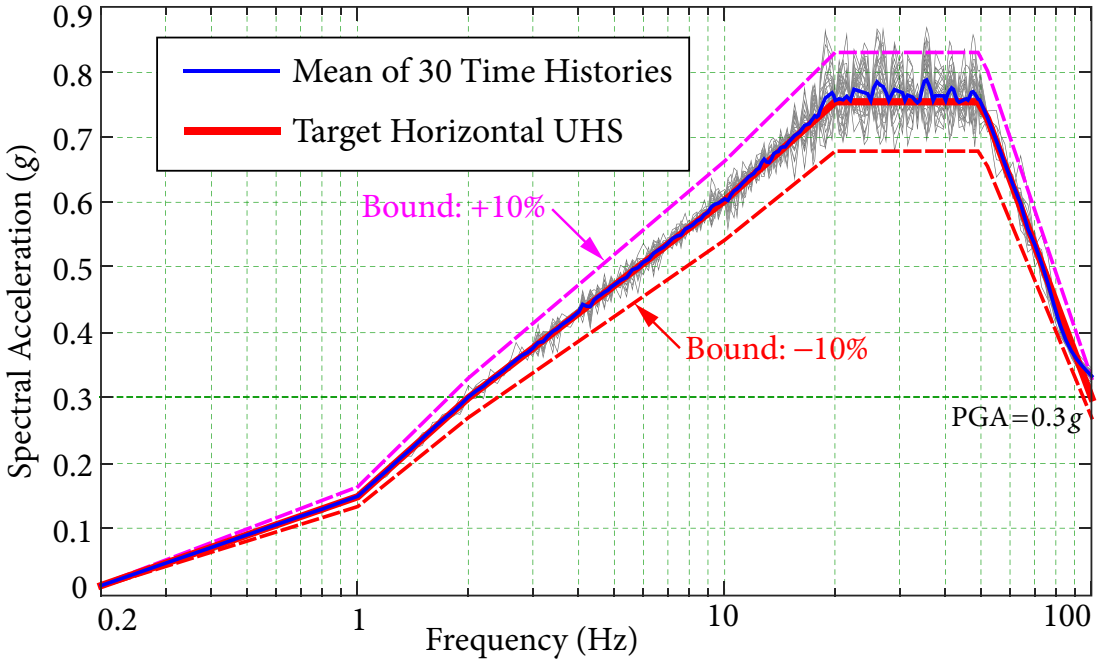

Figure 2.17 Response spectra of compatible time histories

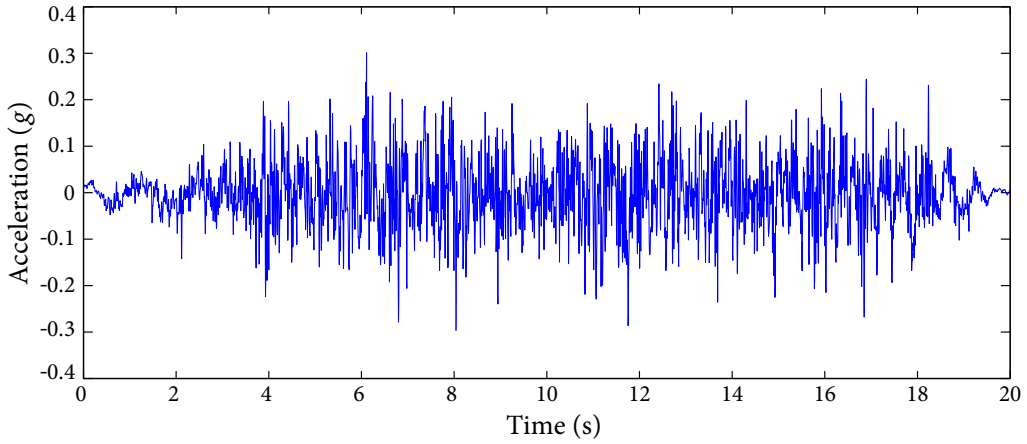

(a) Horizontal Direction 1

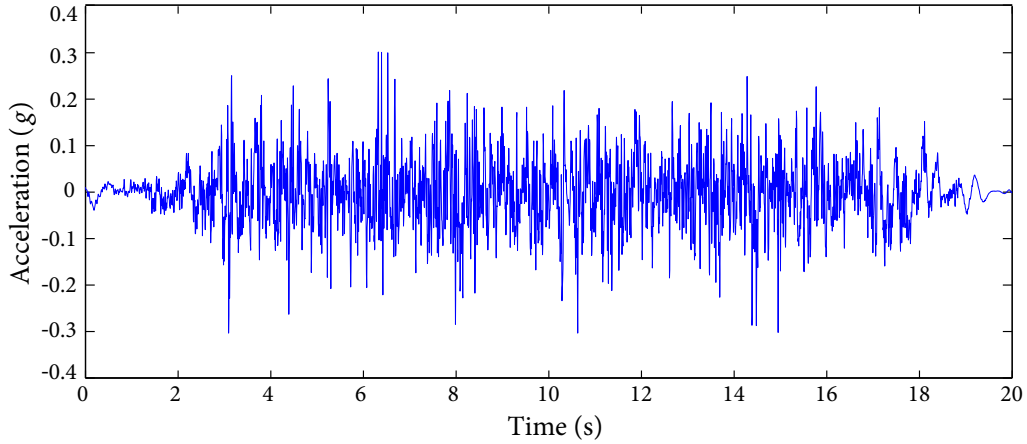

(b) Horizontal Direction 2

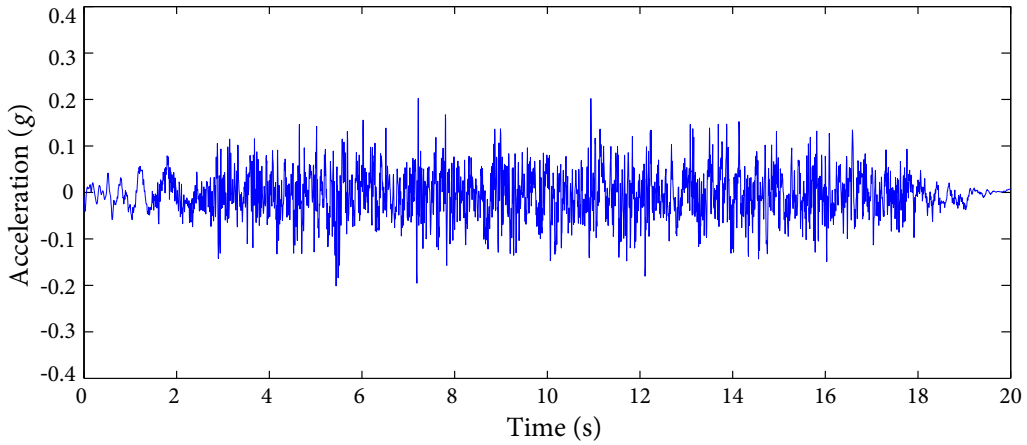

(c) Vertical Direction

Figure 2.18 Tri-directional compatible time histories of CENA UHS

Standard UHS for CENA

The 5% standard Uniform Hazard Spectrum (UHS) proposed by Atkinson and Elgohary (2007) for Central and Eastern North America (CENA) sites anchored at $0.3g$ is chosen as the horizontal GRS; the vertical input GRS is taken as 2/3 of the horizontal GRS. 30 sets of time histories compatible with the standard UHS are generated following the requirements of CSA N289.3 (2010), as shown in Figure 2.17. Compared to design spectrum in USNRC R.G. 1.60, the most apparent characteristic of the standard UHS is the different spectrum shape; the standard UHS has relatively low spectral acceleration values in the intermediate frequency range from 2 to 10 Hz, but contains abundant higher frequency content in the frequency range from 20 to 50 Hz.

For both USNRC R.G. 1.60 GRS and CENA UHS, all spectrum-compatible time histories are generated using the Hilbert-Huang Transform method (Ni *et al.*, 2011; Ni *et al.*, 2013). Samples of the tri-directional compatible time histories for CENA UHS are shown in Figure.

2.3.3 Comparison of FRS

FRS of the Service Building under the Excitation of GRS of USNRC R.G. 1.60

FRS at Node 1 and Node 2 obtained from both time history analyses and the direct spectra-to-spectra method are plotted in Figures 2.19 and 2.20, respectively. These FRS are calculated over 200 frequencies including natural frequencies of the dominant modes of the structure. The mean FRS obtained from time history analyses, which are considered as the "exact" FRS, are highlighted by red dashed lines; the FRS generated by the proposed direct method are represented as black solid lines.

It is seen that FRS generated by the direct method agree extremely well with the "exact" FRS over the entire frequency range. The relative errors are less than 5% at the peaks of FRS, whereas there are large variabilities in FRS from time history analyses, as shown in Figure 2.19 and 2.20. This example demonstrates that time history analysis can lead to approximately 30% overestimation or 20% underestimation at the FRS peaks, even though the time histories are well compatible with the target GRS (within 10% of the target GRS).

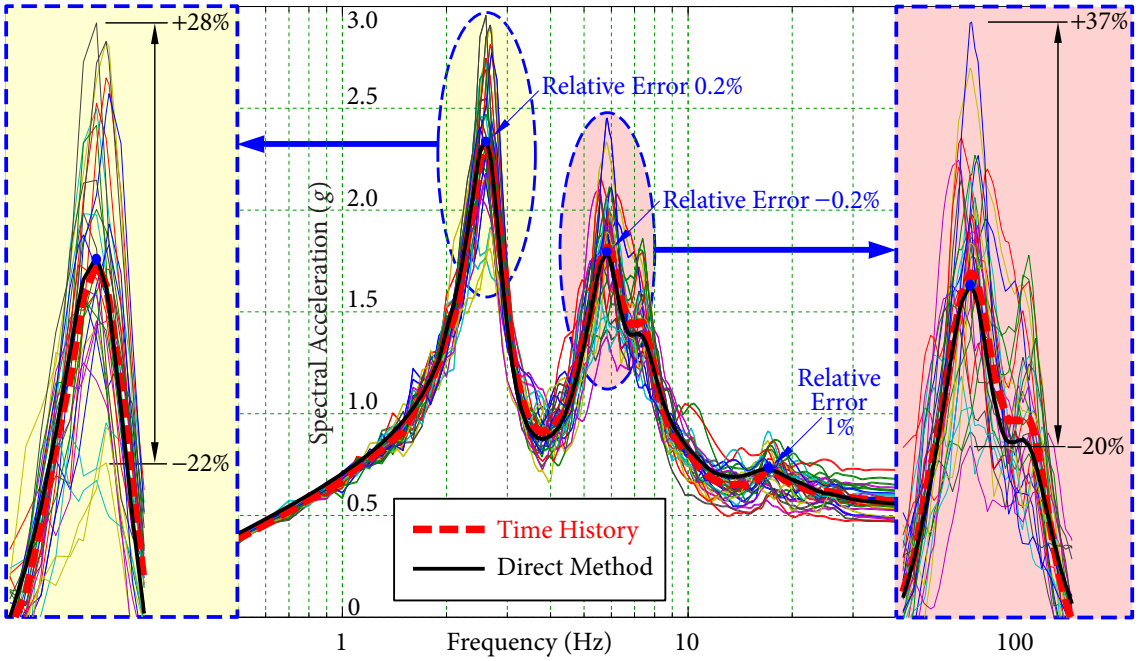

Figure 2.19 FRS for Node 1 (USNRC R.G. 1.60 GRS)

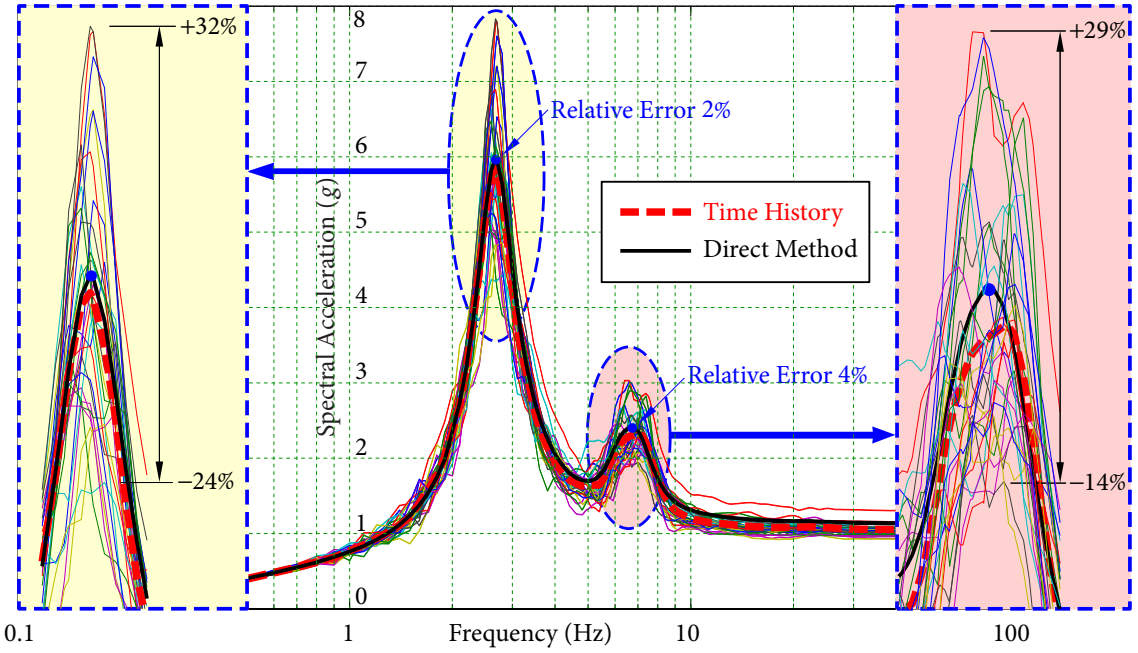

Figure 2.20 FRS for Node 2 (USNRC R.G. 1.60 GRS)

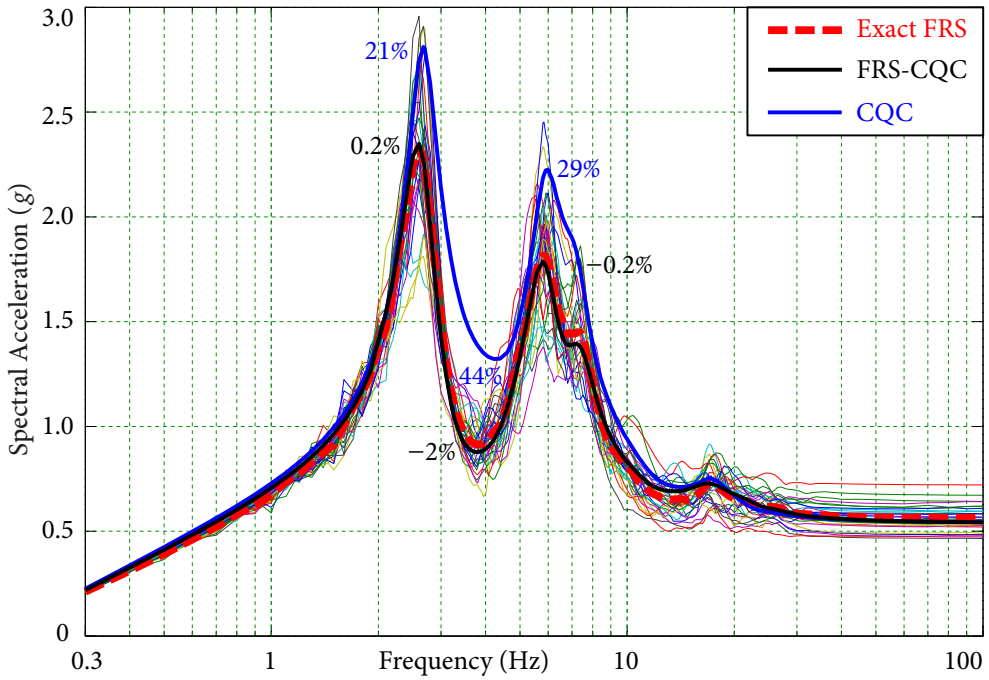

Figure 2.21 Errors in modal combination rules for FRS at Node 1

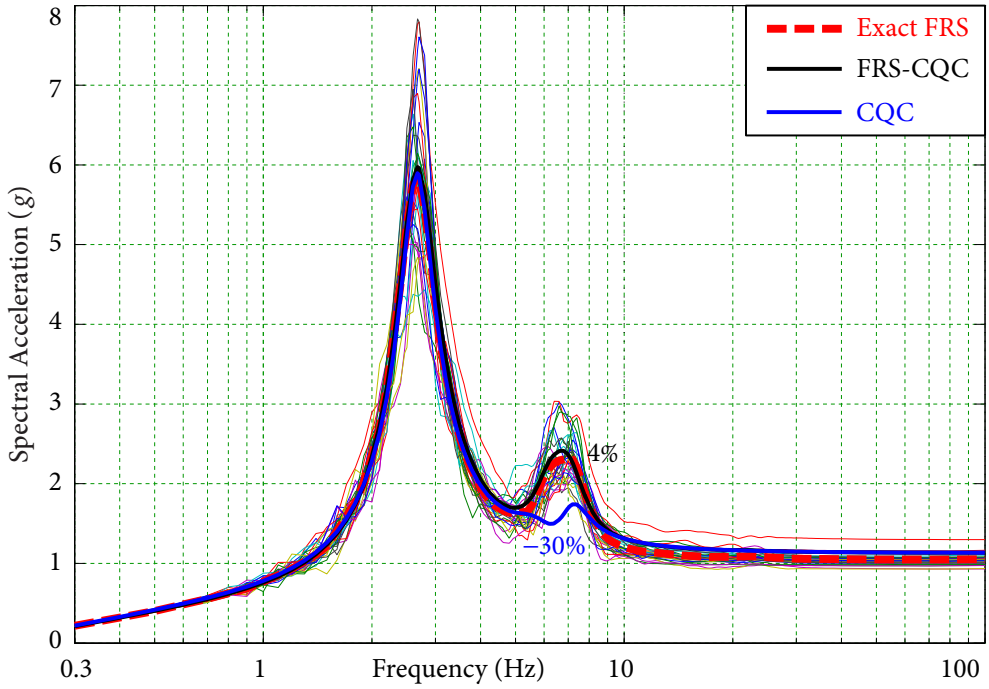

Figure 2.22 Errors in modal combination rules for FRS at Node 2

Furthermore, it is observed that FRS from a single time history analysis may be over-conservative at some peaks but significantly nonconservative at other peaks.

The primary source of variability in time history analysis stems from the inherent uncertainties and randomness of the spectrum-compatible time histories, which are reflected from their rugged spectral shapes. As seen in Figures 2.16 and 2.17, there is an apparent difference between the response spectrum of a spectrum-compatible time history and the target GRS, which has a smooth spectral shape. From equation (2.2.18), it is clear that FRS are amplified GRS. Therefore, this difference is also amplified by an amplification factor, which can range from 5.5 to 7 in tuning cases. For an oscillator mounted on a SDOF structure, a 5% difference in GRS can result in approximately 30% difference at FRS peaks. For an oscillator mounted on a multiple DOF structure, modal responses are multiplied by the contribution factors and combined through equations (2.2.42) and (2.2.58). As a result, variabilities in FRS are combinations of the differences in all modal response and are also significant.

To further verify the significance of modal combination on the determination of FRS, Figures 2.21 and 2.22 show the FRS generated by the direct method using the conventional CQC combination rule. For FRS at Node 1, there are 21%, 29%, and 44% relative errors at the first, second peaks, and the valley between the two peaks, respectively. For Node 2, CQC gives results close to the "exact" FRS around the first peak. However, there is 30% under-estimation at the second peak.

Figure 2.23 illustrates the seismic responses of the first four significant modes at Node 1. The effect of modal combination can be analyzed qualitatively as follows.

- For low frequencies $f < 2$ Hz, the response of the oscillator is contributed mainly by the amplified ground motion. Since the oscillator is a SDOF system, it does not involve modal combination.
- For frequencies from 2 to 20 Hz, which cover the dominant modal frequencies of the structure, each mode has considerable contribution so that the effect of modal combination becomes significant. Conventional CQC combination rule, which is developed to combine structural responses to account for the correlation between

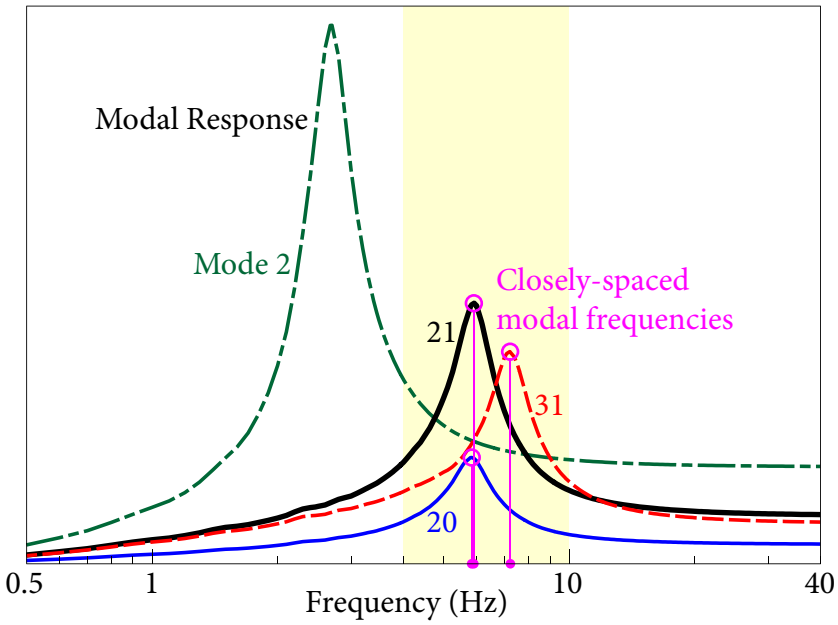

Figure 2.23 Analysis of modal combination of FRS

modal responses of the structure, cannot fully account for the correlation between the responses of the oscillator contributed by different modal responses and the correlation between response of the oscillator contributed by a modal response and the response of a structure mode.

- For high frequencies $f > 20$ Hz, because the oscillator is sufficiently rigid, its response is close to the structural response. The formula of FRS-CQC can be reduced to CQC in this case; hence, the resultant FRS given by these two combination rules are close.

Since structures in nuclear power plants have multiple dominant modes, and some of them are closely-spaced, modal combination rules significantly influence the resultant FRS. It is demonstrated that FRS-CQC combination rule is valid and accurate to combine modal responses.

FRS of the Service Building under the Excitation of Standard UHS for CENA

For Standard UHS for CENA, the proposed direct method is validated by comparing FRS obtained from the direct method with the "exact" FRS, as shown in Figures 2.24 and 2.25. It is seen that FRS given by the proposed direct method agree extremely well with the "exact"

FRS over the entire frequency range, and the relative errors at peaks are mostly less than 5%. Compared to Figures 2.19 and 2.20, there are some differences in the spectral shapes of FRS, particularly over the higher frequency range from 10 to 40 Hz. FRS peak up in this range since the spectral acceleration of UHS reaches the maximum value while the spectral acceleration of R.G. 1.60 GRS decreases.

Peak FRS generated from UHS are generally lower than those from R.G. 1.60 GRS. The reason is that the spectral accelerations of UHS are apparently lower than those of R.G. 1.60 over the frequency range from 2 to 8 Hz, where the dominant modes of the structure contribute most.

Probabilistic Descriptions of FRS Peaks

Another major advantage of the proposed direct method is that it can give probabilistic descriptions for FRS peak values. Using the probabilistic description of tRS developed in the companion paper, FRS with any desired level of NEP p can be determined from the given GRS and the corresponding tRS with NEP p. FRS with 84.1% NEP at Node 1 obtained by time history analyses and the proposed direct spectra-to-spectra method are compared in Figure 2.26 for USNRC R.G. 1.60 GRS and in Figure 2.27 for Standard UHS for CENA. The relative errors at the three FRS peaks are 4.5%, 1%, and 1%, respectively, for USNRC R.G. 1.60 GRS; the relative errors at the four FRS peaks are 0.3%, -1.3%, -0.7%, and -3.8%, respectively, for Standard UHS for CENA. This excellent degree of agreement further demonstrates the accuracy of the proposed method.

It is noted that the mean FRS and FRS with 84.1% NEP given by the proposed direct method are almost the same for non-tuning cases, as shown in Figures 2.26 and 2.27. This can be explained by equation (2.2.23) and Figure 2.4. The amplification factors given by equation (2.2.23) depend on the equivalent damping ratios $\zeta_{0,e}$ and ζ_e, which are determined by tRS and GRS in equation (2.2.33) and have a significant effect on the amplification factors in the perfect-tuning and near-tuning cases but have a negligible effect in non-tuning cases, as shown in Figure 2.4. As a result, for non-tuning cases, the amplification factors are almost the same for all values of the equivalent damping ratios, leading to that FRS for all levels of NEP p are almost the same.

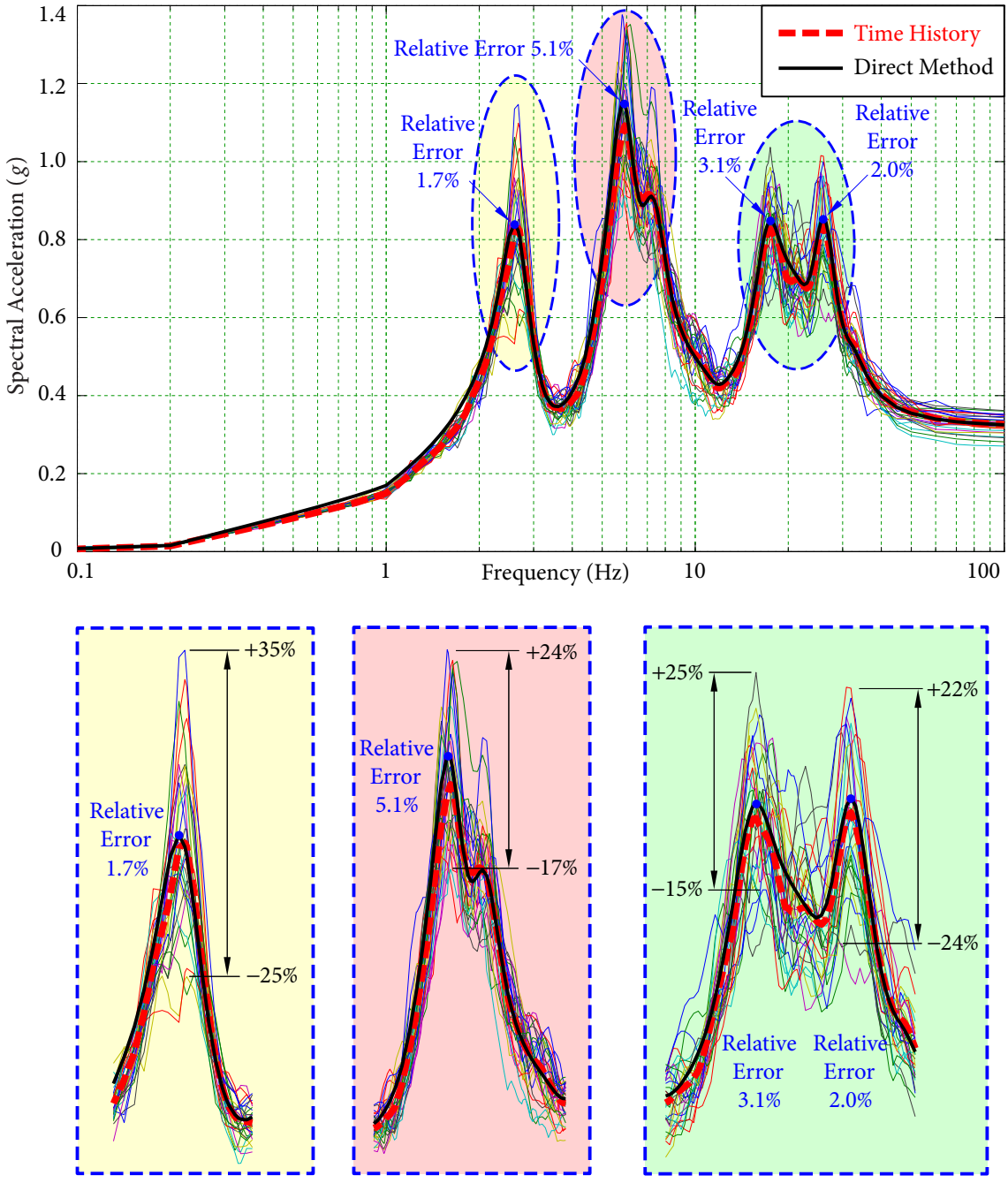

Figure 2.24 FRS for Node 1 (UHS for CENA)

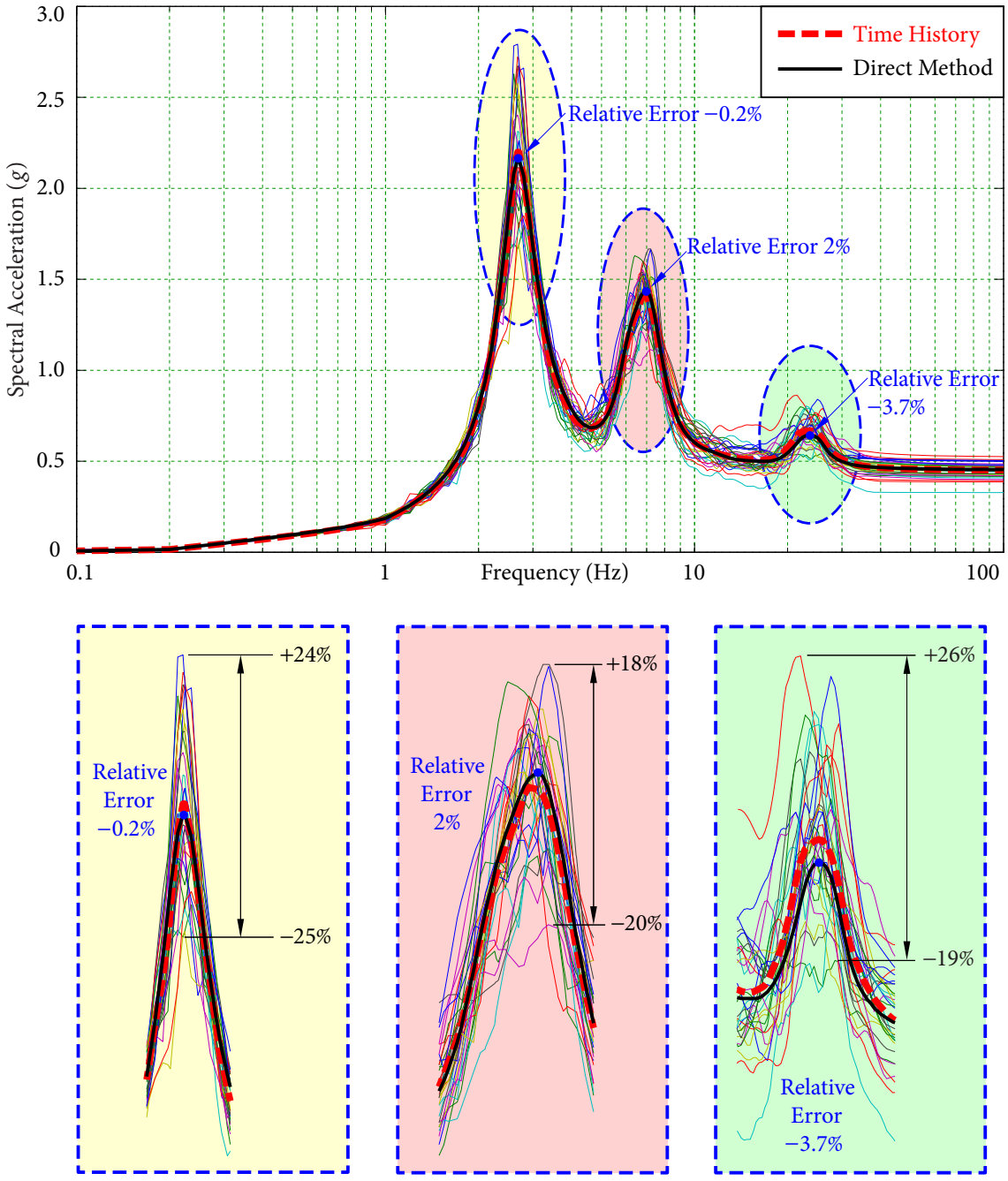

Figure 2.25 FRS for Node 2 (UHS for CENA)

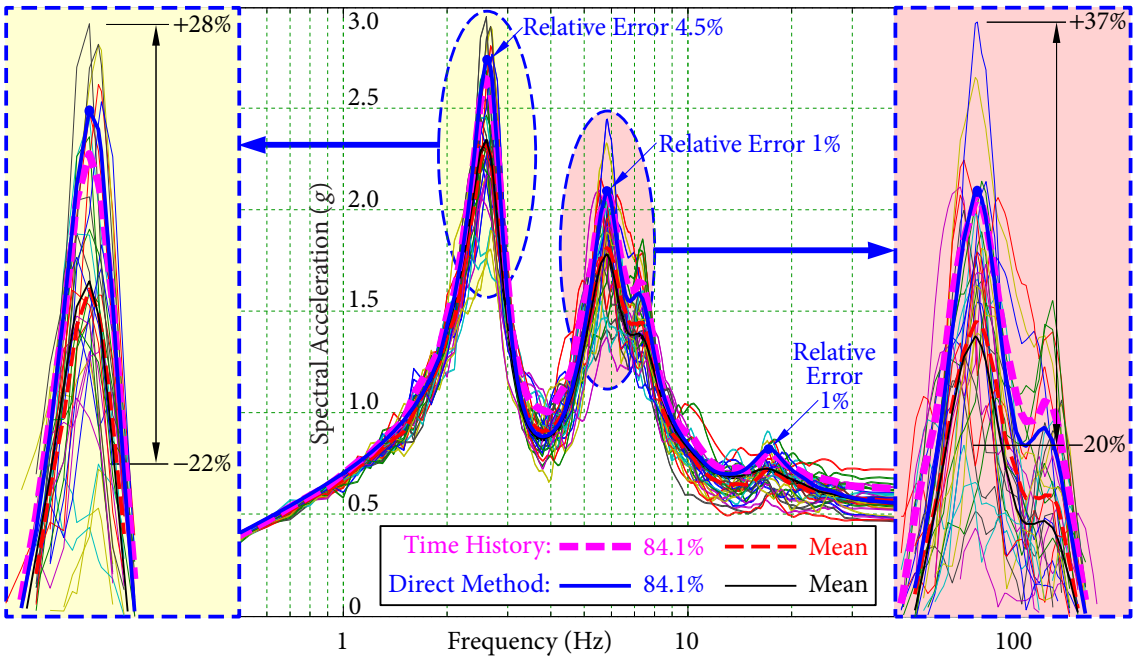

Figure 2.26 Probabilistic description of FRS for Node 1 (USNRC R.G. 1.60 GRS)

Because of the large amplification factors in the perfect-tuning and near-tuning cases, small deviations of the response spectrum of a time history from the target GRS are significantly amplified. Although the compatibility of the time histories is good by satisfying code requirements, as shown in Figures 2.16 and 2.17, there are large variabilities in the FRS from time history analyses, particularly in the perfect-tuning and near-tuning cases, as shown in Figures 2.19, 2.20, 2.24, and 2.25. Peak responses can be overestimated and underestimated by as much as 35% and 25%, respectively. Hence, results from time history analyses using a single set or a small number of sets of spectrum-compatible ground motions are not adequate to give accurate FRS. This observation further highlights the advantage of the proposed direct method, which uses the target GRS as input directly, without generating spectrum-compatible time histories that are the primary source of variabilities.

2.4 Summary

In this chapter, a direct spectra-to-spectra method is developed for accurate and efficient generation of FRS. Seismic response of a SDOF oscillator mounted on a SDOF primary

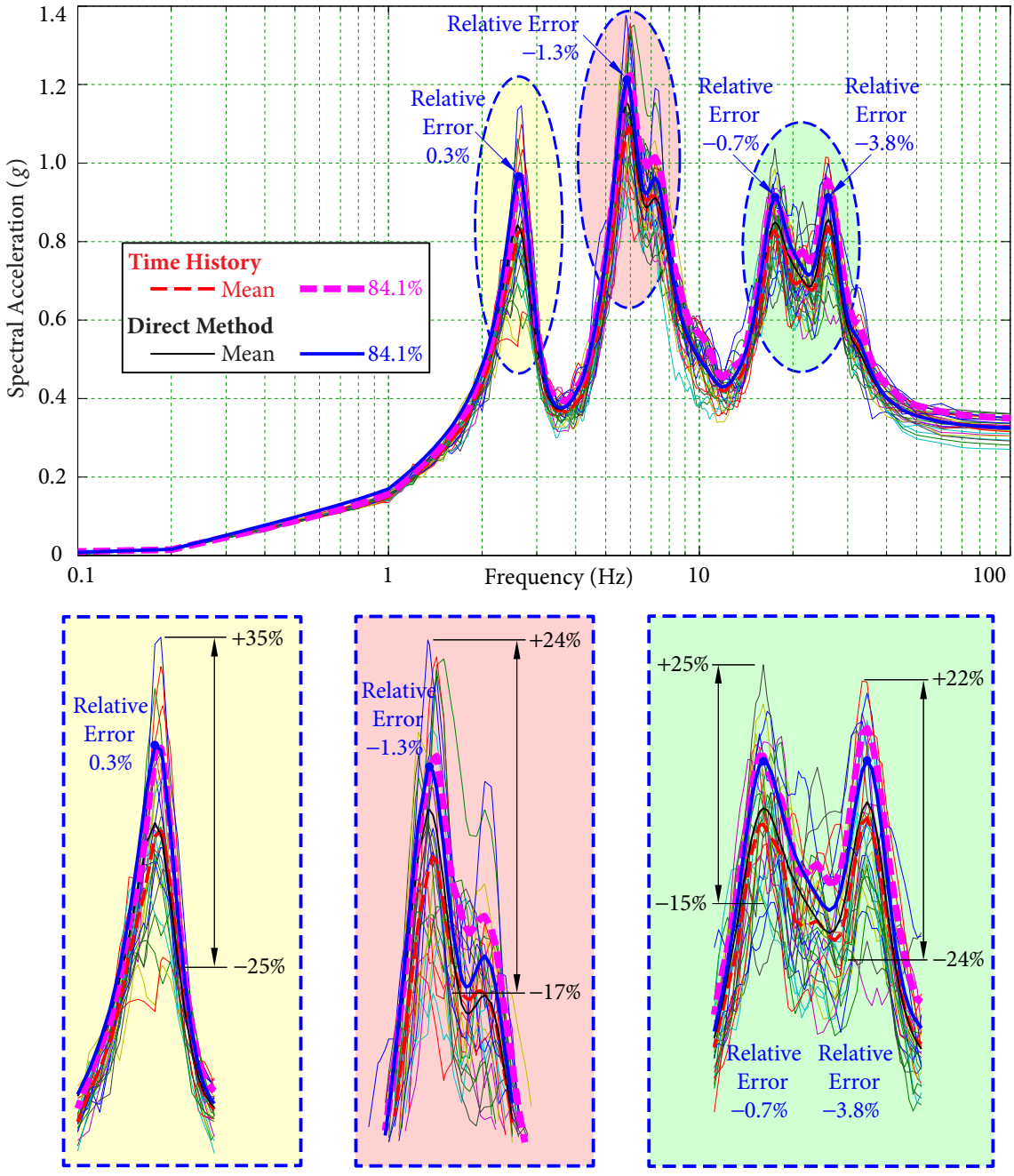

Figure 2.27 Probabilistic description of FRS for Node 1 (UHS for CENA)

structure is studied first. The response of the oscillator is derived analytically based on Duhamel's integral. For the tuning case when the oscillator is resonant with the SDOF primary structure, the concept of tRS is introduced, along with the statistical relationships between tRS and GRS developed from extensive numerical simulations, to give an accurate and complete probabilistic description of FRS, since large variabilities exist in this important case.

The formulation is then extended to a SDOF oscillator mounted on a multiple DOF primary structure. A new modal combination method for generating FRS, called FRS-CQC, is developed based on random vibration theory. FRS-CQC can fully account for the correlation of responses between equipment and its supporting structure with closely-spaced modes.

Numerical examples of a typical service building subjected to tri-directional seismic input are presented. FRS determined by the proposed direct method agree extremely well with the "exact" FRS, which are obtained through a large number of time history analyses, for both conventional Newmark-type GRS (USNRC R.G. 1.60 GRS) and UHS for CENA with significant high frequency spectral accelerations. It is demonstrated that FRS determined by time history analyses have large variabilities, particularly in tuning cases or at FRS peaks; hence, FRS determined by time history methods using a single set or a small number of sets of spectrum-compatible tri-directional time histories are not reliable. Furthermore, it is shown that modal combination methods significantly affect the results; there will be large errors if the conventional CQC or SRSS modal combination methods are applied to determine FRS. The proposed direct spectra-to-spectra method can avoid these deficiencies and give accurate FRS, especially probabilistic descriptions of FRS peaks.

The proposed direct spectra-to-spectra method has three significant and novel features:

1. Using the concept of tRS and the statistical relationships between tRS and GRS, FRS in the perfect-tuning and near-tuning cases can be determined accurately for both conventional Newmark-type GRS and UHS with significant high frequency spectral accelerations.
2. The correlations of responses between equipment and it supporting structure with closely-spaced modes can be fully accounted for through FRS-CQC combination rule.

As a result, the proposed direct method can generate accurate FRS for complex three-dimensional finite element structural models with closely-spaced modes under tri-directional seismic input.

3. From the complete probabilistic descriptions of tRS for given GRS, the proposed direct method can give complete probabilistic descriptions of FRS peaks, i.e., FRS with any desired level of NEP p can be determined.

In summary, the proposed direct spectra-to-spectra method is accurate and efficient, with analytical formulation in terms of basic modal information of the primary structure, prescribed GRS, and the corresponding tRS. It can be conveniently implemented in practice to generate FRS for complex structures with closely-spaced modes.

CHAPTER 3

Generating Floor Response Spectra: Scaling Method

In seismic risk assessment and refurbishment of existing nuclear facilities, it is necessary to develop new FRS as seismic demand for SSCs since the amplitude and spectrum shape of new input ground motion spectrum (GRS) may be significantly different from that of the GRS used in the past seismic design and analysis. Scaling methods, which allow the generation of FRS corresponding to new GRS by multiplying existing FRS with appropriate scaling factors rather than by performing re-analyses of the structure, are efficient and economical approaches. In practice, preliminary estimation of new FRS can generally be obtained by scaling the existing FRS upward for the increase of the new GRS over the previous GRS under acceptable circumstances. Otherwise, a reanalysis of structure is required. It is, of course, desirable for engineers to utilize as much of the existing information and results as possible without repeating the procedure of dynamic analysis, which introduces extra costs and is time consuming. However, in many practical situations, it is challenging to generate FRS not only by scaling but also by analyzing structural responses due to the lack of structural model information.

The direct method for generating FRS developed in Chapter 2 prompted the development of the scaling method presented in this chapter. The analytical formulation of the direct spectra-to-spectramethod provides a strong physical insight into the essential characteristics of FRS, which allows the identification of dynamical information of significant

equivalent modes of the underlying structure from the available FRS and GRS. Scaling factors are then determined in terms of the dynamical information (modal frequencies,modal damping ratios, and modal contribution factors) and input GRS.

3.1 Scaling Problems

In many practical situations, scaling methods are efficient and economical approaches to obtain FRS:

Scaling Problem 1: Knowing FRS $\mathcal{S}_{\mathrm{F}}(f, \zeta_0)$ with one or only a few values of damping ratio, it is required to determine $\mathcal{S}_{\mathrm{F}}(f, \zeta_0')$ for a number of different damping ratios ζ_0'.

Scaling Problem 2: Knowing FRS-I $\mathcal{S}_{\text{F-I}}(f, \zeta_0)$ with one or only a few values of damping ratio for Ground Response Spectra (GRS-I) $\mathcal{S}_{\text{G-I}}(f, \zeta)$, it is required to determine FRS-II $\mathcal{S}_{\text{F-II}}(f, \zeta_0')$ for a number of different damping ratios ζ_0' under different GRS-II $\mathcal{S}_{\text{G-II}}(f, \zeta)$.

In the following, some existing results for both scaling problems are reviewed briefly. The importance and challenges of scaling methods are highlighted.

Scaling Problem 1

Scaling Problem 1 arises quite frequently in practice. Usually FRS corresponding to one or only a few damping ratios are available. However, FRS for various damping ratios, which may range from 2% to 15%, are required.

For example, for many existing nuclear power plants, usually low structural damping ratios were used in the original dynamic models. Also the final FRS curves were presented with low equipment damping ratios up to 5% or 7%. In seismic margin assessment, median damping ratios for structures are required, which are larger than those used in the original dynamic analyses; FRS with higher equipment damping ratios are also required. Engineering activities, driven by schedule and budget, call for a prompt and economical approach to generate the updated FRS for high equipment damping ratios with the high (median) structural damping ratios.

ASCE 4-98 Clause 2.2.1 (1998) provides the following equation to determine $\mathcal{S}_F(f,\zeta)$ from $\mathcal{S}_F(f,\zeta_1)$ and $\mathcal{S}_F(f,\zeta_2)$:

$$\mathcal{S}_F(f,\zeta) = \mathcal{S}_F(f,\zeta_1) + [\mathcal{S}_F(f,\zeta_2) - \mathcal{S}_F(f,\zeta)]\,\frac{\ln\zeta - \ln\zeta_1}{\ln\zeta_2 - \ln\zeta_1}, \tag{3.1.1}$$

which can be written as

$$\frac{\mathcal{S}_F(f,\zeta) - \mathcal{S}_F(f,\zeta_1)}{\mathcal{S}_F(f,\zeta_2) - \mathcal{S}_F(f,\zeta_1)} = \frac{\ln\zeta - \ln\zeta_1}{\ln\zeta_2 - \ln\zeta_1}, \tag{3.1.2}$$

i.e., $\mathcal{S}_F(f,\zeta)$ is determined by linear interpolation in the $\mathcal{S}_F(f,\zeta)$-$\ln\zeta$ plane.

ASCE 4-98 Clause 3.4.2.4 (1998) gives the following equation

$$\mathcal{S}_F(f,\zeta) = \sqrt{\mathcal{S}_F^2(f,\zeta_2) + [\mathcal{S}_F^2(f,\zeta_1) - \mathcal{S}_F^2(f,\zeta_2)]\,\frac{\zeta_1}{\zeta}\left(\frac{\zeta-\zeta_2}{\zeta_1-\zeta_2}\right)}, \quad \text{for } \zeta_1 < \zeta < \zeta_2 \leqslant 3\zeta_1. \tag{3.1.3}$$

Equation (3.1.3) can be written as

$$\frac{\mathcal{S}_F^2(f,\zeta_2) - \mathcal{S}_F^2(f,\zeta)}{\zeta_2 - \zeta} = \frac{\zeta_1}{\zeta}\,\frac{\mathcal{S}_F^2(f,\zeta_2) - \mathcal{S}_F^2(f,\zeta_1)}{\zeta_2 - \zeta_1}. \tag{3.1.4}$$

Note that

$$\frac{\mathcal{S}_F^2(f,\zeta_2) - \mathcal{S}_F^2(f,\zeta)}{\zeta_2 - \zeta} = \frac{\mathcal{S}_F^2(f,\zeta_2) - \mathcal{S}_F^2(f,\zeta_1)}{\zeta_2 - \zeta_1} \tag{3.1.5}$$

amounts to determining $\mathcal{S}_F^2(f,\zeta)$ by linear interpolation in the $\mathcal{S}_F^2(f,\zeta)$-ζ plane. Since $\zeta_1/\zeta < 1$, the slope of the solid line given by equation (3.1.4) is less than the slope of the dashed line given by linear interpolation (3.1.5), as illustrated in Figure 3.1. FRS determined from equation (3.1.4) are more conservative than the results given by linear interpolation in the $\mathcal{S}_F^2(f,\zeta)$-ζ plane.

SQUG GIP Section 4.2.2 (2001) provides two results for IRS:

1. For IRS shape similar to the Bounding Spectrum (without very narrow peaks),

$$\mathcal{S}_F(f,\zeta) = \mathcal{S}_F(f,\zeta_0)\sqrt{\frac{\zeta_0}{\zeta}} \implies \mathcal{S}_F(f,\zeta) \sim \frac{1}{\sqrt{\zeta}}. \tag{3.1.6}$$

   For all $f > f_{\text{Peak}}$ (corresponding to peak of IRS), $\mathcal{S}_F(f,\zeta) \geqslant$ ZPA (zero-period acceleration). Equation (3.1.6) amounts to scaling $\mathcal{S}_F(f,\zeta)$ proportional to $1/\sqrt{\zeta}$.

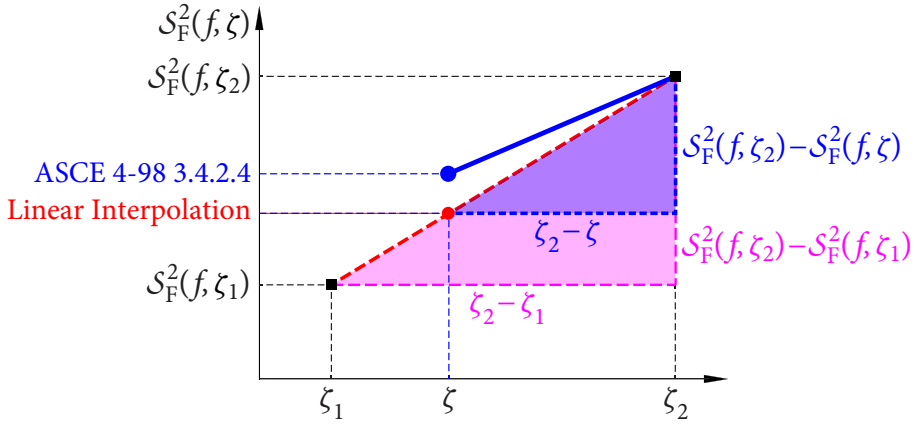

Figure 3.1 Scaling method for FRS given by ASCE 4-98 Clause 3.4.2.4

2. For equipment mounted below about 40 feet above the effective grade and has a fundamental natural frequency greater than about 8 Hz,

   - $f \leqslant 8$ Hz: $\mathcal{S}_F(f,\zeta) = \mathcal{S}_F(f,\zeta_0)\sqrt{\dfrac{\zeta_0}{\zeta}} \implies \mathcal{S}_F(f,\zeta) \sim \dfrac{1}{\sqrt{\zeta}}$;
   - $f \geqslant 20$ Hz: $\mathcal{S}_F(f,\zeta) = \mathcal{S}_F(f,\zeta_0)$, i.e. assuming that damping has no effect;
   - 8 Hz $< f <$ 20 Hz: $\dfrac{\log \mathcal{S}_F(f,\zeta) - \log \mathcal{S}_F(8\text{Hz},\zeta)}{\log f - \log 8} = \dfrac{\log \mathcal{S}_F(20\text{Hz},\zeta) - \log \mathcal{S}_F(8\text{Hz},\zeta)}{\log 20 - \log 8}$,

     i.e., $\mathcal{S}_F(f,\zeta)$ is obtained from linear interpolation in $\log \mathcal{S}_F(f,\zeta)$-$\log f$ plane between 8 Hz and 20 Hz.

From this summary, it is clearly seen that existing scaling approaches are essentially

- a simple scaling, such as equation (3.1.6) with a uniform scaling factor for all frequency f; or
- linear interpolation based on various assumptions between $\mathcal{S}_F(f,\zeta)$ and ζ or f, which are not valid when the equipment damping ratios of required FRS are out the range, or when only one FRS with 5% equipment damping ratio is available.

Scaling Problem 2

An accurate and reliable method for Scaling Problem 2 is important in many engineering projects. For example, in a life-extension project of an existing nuclear power plant, $\mathcal{S}_{F\text{-I}}(f,\zeta)$ are usually available for Design Basis Earthquake (DBE) $\mathcal{S}_{G\text{-I}}(f,\zeta)$. $\mathcal{S}_{F\text{-II}}(f,\zeta)$ are

required for site-specific ground motion response spectra (GMRS) or review-level earthquakes (RLE) $\mathcal{S}_{\text{G-II}}(f,\zeta)$ in seismic margin analysis. Project scope and budget may not warrant a complete seismic structural analysis to obtain $\mathcal{S}_{\text{F-II}}(f,\zeta)$.

In rehabilitation projects, sometimes structures need to be strengthened due to a higher seismicity $\mathcal{S}_{\text{G-II}}(f,\zeta)$ than the original design $\mathcal{S}_{\text{G-I}}(f,\zeta)$. It is tricky to decide which strengthen scheme is the most economical from the seismic point of view. A quick yet accurate approach to determine $\mathcal{S}_{\text{F-II}}(f,\zeta)$ from $\mathcal{S}_{\text{G-II}}(f,\zeta)$ will assist engineers to decide which strengthen scheme is optimal.

Similarly, in a new-build, $\mathcal{S}_{\text{F-I}}(f,\zeta)$ are available for a generic design based on a standard GRS $\mathcal{S}_{\text{G-I}}(f,\zeta)$, such as those in CSA N289.3 (2010) or USNRC R.G. 1.60 (1973). An efficient and good estimate of $\mathcal{S}_{\text{F-II}}(f,\zeta)$ for site-specific GRS $\mathcal{S}_{\text{G-II}}(f,\zeta)$ is critical for feasibility analysis, budgeting, scheduling, bidding and tendering, and procurement of important equipment, which may take years to manufacture, before the site-specific design is finalized and a complete seismic analysis is performed.

It is obviously desirable for engineers to use as much of the available information and results of previous analyses as possible without performing a complete dynamic analysis, which is time consuming and introduces extra costs. However, the existing scaling methods recommended in EPRI NP-6041-SL (1991) basically give approximate estimates with an uniform scaling factor and are restricted to some special cases. Because of their crude approximations, they are not widely used in nuclear industry.

Objective and Scope

The primary challenges and difficulties in developing FRS based on results of previous analyses include:

1. Related to Scaling Problem 1, FRS with various equipment damping ratios, which may range from 2% to 15%, are required when FRS corresponding to only a few damping ratios (e.g., 5%) are available.
2. Differences in the spectral shapes between GRS-I of the previous analysis and the new GRS-II may result in significant variations in the FRS shapes.

3. In some technical reports of nuclear facilities constructed decades ago, only the final resultant FRS-I are available. Therefore, it is challenging to develop FRS-II not only by scaling method but also by a re-analysis of structural response due to the lack of structural model information.

Despite the important applications of accurate and reliable scaling methods for generating FRS in the nuclear industry, there have been no significant progress in developing such methods in the past decades due to these theoretical and technical challenges.

Consequently, FRS-II have been developed by re-analysis rather than by scaling in almost all cases. Time history method is a most commonly used method for generating FRS in current practice. However, due to the inherent randomness and uncertainty of spectrum-compatible time histories which are generated as intermediate seismic inputs from a target response spectrum, time history method introduces large variabilities in FRS, particularly at FRS peaks which are of primary interest for engineers. In order to obtain accurate FRS, a large number of time history analyses are needed; it is, however, excessively time-consuming and computationally expensive.

The direct spectra-to-spectra method developed in chapter 2 prompted the development of the scaling method presented in this chapter. By introducing the concept of t-response spectra (tRS) and developing statistical relationships between tRS and GRS to deal with tuning or resonance between the equipment and primary supporting structure, a direct spectra-to-spectra method for generating FRS is developed. Only basic modal information of the structure (including modal frequencies, modal damping ratios, modal participation factors, and mode shapes at the locations of interest along with input GRS) is needed. It has been demonstrated that this highly efficient direct method can provide accurate FRS, especially give probabilistic descriptions at FRS peaks, matching those obtained by time history analyses with a large number of time histories.

In this chapter, a scaling method for solving the two scaling problems based on the direct spectra-to-spectra method developed in Chapter 2 is presented. In Section 3.2, a system identification procedure is developed to obtain the modal information of significant equivalent modes of the underlying structure. In Section 3.3, procedures for the two scaling problems are developed. Numerical examples for scaling FRS for a typical service

building in a nuclear power plant are presented in Section 3.4 to demonstrate the accuracy and advantages of the proposed scaling method, which is efficient, accurate, and easy to implement.

3.2 System Identification

An essential task in a scaling method for generating FRS is system identification: to recover the most significant dynamical characteristics of the underlying structure from $\mathcal{S}_{\text{G-I}}(f,\zeta)$ and available $\mathcal{S}_{\text{F-I}}(f,\zeta)$. The formulation of the direct spectra-to-spectra method (Jiang *et al.*, 2015) provides a strong physical insight into FRS and is ideally suited for system identification.

It is known that FRS is contributed primarily by a number of significant modes of the structure, and FRS peaks occur at the frequencies of these modes. Therefore, for the mth DOF (corresponding to the nth node in direction j), the first step is to extract the significant equivalent modal information (frequencies and the corresponding spectral accelerations) from the available FRS-I.

It should be noted that the available FRS have usually been broadened and smoothed, which means some spectral values may have been modified artificially and thus inappropriate to be used for identifying the structural information. Nevertheless, since the plateaus of FRS result from broadening (normally by $\pm 15\%$) the peaks of raw FRS, it is reasonable to use the middle point at an FRS plateau for the natural frequency of a significant structural mode and the corresponding spectral acceleration. If there is a wide plateau, it may be assumed that it is the result of broadening and smoothing from more than one peak, as shown in Figure 3.2. In this case, two or more significant modes may be taken considering that the corners are usually the results of broadening from a peak by $\pm 15\%$; however, it is understood that the broadened-and-smoothed FRS may not accurately reflect the underlying raw FRS.

The number of the significant structural modes can be larger than the number of FRS plateaus due to the possible existence of closely-spaced modes. However, a cluster of closely-spaced modes can be treated as one synthesized mode with the same frequency and an equivalent modal contribution factor. This assumption may not be able to reproduce

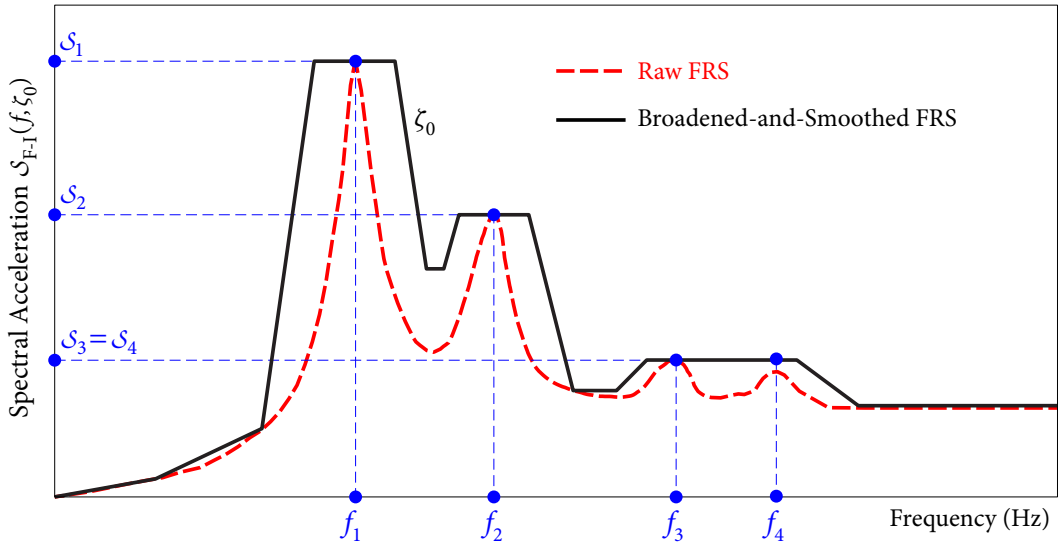

Figure 3.2 Broadened-and-Smoothed FRS

exactly the same dynamical information as the original structure; but it simplifies the calculation for generating FRS without compromising the accuracy.

In general, the available FRS-I in direction i is obtained under tri-directional excitations. In system identification, the available FRS-I and GRS-I in direction i are used to obtain the equivalent significant modes of the underlying structure. Hence, the equivalent system contains the significant dynamic characteristics of generating FRS in direction i under tri-directional seismic excitations from GRS in direction i. As a result, even though only GRS in direction i is used in generating FRS in the proposed scaling method, the generated FRS contains the effect of tri-directional seismic excitations.

Suppose that GRS-I $\mathcal{S}_{\text{G-I}}(f,\zeta_0)$ and FRS-I $\mathcal{S}_{\text{F-I}}(f,\zeta_0)$ for the mth DOF (corresponding to the nth node in direction j) of the original structure are available. For clarity of presentation, the subscript m signifying the mth DOF is dropped. It is assumed that there are $\mathcal{N}$ significant modes in the underlying structure, where $\mathcal{N}$ may be slightly larger than the number of plateaus in FRS-I.

As an example of illustration, for a given FRS-I as shown in Figure 3.2, the frequencies of the four significant modes f_k, $k=1,2,3,4$, and the corresponding spectra accelerations $\mathcal{S}_k=\mathcal{S}_{\text{F-I}}(f_k,\zeta_0)$ can be easily obtained by inspection and simple calculation.

The maximum value of the contribution of the kth significant mode to the absolute acceleration of the oscillator mounted in the mth DOF is, from equation (2.2.42),

$$R_k = \underbrace{\varphi_k \Gamma_k}_{X_k} \underbrace{\sqrt{[\mathcal{AF}_{0,k}\, \mathcal{S}_{\text{G-I}}(f_0, \zeta_0)]^2 + [\mathcal{AF}_k\, \mathcal{S}_{\text{G-I}}(f_k, \zeta_k)]^2}}_{a_k}, \tag{3.2.1}$$

where ζ_0 is the damping ratio of the FRS, ζ_k is the damping ratio of the significant mode k of the underlying structure, and the amplification factors $\mathcal{AF}_{0,k}$ and $\mathcal{AF}_k$ can be evaluated from equation (2.2.43). Note that the superscript i is dropped since only the direction corresponding to the mth DOF is considered. Hence, the value of a_k can be easily determined. The unknown quantity X_k characterizes the contribution factor of significant mode k in the response of the mth DOF.

From equation (2.2.58), the FRS-I value of the mth DOF at frequency f_0 is given by

$$[\mathcal{S}_{\text{F-I}}(f_0, \zeta_0)]^2 = \sum_{k=1}^{\mathcal{N}} \sum_{\kappa=1}^{\mathcal{N}} \rho_{k\kappa} R_k R_\kappa. \tag{3.2.2}$$

Setting $f_0 = f_s$, $s = 1, 2, \ldots, \mathcal{N}$, where f_s is the frequency of the sth significant mode, substituting equation (3.2.1) into (3.2.2), and denoting $a_k\big|_{f_0 = f_s} = a_{k;s}$ give

$$\sum_{k=1}^{\mathcal{N}} \sum_{\kappa=1}^{\mathcal{N}} \rho_{k\kappa}\, a_{k;s}\, a_{\kappa;s}\, X_k X_\kappa = [\mathcal{S}_{\text{F-I}}(f_s, \zeta_0)]^2 = \mathcal{S}_s^2, \quad s = 1, 2, \ldots, \mathcal{N}, \tag{3.2.3}$$

where, with $f_0 = f_s$,

$$a_{k;s} = \sqrt{[\mathcal{AF}_{0,k}\, \mathcal{S}_{\text{G-I}}(f_0, \zeta_0)]^2 + [\mathcal{AF}_k\, \mathcal{S}_{\text{G-I}}(f_k, \zeta_k)]^2},$$

$$\mathcal{AF}_{0,k} = \frac{r_k^2}{\sqrt{(1 - r_k^2)^2 + (2\,\zeta_{\text{e}}\, r_k)^2}}, \quad \mathcal{AF}_k = \frac{1}{\sqrt{(1 - r_k^2)^2 + (2\,\zeta_{\text{e}}\, r_k)^2}}, \quad r_k = \frac{f_k}{f_0},$$

$$\zeta_{\text{e}} = \frac{\mathcal{S}_{\text{G-I}}(f_0, \zeta_0)}{\sqrt{2} \cdot \mathcal{S}^{\text{t}}_{\text{G-I}}(f_0, \zeta_0)}.$$

For a damping ratio ζ_0, there are $\mathcal{N}$ spectral accelerations at the frequencies f_s, $s = 1, 2, \ldots, \mathcal{N}$, of the significant modes. Hence, there are $\mathcal{N}$ quadratic equations in (3.2.3) for $\mathcal{N}$ unknowns X_k, which can be readily solved numerically. It is noted that the solution sets of the quadratic

system are generally non-unique. For instance, the number of possible solution sets may be up to four when $\mathcal{N}=2$ since the solutions can be graphically represented as the intersections of two ellipses. An effective way to find the most realistic solutions is by taking advantage of the modal property

$$\sum_{k=1}^{\mathcal{N}} \Gamma_k \varphi_k = \sum_{k=1}^{\mathcal{N}} X_k \to 1. \tag{3.2.4}$$

It should be emphasized that X_k denote the equivalent modal contribution factors which may not represent the underlying system exactly. Therefore, the summation of X_k is expected to approach 1 rather than equal to 1 exactly; the problem can be interpreted as an optimization problem of minimizing the objective function

$$f(\mathbf{X}) = \left| \sum_{k=1}^{\mathcal{N}} X_k - 1 \right|, \tag{3.2.5}$$

subject to nonlinear constraints

$$\left| g_s(\mathbf{X}) - \mathcal{S}_s^2 \right| \leqslant \varepsilon_s \cdot \mathcal{S}_s^2, \quad s = 1, 2, \ldots, \mathcal{N}, \tag{3.2.6}$$

where

$$g_s(\mathbf{X}) = \sum_{k=1}^{\mathcal{N}} \sum_{\kappa=1}^{\mathcal{N}} \rho_{k\kappa}\, a_{k;s}\, a_{\kappa;s}\, X_k X_\kappa, \tag{3.2.7}$$

and ε_s are error tolerances which are usually set as small as 10^{-2} to 10^{-3}. This optimization process can be easily implemented by many mathematical software packages, such as *Excel*. With the above discussion, an efficient method of identifying significant equivalent modal information of the underlying structure is summarized in Figure 3.3.

3.3 Scaling of FRS

A scaling method is advantageous in the following situations:

- For some structures built a few decades ago, dynamical information of the structures may not be available. A complete dynamic analysis is not possible unless finite element models are established from scratch.
- Even if complete finite element models of structures are available, it may not be desirable to perform dynamic analysis to generate FRS due to project constraints, such as scope and budget constraints.

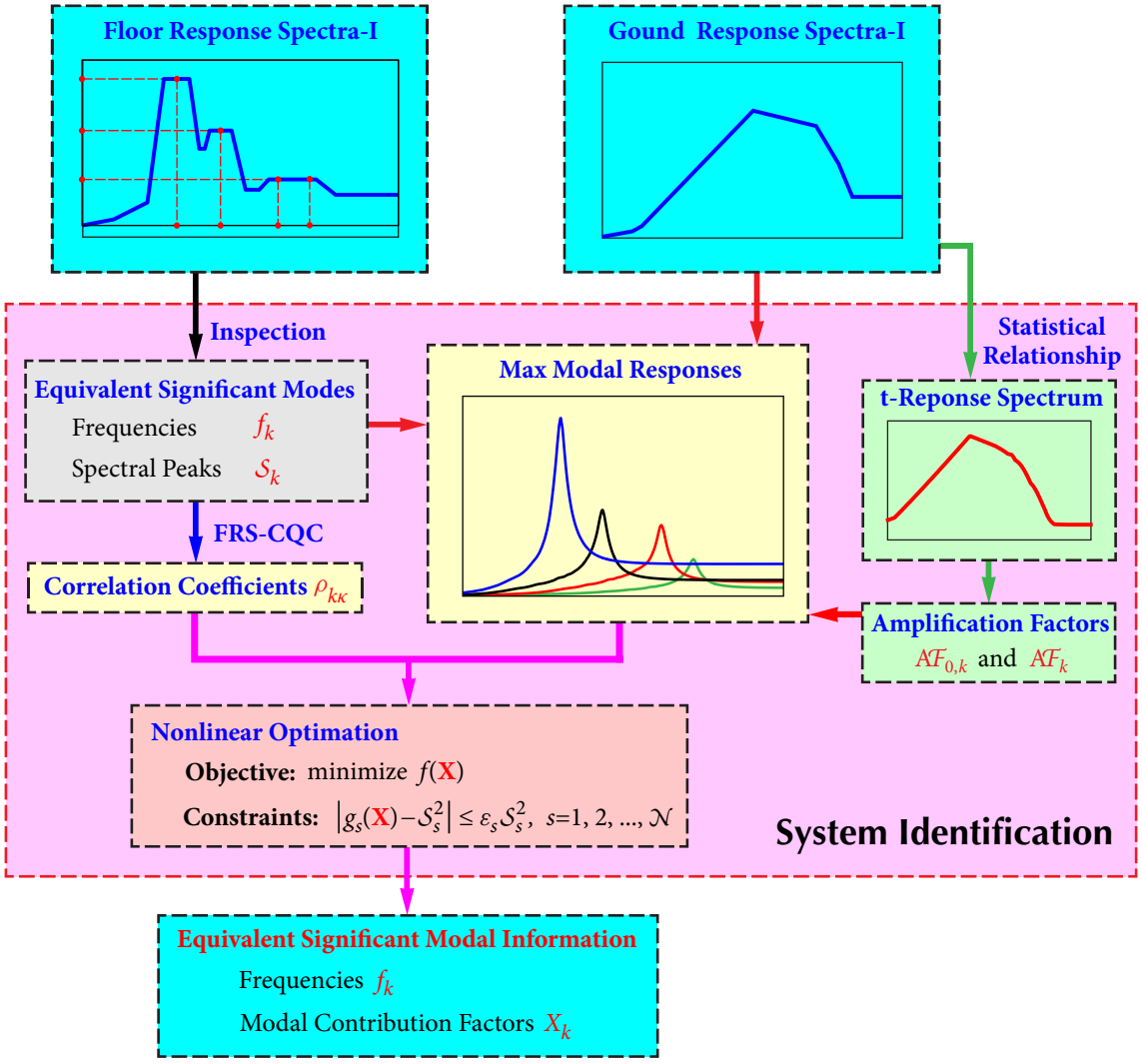

Figure 3.3 Procedure of system identification

In engineering projects when a scaling method is called for to generate FRS, it is assumed that a set of tri-directional FRS $\mathcal{S}^i_{\text{F-I}}(f, \zeta_0)$ and the corresponding tri-directional GRS $\mathcal{S}^i_{\text{G-I}}(f, \zeta_0)$ are available for some values of damping coefficient ζ_0 (e.g., 5%), where the superscript i ($i = 1, 2, 3$) denotes the direction of the spectrum. As discussed in Section 3.2, it is assumed that FRS in direction i is completely due to seismic excitation in direction i; hence, the superscript i is dropped for clarity of presentation.

The analytical formulation of the direct spectra-to-spectra method for generating FRS developed by Jiang *et al.* (2015) provides an ideal avenue for a scaling method. For the mth DOF of the original system, the proposed scaling method involves the following steps:

1. Extract frequencies f_k and determine the modal contribution factors X_k, $k = 1, 2, \ldots, \mathcal{N}$, of the significant modes of the underlying structure from the available $\mathcal{S}_{\text{G-I}}(f, \zeta_0)$ and $\mathcal{S}_{\text{F-I}}(f, \zeta_0)$, as presented in Section 3.2.
2. Using the extracted dynamical information of the underlying structure,
   - **Scaling problem 1:** scale $\mathcal{S}_{\text{F-I}}(f, \zeta_0)$ to generate $\mathcal{S}_{\text{F-I}}(f, \zeta_0')$ for required damping values ζ_0'.
   - **Scaling problem 2:** scale $\mathcal{S}_{\text{F-I}}(f, \zeta_0)$ to generate $\mathcal{S}_{\text{F-II}}(f, \zeta_0')$, corresponding to the new GRS $\mathcal{S}_{\text{G-II}}(f, \zeta_0)$, for required damping values ζ_0'.

3.3.1 Scaling GRS to Different Damping Ratios

In contrast to the primary structures in nuclear power plants, whose modal damping ratios are usually from 5% to 7%, components and various types of equipment are generally made of different materials so that their damping ratios can range from 2% to 15%. In order to assess the seismic demands for different types of equipment accurately, GRS and FRS with the corresponding damping ratios are needed.

Based on equation (2.2.42) for the modal response

$$\left|\ddot{u}_{0,k}\right|^2_{\max} = \left[\mathcal{AF}_{0,k}\, \mathcal{S}_{\text{G}}(\omega_0, \zeta_0)\right]^2 + \left[\mathcal{AF}_k\, \mathcal{S}_{\text{G}}(\omega_k, \zeta_k)\right]^2, \tag{3.3.1}$$

it can be anticipated that the change of the equipment damping ratio ζ_0 will affect the the amplification factors $\mathcal{AF}_{0,k}$ and $\mathcal{AF}_k$, as well as the ground input $\mathcal{S}_{\text{G}}(\omega_0, \zeta_0)$. It was demonstrated that the damping effect on the amplification factors are negligible for non-tuning cases (Jiang *et al.*, 2015). When the equipment is relatively much stiffer than the structure, the modal response of the structure-equipment system is reduced to the structural modal response $\mathcal{S}_{\text{G}}(\omega_k, \zeta_k)$. As a result, the equipment damping ratio has no effect in this case. When the equipment is relatively much more flexible than the structure, the modal response of the structure-equipment system is reduced to the response of the equipment

supported directly on the ground, i.e., $\mathcal{S}_{\mathrm{G}}(\omega_0, \zeta_0)$. Consequently, the effect damping effect on FRS is the same as that on GRS.

However, the most-common standards and codes, such as ASCE 43-05 (2005), NUREG CR-0098 (1978), and CSA N289.3 (2010), provide GRS for only 5% damping. Therefore, Damping Correction Factors (DCF) defined as

$$\mathcal{D}(\omega; \zeta_0, \zeta_0') = \frac{\mathcal{S}_{\mathrm{G}}(\omega, \zeta_0')}{\mathcal{S}_{\mathrm{G}}(\omega, \zeta_0)} \tag{3.3.2}$$

is used to adjust GRS $\mathcal{S}_{\mathrm{G}}(\omega, \zeta_0)$ corresponding to $\zeta_0 = 5\%$ damping ratio to GRS $\mathcal{S}_{\mathrm{G}}(\omega, \zeta_0')$ of another damping level ζ_0'. A comprehensive study on DCF for horizontal GRS was conducted by Cameron and Green (2007), in which DCF is tabulated for various damping ratios, site conditions, and earthquake magnitudes.

3.3.2 Generating FRS for Different Damping Ratios Using the Direct Method

Consider the underlying structure with the significant modes identified in Section 3.2 under the excitation of $\mathcal{S}_{\mathrm{G}}(\omega, \zeta_0)$. For the tuning case when $\omega_0 = \omega_k$, the maximum absolute acceleration of an oscillator with frequency ω_0 and damping ζ_0 due to excitation of the kth mode is given by equation (2.2.35) with the equivalent damping ratio given by equation (2.2.36), which can be written as, using equation (3.3.2),

$$\left|\ddot{u}_{0,k}\right|_{\max} = \frac{\sqrt{\mathcal{D}(\omega_0; \zeta_k, \zeta_0)^2 + 1}}{2\,\zeta_{\mathrm{e}}}\, \mathcal{S}_{\mathrm{G}}(\omega_0, \zeta_k). \tag{3.3.3}$$

For $\zeta_0 = \zeta_k$, $\mathcal{D}(\omega_0; \zeta_k, \zeta_0) = 1$, the modal response reduces to $\left|\ddot{u}_{0,k}\right|_{\max} = \mathcal{S}_{\mathrm{G}}(\omega_0, \zeta_k)/(\sqrt{2}\,\zeta_{\mathrm{e}})$.

From equation (3.3.3), the ratio of the modal responses with equipment damping ratio ζ_0' to the modal response with equipment damping ratio ζ_0 is given by

$$\frac{\left|\ddot{u}_{0,k}'\right|_{\max}}{\left|\ddot{u}_{0,k}\right|_{\max}} = \sqrt{\frac{\mathcal{D}(\omega_0; \zeta_k, \zeta_0')^2 + 1}{2}} \cdot \frac{\zeta_{\mathrm{e}}}{\zeta_{\mathrm{e}}'}, \tag{3.3.4}$$

where ζ_{e}' is the equivalent damping coefficient corresponding to modal damping ζ_k and equipment damping $\zeta_0' \neq \zeta_k$.

Since the physical meaning of tRS is the modal response of an equipment-structure system in perfect-tuning, equation (3.3.4) can be written as

$$\frac{\mathcal{S}_{\mathrm{G}}(\omega_0, \zeta_0' \neq \zeta_k)}{\mathcal{S}_{\mathrm{G}}^{\mathrm{t}}(\omega_0, \zeta_0 = \zeta_k)} = \sqrt{\frac{\mathcal{D}(\omega_0; \zeta_k, \zeta_0')^2 + 1}{2}} \cdot \frac{\zeta_{\mathrm{e}}}{\zeta_{\mathrm{e}}'}, \tag{3.3.5}$$

where, following Jiang *et al.* (2015),

$$\mathcal{S}_{\mathrm{G}}^{\mathrm{t}}(\omega_0, \zeta_0 = \zeta_k) = \frac{1}{2} \cdot \left| \frac{\partial \dot{u}_k(\zeta_k)}{\partial \zeta_k} \right|_{\max}, \tag{3.3.6a}$$

$$\mathcal{S}_{\mathrm{G}}(\omega_0, \zeta_0' \neq \zeta_k) = \frac{1}{2} \cdot \left| \frac{\dot{u}_k(\zeta_0') - \dot{u}_k(\zeta_k)}{\zeta_0' - \zeta_k} \right|_{\max}. \tag{3.3.6b}$$

To determine $\mathcal{S}_{\mathrm{G}}(\omega_0, \zeta_0' \neq \zeta_k)$, consider the maximum modal velocity $\dot{u}_k(\zeta)$, which decreases monotonically with the modal damping ratio ζ_k, as illustrated in Figure 3.4 (without loss of generality, the case of $\zeta_0' > \zeta_k$ is shown):

- From equation (3.3.6a), tRS $\mathcal{S}_{\mathrm{G}}^{\mathrm{t}}(\omega_0, \zeta_0 = \zeta_k)$ and $\mathcal{S}_{\mathrm{G}}^{\mathrm{t}}(\omega_0, \zeta_0' \neq \zeta_k)$ are equal to half of the slopes of the tangent line at point A (with $\zeta_0 = \zeta_k$) and point B (with $\zeta_0' \neq \zeta_k$), respectively.
- From equation (3.3.6b), $\mathcal{S}_{\mathrm{G}}(\omega_0, \zeta_0' \neq \zeta_k)$ is equal to half of the slope of the secant connecting points A and B.
- From the Mean Value Theorem in calculus, there exists $\bar{\zeta}$ between ζ_0 and ζ_0' such that

$$\mathcal{S}_{\mathrm{G}}^{\mathrm{t}}(\omega_0, \bar{\zeta}) = \mathcal{S}_{\mathrm{G}}(\omega_0, \zeta_0' \neq \zeta_k), \tag{3.3.7}$$

  where $\bar{\zeta} = \alpha \cdot \zeta_0' + (1-\alpha) \cdot \zeta_k$, $0 < \alpha < 1$, i.e., the slope of the tangent line at some point C (with $\bar{\zeta}$) is equal to the slope of the secant connecting points A and B.

An in-depth parametric study is performed to quantify the relationship between $\mathcal{S}_{\mathrm{G}}(\omega_0, \zeta_0' \neq \zeta_k)$ and $\mathcal{S}_{\mathrm{G}}^{\mathrm{t}}(\omega_0, \bar{\zeta})$. It is found that, when $\alpha = 0.5$ in which $\bar{\zeta}$ represents the average damping ratio of equipment and structure modes, equation (3.3.7) gives sufficiently accurate approximations for $\mathcal{S}_{\mathrm{G}}(\omega_0, \zeta_0' \neq \zeta_k)$ over the frequency range from 0.1 Hz to 100 Hz. It is anticipated that the accuracy of this approximation will be affected by the damping ratio difference $\Delta\zeta = |\zeta_0' - \zeta_k|$; therefore, a correction factor is introduced in equation (3.3.7) to

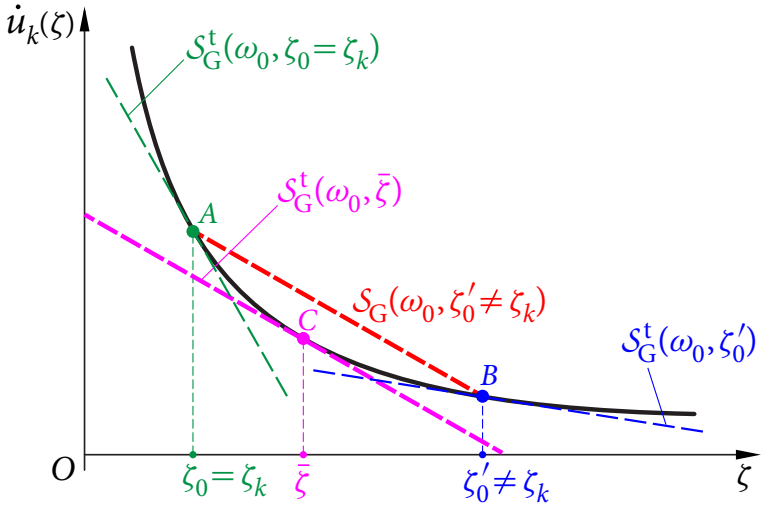

Figure 3.4 t-spectrum correction factor

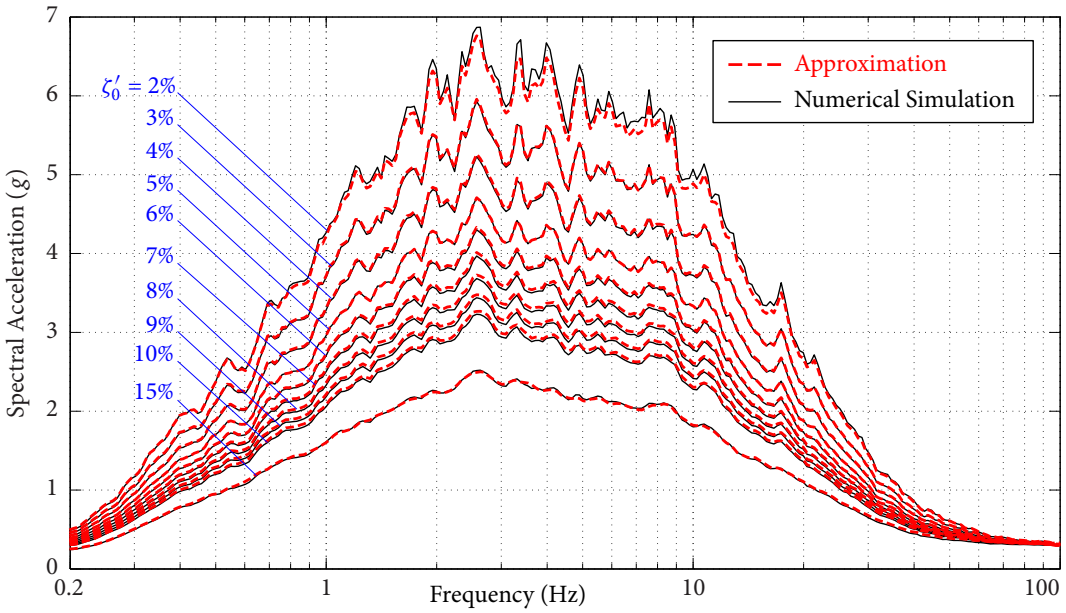

Figure 3.5 Comparison of approximate $\mathcal{S}_G(\omega_0, \zeta_0')$ with numerical simulation

yield

$$\mathcal{S}_G(\omega_0, \zeta_0' \neq \zeta_k) = \mathcal{S}_G^t(\omega_0, \bar{\zeta}) \cdot \left(1 + \left|\zeta_0' - \zeta_k\right|\right), \quad \bar{\zeta} = \frac{1}{2}(\zeta_0' + \zeta_k). \tag{3.3.8}$$

Figure 3.5 shows a comparison of $\mathcal{S}_G(\omega_0, \zeta_0' \neq \zeta_k)$ approximated by equation (3.3.8) and the mean value calculated by numerical simulations from 30 time histories compatible with 5% USNRC R.G. 1.60 GRS (1973), where the damping ratio of structural mode $\zeta_k = 5\%$, and

the equipment damping ratio ζ_0' varies from 2% to 15%. It can be concluded that equation (3.3.8) provides excellent approximations over the entire frequency range and for various equipment damping ratios. It is observed that the responses are more sensitive for lower equipment damping ratios, say $\zeta_0' < 5\%$.

From equations (3.3.5) and (3.3.8) the equivalent damping ratio $\zeta_{k,\mathrm{e}}'$ for modal damping ζ_k and any equipment damping ratio ζ_0' can be obtained as

$$\zeta_{\mathrm{e}}' = \zeta_{\mathrm{e}} \cdot \frac{\mathcal{S}_{\mathrm{G}}^{\mathrm{t}}(\omega_0, \zeta_k)}{\mathcal{S}_{\mathrm{G}}^{\mathrm{t}}\big(\omega_0, \frac{1}{2}(\zeta_0'+\zeta_k)\big) \cdot \big(1+\big|\zeta_0'-\zeta_k\big|\big)} \cdot \sqrt{\frac{\mathcal{D}(\omega_0;\zeta_k,\zeta_0')^2+1}{2}}. \tag{3.3.9}$$

The method for determining tRS $\mathcal{S}_{\mathrm{G}}^{\mathrm{t}}(\omega_0, \zeta)$ for any frequencies and damping ratios is well developed in Li *et al.*, 2015, whereas DCF $\mathcal{D}(\omega_0;\zeta_k,\zeta_0')$ is tabulated in Cameron and Green (2007).

FRS of the mth DOF of the original structure for damping ratio ζ_0' can then be obtained using equations (2.2.35), (2.2.36), (2.2.42) and (2.2.43):

$$[\mathcal{S}_{\mathrm{F}}(\omega_0, \zeta_0')]^2 = \sum_{k=1}^{\mathcal{N}} \sum_{\kappa=1}^{\mathcal{N}} \rho_{k\kappa}\, R_k R_\kappa, \tag{3.3.10}$$

where

$$\begin{gathered} R_k = X_k \sqrt{[\mathit{AF}_{0,k}\, \mathcal{S}_{\mathrm{G}}(\omega_0, \zeta_0')]^2 + [\mathit{AF}_k\, \mathcal{S}_{\mathrm{G}}(\omega_k, \zeta_k)]^2}, \\ \mathit{AF}_{0,k} = \frac{r_k^2}{\sqrt{(1-r_k^2)^2 + (2\,\zeta_{\mathrm{e}}' r_k)^2}}, \quad \mathit{AF}_k = \frac{1}{\sqrt{(1-r_k^2)^2 + (2\,\zeta_{\mathrm{e}}' r_k)^2}}, \quad r_k = \frac{\omega_k}{\omega_0}, \end{gathered} \tag{3.3.11}$$

and the equivalent damping ratio ζ_{e}' is given by equation (3.3.9).

3.3.3 Scaling Problem 1

Given $\mathcal{S}_{\text{G-I}}(f, \zeta_0)$, the procedure of scaling $\mathcal{S}_{\text{F-I}}(f, \zeta_0)$ to $\mathcal{S}_{\text{F-I}}(f, \zeta_0')$ for a desired damping value ζ_0' is as follows:

1. **System Identification:** Identify significant modes from $\mathcal{S}_{\text{G-I}}(f, \zeta_0)$ and $\mathcal{S}_{\text{F-I}}(f, \zeta_0)$ and obtain frequencies f_k and modal contribution factors X_k, $k = 1, 2, \ldots, \mathcal{N}$.

2. **Direct Method:** Using the direct method, equations (3.3.9) to (3.3.11), from $\mathcal{S}_{\text{G-I}}(f, \zeta_0)$ determine $\mathcal{S}^{\text{D}}_{\text{F-I}}(f, \zeta_0)$ and $\mathcal{S}^{\text{D}}_{\text{F-I}}(f, \zeta_0')$ for the desired damping ratio ζ_0', where the superscript "D" stands for "Direct Method".
3. **Scaling FRS**
   - If $\mathcal{S}_{\text{F-I}}(f, \zeta_0)$ is raw FRS, determine the scaling factor as

$$\mathcal{R}^{\text{FRS-I}}(f, \zeta_0, \zeta_0') = \frac{\mathcal{S}^{\text{D}}_{\text{F-I}}(f, \zeta_0')}{\mathcal{S}^{\text{D}}_{\text{F-I}}(f, \zeta_0)}. \tag{3.3.12}$$

     The scaled FRS-I for damping ratio ζ_0' is obtained from the available $\mathcal{S}_{\text{F-I}}(f, \zeta_0)$ as

$$\mathcal{S}_{\text{F-I}}(f, \zeta_0') = \mathcal{R}^{\text{FRS-I}}(f, \zeta_0, \zeta_0') \times \mathcal{S}_{\text{F-I}}(f, \zeta_0). \tag{3.3.13}$$

   - If $\mathcal{S}_{\text{F-I}}(f, \zeta_0)$ has been broadened and smoothed, the scaling factor (3.3.12) is not used in this case, since the broadened-and-smoothed FRS-I contains a large amount of artificially modified information which is inappropriate to use for scaling. $\mathcal{S}^{\text{D}}_{\text{F-I}}(f, \zeta_0')$ is used as $\mathcal{S}_{\text{F-I}}(f, \zeta_0')$.
   - $\mathcal{S}_{\text{F-I}}(f, \zeta_0')$ is then broadened and smoothed as needed.

3.3.4 Scaling Problem 2

Given $\mathcal{S}_{\text{G-I}}(f, \zeta_0)$ and $\mathcal{S}_{\text{F-I}}(f, \zeta_0)$, the procedure of scaling $\mathcal{S}_{\text{F-I}}(f, \zeta_0)$ to obtain $\mathcal{S}_{\text{F-II}}(f, \zeta_0')$ for a new $\mathcal{S}_{\text{G-II}}(f, \zeta_0)$ and desired damping value ζ_0' is as follows:

1. **System Identification:** Identify significant modes from $\mathcal{S}_{\text{G-I}}(f, \zeta_0)$ and $\mathcal{S}_{\text{F-I}}(f, \zeta_0)$ and obtain frequencies f_k and modal contribution factors X_k, $k = 1, 2, \ldots, \mathcal{N}$.
2. **Direct Method:** Using the direct method, equations (3.3.9) to (3.3.11), determine
   - $\mathcal{S}^{\text{D}}_{\text{F-I}}(f, \zeta_0)$ from $\mathcal{S}_{\text{G-I}}(f, \zeta_0)$,
   - $\mathcal{S}^{\text{D}}_{\text{F-II}}(f, \zeta_0')$ from $\mathcal{S}_{\text{G-II}}(f, \zeta_0)$ and for the desired damping ratio ζ_0'.
3. **Scaling FRS**
   - If $\mathcal{S}_{\text{F-II}}(f, \zeta_0)$ is raw FRS, determine the scaling factor as

$$\mathcal{R}^{\text{FRS-II}}(f, \zeta_0, \zeta_0') = \frac{\mathcal{S}^{\text{D}}_{\text{F-II}}(f, \zeta_0')}{\mathcal{S}^{\text{D}}_{\text{F-I}}(f, \zeta_0)}. \tag{3.3.14}$$

The scaled FRS-II for $\mathcal{S}_{\text{G-II}}(f, \zeta_0)$ and for damping ratio ζ_0' is obtained from the available $\mathcal{S}_{\text{F-I}}(f, \zeta_0)$ as

$$\mathcal{S}_{\text{F-II}}(f, \zeta_0') = \mathcal{R}^{\text{FRS-II}}(f, \zeta_0, \zeta_0') \times \mathcal{S}_{\text{F-I}}(f, \zeta_0). \tag{3.3.15}$$

- If $\mathcal{S}_{\text{F-I}}(f, \zeta_0)$ has been broadened and smoothed, the scaling factor (3.3.14) is not used. $\mathcal{S}^{\text{D}}_{\text{F-II}}(f, \zeta_0')$ is used as $\mathcal{S}_{\text{F-II}}(f, \zeta_0')$.
- $\mathcal{S}_{\text{F-II}}(f, \zeta_0')$ is then broadened and smoothed as needed.

3.4 Numerical Application

To verify the accuracy and demonstrate the efficiency of the proposed scaling methods for generating FRS, numerical examples are presented for the two scaling problems.

A typical service building in nuclear power plants is selected as the primary structure. A three-dimensional finite element model of the building is established by the commercial finite element analysis software *STARDYNE*, as shown in Figure 2.13. Details about the model were described in Chapter 2. Two types of ground response spectra, i.e., USNRC R.G. 1.60 GRS (1973) and Standard Uniform Hazard Spectra (UHS) for Central and Eastern North America (CENA) (Atkinson and Elgohary, 2007), between which significant differences exist in the spectral shapes, are considered as GRS-I and GRS-II, respectively. Figure 3.6 illustrates the two GRS with 5% damping ratio anchored at $0.3g$ peak ground acceleration (PGA). It can be observed that USNRC R.G. 1.60 GRS possesses more intermediate frequency content (1-10 Hz), whereas CENA UHS are abundant in high frequency range (20-50 Hz).

In this study, 30 sets of tri-directional spectrum-compatible time histories are generated using the Hilbert-Huang Transform method (Ni *et al.*, 2011; Ni *et al.*, 2013) for each GRS type. FRS at two nodes as indicated in Figure 2.13 are obtained through performing numerical time history analyses of the structure, and the mean FRS from the 30 sets of simulations are considered as "exact" FRS at the locations. Herein, only the mean FRS with 5% damping ratio produced by time histories compatible with USNRC R.G. 1.60 GRS are treated as available FRS-I; all other mean FRS will be used as benchmark for validating the proposed scaling method.

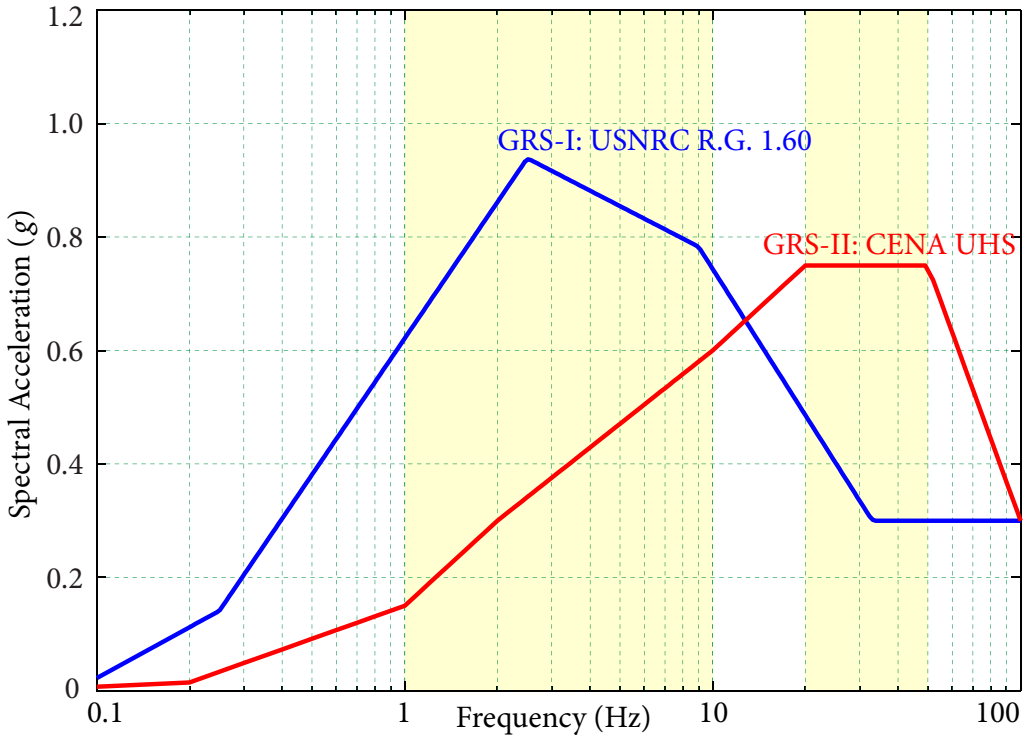

Figure 3.6 Two types of input ground response spectra

3.4.1 Equivalent Modal Information

In this Section, modal information of the equivalent structural modes is identified from the existing FRS-I using the method developed in Section 3.2.

The exact FRS-I at Node 1 with 5% damping ratio is shown as the black dashed line in Figure 3.7, which is considered as the available $\mathcal{S}_{\text{F-I}}(f, \zeta_0 = 5\%)$. It can be seen that there are three peaks located around 2.5 Hz, 5.8 Hz, and 18 Hz, where significant modes generally exist. It is also observed that the second peak has a wider band, indicating that there may exist multiple closely-spaced modes in the range from 5.5 to 7.5 Hz. In addition, it should be noted that, although the third peak is relatively lower, flat and wide, some significant modes may exist in higher frequency range (20 to 30 Hz), since GRS-I has lower spectral values and decreases drastically in this range. Hence, the first question arises from implementing the proposed method is choosing a suitable number of significant equivalent modes.

Number of Significant Equivalent Modes

It is discussed in Section 3.2 that the number of equivalent modes can be equal to or larger than the number of FRS peaks. In order to study the effect of the number of equivalent modes, FRS-I is approximated by 3, 4, 5, and 6 equivalent modes using the proposed method for system identification. The circles in Figures 3.7 to 3.10 represent the critical points used for locating the frequencies of significant equivalent modes and the corresponding spectral accelerations. All the critical points are selected at the FRS peaks or the knees of the curve, and the number of critical points is equal to the number of significant equivalent modes. The coordinates of the critical points and modal information of the identified equivalent modes are listed in Table 3.1, where f_k, $\mathcal{S}_k$, and X_k denote the frequencies, spectral accelerations, and contribution factors of the equivalent modes, respectively. An appropriate way of verifying the accuracy of the extracted equivalent modal information is using the modal information to reproduce FRS-I. The colored solid lines in Figures 3.7 to 3.10 are the FRS-I generated through the direct spectra-to-spectra method using the equivalent modal information.

Some remarkable features can be observed from Figures 3.7 to 3.10 and Table 3.1:

1. All the reproduced FRS-I agree well with the exact FRS-I. The FRS match perfectly at the critical points, the information of which are employed for the nonlinear constraints in equation (3.2.6). The FRS at other points generally converge to the exact values as the number of modes increases, and 5-equivalent-mode approximation can give sufficient accuracy.
2. Comparing Figures 3.7 to 3.10, assuming multiple closely-spaced modes at the second peak, where the relatively wider peak occurs, can give better approximation as anticipated.
3. One exception is that the 4-mode approximation does not produce a better result than the 3-mode approximation. This phenomenon can be explained by the equivalent modal information listed in Table 3.1. From the sum of the contribution factors, it is seen that the optimal solutions for the 4-mode approximation are weakly satisfactory to model the real physical structural system in this case. However, it will be seen that

these discrepancies do not have a significant effect when scaling factors are employed to generate FRS-II in the following examples.

4. In spite of lower spectral acceleration in higher frequency range (20 to 30 Hz), the contribution factors of these modes are considerably large. In the following examples, it will be seen that these modes have a significant effect when scaling FRS-I to FRS-II, which corresponds to a GRS-II with rich high-frequency content.

Table 3.1 Equivalent Modal information at Node 1

	3-Mode Approximation			4-Mode Approximation		
Mode	f_k (Hz)	$\mathcal{S}_k$ (g)	X_k	f_k (Hz)	$\mathcal{S}_k$ (g)	X_k
1	2.6	2.33	0.41045	2.6	2.33	0.42045
2	5.8	1.82	0.35426	5.8	1.82	0.36846
3	17.5	0.72	0.20915	17.5	0.72	0.18337
4				26.0	0.62	−0.18246
		$\sum X_k$	0.974		$\sum X_k$	0.790

	5-Mode Approximation			6-Mode Approximation		
Mode	f_k (Hz)	$\mathcal{S}_k$ (g)	X_k	f_k (Hz)	$\mathcal{S}_k$ (g)	X_k
1	2.6	2.33	0.40911	2.6	2.33	0.40814
2	5.8	1.82	0.34412	5.8	1.82	0.31816
3	7.2	1.44	0.21987	6.6	1.50	0.12831
4	17.5	0.72	−0.17889	7.2	1.45	0.12149
5	26.0	0.62	0.17037	17.0	0.72	−0.17207
6				26.0	0.62	0.17321
		$\sum X_k$	0.965		$\sum X_k$	0.977

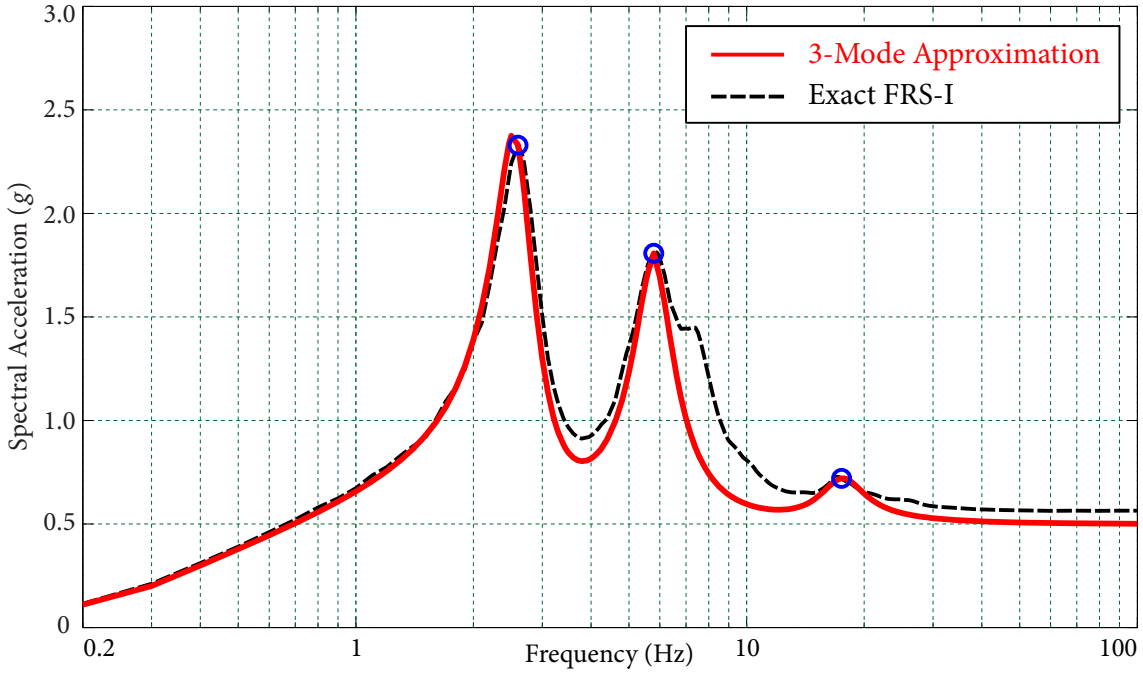

Figure 3.7 3 Equivalent Modes Approximation of FRS-I at Node 1

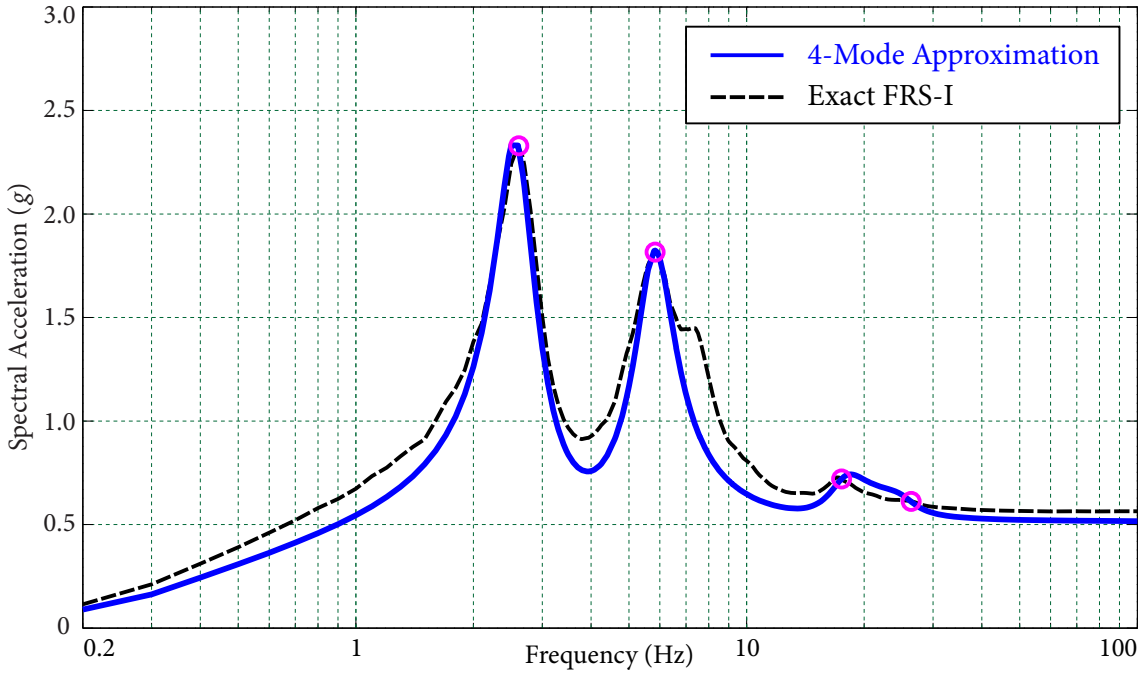

Figure 3.8 4 Equivalent Modes Approximation of FRS-I at Node 1

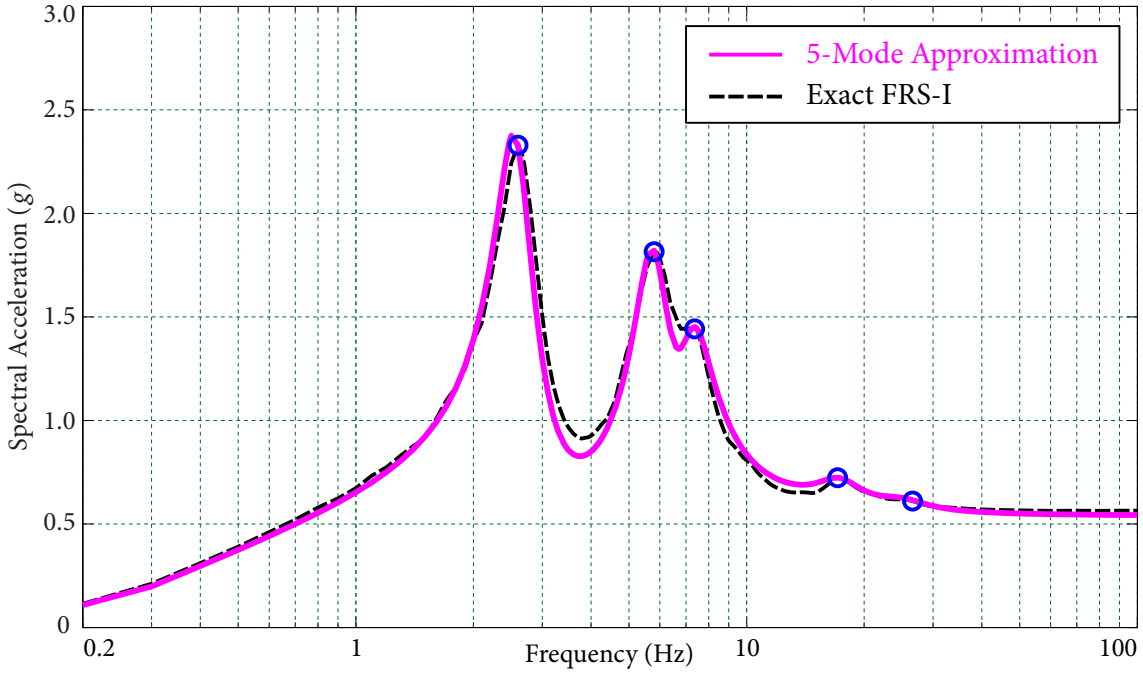

Figure 3.9 5 Equivalent Modes Approximation of FRS-I at Node 1

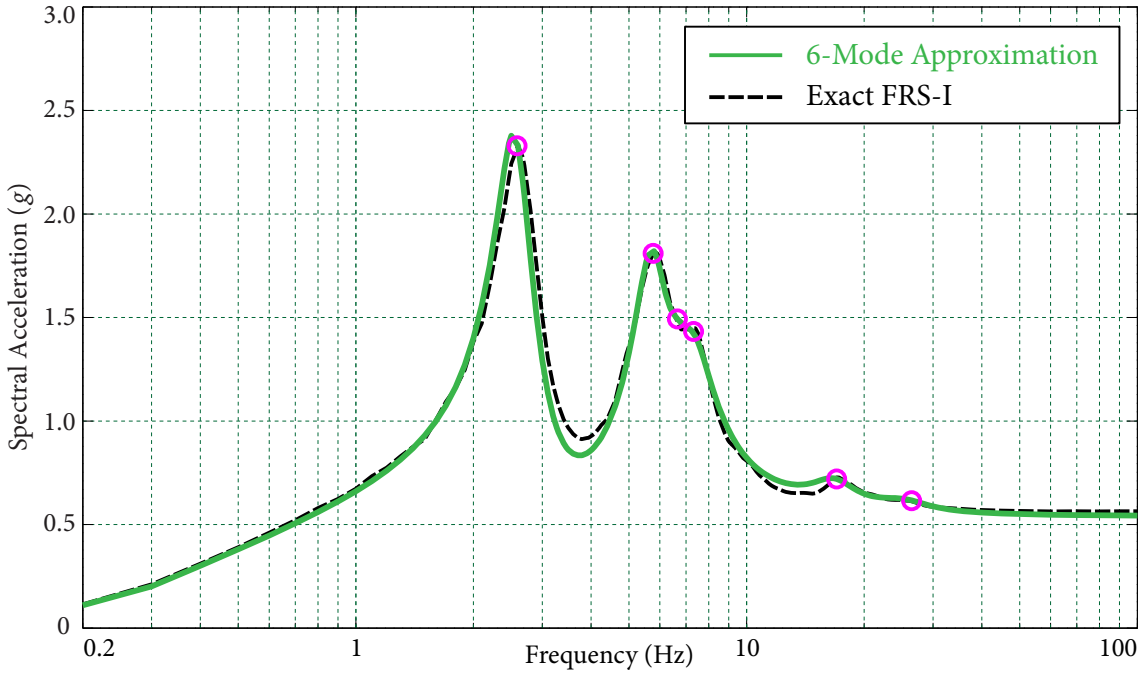

Figure 3.10 6 Equivalent Modes Approximation of FRS-I at Node 1

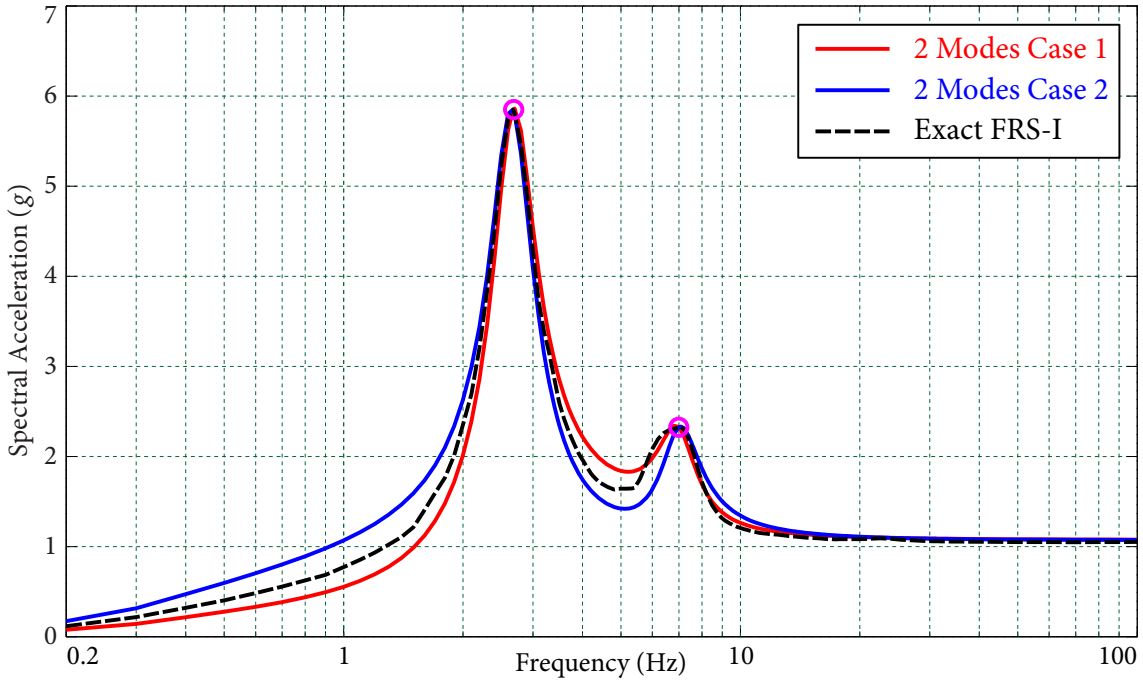

Figure 3.11 2 Equivalent Modes Approximation of FRS-I at Node 2

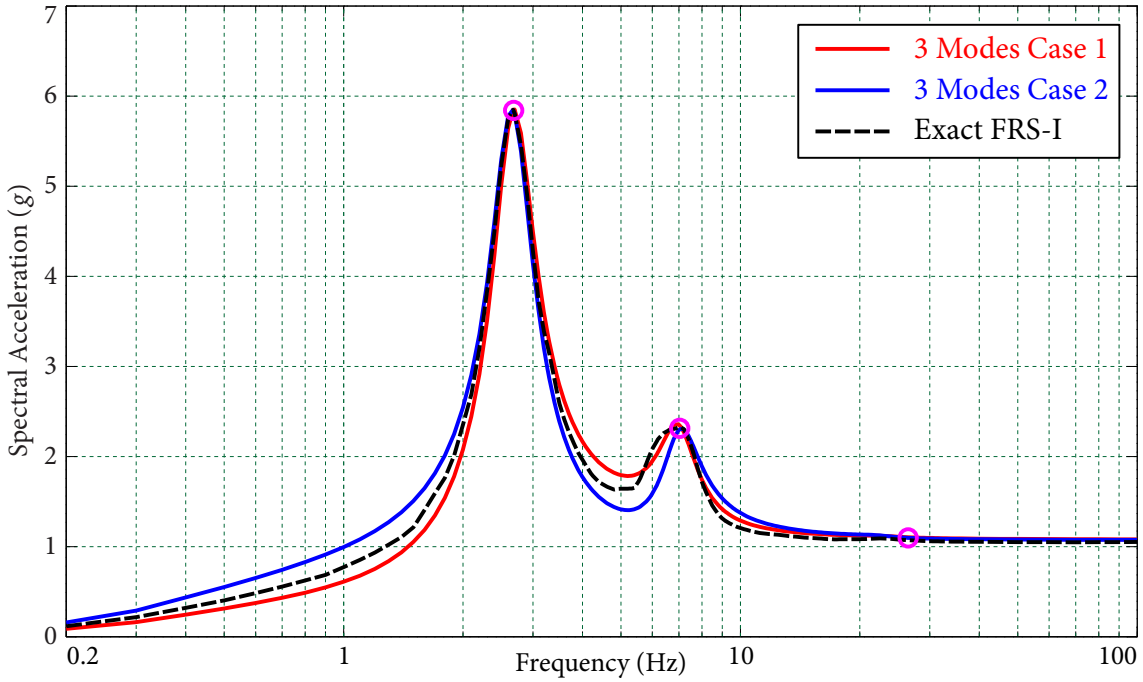

Figure 3.12 3 Equivalent Modes Approximation of FRS-I at Node 2

Multiple Solutions

In some cases, there may be multiple solutions for the optimization problem. The black dash line in Figure 3.11 shows the exact FRS-I at Node 2, which possesses two normal peaks. The equivalent modal information at Node 2 is identified by 2- and 3-mode approximations, as listed in Table 2. Two sets of solutions are obtained for each approximation. The accuracy of the identified modal information is again verified by reproducing FRS-I using the extracted information in the direct spectra-to-spectra method. The red and blue solid lines in Figures 3.11 and 3.12 represent the reproduced FRS-I based on the two sets of equivalent modal information. Some observations from Figures 3.11, 3.12, and Table 3.2 are:

1. The sum of the contribution factors for each solution set is quite different from 1.0 (for the real modal information of structure) for each approximation.
2. As the number of equivalent modes increases, the two sets of solutions approach the real modal information of the structure, and the reproduced FRS-I thus converge to the exact FRS-I.
3. The discrepancies of the reproduced FRS-I mainly occur at low frequency range (far less than the natural frequency of the first dominant mode) and the valley between the two peaks. However, these discrepancies do not have a significant effect when scaling factors are used to scale FRS, as shown in the following examples.

Table 3.2 Equivalent Modal information at Node 2

	2-Mode Approximation				3-Mode Approximation			
Mode	f_k (Hz)	$\mathcal{S}_k$ (g)	X_k Set-1	X_k Set-2	f_k (Hz)	$\mathcal{S}_k$ (g)	X_k Set-1	X_k Set-2
1	2.676	5.850	1.10103	1.08536	2.676	5.850	1.10028	1.08801
2	7.000	2.324	−0.41993	0.43529	7.000	2.324	−0.43149	0.42562
3					23.500	1.100	0.10966	−0.11178
		$\sum X_k$	0.681	1.521		$\sum X_k$	0.778	1.402

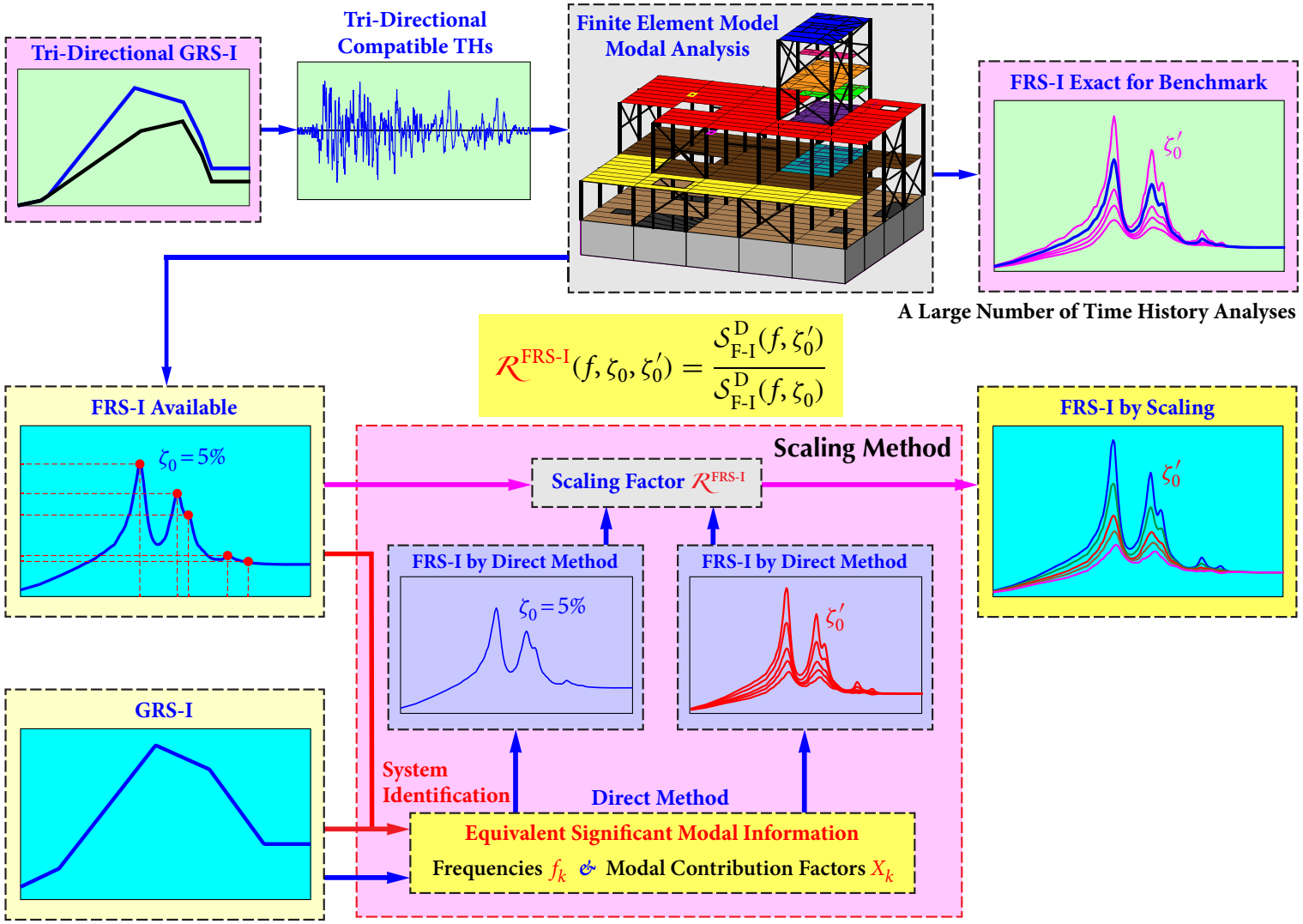

Figure 3.13 Procedure of scaling problem 1

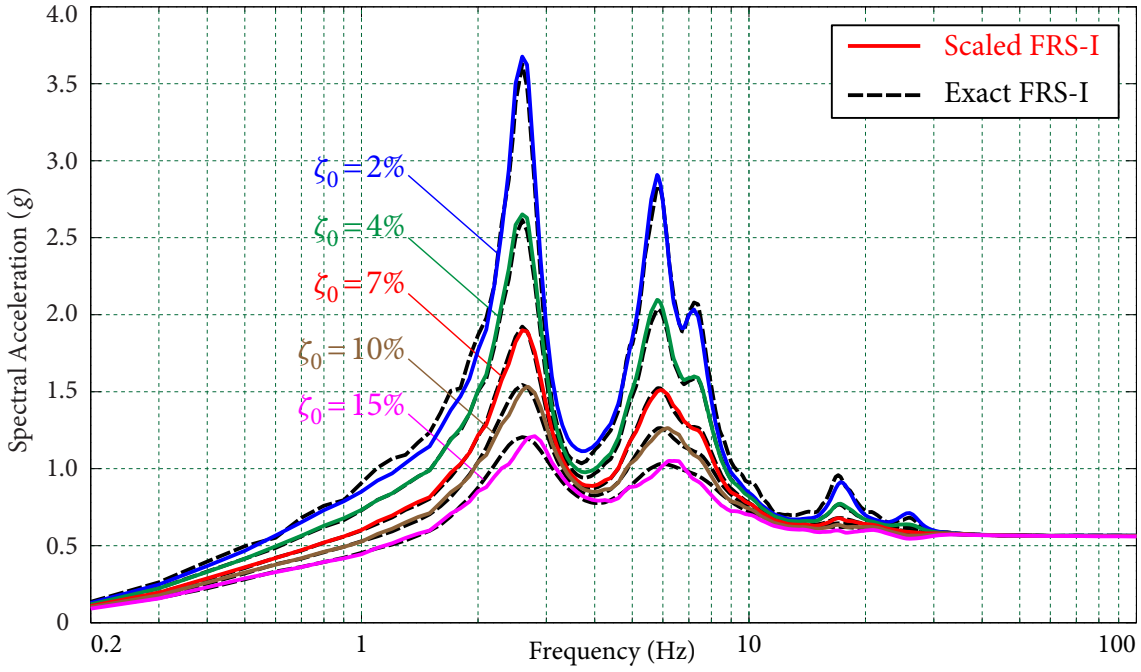

Figure 3.14 Scaling FRS-I with various damping ratios at Node 1

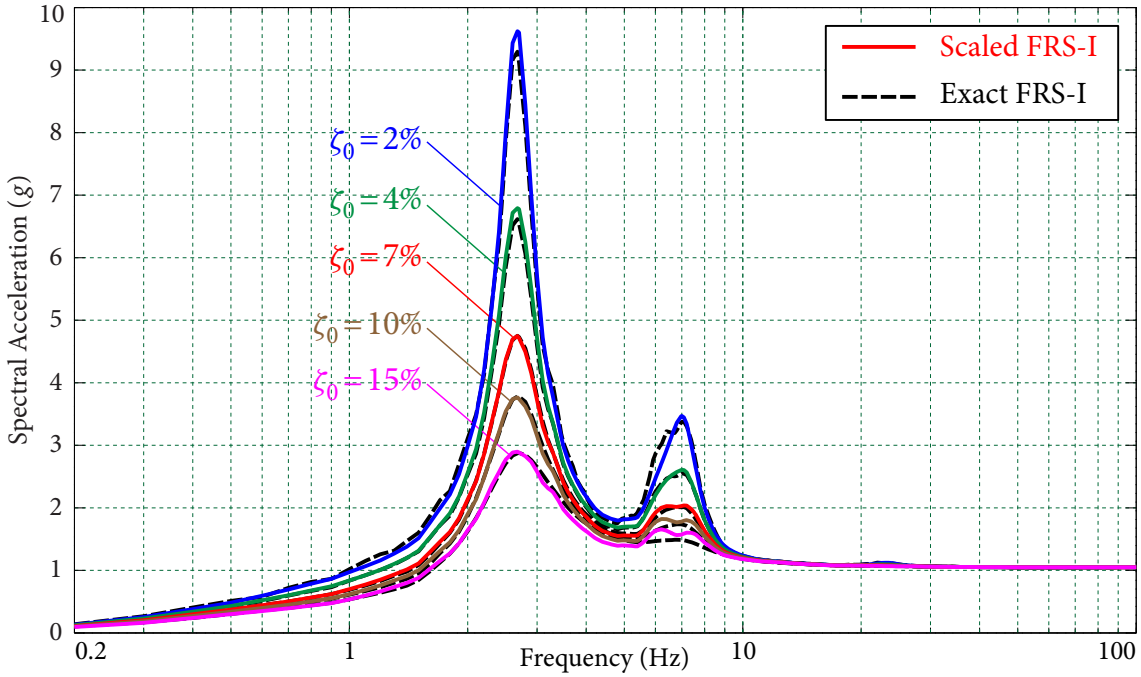

Figure 3.15 Scaling FRS-I to various damping ratios at Node 2

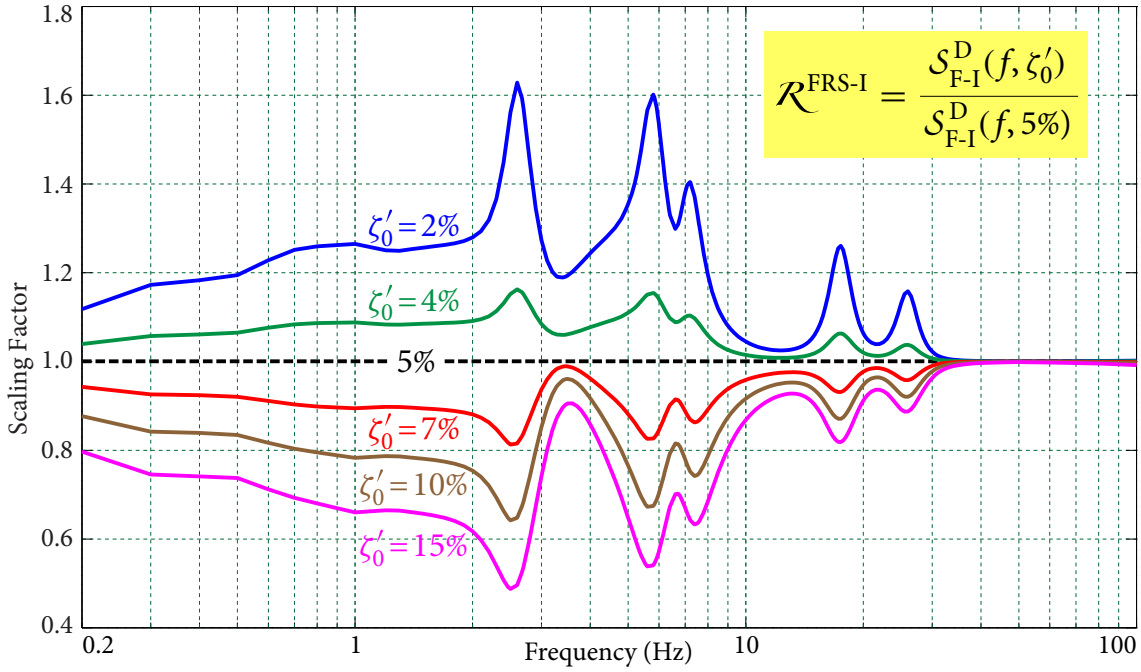

Figure 3.16 Scaling factors for various damping ratios at Node 1

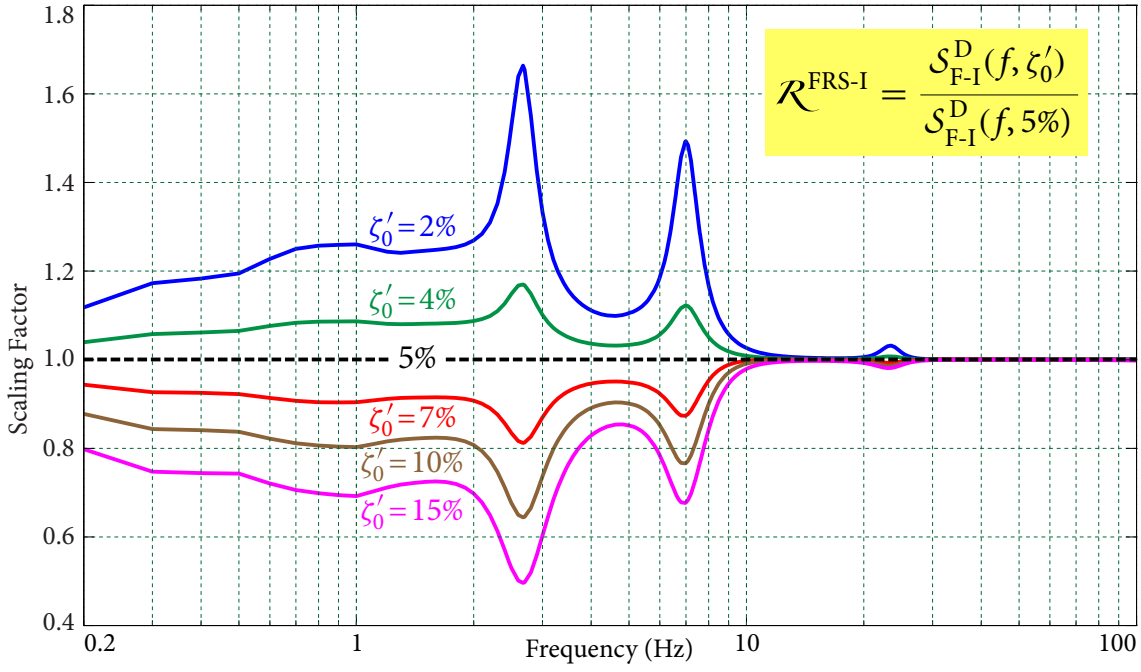

Figure 3.17 Scaling factors for various damping ratios at Node 2

3.4.2 Scaling Problem 1 – Scaling FRS to Various Damping Ratios

Based on the above validation of identified equivalent modal information, 5- and 3-mode approximations are applied to generate the scaling factors given by equation (3.3.12) for scaling FRS-I with 5% damping ratio to FRS with other damping ratios at Nodes 1 and 2, respectively. Then, multiplying the scaling factors with the exact FRS-I results in FRS with other damping ratios. The procedure for scaling problem 1 is illustrated in Figure 3.13.

Figures 3.14 and 3.15 show the comparison of the "exact" FRS (obtained from the mean of 30 time history analyses) and FRS obtained from the proposed scaling method, for 2%, 4%, 7%, 10%, and 15% equipment damping ratios, at the two nodes. It is seen that the scaled FRS agree excellently with the exact FRS over the entire frequency range and for various damping ratios.

Scaling factors for the two nodes are plotted in Figures 3.16 and 3.17. It is important to note that the shapes of the scaling factors are quite similar to the shapes of the FRS which are functions of frequency and damping ratio. Furthermore, peaks emerge at the natural frequencies of the equivalent modes, which indicates that the scaling of FRS depends on the modal information of the structure. Therefore, using a constant scaling factor to scale FRS will lead to inconsistent conservatism or underestimation in any situations. At low frequencies, the scaling factors are nearly constant since FRS are close to GRS based on the physical interpretation of the formula of the direct spectra-to-spectra method (Jiang *et al.*, 2015). In very high frequency range, scaling factors converge to 1 as FRS approach the structural responses at the node, which are independent of the equipment damping ratios.

3.4.3 Scaling Problem 2 – Scaling FRS for Different GRS

For Scaling Problem 2, i.e., scaling $\mathcal{S}_{\text{F-I}}(f, \zeta_0)$ corresponding to $\mathcal{S}_{\text{G-I}}(f, \zeta_0)$ to obtain $\mathcal{S}_{\text{F-II}}(f, \zeta_0')$ corresponding to $\mathcal{S}_{\text{G-II}}(f, \zeta_0)$, the scaling factors are determined using equation (3.3.14). The procedure for scaling problem 2 is illustrated in Figure 3.18.

For Node 1, the scaling factors are calculated using the modal information approximated by 3, 4, 5 and 6 equivalent modes; the reproduced FRS-II using the equivalent modal information in the scaling method are compared with the exact FRS-II in Figures 3.19 to

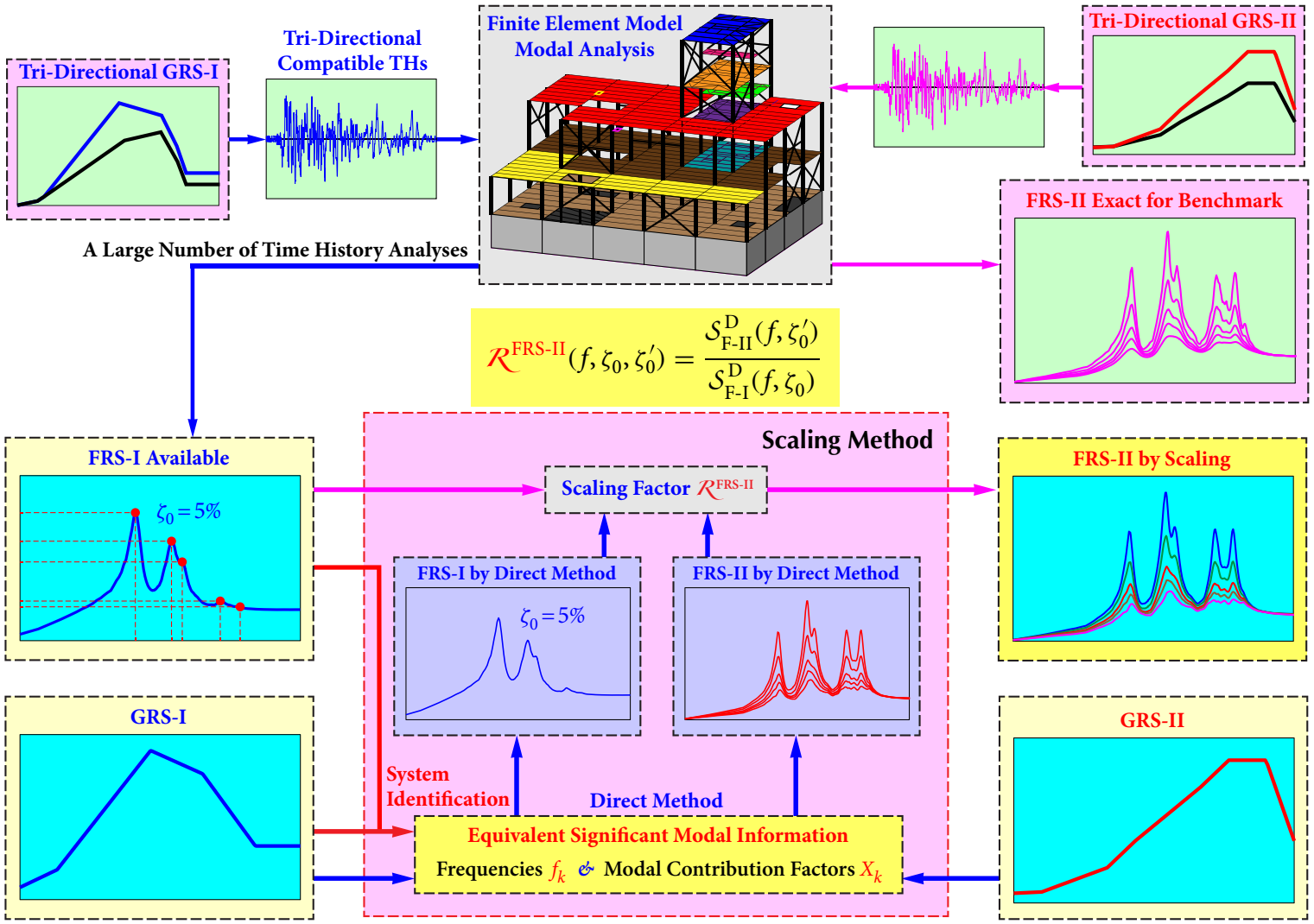

Figure 3.18 Procedure of scaling problem 2

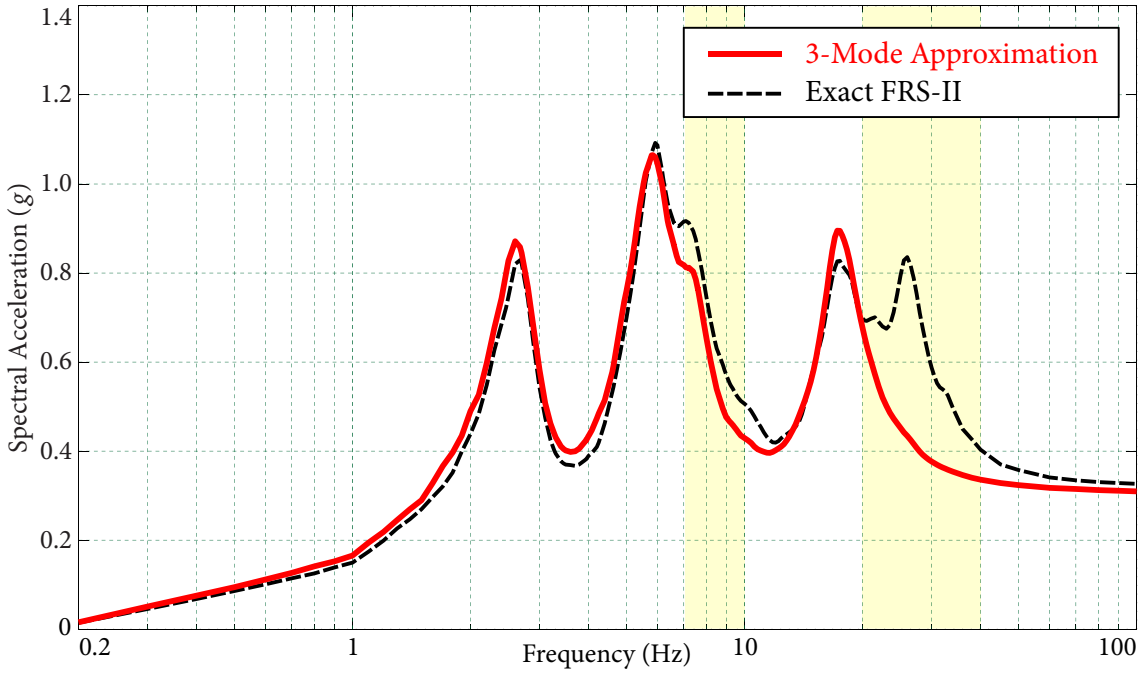

Figure 3.19 3 Equivalent Modes Approximation of FRS-II at Node 1

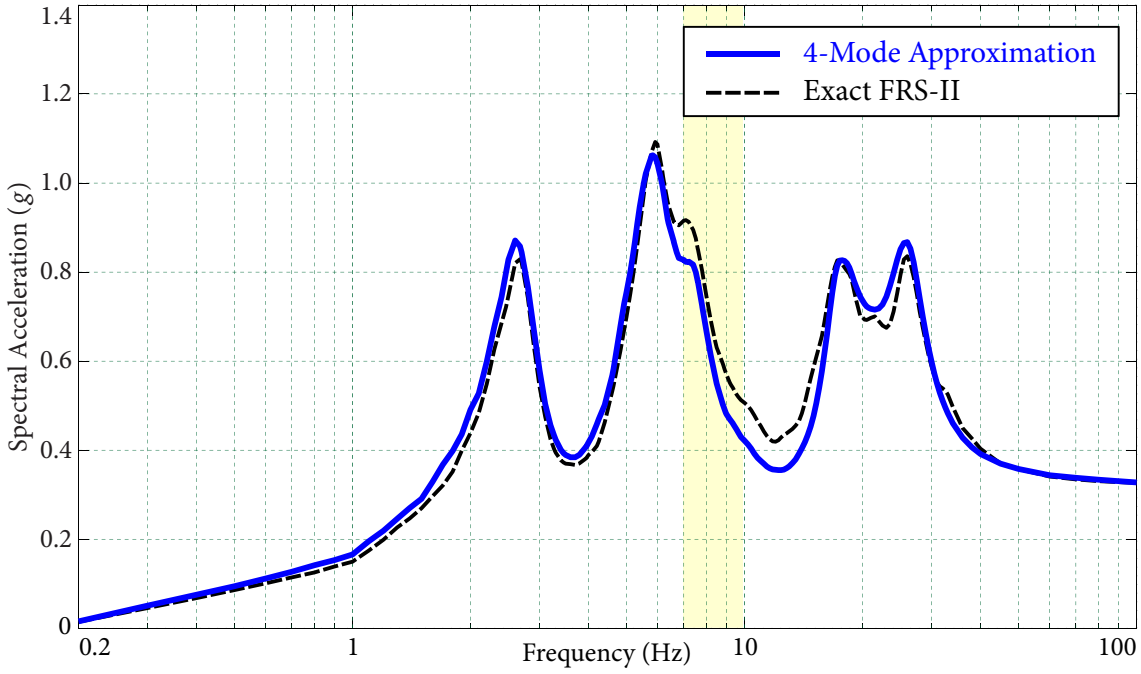

Figure 3.20 4 Equivalent Modes Approximation of FRS-II at Node 1

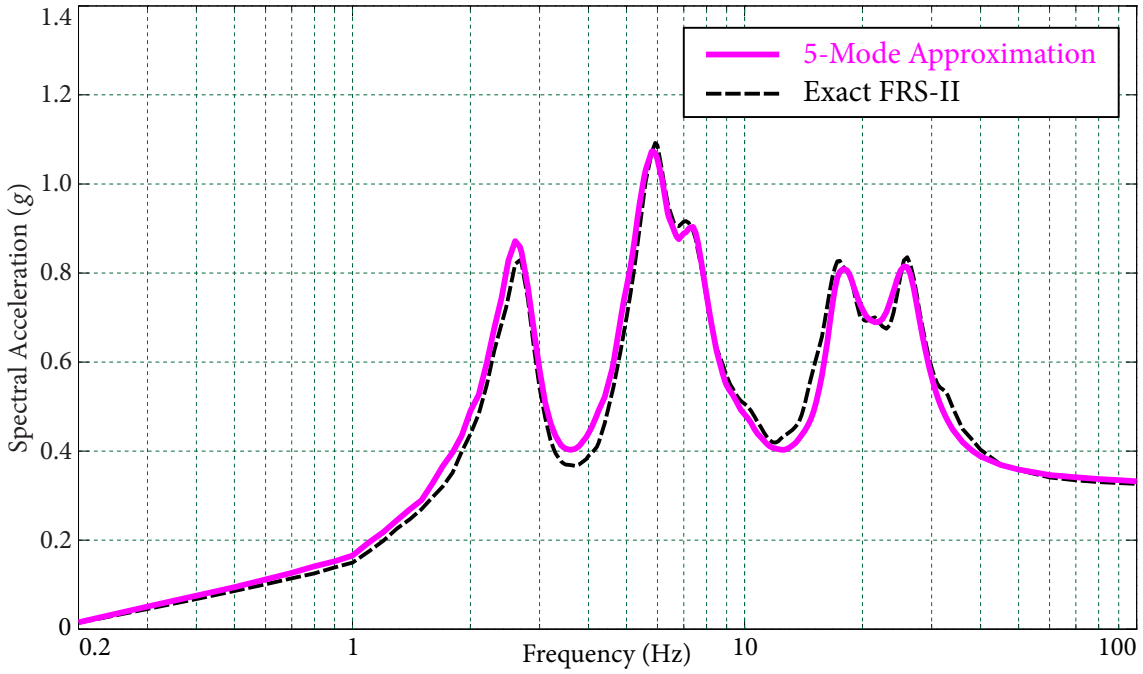

Figure 3.21 5 Equivalent Modes Approximation of FRS-II at Node 1

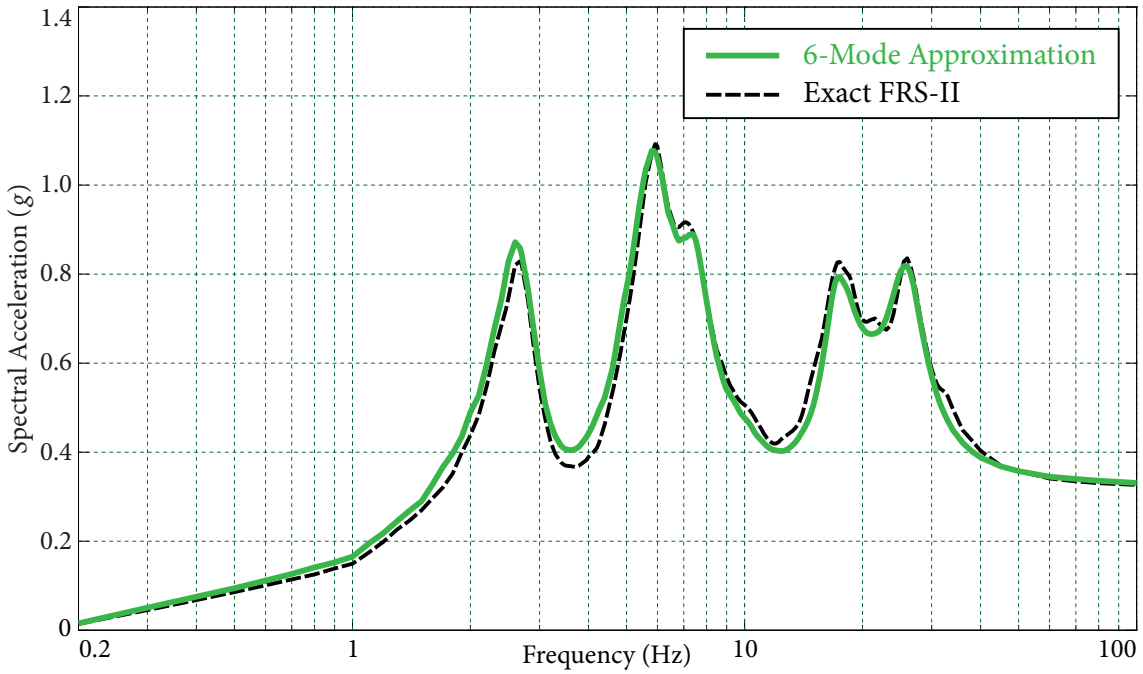

Figure 3.22 6 Equivalent Modes Approximation of FRS-II at Node 1

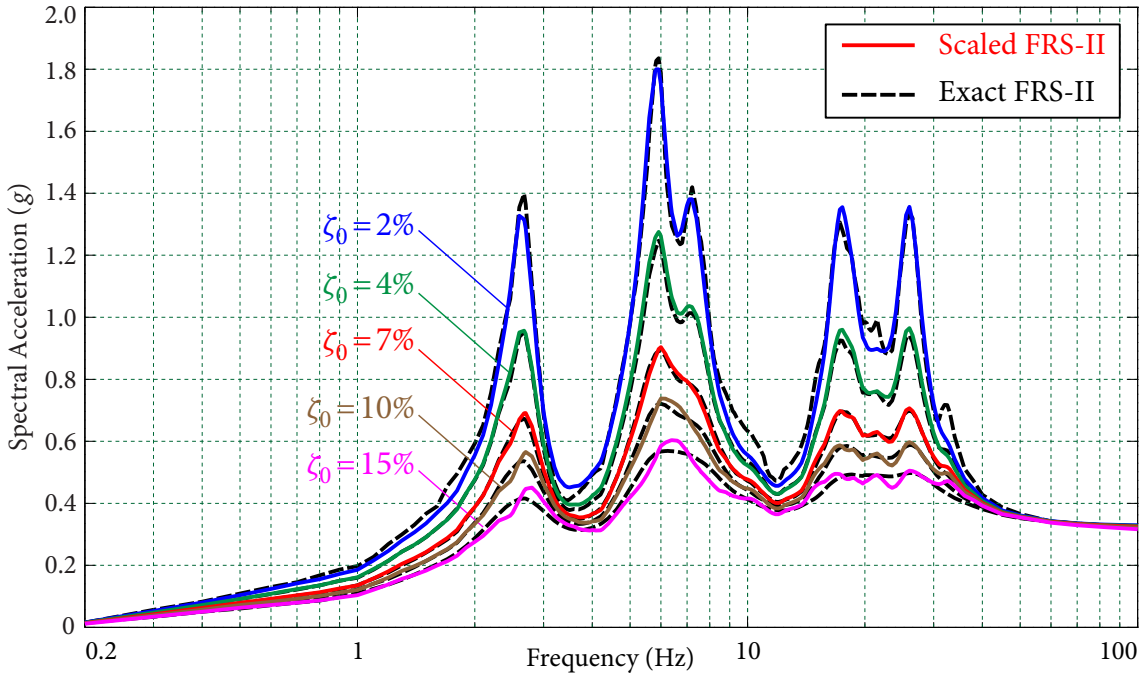

Figure 3.23 Scaling FRS-II to various damping ratios at Node 1

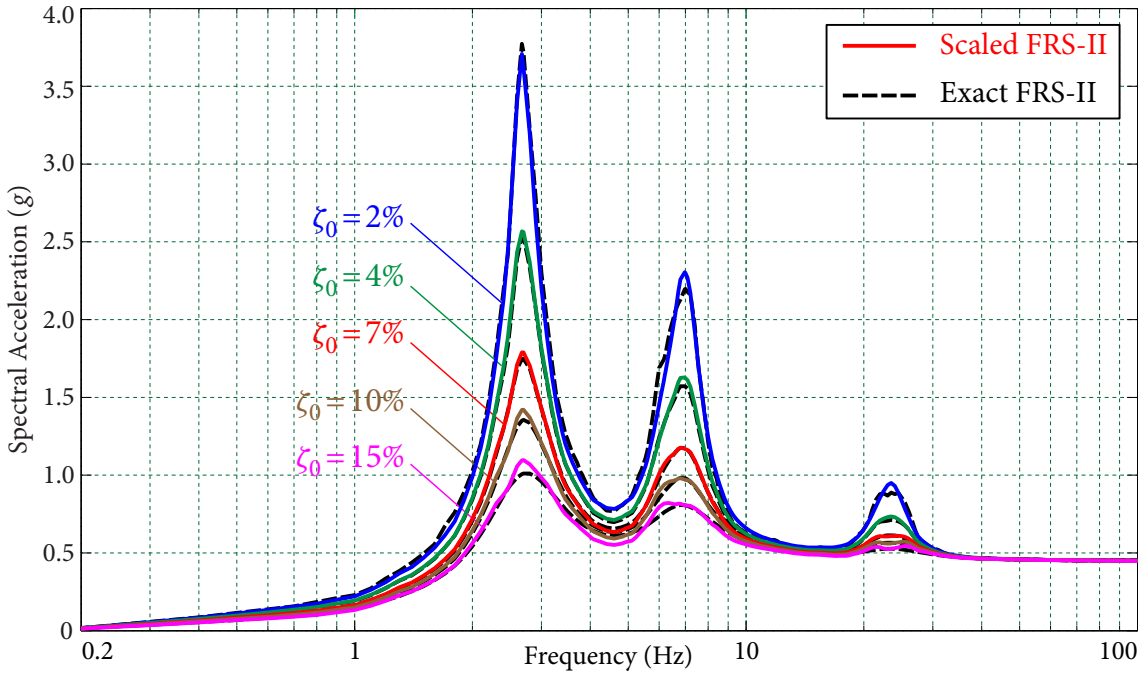

Figure 3.24 Scaling FRS-II to various damping ratios at Node 2

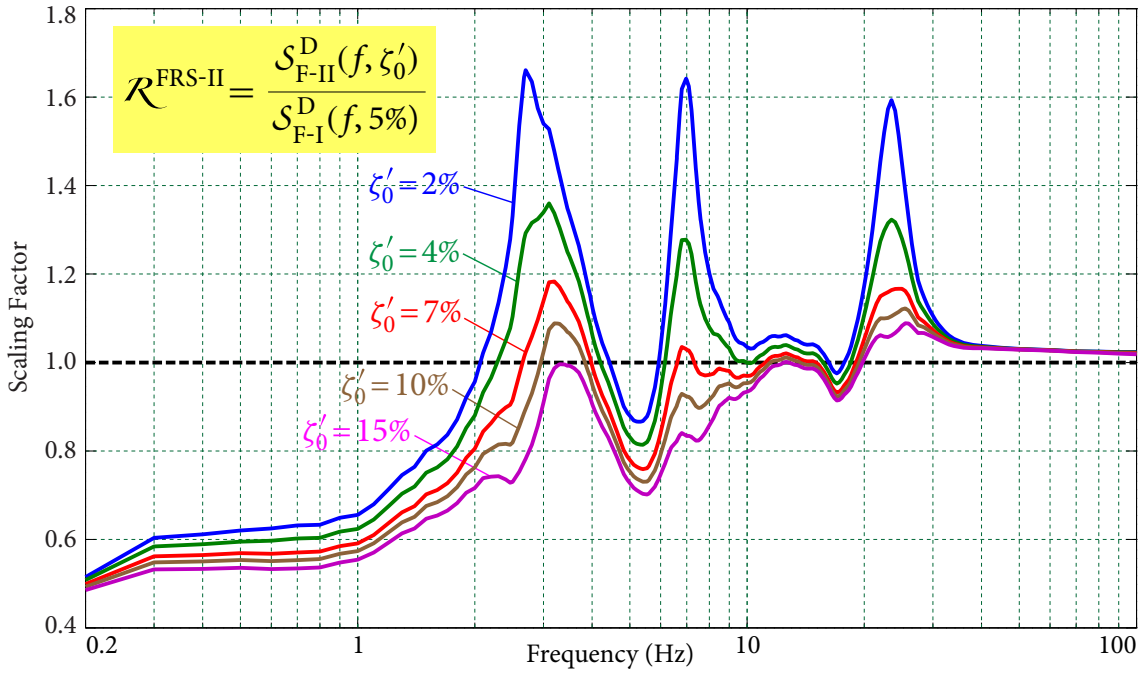

Figure 3.25 Scaling factors for various damping ratios at Node 1

3.22. It is observed that all approximations lead to excellent agreement with the exact results, except for the high frequency range for the 3-mode approximation. This error is caused by ignoring contributions from the high-frequency modes. As discussed earlier, although these modes may not have pronounced effect on FRS-I resulting from a GRS-I that is lack of high frequency content, their effect will be activated and significantly amplified when the input GRS is rich in high frequency content. Consequently, it is reasonable and necessary to assume a few high frequency modes in the higher frequency range (20 to 30 Hz) where GRS-II possesses abundant high frequency content. Another observation is that the 4-mode approximation produces better results in Figure 3.20 compared to Figure 3.8.

It is also found that the reproduced FRS-II from two sets of solutions for the modal information (listed in Table 3.2) of Node 2 almost coincide and agree very well with the exact FRS-II. This phenomenon highlights the advantage of the scaling method: even though there may be significant discrepancy between the identified equivalent modal information and that of the real structure, the scaling method can still generate FRS with sufficient accuracy.

FRS-II with various damping ratios obtained using the scaling method are shown in Figures 3.23 and 3.24, in which 5 and 3 equivalent modes, respectively, are used for Nodes 1 and 2. It is seen that FRS-II obtained using the scaling method agree very well with the exact results. The scaling factor given by equation (3.3.14) is shown in Figure 3.25 for Node 1. It is noted that the peaks of the scaling factor may not occur at equivalent modal frequencies, since the scaling factors depend on not only the modal information but also the differences in the spectral shapes.

3.4.4 Scaling Broadened FRS

In practice, the available FRS-I are usually broadened and smoothed, and raw FRS may not be available. As shown in Figure 3.26, the blue solid line represents the broadened-and-smoothed FRS-I at Node 1. The black dash line is the raw FRS-I; it is shown in this figure for reference only and its information will not be used in the following analysis.

Different from the raw FRS-I where the locations of FRS-I peaks can be accurately identified, peaks of broadened FRS-I are generally assumed at the middle points of the plateaus. Thus, three critical points are selected from the three middle point of the plateaus. Besides these three points, other critical points are selected approximately based on the shape of the broadened FRS-I. It should be noted that these critical points are not necessary on the original raw FRS-I, which is assumed to be unknown. Since the second peak has wide band, it is assumed that there are three closely-spaced modes in the second peak plateau. In addition, a high-frequency mode is assumed in the higher frequency range. Therefore, the available FRS-I is approximated by 6 equivalent modes. The equivalent modal information obtained by applying the system identification technique and the coordinates of the selected critical points are listed in Table 3.3.

To evaluate the accuracy of the equivalent modal information, FRS-I is reproduced by using the identified equivalent modal information in the direct method and plotted as red solid line in Figure 3.26. It can be seen that there are certain shifts at FRS-I peaks compared to the original raw FRS-I due to the bias in selecting critical points; however, these differences are not significant after broadening and smoothing.

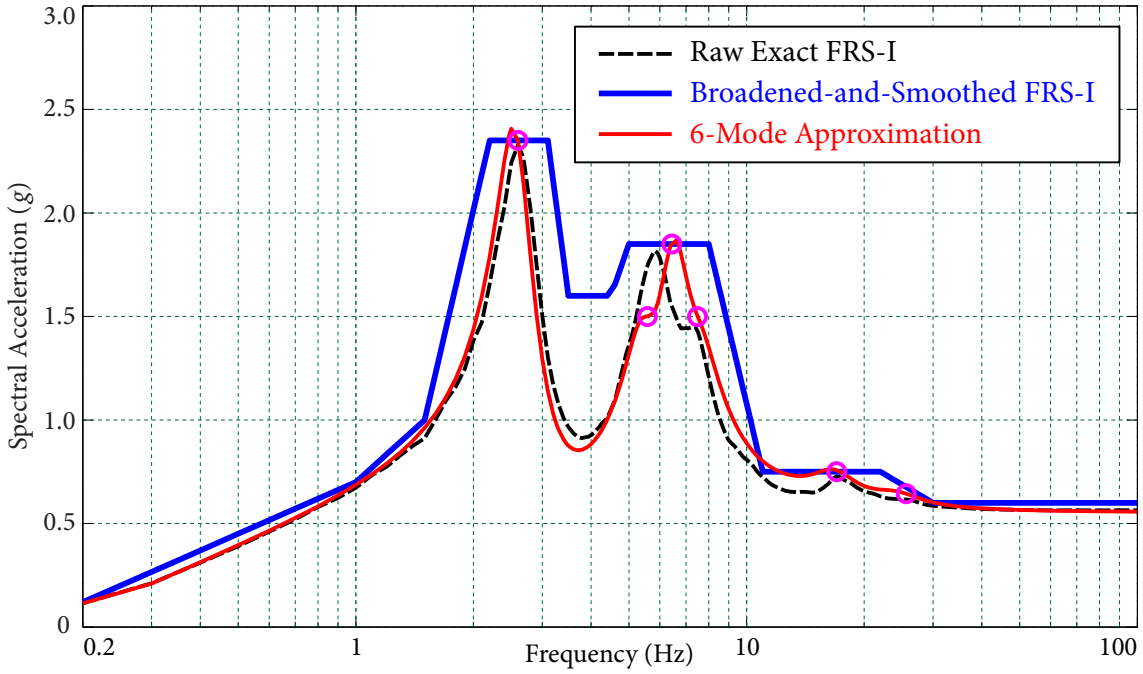

Figure 3.26 Verification of identified modal information

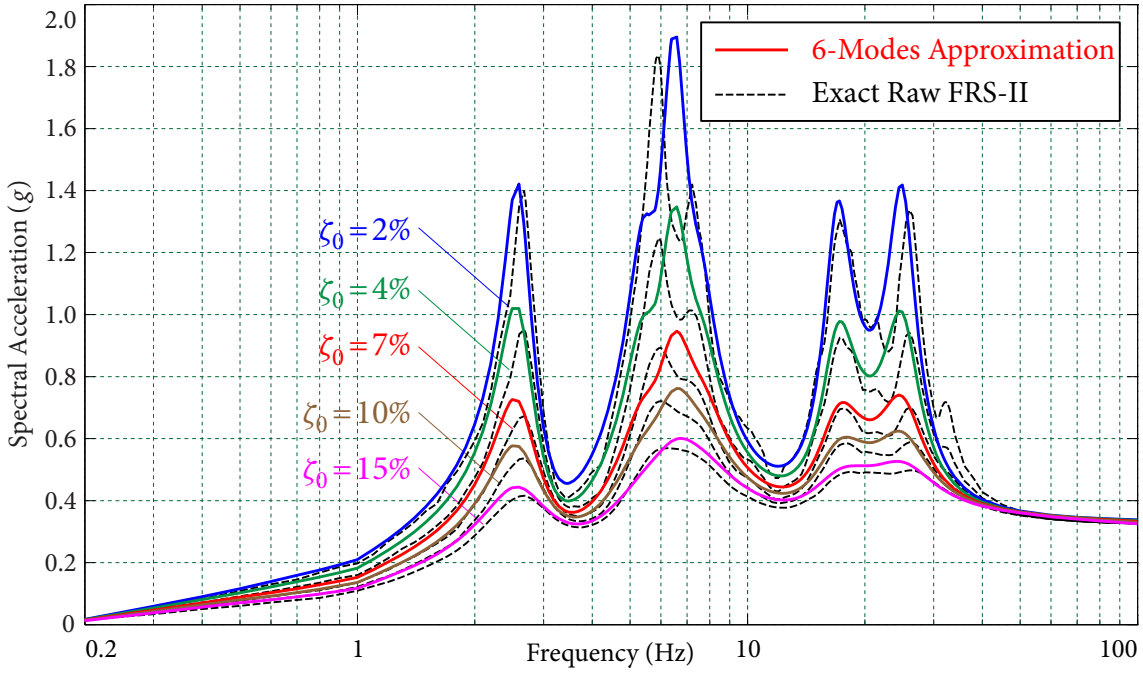

Figure 3.27 Comparison of FRS-II

Table 3.3 Equivalent modal information of 6 mode-approximation for broadened FRS

Mode	f_k (Hz)	$\mathcal{S}_k$ (g)	X_k	Mode	f_k (Hz)	$\mathcal{S}_k$ (g)	X_k
1	2.6	2.35	0.40907	4	7.5	1.50	0.10277
2	5.5	1.50	0.16376	5	17.0	0.75	−0.18680
3	6.5	1.85	0.34813	6	25.0	0.65	0.18178

The equivalent modal information is then employed in the direct spectra-to-spectra method to generate FRS-II as discussed in Section 3.3.4. In Figure 3.27, FRS-II determined from the equivalent modal information are compared with the exact FRS-II. The FRS-II obtained from the direct method can match the exact FRS-II very well after both are broadened and smoothed.

It is worthy to emphasize that scaling factor is not used in this case, since the raw FRS-I is assumed unavailable and the broadened-and-smoothed FRS-I contains a large amount of artificially modified information which is inappropriate to use for scaling. Nevertheless, the direct spectra-to-spectra method can procedure adequately accurate FRS-II when an appropriate number of equivalent modes are included.

3.5 Summary

In this study, a scaling method for generating FRS is presented based on the previously-developed direct spectra-to-spectra method for generating FRS, which requires only the basic modal information of structures and the input GRS. The analytical formulation of the direct spectra-to-spectra method provides a strong physical insight into FRS, which allows the identification of dynamical information of the significant equivalent modes of the underlying structure from the available FRS-I and GRS-I. Scaling factors are then determined in terms of the dynamical information (including modal frequencies, damping ratios, and contribution factors) and the input GRS-I and GRS-II.

Numerical examples of a typical service building in nuclear power plants show that the FRS obtained by this scaling method agree very well with the numerically "exact" FRS which

are obtained from a large number of time history analyses, even when there are significant differences between the spectral shapes of GRS-I and GRS-II. It is also demonstrated that this method provides accurate FRS with various equipment damping ratios.

The proposed method is efficient, accurate, and convenient to implement. It allows engineers to generate accurate FRS for different GRS and for various damping ratios by using as much of the available results as possible without performing a complete dynamic analysis, which introduces extra costs and is time consuming.

However, it should be noted that the accuracy of scaled FRS-I or FRS-II obviously depends on the accuracy of the available FRS-I; for example, if the available FRS-I contains excessive conservatism, the scaled FRS-I or FRS-II would contain the same level of conservatism.

In Appendix A: *Benchmark Studies to Verify an Approximate Method for Spectra Scaling* of EPRI 1002988 (EPRI, 2002, p.A-1), it is commented that "More sophisticated scaling procedures can be applied providing that the eigensolutions for the original models are available. These scaling procedures can utilize random vibration theory, direct generation computer programs, also based on random vibration theory, or time history solutions. In some cases, the eigensolution outputs in the analysis reports are only partially complete. . . . spectra are scaled . . . by more simplified procedures using only frequencies and participation factors."

It should be emphasized that the scaling method developed in this study does not require any information on the underlying structure yet still yields excellent FRS results. The dynamic information of the equivalent significant modes of the underlying structure are recovered by using system identification based on the direct method (Jiang *et al.*, 2015), which has been demonstrated to be very accurate as long as the available FRS are reasonable. If eigensolutions are available, then there is no need to use scaling methods. The direct method (Jiang *et al.*, 2015) can be applied to generate FRS with accuracy matching those obtained from a large number of time history analyses and with complete probabilistic descriptions of FRS peaks (any level of NEP p). On the other hand, if partial modal information (modal frequencies) is available, it can be useful in system identification in helping to locate significant modes, especially high frequency modes; this is particularly important when available FRS-I has been broadened and smoothed.

C H A P T E R 4

Generating Floor Response Spectra: Considering Soil-Structure Interaction

4.1 Introduction

In seismic design and assessment of structures, the input earthquake excitations, which are in terms of site-specific ground response spectra or time histories, are provided by seismologists or specified in design codes. Civil engineers can obtain seismic responses of a structure subjected to the prescribed seismic input by performing dynamic analysis. It is reasonable to conduct this procedure when the structure is founded on rigid bedrock. However, it has been demonstrated that the effect of interaction between the structure and its surrounding soil is not negligible (Wolf, 1985; 1987):

- Seismic responses at the foundation of the structure are different from the free-field responses at the site due to the presence of the structure.
- The structure will interact with the surrounding soil, leading to a further change of the seismic motion at the base.

The typical myth about the effect of soil-structure interaction (SSI) is that considering SSI will reduce the overall seismic responses of the structure, since it elongates the fundamental period of the structure which mostly corresponds to a lower spectral acceleration in a ground response spectrum. In addition, the effective damping of a soil-structure system, which consists of structural damping, soil material damping, and soil radiation damping,

is considerably higher than that of the structure, leading to more energy dissipation and further reduction of the responses. However, it is well understood that FRS peaks occur at the frequencies of the structure dominant modes. Considering the SSI effect results in shifting of structural natural frequencies, and thus leads to shifting of FRS peaks, which could possibly approach the resonant frequencies of equipment mounted on the structure. Consequently, the seismic input to equipment could be significantly increased. Figure 4.2 illustrates this effect: the frequency of the dominant mode of a structure reduces from 5.8 Hz to 4.5 Hz and the FRS peak shifts from 5.8 Hz to 4.5 Hz when the SSI effect is taken into account. Although the FRS peak value for the soil-structure system is less than that for the fixed-base structure, the increase of the seismic input can be as large as 40% (from 1.5g to 2.1g) for an equipment with a natural frequency of 4.5 Hz.

Therefore, seismic input and structural analysis should not be considered independently when the structure is founded on relatively soft soil. The effect of soil will be considered in two major steps of soil-structure interaction analysis:

1. Since response spectra are normally prescribed at the bedrock or ground surface, a site response analysis is performed to determine the foundation input response spectra (FIRS) base on wave propagation theory. The free-field can be generally modelled as a series of soil layers with certain properties and depth resting on the bedrock, which is usually regarded as an elastic homogeneous half-space as shown in Figure 4.1.

2. A dynamic analysis of the structure is conduct using FIRS, considering the interaction between the structure and the surrounding soil.

The most straightforward approach for considering SSI effect is to model the soil-structure system as an integral part, then perform dynamic analysis for the entire system. This method is referred as the complete method of SSI analysis. However, in contrast to the structure, which can be modelled with sufficient accuracy by a system with a finite number of degrees-of-freedom, the soil medium is essentially an unbounded domain. Therefore, the modelling of the soil is accomplished by a truncated soil medium with so-called artificial boundaries, as shown in Figure 4.3. Conceptually, the artificial boundary conditions are capable of representing the dynamic properties of the missing soil, and perfectly absorbing

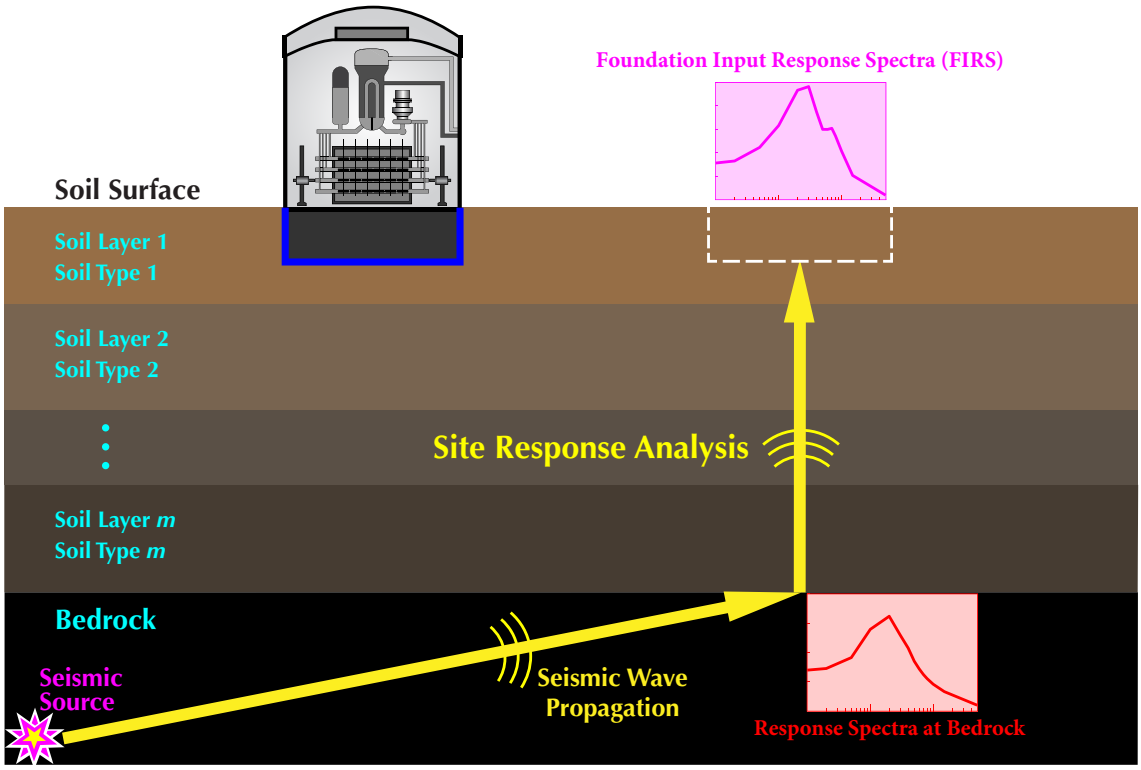

Figure 4.1 Soil-Structure Interaction

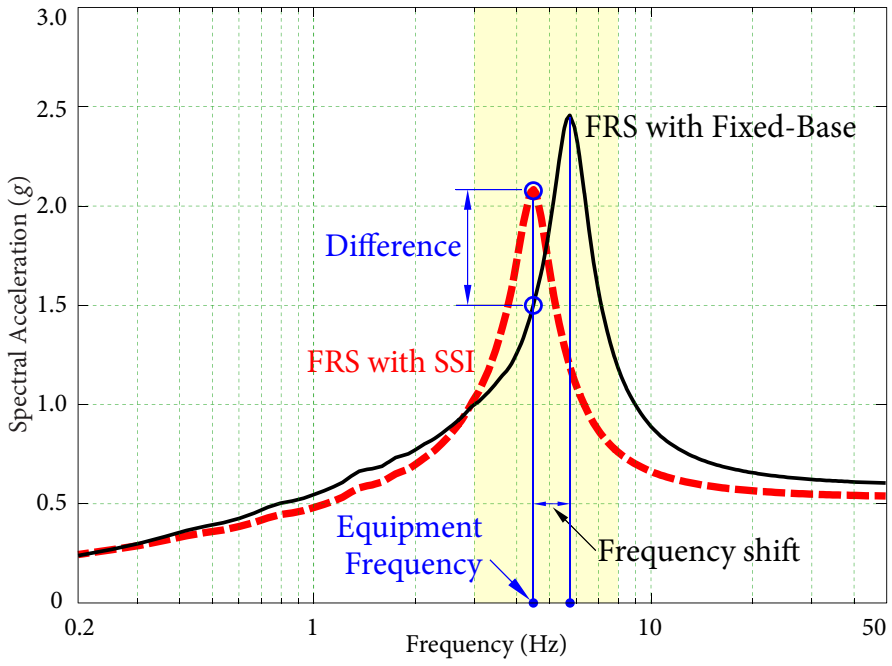

Figure 4.2 Effect of SSI on FRS

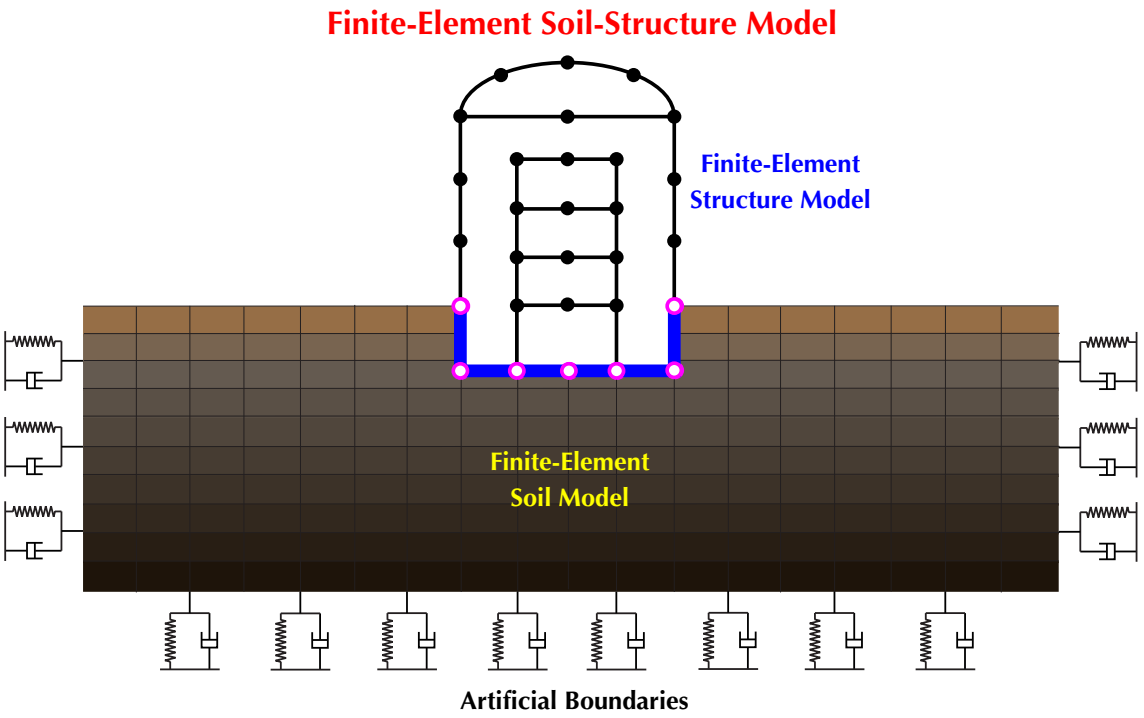

Figure 4.3 Complete method for SSI analysis

the incoming waves. Some types of artificial boundaries were developed under different assumptions. (Smith, 1974; Deeks and Randolph, 1994; Wolf and Song, 1996)

However, the complete method requires solving a large system of coupled equations with excessive degrees-of-freedom, which is not only computationally expensive but also inefficient since only the responses of the structure are of interest. Moreover, when the properties of the structure or soil are changed, the entire analysis procedure has to be repeated.

For these reasons, the substructure method for SSI analysis (Gutierrez and Chopra, 1978), which is theoretically equivalent to the complete method, yet allows to divide the systems into more manageable parts and to analyze these parts separately using appropriate methods, has been developed. Some commercial finite element analysis software packages, such as *SASSI* (Lysmer *et al.*, 1983), *ACS SASSI* (Ghiocel, 2015) were developed on the basis of the substructure method, and are currently employed in practice to perform dynamic analysis for soil-structure systems. However, the seismic inputs required by *ACS SASSI*

are spectrum-compatible time histories, which means that the deficiencies of time history analysis for generating FRS, as discussed in Chapter 1, are inevitable.

Furthermore, when soil is involved in analysis, it is important to consider uncertainties in soil. CSA N289.3 (2010) requires that uncertainties in soil properties and modelling of SSCs be considered in a time history analysis. Furthermore, maximum of maxima of the resultant FRS is used for design. Apparently, this approach is extremely time-consuming, and the results are excessively conservative.

As a result, it is desirable to develop an efficient and accurate method for generating FRS taking into account the SSI effect. Some methods have been developed to perform a modal analysis for the soil-structure system represented by a structure supported by lumped-parameter soil springs, and equivalent modal damping ratios for the system are utilized to decouple the equations of motion (Roesset *et al.*, 1973; Tsai, 1973). Researchers also employed modified base excitations to address the SSI effect (Jennings and Bielak, 1973; Wu and Smith, 1995) by applying the mode superposition principle. However, these methods are not developed for a response spectrum analysis. It has been demonstrated that the spectra-to-spectra method developed gives excellent results of FRS for a fixed-base structure; the objective of the following study is to extend this method to treat the effect of SSI by utilizing modified response spectra.

4.2 Substructure Method

4.2.1 Dynamic Stiffness Matrix

For a multiple degrees-of-freedom (DOF) linear system, the equation of motion is of the form

$$\mathbf{M}\ddot{\mathbf{x}}(t) + \mathbf{C}\dot{\mathbf{x}}(t) + \mathbf{K}\mathbf{x}(t) = \mathbf{p}(t), \tag{4.2.1}$$

where $\mathbf{M}$, $\mathbf{C}$, $\mathbf{K}$ are the mass, damping, and stiffness matrices, respectively, $\mathbf{p}(t)$ is the load vector, and $\mathbf{x}(t)$ is the response vector. Under harmonic excitation $\mathbf{p}(t) = \mathbf{P}e^{i\omega t}$, the response $\mathbf{x}(t)$ can be expressed as $\mathbf{x}(t) = \mathbf{X}e^{i\omega t}$. Substituting $\mathbf{x}(t)$ into equation (4.2.1) yields

$$\mathbf{S}\mathbf{X} = \mathbf{P}, \tag{4.2.2}$$

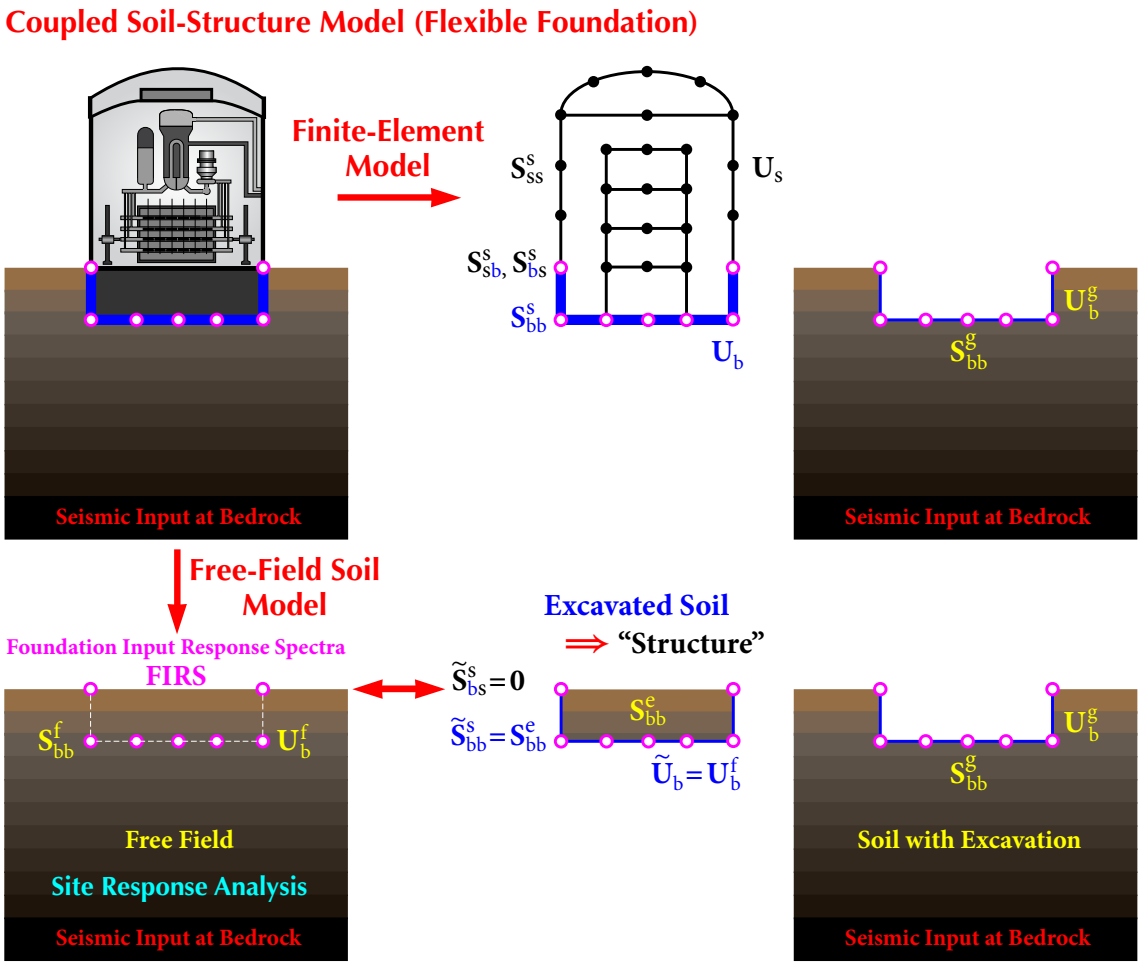

Figure 4.4 Coupled Soil-Structure Model

where $\mathbf{S}$ is the frequency dependent *dynamic stiffness matrix* given by

$$\mathbf{S} = -\omega^2 \mathbf{M} + \mathrm{i}\omega \mathbf{C} + \mathbf{K}. \tag{4.2.3}$$

In terms of the dynamic stiffness matrix, the equation of motion (4.2.1) can be express as an equation of dynamic equilibrium (4.2.2).

4.2.2 Substructure Model for Flexible Foundation

The coupled soil-structure model is shown in Figure 4.4. Let $\mathbf{U}_s$ and $\mathbf{U}_b$ be amplitudes of the absolute displacement vectors of the superstructure and foundation, respectively, where the subscripts "s" and "b" stand for the degrees-of-freedom of "structure" and "base" (or

boundary of soil-structure interface), respectively. The equation of dynamic equilibrium of the structure is given by

$$\begin{bmatrix} \mathbf{S}_{ss}^{s} & \mathbf{S}_{sb}^{s} \\ \mathbf{S}_{bs}^{s} & \mathbf{S}_{bb}^{s} \end{bmatrix} \begin{Bmatrix} \mathbf{U}_{s} \\ \mathbf{U}_{b} \end{Bmatrix} = \begin{Bmatrix} \mathbf{P}_{s} \\ \mathbf{P}_{b} \end{Bmatrix}, \tag{4.2.4}$$

where $\mathbf{P}_s$ is the amplitude vector of the load applied on the nodes of the structure, and $\mathbf{P}_b$ is the amplitude vector of the interaction forces between the structure and soil. For earthquake excitation, the nodes of the structure not in contact with the soil are not loaded, i.e., $\mathbf{P}_s = \mathbf{0}$, and hence

$$\mathbf{S}_{ss}^{s}\,\mathbf{U}_{s} + \mathbf{S}_{sb}^{s}\,\mathbf{U}_{b} = \mathbf{0}. \tag{4.2.5}$$

Let $\mathbf{S}_{bb}^{g}$ be the dynamic stiffness matrix of the soil with excavation, and $\mathbf{U}_{b}^{g}$ be the amplitudes of absolute displacement vector of the soil with excavation under the earthquake excitation. The subscript "g" stands for ground or the soil with excavation. The interaction forces of the soil depend on the relative motion between the foundation (base) and the soil at the interface, i.e.,

$$\mathbf{P}_{b} = \mathbf{S}_{bb}^{g}\,(\mathbf{U}_{b} - \mathbf{U}_{b}^{g}). \tag{4.2.6}$$

Equation (4.2.4) becomes

$$\begin{bmatrix} \mathbf{S}_{ss}^{s} & \mathbf{S}_{sb}^{s} \\ \mathbf{S}_{bs}^{s} & \mathbf{S}_{bb}^{s} + \mathbf{S}_{bb}^{g} \end{bmatrix} \begin{Bmatrix} \mathbf{U}_{s} \\ \mathbf{U}_{b} \end{Bmatrix} = \begin{Bmatrix} \mathbf{0} \\ \mathbf{S}_{bb}^{g}\,\mathbf{U}_{b}^{g} \end{Bmatrix}. \tag{4.2.7}$$

In equation (4.2.7), the earthquake excitation is characterized by $\mathbf{U}_{b}^{g}$, which is the motion of the nodes on the soil-structure interface of the soil with excavation. It is desirable to replace $\mathbf{U}_{b}^{g}$ by the free-field motion $\mathbf{U}_{b}^{f}$ that does not depend on the excavation.

4.2.3 Free-Field Soil Model

The free-field soil can be divided into the excavated soil and the soil without excavation as shown in Figure 4.4. Regarding the excavated soil as a "structure", referring to the coupled soil-structure model and equation (4.2.7), one has $\tilde{\mathbf{U}}_b = \mathbf{U}_b^f$, $\tilde{\mathbf{S}}_{bs}^{s} = \mathbf{0}$, and hence $\tilde{\mathbf{S}}_{bb}^{s} = \mathbf{S}_{bb}^{e}$, which is the dynamic stiffness matrix of the excavated soil; the subscript "e" stands for

excavated soil. Hence, the second block-row of equation (4.2.7) gives

$$\begin{bmatrix} \tilde{\mathbf{S}}^{s}_{bs} & \tilde{\mathbf{S}}^{s}_{bb} + \mathbf{S}^{g}_{bb} \end{bmatrix} \begin{Bmatrix} \times \\ \mathbf{U}^{f}_{b} \end{Bmatrix} = \left\{ \mathbf{S}^{g}_{bb} \mathbf{U}^{g}_{b} \right\} \implies (\mathbf{S}^{e}_{bb} + \mathbf{S}^{g}_{bb}) \mathbf{U}^{f}_{b} = \mathbf{S}^{g}_{bb} \mathbf{U}^{g}_{b}. \tag{4.2.8}$$

Note that adding the excavated soil to the soil with excavation leads to the free-field system, i.e.,

$$\mathbf{S}^{g}_{bb} + \mathbf{S}^{e}_{bb} = \mathbf{S}^{f}_{bb}, \quad \text{or} \quad \mathbf{S}^{g}_{bb} = \mathbf{S}^{f}_{bb} - \mathbf{S}^{e}_{bb}. \tag{4.2.9}$$

Hence, equation (4.2.8) can be written as

$$\mathbf{S}^{f}_{bb} \mathbf{U}^{f}_{b} = \mathbf{S}^{g}_{bb} \mathbf{U}^{g}_{b}, \tag{4.2.10}$$

where $\mathbf{S}^{f}_{bb}$ is the dynamic stiffness matrix of the free-field that is discretized at the nodes at which the structure is inserted, and $\mathbf{U}^{f}_{b}$ is the free-field motion at the nodes of the soil-structure interface. Hence, $\mathbf{U}^{f}_{b}$ is the free-field response of the soil at the foundation level; the acceleration response spectra of $\ddot{\mathbf{u}}^{f}_{b}$ are the Foundation Input Response Spectra (FIRS), which can be obtained from a site response analysis of the free-field.

Using equation (4.2.10), equation (4.2.7) becomes

$$\begin{bmatrix} \mathbf{S}^{s}_{ss} & \mathbf{S}^{s}_{sb} \\ \mathbf{S}^{s}_{bs} & \mathbf{S}^{s}_{bb} + \mathbf{S}^{g}_{bb} \end{bmatrix} \begin{Bmatrix} \mathbf{U}_{s} \\ \mathbf{U}_{b} \end{Bmatrix} = \begin{Bmatrix} \mathbf{0} \\ \mathbf{S}^{f}_{bb} \mathbf{U}^{f}_{b} \end{Bmatrix}. \tag{4.2.11}$$

Equation (4.2.11) is the equation of motion of the structure supported on a generalized spring characterized by the dynamic stiffness matrix $\mathbf{S}^{g}_{bb}$, and the other end of the spring is subjected to earthquake excitation $\mathbf{U}^{f}_{b}$, which is free-field response at the foundation level.

Using equation (4.2.9), equation (4.2.11) can also be written as

$$\begin{bmatrix} \mathbf{S}^{s}_{ss} & \mathbf{S}^{s}_{sb} \\ \mathbf{S}^{s}_{bs} & (\mathbf{S}^{s}_{bb} - \mathbf{S}^{e}_{bb}) + \mathbf{S}^{f}_{bb} \end{bmatrix} \begin{Bmatrix} \mathbf{U}_{s} \\ \mathbf{U}_{b} \end{Bmatrix} = \begin{Bmatrix} \mathbf{0} \\ \mathbf{S}^{f}_{bb} \mathbf{U}^{f}_{b} \end{Bmatrix}. \tag{4.2.12}$$

4.2.4 Substructure Model for Rigid Foundation

In many engineering applications, such as in nuclear power plants, the foundations can be assumed to be rigid. In this case, the free-field earthquake excitation is applied at only

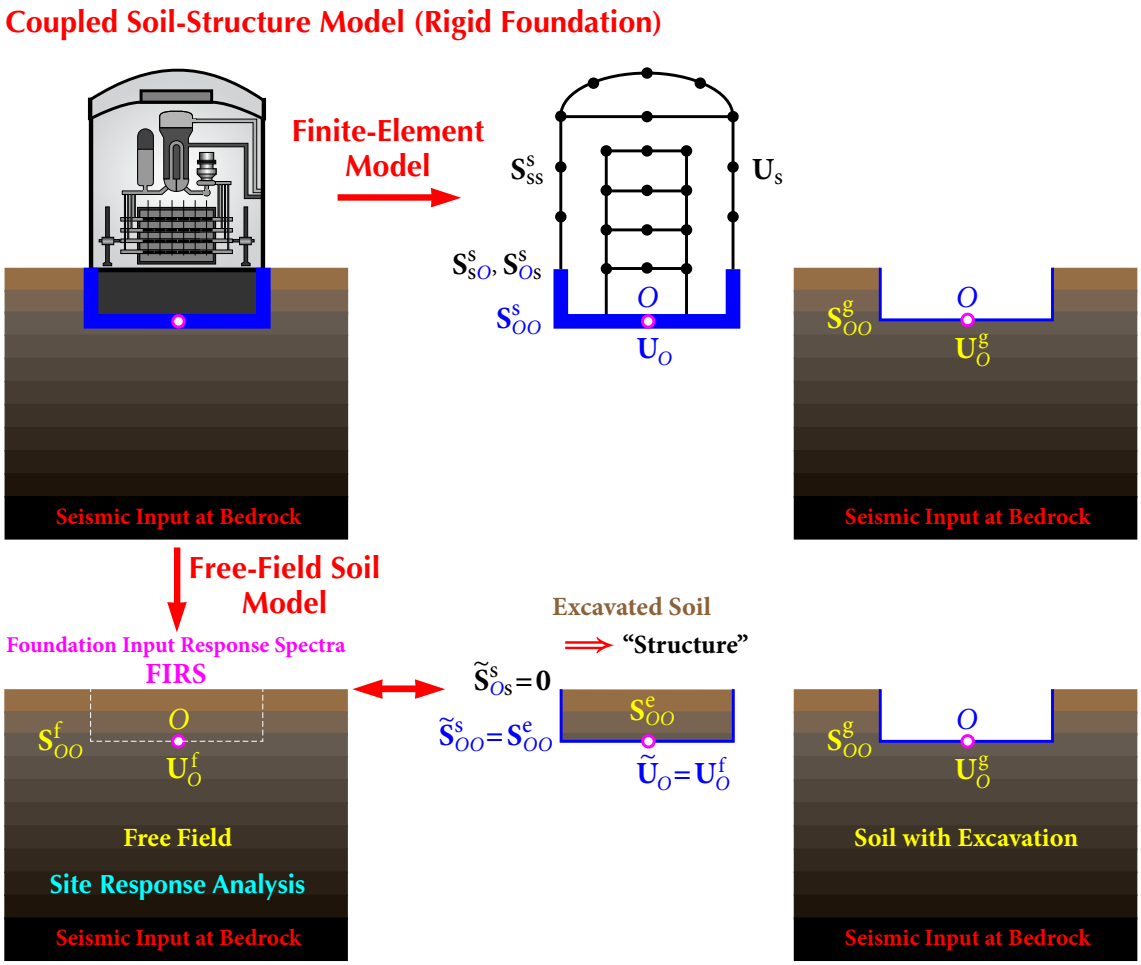

Figure 4.5 Coupled Soil-Structure Model with Rigid Foundation

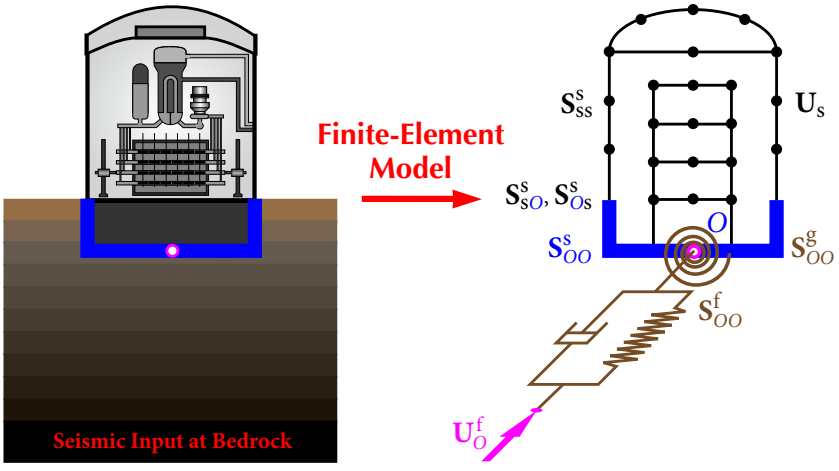

Figure 4.6 Soil-Spring Model of SSI with Rigid Foundation

one node O on the foundation (Figure 4.5). Hence, referring to the general case of flexible foundation (Section 4.2.2), one has

$$\mathbf{S}^{\mathrm{s}}_{\mathrm{bb}} \Longrightarrow \mathbf{S}^{\mathrm{s}}_{OO}, \quad \mathbf{S}^{\mathrm{s}}_{\mathrm{bs}} \Longrightarrow \mathbf{S}^{\mathrm{s}}_{O\mathrm{s}}, \quad \mathbf{S}^{\mathrm{s}}_{\mathrm{sb}} \Longrightarrow \mathbf{S}^{\mathrm{s}}_{\mathrm{s}O}, \quad \mathbf{S}^{\mathrm{g}}_{\mathrm{bb}} \Longrightarrow \mathbf{S}^{\mathrm{g}}_{OO}, \quad \mathbf{S}^{\mathrm{f}}_{\mathrm{bb}} \Longrightarrow \mathbf{S}^{\mathrm{f}}_{OO},$$
$$\mathbf{U}_{\mathrm{b}} \Longrightarrow \mathbf{U}_O, \quad \mathbf{U}^{\mathrm{g}}_{\mathrm{b}} \Longrightarrow \mathbf{U}^{\mathrm{g}}_O, \quad \mathbf{U}^{\mathrm{f}}_{\mathrm{b}} \Longrightarrow \mathbf{U}^{\mathrm{f}}_O.$$

Equation (4.2.11) then becomes

$$\begin{bmatrix} \mathbf{S}^{\mathrm{s}}_{\mathrm{ss}} & \mathbf{S}^{\mathrm{s}}_{\mathrm{s}O} \\ \mathbf{S}^{\mathrm{s}}_{O\mathrm{s}} & \mathbf{S}^{\mathrm{s}}_{OO}+\mathbf{S}^{\mathrm{g}}_{OO} \end{bmatrix} \begin{Bmatrix} \mathbf{U}_{\mathrm{s}} \\ \mathbf{U}_O \end{Bmatrix} = \begin{Bmatrix} \mathbf{0} \\ \mathbf{S}^{\mathrm{f}}_{OO}\mathbf{U}^{\mathrm{f}}_O \end{Bmatrix}. \tag{4.2.13}$$

Equation (4.2.13) is the equation of motion of the structure supported on a generalized spring characterized by the dynamic stiffness matrix $\mathbf{S}^{\mathrm{g}}_{OO}$ at node O, and the other end of the spring is subjected to earthquake excitation $\mathbf{U}^{\mathrm{f}}_O$, which is free-field response at the foundation level (node O as shown in Figure 4.6). Using equation (4.2.9), equation (4.2.13) can also be written as

$$\begin{bmatrix} \mathbf{S}^{\mathrm{s}}_{\mathrm{ss}} & \mathbf{S}^{\mathrm{s}}_{\mathrm{s}O} \\ \mathbf{S}^{\mathrm{s}}_{O\mathrm{s}} & (\mathbf{S}^{\mathrm{s}}_{OO}-\mathbf{S}^{\mathrm{e}}_{OO})+\mathbf{S}^{\mathrm{f}}_{OO} \end{bmatrix} \begin{Bmatrix} \mathbf{U}_{\mathrm{s}} \\ \mathbf{U}_O \end{Bmatrix} = \begin{Bmatrix} \mathbf{0} \\ \mathbf{S}^{\mathrm{f}}_{OO}\mathbf{U}^{\mathrm{f}}_O \end{Bmatrix}. \tag{4.2.14}$$

For a structure with N nodes (not including the rigid foundation), each node has 6 DOF (three translational and three rotational). The rigid foundation has one node O with 6 DOF. The dimensions of the vectors $\mathbf{U}_{\mathrm{s}}$, $\mathbf{U}_O$, and $\mathbf{U}^{\mathrm{f}}_O$ are $6N$, 6, and 6, respectively. The dimensions of the dynamic stiffness sub-matrices of the structure $\mathbf{S}^{\mathrm{s}}_{\mathrm{ss}}$, $\mathbf{S}^{\mathrm{s}}_{\mathrm{s}O}$, $\mathbf{S}^{\mathrm{s}}_{O\mathrm{s}}$, $\mathbf{S}^{\mathrm{s}}_{OO}$ are $6N\times 6N$, $6N\times 6$, $6\times 6N$, and 6×6, respectively. The dimensions of the dynamic stiffness sub-matrices of the soil $\mathbf{S}^{\mathrm{f}}_{OO}$, $\mathbf{S}^{\mathrm{g}}_{OO}$, and $\mathbf{S}^{\mathrm{e}}_{OO}$ are all 6×6.

4.2.5 Fixed-Base Model for Rigid Foundation

If the soil is firm enough so that the structure can be considered as fixed-base as shown in Figure 4.7, the motion of point O of the basemat is the earthquake input to the structure. From the first block-row of equation (4.2.13), one has

$$\mathbf{S}^{\mathrm{s}}_{\mathrm{ss}}\mathbf{U}_{\mathrm{s}} + \mathbf{S}^{\mathrm{s}}_{\mathrm{s}O}\mathbf{U}_O = \mathbf{0} \implies \mathbf{U}_{\mathrm{s}} = \mathbf{S}^{\mathrm{fb}}\mathbf{U}_O, \quad \mathbf{S}^{\mathrm{fb}} = -\left(\mathbf{S}^{\mathrm{s}}_{\mathrm{ss}}\right)^{-1}\mathbf{S}^{\mathrm{s}}_{\mathrm{s}O}, \tag{4.2.15}$$

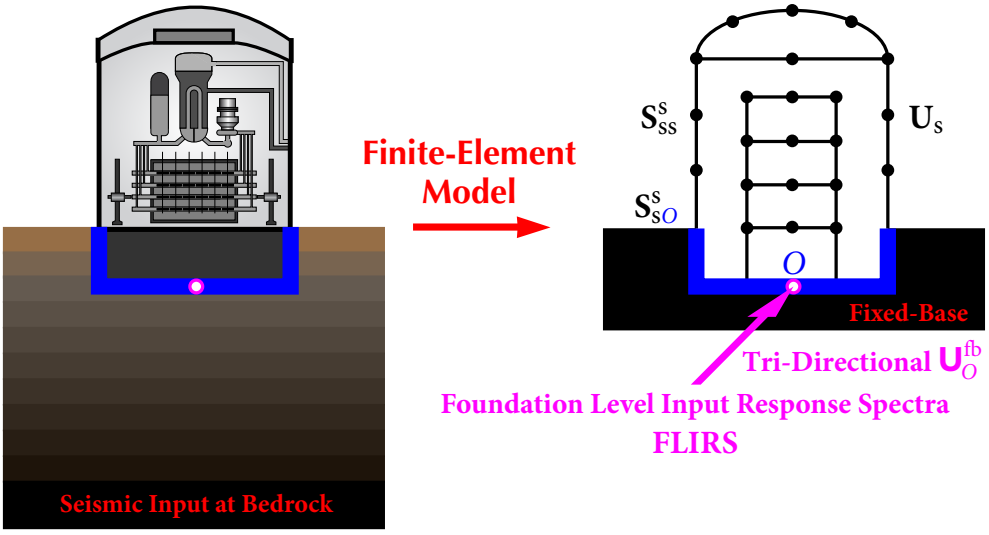

Figure 4.7 Fixed-Base Model with Rigid Foundation

where $\mathbf{S}^{\text{fb}}$ is the dynamic stiffness matrix for fixed-base analysis, the superscript "fb" stands for fixed-base.

In seismic analyses, rotational ground motions are not considered and only translational ground motions are considered. Re-organize vector $\mathbf{U}_{\text{s}}$ and rewrite $\mathbf{U}_O$ as

$$\mathbf{U}_{\text{s}} = \begin{Bmatrix} \mathbf{U}_{\text{s,T}} \\ \mathbf{U}_{\text{s,R}} \end{Bmatrix}_{6N\times 1}, \qquad \mathbf{U}_O = \begin{Bmatrix} \mathbf{U}^{\text{fb}}_O \\ \mathbf{0} \end{Bmatrix}_{6\times 1}, \tag{4.2.16}$$

in which the subscripts "T" and "R" stand for translational and rotational degrees-of-freedom, respectively. Re-arranging and partitioning $\mathbf{S}^{\text{fb}}$ accordingly, one has

$$\mathbf{S}^{\text{fb}} = \begin{bmatrix} \mathbf{S}^{\text{fb}}_{\text{TT}} & \mathbf{S}^{\text{fb}}_{\text{TR}} \\ \mathbf{S}^{\text{fb}}_{\text{RT}} & \mathbf{S}^{\text{fb}}_{\text{RR}} \end{bmatrix}_{6N\times 6}, \tag{4.2.17}$$

in which each submatrix is of dimension $3N\times 3$. Equation (4.2.15) can be written as

$$\begin{Bmatrix} \mathbf{U}_{\text{s,T}} \\ \mathbf{U}_{\text{s,R}} \end{Bmatrix} = \begin{bmatrix} \mathbf{S}^{\text{fb}}_{\text{TT}} & \mathbf{S}^{\text{fb}}_{\text{TR}} \\ \mathbf{S}^{\text{fb}}_{\text{RT}} & \mathbf{S}^{\text{fb}}_{\text{RR}} \end{bmatrix} \begin{Bmatrix} \mathbf{U}^{\text{fb}}_O \\ \mathbf{0} \end{Bmatrix} = \begin{Bmatrix} \mathbf{S}^{\text{fb}}_{\text{TT}}\,\mathbf{U}^{\text{fb}}_O \\ \mathbf{S}^{\text{fb}}_{\text{RT}}\,\mathbf{U}^{\text{fb}}_O \end{Bmatrix}. \tag{4.2.18}$$

Multiplying the first block-row of equation (4.2.18) by $\left(\mathbf{S}^{\text{fb}}_{\text{TT}}\right)^T$ yields

$$\left(\mathbf{S}^{\text{fb}}_{\text{TT}}\right)^T \mathbf{U}_{\text{s,T}} = \left[\left(\mathbf{S}^{\text{fb}}_{\text{TT}}\right)^T \mathbf{S}^{\text{fb}}_{\text{TT}}\right] \mathbf{U}^{\text{fb}}_O. \tag{4.2.19}$$

The reason for performing this manipulation is to make $[(\mathbf{S}_{TT}^{fb})^T \mathbf{S}_{TT}^{fb}]$ a square matrix of dimension 3×3, the purpose of which will be clear in Section 4.3.

The tri-directional (translational) acceleration response spectra $\mathbf{U}_O^{fb}$ applied at the foundation of a *fixed-base* structure are called Foundation Level Input Response Spectra (FLIRS), as shown in Figure 4.7. It is important to note that FLIRS are different from Foundation Input Response Spectra (FIRS), which are the acceleration response spectra at the elevation of the foundation of the *free-field*, as illustrated in Figure 4.5.

The concept of FLIRS, which are the seismic input to fixed-base structures, is important in seismic design and assessment of nuclear power plants. Generic design of a nuclear power plant is based on fixed-base analysis under the tri-directional seismic excitations represented by standard GRS, such as those in CSA N289.3 or USNRC R.G. 1.60, anchored at a specific Peak Ground Acceleration (PGA). By comparing the site-specific FLIRS with the standard GRS, based on which the generic nuclear power plant is designed, initial feasibility of the generic design at the desired site can be assessed and Systems, Structures, and Components (SSCs) that may be vulnerable can be identified.

Since the dimension of the dynamic stiffness sub-matrix $\mathbf{S}_{ss}^{s}$ is $6N\times6N$, the evaluation of its inverse in equation (4.2.15) could be numerically challenging when N is large. To take advantage of the modal properties of the structure, a modal analysis is conducted.

For a three-dimensional model of a structure with N nodes (not including rigid foundation), a typical node n has six DOF: three translational DOF $u_{n,1}$, $u_{n,2}$, $u_{n,3}$, and three rotational DOF $u_{n,4}$, $u_{n,5}$, $u_{n,6}$. The structure is subjected to tri-directional seismic excitations at the foundation. The relative displacement vector $\mathbf{x}$ of dimension $6N$ is governed by (see, e.g., Jiang *et al.*, 2015)

$$\mathbf{M}\ddot{\mathbf{x}}(t) + \mathbf{C}\dot{\mathbf{x}}(t) + \mathbf{K}\mathbf{x}(t) = -\mathbf{M}\sum_{i=1}^{3} \boldsymbol{\mathcal{T}}^i \ddot{u}_g^i(t), \tag{4.2.20}$$

where

$$\mathbf{x} = \begin{Bmatrix} \mathbf{x}_1 \\ \mathbf{x}_2 \\ \vdots \\ \mathbf{x}_N \end{Bmatrix}, \quad \mathbf{x}_n = \begin{Bmatrix} x_{n,1} \\ x_{n,2} \\ \vdots \\ x_{n,6} \end{Bmatrix}, \quad \boldsymbol{\mathcal{T}}^i = \begin{Bmatrix} \mathbf{1}^i \\ \mathbf{1}^i \\ \vdots \\ \mathbf{1}^i \end{Bmatrix}, \quad \mathbf{1}^i = \begin{Bmatrix} \delta_{i1} \\ \delta_{i2} \\ \vdots \\ \delta_{i6} \end{Bmatrix}, \tag{4.2.21}$$

$\mathbf{M}$, $\mathbf{C}$, $\mathbf{K}$ are, respectively, the mass, damping, and stiffness matrices of dimension $6N\times 6N$, $\mathbf{x}_n$ is the relative displacement vector of node n, $\boldsymbol{\mathcal{I}}^i$ is the influence vector of the seismic excitation in direction i, and δ_{ij} denotes the Kronecker delta function.

For a structure-foundation system resting on soil, the base excitations may also contain rotational components, equation (4.2.20) can be extended to

$$\mathbf{M}\ddot{\mathbf{x}}(t)+\mathbf{C}\dot{\mathbf{x}}(t)+\mathbf{K}\mathbf{x}(t)=-\mathbf{M}\boldsymbol{\mathcal{I}}\ddot{\mathbf{u}}_O(t), \tag{4.2.22}$$

where node O is at the rigid foundation, and

$$\boldsymbol{\mathcal{I}}=[\,\boldsymbol{\mathcal{I}}^1\ \boldsymbol{\mathcal{I}}^2\ \boldsymbol{\mathcal{I}}^3\ \boldsymbol{\mathcal{I}}^4\ \boldsymbol{\mathcal{I}}^5\ \boldsymbol{\mathcal{I}}^6\,],\qquad \ddot{\mathbf{u}}_O(t)=\left\{\ddot{u}_O^1(t),\,\ddot{u}_O^2(t),\,\ddot{u}_O^3(t),\,\ddot{\theta}_O^1(t),\,\ddot{\theta}_O^2(t),\,\ddot{\theta}_O^3(t)\right\}^T.$$

Here $\boldsymbol{\mathcal{I}}^i$ are defined in equation (4.2.21) for $i=1,2,3$, and

$$\boldsymbol{\mathcal{I}}^4=\begin{Bmatrix}\mathbf{r}_1^1\\ \mathbf{r}_1^2\\ \vdots\\ \mathbf{r}_1^N\end{Bmatrix},\quad \mathbf{r}_1^n=\begin{Bmatrix}0\\ -\bar{z}_n\\ 0\\ 1\\ 0\\ 0\end{Bmatrix},\quad \boldsymbol{\mathcal{I}}^5=\begin{Bmatrix}\mathbf{r}_2^1\\ \mathbf{r}_2^2\\ \vdots\\ \mathbf{r}_2^N\end{Bmatrix},\quad \mathbf{r}_2^n=\begin{Bmatrix}\bar{z}_n\\ 0\\ 0\\ 0\\ 1\\ 0\end{Bmatrix},\quad \boldsymbol{\mathcal{I}}^6=\begin{Bmatrix}\mathbf{r}_3^1\\ \mathbf{r}_3^2\\ \vdots\\ \mathbf{r}_3^N\end{Bmatrix},\quad \mathbf{r}_3^n=\begin{Bmatrix}-\bar{y}_n\\ \bar{x}_n\\ 0\\ 0\\ 0\\ 1\end{Bmatrix},$$

$\bar{x}_n$, $\bar{y}_n$, and $\bar{z}_n$ represent the coordinates of the nth node in a Cartesian coordinate system with its origin located at Node O.

Letting $\mathbf{x}(t)=\mathbf{X}\mathrm{e}^{\mathrm{i}\omega t}$ and $\mathbf{u}_O(t)=\mathbf{U}_O\,\mathrm{e}^{\mathrm{i}\omega t}$, equation (4.2.22) becomes

$$(-\omega^2\mathbf{M}+\mathrm{i}\omega\mathbf{C}+\mathbf{K})\mathbf{X}=\omega^2\mathbf{M}\boldsymbol{\mathcal{I}}\mathbf{U}_O. \tag{4.2.23}$$

Applying the modal transformation $\mathbf{X}=\boldsymbol{\Phi}\mathbf{Q}$, where $\boldsymbol{\Phi}$ is the modal matrix, substituting into equation (4.2.23), and multiplying $\boldsymbol{\Phi}^T$ from the left yield

$$(-\omega^2\boldsymbol{\Phi}^T\mathbf{M}\boldsymbol{\Phi}+\mathrm{i}\omega\boldsymbol{\Phi}^T\mathbf{C}\boldsymbol{\Phi}+\boldsymbol{\Phi}^T\mathbf{K}\boldsymbol{\Phi})\mathbf{Q}=\omega^2\boldsymbol{\Phi}^T\mathbf{M}\boldsymbol{\mathcal{I}}\mathbf{U}_O. \tag{4.2.24}$$

Employing the orthogonality gives

$$\mathrm{diag}\left\{-\omega^2+\mathrm{i}2\zeta_n\omega_n\omega+\omega_n^2\right\}\mathbf{Q}=\omega^2\boldsymbol{\Gamma}\mathbf{U}_O, \tag{4.2.25}$$

where $\boldsymbol{\Gamma}$ is a $6N\times 6$ matrix of the modal participation factors given by

$$\boldsymbol{\Gamma}=\frac{\boldsymbol{\Phi}^T\mathbf{M}\boldsymbol{\mathcal{I}}}{\boldsymbol{\Phi}^T\mathbf{M}\boldsymbol{\Phi}}. \tag{4.2.26}$$

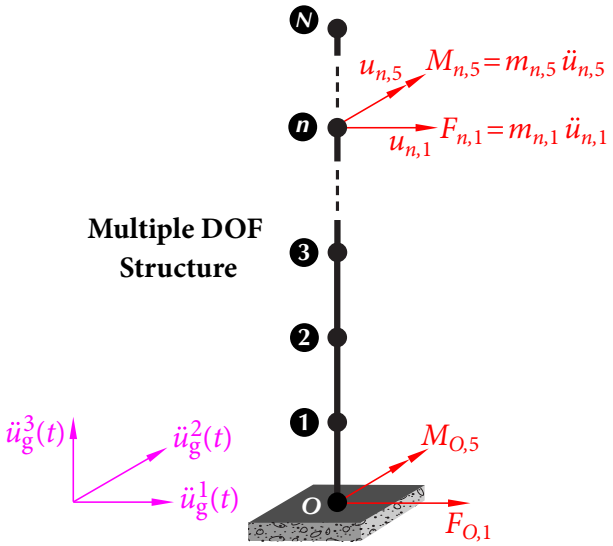

Figure 4.8 Dynamic equilibrium of structure-foundation system

Hence,

$$\mathbf{X} = \omega^2 \mathbf{\Phi H \Gamma U}_O, \tag{4.2.27}$$

where $\mathbf{H}$ is a diagonal matrix of the complex frequency response functions, i.e.,

$$\mathbf{H} = \text{diag}\left\{\frac{1}{\omega_n^2 - \omega^2 + \mathrm{i}2\zeta_n\omega_n\omega}\right\}. \tag{4.2.28}$$

Since the relative displacement $\mathbf{x} = \mathbf{u} - \boldsymbol{\mathcal{I}}\mathbf{u}_O$, substituting into equation (4.2.27) gives

$$\mathbf{U} = (\omega^2 \mathbf{\Phi H \Gamma} + \boldsymbol{\mathcal{I}})\,\mathbf{U}_O. \tag{4.2.29}$$

Comparing equation (4.2.29) with equations (4.2.15), one obtains

$$\mathbf{S}^{\text{fb}} = \omega^2 \mathbf{\Phi H \Gamma} + \boldsymbol{\mathcal{I}}. \tag{4.2.30}$$

Based on Newton's second law, the dynamic force equilibrium of the structure-foundation system in Direction 1, as illustrated in Figure 4.8, is given by

$$-\omega^2\left(\sum_{n=1}^{N} m_{n,1}\,U_{n,1} + m_{O,1}\,U_{O,1}\right) = F_{O,1}, \tag{4.2.31}$$

in which $F_{O,1}$ is the interaction force in Direction 1. The first term can be written in a matrix form as

$$-\omega^2\left[(\boldsymbol{\mathcal{I}}^1)^T\mathbf{M}\mathbf{U} + m_{O,1}\,U_{O,1}\right] = F_{O,1}. \tag{4.2.32}$$

Similarly, taking moment about Node O, the dynamic moment equilibrium of the structure-foundation system in Direction 5 is given by

$$-\omega^2\left[\sum_{n=1}^{N}\left(m_{n,5}\,U_{n,5}+m_{n,1}\,U_{n,1}\,\bar{z}_n\right)+m_{O,5}\,U_{O,5}\right]=M_{O,5}, \tag{4.2.33}$$

in which the summation term can be expressed into a matrix form as

$$-\omega^2\left[(\boldsymbol{\mathcal{I}}^5)^T\mathbf{M}\mathbf{U}+m_{O,5}\,U_{O,5}\right]=M_{O,5}. \tag{4.2.34}$$

The dynamic equilibrium in the other directions can be derived similarly as equations (4.2.32) and (4.2.34). Therefore, the dynamic equilibrium equation of the entire structure-foundation system can be obtained as

$$-\omega^2\left(\boldsymbol{\mathcal{I}}^T\mathbf{M}\mathbf{U}+\mathbf{M}_O\,\mathbf{U}_O\right)=\mathbf{F}_O, \tag{4.2.35}$$

where the first term represents the resultant of the superstructure's motion about the foundation at the Node O, $\mathbf{M}_O$ is a 6×6 mass matrix of the foundation, and $\mathbf{F}_O$ denotes the vector of soil-structure interaction forces acting on the foundation, which are given by $\mathbf{F}_O=\mathbf{S}^{\mathrm{f}}_{OO}(\mathbf{U}^{\mathrm{f}}_O-\mathbf{U}_O)$ from equation (4.2.6).

Therefore, equation (4.2.35) can be rewritten as

$$-\omega^2\,\boldsymbol{\mathcal{I}}^T\mathbf{M}\mathbf{U}+\left(-\omega^2\mathbf{M}_O+\mathbf{S}^{\mathrm{f}}_{OO}\right)\mathbf{U}_O=\mathbf{S}^{\mathrm{f}}_{OO}\,\mathbf{U}^{\mathrm{f}}_O. \tag{4.2.36}$$

Comparing with the second block-row of equation (4.2.14), a structure founded on the ground surface implies $\mathbf{S}^{\mathrm{e}}_{OO}=\mathbf{0}$; hence

$$\mathbf{S}^{\mathrm{s}}_{\mathrm{Os}}=-\omega^2\,\boldsymbol{\mathcal{I}}^T\mathbf{M},\qquad \mathbf{S}^{\mathrm{s}}_{OO}=-\omega^2\mathbf{M}_O. \tag{4.2.37}$$

4.3 Foundation Level Input Response Spectra (FLIRS)

As discussed in Section 4.2.5, it is desirable to determine the equivalent FLIRS for the structure with rigid foundation (studied in Section 4.2.4) in seismic design and assessment. In SSI analysis, a fixed-base analysis can be performed using the equivalent FLIRS as the seismic input, instead of a coupled soil-structure analysis using FIRS as the seismic input.

From the first block-row of equation (4.2.14), one obtains

$$\mathbf{U}_{\mathrm{s}}=-\left(\mathbf{S}^{\mathrm{s}}_{\mathrm{ss}}\right)^{-1}\mathbf{S}^{\mathrm{s}}_{\mathrm{s}O}\,\mathbf{U}_O=\mathbf{S}^{\mathrm{fb}}\,\mathbf{U}_O. \tag{4.3.1}$$

From the second block-row of equation (4.2.14), one has

$$\mathbf{S}_{Os}^{s}\mathbf{U}_{s}+[(\mathbf{S}_{OO}^{s}-\mathbf{S}_{OO}^{e})+\mathbf{S}_{OO}^{f}]\mathbf{U}_{O}=\mathbf{S}_{OO}^{f}\mathbf{U}_{O}^{f}. \tag{4.3.2}$$

Substituting equation (4.3.1) into (4.3.2) yields

$$\mathbf{S}_{Os}^{s}\mathbf{S}^{fb}\mathbf{U}_{O}+[(\mathbf{S}_{OO}^{s}-\mathbf{S}_{OO}^{e})+\mathbf{S}_{OO}^{f}]\mathbf{U}_{O}=\mathbf{S}_{OO}^{f}\mathbf{U}_{O}^{f},$$

which gives

$$\underbrace{\mathbf{U}_{O}}_{6\times1}=\underbrace{\mathbf{S}^{-1}}_{6\times6}\underbrace{\mathbf{S}_{OO}^{f}}_{6\times6}\underbrace{\mathbf{U}_{O}^{f}}_{6\times1},\qquad \mathbf{S}=\underbrace{\mathbf{S}_{Os}^{s}}_{6\times6N}\underbrace{\mathbf{S}^{fb}}_{6N\times6}+\underbrace{(\mathbf{S}_{OO}^{s}-\mathbf{S}_{OO}^{e})+\mathbf{S}_{OO}^{f}}_{6\times6}. \tag{4.3.3}$$

Note that $\mathbf{S}^{-1}\mathbf{S}_{OO}^{f}$ is a square matrix of dimension 6×6; partition it as follows:

$$\mathbf{S}^{-1}\mathbf{S}_{OO}^{f}=\mathbf{T}=\begin{bmatrix}\mathbf{T}_{TT} & \mathbf{T}_{TR}\\ \mathbf{T}_{RT} & \mathbf{T}_{RR}\end{bmatrix}_{6\times6}, \tag{4.3.4}$$

in which each submatrix is of dimension 3×3.

Substituting equation (4.2.37) into equation (4.3.3) yields

$$\mathbf{S}=-\omega^{2}(\boldsymbol{\mathcal{I}}^{T}\mathbf{M}\mathbf{S}^{fb}+\mathbf{M}_{O})+\mathbf{S}_{OO}^{f}. \tag{4.3.5}$$

Since the earthquake influence matrix $\boldsymbol{\mathcal{I}}$ and the fixed-base model structural response transfer matrix $\mathbf{S}^{fb}$ are dimensionless, and $\mathbf{S}_{OO}^{f}$ denotes the dynamic stiffness of the soil springs, equation (4.3.5) can be expressed in terms of a standard dynamic stiffness matrix as

$$\mathbf{S}=-\omega^{2}\tilde{\mathbf{M}}+\mathrm{i}\omega\mathbf{C}^{f}+\mathbf{K}^{f}, \tag{4.3.6}$$

where $\tilde{\mathbf{M}}=\boldsymbol{\mathcal{I}}^{T}\mathbf{M}\mathbf{S}^{fb}+\mathbf{M}_{O}$ is a 6×6 mass matrix which is determined by the structure and foundation mass matrices, influence matrix, and the fixed-base structure transfer matrix $\mathbf{S}^{fb}$; $\mathbf{K}^{f}$ and $\mathbf{C}^{f}$ are the stiffness and damping matrices of soil springs, respectively.

Therefore, the problem can be interpreted as a synthesized 6-DOF mass, which is frequency-dependent, supported by generalized soil springs. With a better understanding of the physical behaviour of the soil-structure system, the advantage of the proposed direct method becomes evident: When the properties of a structure or soil are changed,

only the synthesized mass or the stiffnesses of the generalized soil springs need to change; as a result, a reanalysis of the entire system, which is time-consuming, can be avoided. Furthermore, the required computational effort is reduced significantly, since it is needed to evaluate the inverse of a 6×6 matrix rather than a $6N\times 6N$ matrix, which may lead to numerical difficulties for a large-scale system.

In a site response analysis, the soil medium is modelled as a series of semi-infinite layers on a half-space, and the rotational responses of free-field should be very small under the translational excitation at bedrock. Hence, the rotational input at foundation level is negligible compared to the translational input; the rotational input is usually not given by a site response analysis and is taken as 0.

From equations (4.3.1) and (4.3.3), one has $\mathbf{U}_{\mathrm{s}} = \mathbf{S}^{\mathrm{fb}}\,\mathbf{T}\,\mathbf{U}^{\mathrm{f}}_{O}$, i.e.,

$$\begin{aligned}\begin{Bmatrix}\mathbf{U}_{\mathrm{s,T}}\\ \mathbf{U}_{\mathrm{s,R}}\end{Bmatrix}_{6N\times 1} &= \begin{bmatrix}\mathbf{S}^{\mathrm{fb}}_{\mathrm{TT}} & \mathbf{S}^{\mathrm{fb}}_{\mathrm{TR}}\\ \mathbf{S}^{\mathrm{fb}}_{\mathrm{RT}} & \mathbf{S}^{\mathrm{fb}}_{\mathrm{RR}}\end{bmatrix}_{6N\times 6}\begin{bmatrix}\mathbf{T}_{\mathrm{TT}} & \mathbf{T}_{\mathrm{TR}}\\ \mathbf{T}_{\mathrm{RT}} & \mathbf{T}_{\mathrm{RR}}\end{bmatrix}_{6\times 6}\begin{Bmatrix}\mathbf{U}^{\mathrm{f}}_{O,\mathrm{T}}\\ \mathbf{0}\end{Bmatrix}_{6\times 1}\\ &= \begin{bmatrix}\mathbf{S}^{\mathrm{fb}}_{\mathrm{TT}} & \mathbf{S}^{\mathrm{fb}}_{\mathrm{TR}}\\ \mathbf{S}^{\mathrm{fb}}_{\mathrm{RT}} & \mathbf{S}^{\mathrm{fb}}_{\mathrm{RR}}\end{bmatrix}\begin{bmatrix}\mathbf{T}_{\mathrm{TT}}\,\mathbf{U}^{\mathrm{f}}_{O,\mathrm{T}}\\ \mathbf{T}_{\mathrm{RT}}\,\mathbf{U}^{\mathrm{f}}_{O,\mathrm{T}}\end{bmatrix} = \begin{Bmatrix}\mathbf{S}^{\mathrm{fb}}_{\mathrm{TT}}\,\mathbf{T}_{\mathrm{TT}}\,\mathbf{U}^{\mathrm{f}}_{O,\mathrm{T}} + \mathbf{S}^{\mathrm{fb}}_{\mathrm{TR}}\,\mathbf{T}_{\mathrm{RT}}\,\mathbf{U}^{\mathrm{f}}_{O,\mathrm{T}}\\ \mathbf{S}^{\mathrm{fb}}_{\mathrm{RT}}\,\mathbf{T}_{\mathrm{TT}}\,\mathbf{U}^{\mathrm{f}}_{O,\mathrm{T}} + \mathbf{S}^{\mathrm{fb}}_{\mathrm{RR}}\,\mathbf{T}_{\mathrm{RT}}\,\mathbf{U}^{\mathrm{f}}_{O,\mathrm{T}}\end{Bmatrix}.\end{aligned} \tag{4.3.7}$$

Note that it is not possible to have a single set of tri-directional translational FLIRS in a fixed-base analysis to give both correct translational responses $\mathbf{U}_{\mathrm{s,T}}$ and rotational responses $\mathbf{U}_{\mathrm{s,R}}$. In the generation of floor response spectra (FRS), only translational responses are needed. Hence, from the first block-row of equation (4.3.7), one has

$$\mathbf{U}_{\mathrm{s,T}} = \mathbf{S}^{\mathrm{fb}}_{\mathrm{TT}}\,\mathbf{T}_{\mathrm{TT}}\,\mathbf{U}^{\mathrm{f}}_{O,\mathrm{T}} + \mathbf{S}^{\mathrm{fb}}_{\mathrm{TR}}\,\mathbf{T}_{\mathrm{RT}}\,\mathbf{U}^{\mathrm{f}}_{O,\mathrm{T}}. \tag{4.3.8}$$

Multiplying $\left(\mathbf{S}^{\mathrm{fb}}_{\mathrm{TT}}\right)^{T}$ from the left yields

$$\begin{aligned}\left(\mathbf{S}^{\mathrm{fb}}_{\mathrm{TT}}\right)^{T}\mathbf{U}_{\mathrm{s,T}} &= \left\{\left(\mathbf{S}^{\mathrm{fb}}_{\mathrm{TT}}\right)^{T}\mathbf{S}^{\mathrm{fb}}_{\mathrm{TT}}\,\mathbf{T}_{\mathrm{TT}} + \left(\mathbf{S}^{\mathrm{fb}}_{\mathrm{TT}}\right)^{T}\mathbf{S}^{\mathrm{fb}}_{\mathrm{TR}}\,\mathbf{T}_{\mathrm{RT}}\right\}\mathbf{U}^{\mathrm{f}}_{O,\mathrm{T}}\\ &= \left[\left(\mathbf{S}^{\mathrm{fb}}_{\mathrm{TT}}\right)^{T}\mathbf{S}^{\mathrm{fb}}_{\mathrm{TT}}\right]\left\{\mathbf{T}_{\mathrm{TT}} + \left[\left(\mathbf{S}^{\mathrm{fb}}_{\mathrm{TT}}\right)^{T}\mathbf{S}^{\mathrm{fb}}_{\mathrm{TT}}\right]^{-1}\left(\mathbf{S}^{\mathrm{fb}}_{\mathrm{TT}}\right)^{T}\mathbf{S}^{\mathrm{fb}}_{\mathrm{TR}}\,\mathbf{T}_{\mathrm{RT}}\right\}\mathbf{U}^{\mathrm{f}}_{O,\mathrm{T}}.\end{aligned} \tag{4.3.9}$$

Since $\left[\left(\mathbf{S}^{\mathrm{fb}}_{\mathrm{TT}}\right)^{T}\mathbf{S}^{\mathrm{fb}}_{\mathrm{TT}}\right]$ is a square matrix of dimension 3×3, it is straightforward to determine its inverse. Thus, the purpose of the transformation in equation (4.2.19) becomes evident.

Comparing equation (4.3.9) with equation (4.2.19), one obtains the equivalent FLIRS as

$$\mathbf{U}_O^{\mathrm{fb}} = \boldsymbol{\mathcal{T}}\,\mathbf{U}_{O,\mathsf{T}}^{\mathrm{f}}, \tag{4.3.10}$$

where $\boldsymbol{\mathcal{T}}$ is a complex transfer matrix from FIRS (generated by $\mathbf{U}_{O,\mathsf{T}}^{\mathrm{f}}$) to FLIRS (generated by $\mathbf{U}_O^{\mathrm{fb}}$), given as

$$\underbrace{\boldsymbol{\mathcal{T}}}_{3\times3} = \underbrace{\mathbf{T}_{\mathsf{TT}}}_{3\times3} + \underbrace{[(\mathbf{S}_{\mathsf{TT}}^{\mathrm{fb}})^T\mathbf{S}_{\mathsf{TT}}^{\mathrm{fb}}]^{-1}}_{3\times3}\underbrace{(\mathbf{S}_{\mathsf{TT}}^{\mathrm{fb}})^T}_{3\times3N}\underbrace{\mathbf{S}_{\mathsf{TR}}^{\mathrm{fb}}}_{3N\times3}\underbrace{\mathbf{T}_{\mathsf{RT}}}_{3\times3}. \tag{4.3.11}$$

The first and second term of $\boldsymbol{\mathcal{T}}$ denote the contributions from the translational and rotational motions of the foundation in the soil-structure system, respectively.

It is important to emphasize that, although the FLIRS given by equation (4.3.10) would not give correct rotational responses $\mathbf{U}_{\mathrm{s},\mathsf{R}}$ of a structure, it gives exact translation responses and hence exact FRS because only translational responses are required to generate FRS. Therefore, the fixed-base analysis of the structure under the excitation of FLIRS $\mathbf{U}_O^{\mathrm{fb}}$ given by equation (4.3.10) gives exactly the same FRS as a full coupled soil-structure analysis under the excitation of FIRS $\mathbf{U}_{O,\mathsf{T}}^{\mathrm{f}}$.

Based on the theory of random vibration, the relation between the power spectral density functions of $\mathbf{U}_O^{\mathrm{fb}}$ and $\mathbf{U}_{O,\mathsf{T}}^{\mathrm{f}}$ can be determined by

$$\mathbf{S}_{\ddot{U}\ddot{U}}^{\mathrm{fb}}(\omega) = \left[\left|\boldsymbol{\mathcal{T}}(\omega)\right|^2\right]\mathbf{S}_{\ddot{U}\ddot{U}}^{\mathrm{f}}(\omega), \tag{4.3.12}$$

where $\mathbf{S}_{\ddot{U}\ddot{U}}^{\mathrm{fb}}(\omega)$ and $\mathbf{S}_{\ddot{U}\ddot{U}}^{\mathrm{f}}(\omega)$ are the 3×1 vectors of the power spectral density functions of $\mathbf{U}_O^{\mathrm{fb}}$ and $\mathbf{U}_{O,\mathsf{T}}^{\mathrm{f}}$, respectively. In equation (4.3.12), $\left[\left|\boldsymbol{\mathcal{T}}(\omega)\right|^2\right]$ denotes a matrix in which each element is equal to the squared modulus of the corresponding element in $\boldsymbol{\mathcal{T}}$. For a complex number $a+\mathrm{i}b$, its modulus is defined as $\left|a+\mathrm{i}b\right| = \sqrt{a^2+b^2}$. It is found that, for structures in nuclear power plants, the off-diagonal terms of $\boldsymbol{\mathcal{T}}$ are relatively small compared to the diagonal terms, and thus may be neglected. It means that the motion of the foundation in one direction is only induced by the excitations in the same direction.

It is known that the mean square response of a SDOF oscillator under a base excitation $\mathbf{U}_{O,\mathsf{T}}^{\mathrm{f}}$ can be obtained by

$$\mathrm{E}\left[\ddot{X}_0^2(t)\right] = \int_{-\infty}^{\infty}\left|\omega_0^2 H_0(\omega)\right|^2\mathbf{S}_{\ddot{U}\ddot{U}}^{\mathrm{f}}(\omega)\,\mathrm{d}\omega, \tag{4.3.13}$$

in which $H_0(\omega)$ is the complex frequency response function characterized by the circular frequency ω_0 and damping ratio ζ_0 of the SDOF oscillator. For excitations with wide-band power spectral densities, $\boldsymbol{S}^{\mathrm{f}}_{\ddot{U}\ddot{U}}(\omega)$ can be approximated by constant $\boldsymbol{S}^{\mathrm{f}}_{\ddot{U}\ddot{U}}$. From equations (4.3.12) and (4.3.13), the ratios between the mean square responses of a SDOF oscillator under base excitation $\mathbf{U}^{\mathrm{fb}}_{O}$ and those under base excitation $\mathbf{U}^{\mathrm{f}}_{O,\mathrm{T}}$ can be calculated by

$$\boldsymbol{\mathcal{R}}^2(\omega_0,\zeta_0)=\frac{\displaystyle\int_{-\infty}^{\infty}\left|\omega_0^2 H_0(\omega)\right|^2\left[\left|\boldsymbol{\mathcal{T}}(\omega)\right|^2\right]\boldsymbol{S}^{\mathrm{f}}_{\ddot{U}\ddot{U}}(\omega)\,\mathrm{d}\omega}{\displaystyle\int_{-\infty}^{\infty}\left|\omega_0^2 H_0(\omega)\right|^2\boldsymbol{S}^{\mathrm{f}}_{\ddot{U}\ddot{U}}(\omega)\,\mathrm{d}\omega}=\frac{\displaystyle\int_{-\infty}^{\infty}\left|H_0(\omega)\right|^2\left[\left|\boldsymbol{\mathcal{T}}(\omega)\right|^2\right]\mathbf{1}\,\mathrm{d}\omega}{\displaystyle\int_{-\infty}^{\infty}\left|H_0(\omega)\right|^2\,\mathrm{d}\omega},\tag{4.3.14}$$

where $\mathbf{1}$ is the 3×1 vector with all elements being 1. Equation (4.3.14) can be easily evaluated numerically.

The maximum response of a SDOF oscillator, which is by definition the response spectrum, is usually related to its root mean square response through a peak factor as

$$\mathcal{S}_{\mathrm{A}}(\omega_0,\zeta_0)=\left|X_0(t)\right|_{\max}=\mathcal{P}\cdot\sqrt{\mathrm{E}\left[X_0^2(t)\right]}.\tag{4.3.15}$$

Combining equations (4.3.14) and (4.3.15) yields the tri-directional fixed-base FLIRS

$$\boldsymbol{\mathcal{S}}^{\mathrm{fb}}_{\mathrm{A}}(\omega_0,\zeta_0)=\frac{\mathcal{P}^{\mathrm{fb}}}{\mathcal{P}^{\mathrm{f}}}\cdot\boldsymbol{\mathcal{R}}(\omega_0,\zeta_0)\,\boldsymbol{\mathcal{S}}^{\mathrm{f}}_{\mathrm{A}}(\omega_0,\zeta_0).\tag{4.3.16}$$

For responses in earthquake engineering, the values of peak factors $\mathcal{P}^{\mathrm{fb}}$ and $\mathcal{P}^{\mathrm{f}}$ are not different significantly; they are often assigned the numerical value 3. Hence

$$\boldsymbol{\mathcal{S}}^{\mathrm{fb}}_{\mathrm{A}}(\omega_0,\zeta_0)=\boldsymbol{\mathcal{R}}(\omega_0,\zeta_0)\,\boldsymbol{\mathcal{S}}^{\mathrm{f}}_{\mathrm{A}}(\omega_0,\zeta_0),\tag{4.3.17}$$

in which $\boldsymbol{\mathcal{R}}(\omega_0,\zeta_0)$ can be interpreted as response spectrum modification factors from FIRS to FLIRS.

4.4 Generating FRS Considering SSI

For a structure in a nuclear power plant with its rigid foundation embedded in layered soil, a procedure for generating FRS considering SSI is illustrated in Figure 4.9 and is summarized as follows:

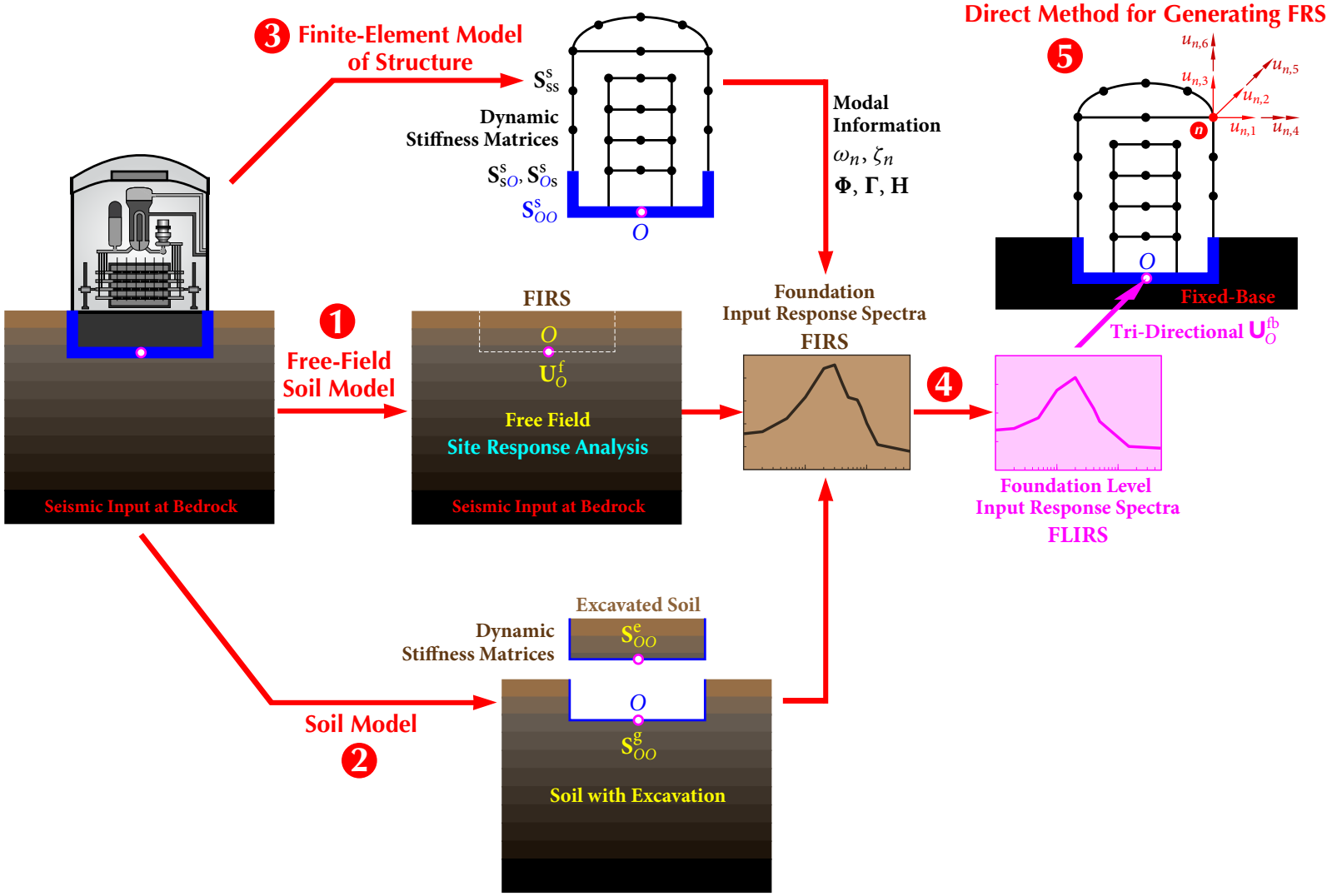

Figure 4.9 Procedure for generating FRS considering SSI

1. Consider the layered soil as a free-field. With seismic input applied at the bedrock, a site response analysis is performed to obtain the Foundation Input Response Spectra (FIRS) $\mathbf{U}_O^{\mathrm{f}}$ or $\mathbf{U}_{O,\mathrm{T}}^{\mathrm{f}}$ at the elevation of the foundation.
2. Establish a model of the layered soil. Determined the dynamic stiffness matrices of the excavated soil $\mathbf{S}_{OO}^{\mathrm{e}}$ and the soil with excavation $\mathbf{S}_{OO}^{\mathrm{g}}$. The dynamic stiffness matrix of the free-field is $\mathbf{S}_{OO}^{\mathrm{f}} = \mathbf{S}_{OO}^{\mathrm{g}} + \mathbf{S}_{OO}^{\mathrm{e}}$.
3. Set up a finite element model of the structure. Determine the dynamic stiffness matrices $\mathbf{S}_{\mathrm{ss}}^{\mathrm{s}}$, $\mathbf{S}_{\mathrm{s}O}^{\mathrm{s}}$, $\mathbf{S}_{O\mathrm{s}}^{\mathrm{s}}$, $\mathbf{S}_{OO}^{\mathrm{s}}$. Perform a modal analysis to obtain the modal frequencies ω_n, modal damping coefficients ζ_n, modal matrix $\boldsymbol{\Phi}$, and matrix of modal contribution factors $\boldsymbol{\Gamma}$.
4. Determine the Foundation Level Input Response Spectra (FLIRS):

   - $\mathbf{S}^{\mathrm{fb}} = \omega^2 \boldsymbol{\Phi}\mathbf{H}\boldsymbol{\Gamma} + \boldsymbol{\mathcal{I}} = \begin{bmatrix} \mathbf{S}_{\mathrm{TT}}^{\mathrm{fb}} & \mathbf{S}_{\mathrm{TR}}^{\mathrm{fb}} \\ \mathbf{S}_{\mathrm{RT}}^{\mathrm{fb}} & \mathbf{S}_{\mathrm{RR}}^{\mathrm{fb}} \end{bmatrix}_{6N\times 6}$

     $\mathbf{H} = \mathrm{diag}\left\{ \dfrac{1}{\omega_n^2 - \omega^2 + \mathrm{i}\,2\zeta_n\omega_n\omega} \right\}_{6N\times 6N}$

     $\boldsymbol{\Gamma} = \dfrac{\boldsymbol{\Phi}^T\mathbf{M}\boldsymbol{\mathcal{I}}}{\boldsymbol{\Phi}^T\mathbf{M}\boldsymbol{\Phi}}$ is a $6N\times 6$ matrix of the modal participation factors.

     $\boldsymbol{\mathcal{I}} = [\,\boldsymbol{\mathcal{I}}^1\ \boldsymbol{\mathcal{I}}^2\ \boldsymbol{\mathcal{I}}^3\ \boldsymbol{\mathcal{I}}^4\ \boldsymbol{\mathcal{I}}^5\ \boldsymbol{\mathcal{I}}^6\,]_{6N\times 6}$

   - $\mathbf{S} = \mathbf{S}_{O\mathrm{s}}^{\mathrm{s}}\mathbf{S}^{\mathrm{fb}} + \left(\mathbf{S}_{OO}^{\mathrm{s}} - \mathbf{S}_{OO}^{\mathrm{e}}\right) + \mathbf{S}_{OO}^{\mathrm{f}}$

     Determine the inverse $\mathbf{S}^{-1}$. The dimension is 6×6.

   - $\begin{bmatrix} \mathbf{T}_{\mathrm{TT}} & \mathbf{T}_{\mathrm{TR}} \\ \mathbf{T}_{\mathrm{RT}} & \mathbf{T}_{\mathrm{RR}} \end{bmatrix}_{6\times 6} = \mathbf{S}^{-1}\mathbf{S}_{OO}^{\mathrm{f}}$

   - Transfer matrix: $\boldsymbol{\mathcal{T}} = \mathbf{T}_{\mathrm{TT}} + [\left(\mathbf{S}_{\mathrm{TT}}^{\mathrm{fb}}\right)^T\mathbf{S}_{\mathrm{TT}}^{\mathrm{fb}}]^{-1}\left(\mathbf{S}_{\mathrm{TT}}^{\mathrm{fb}}\right)^T\mathbf{S}_{\mathrm{TR}}^{\mathrm{fb}}\,\mathbf{T}_{\mathrm{RT}}$

   - FLIRS modification factor: $\mathcal{R}^2(\omega_0,\zeta_0) = \dfrac{\displaystyle\int_{-\infty}^{\infty} \left|H_0(\omega)\right|^2 \left[\left|\boldsymbol{\mathcal{T}}(\omega)\right|^2\right]\mathbf{1}\,\mathrm{d}\omega}{\displaystyle\int_{-\infty}^{\infty} \left|H_0(\omega)\right|^2\,\mathrm{d}\omega}$

- FLIRS: $\boldsymbol{\mathcal{S}}_{\mathrm{A}}^{\mathrm{fb}}(\omega_0, \zeta_0) = \boldsymbol{\mathcal{R}}(\omega_0, \zeta_0)\, \boldsymbol{\mathcal{S}}_{\mathrm{A}}^{\mathrm{f}}(\omega_0, \zeta_0)$

5. The FLIRS $\boldsymbol{\mathcal{S}}_{\mathrm{A}}^{\mathrm{fb}}(\omega_0, \zeta_0)$ are input to the fixed-base finite-element model of the structure to generate the required FRS, which are exactly the same as the FRS obtained from a full coupled soil-structure analysis under the excitation of FIRS.

   Hence, when the direct spectra-to-spectra method developed by Jiang *et al.* (2015) is applied to the fixed-base structure under the excitation of FLIRS $\boldsymbol{\mathcal{S}}_{\mathrm{A}}^{\mathrm{fb}}(\omega_0, \zeta_0)$, FRS with complete probabilistic descriptions of FRS peaks, i.e., FRS with any desired level of NEP p can be obtained. If the method of time history is applied, such a result could only be obtained from a large number of coupled soil-structure analyses using a commercial finite-element software, such as *ACS SASSI*, with a large number of generated time histories compatible with the FIRS.

4.5 Numerical Example

To verify the accuracy and efficiency of the proposed method, FRS of a typical reactor building in nuclear power plants founded on the surface of a homogeneous half-space are generated following the procedure summarized in Section 4.4. The resultant FRS are then compared with the mean FRS obtained from a large number of time history analyses, which is referred as the "exact" FRS for benchmark. Based on the physical meaning of the formulation in the proposed method, some key parameters, which affect the resultant FRS when the SSI effect is accounted, are investigated.

Model information

The selected reactor building consists of a containment and an internal structure that are supported by a circular disk foundation with a radius of 19.8 m, as shown in Figure 4.10. Using the commercial finite element software *STARDYNE*, the building is modelled as a lumped-parameter system which can characterize the most significant dynamic properties of the structure. There are total 12 nodes for both the superstructure and the foundation, and each node has 6 DOF. Therefore, the model is a 6×12 DOF system. For a fixed-base model, the DOF at Node *O*, which denotes the foundation, are constrained. The model is

symmetric about X- and Y-axes, and the finite element model information is described in Tables 4.1 and 4.2 (Li *et al.*, 2005).

The underlying soil is chosen as an infinite homogenous half-space. To consider the variability of the soil properties, three soil cases with different shear modulus, including Case 1: Lower Bound (LB, −30%), Case 2: Best Estimate (BE), and Case 3: Upper Bound (UB, +30%), are studied. For each case, the stiffnesses of the soil springs in the three translational and three rotational directions are calculated by the formula recommended in ASCE 4-98 Standard (1998, Page 25) and are listed in Table 4.3. The radiation and material damping of the soil is treated as one damping ratio of 0.3 and 0.1 for translational and rotational components, respectively.

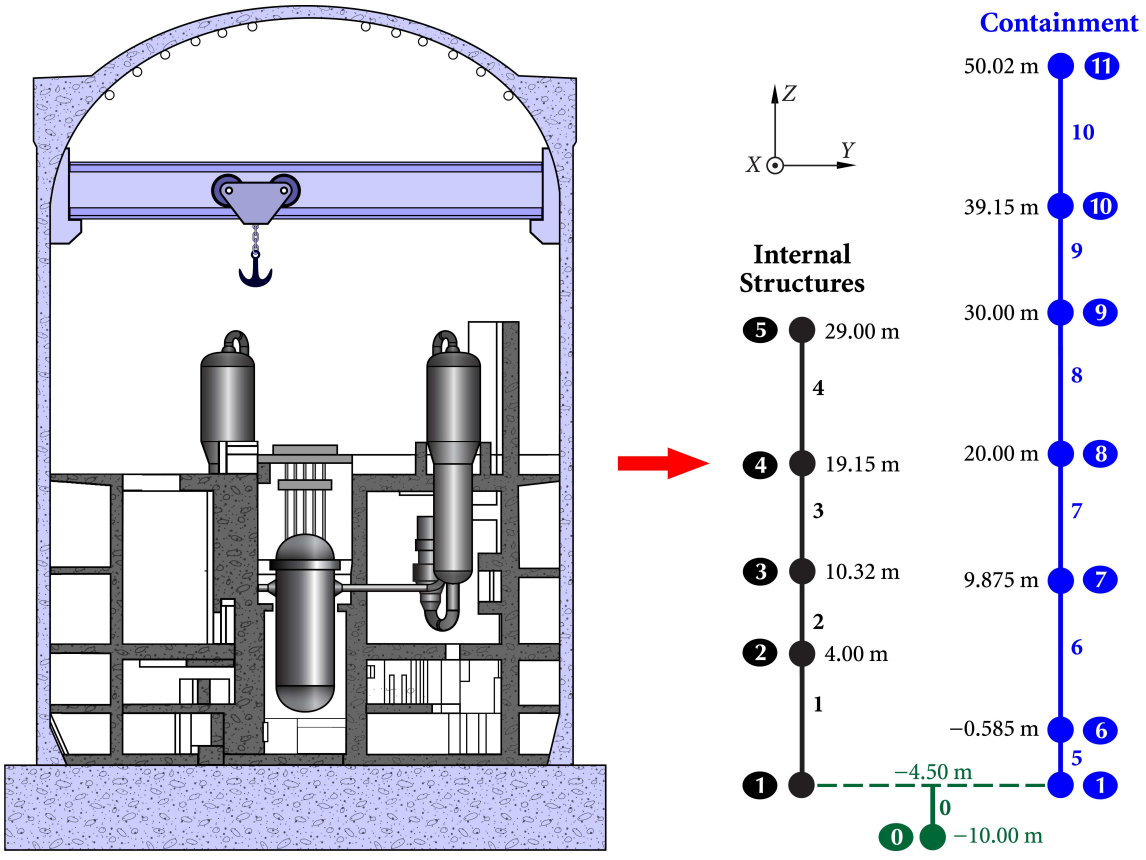

Figure 4.10 Primary and secondary systems in a nuclear power plant

Table 4.1 Nodal information of reactor building model

Node	Elevation (m)	Mass ($\times 10^6$ kg)	Moment of inertia ($\times 10^6$ kg $\cdot$ m^2)	
			$I_{xx} = I_{yy}$	I_{zz}
0	-10	8425	843	1643
1	-4.5	13420	1260	1931
2	4	5710	370	0
3	10.32	5970	394	0
4	19.15	6750	500	0
5	29	1270	110	0
6	-0.585	2288	424	824
7	9.875	3033	568	1087
8	20	2960	554	1063
9	30	2960	554	1063
10	39.15	3068	562	1081
11	50.02	6271	910	1727

Table 4.2 Beam Element Properties of reactor building model

Section	Beam	Area (m^2)	Shear area (m^2)	Second area moment (m^4)
1	0	1204	1084.7	115436
2	1	50	19	5720
3	2	110	70	8160
4	3	140	70	8160
5	4	60	30	325
6	5	176	88	30570
7	6-10	107	53.5	19241

Table 4.3 Soil properties and equivalent stiffness

Case	Shear modules (MPa)	Shear velocity (m/s)	Soil spring stiffness			
			Translational ($\times 10^{11}$ N/m)		Rotational ($\times 10^{14}$ N·m/rad)	
			$K_x = K_y$	K_z	$K_{rx} = K_{ry}$	K_{rz}
1 (LB)	6790	1616	6.57	7.79	2.04	2.81
2 (BE)	9700	1931	9.38	11.1	2.91	4.02
3 (UB)	12610	2202	12.2	14.5	3.78	5.22
Soft soil	1358	323	1.31	1.56	0.41	0.56

Foundation input response spectra

The R.G. 1.60 response spectra (USNRC, 1973) are assumed as the foundation input response spectra (FIRS) obtained from a site response analysis. The peak ground accelerations are anchored to $0.3g$ and $0.2g$ for the horizontal and vertical directions, respectively. 30 sets of tri-directional time histories, which are compatible with the target FIRS as shown in Figure 2.16, are generated by the Hilbert-Huang Transform method (Ni *et al.*, 2013, 2011), and will be used for performing time history analyses to provide the "exact" FRS for benchmark.

Effect of soil-structure interaction on FRS

The effect of SSI on FRS is studied first by comparing the mean FRS obtained from the 30 sets of time history analyses. The mean FRS at Node 5 for a fixed-base model and the Case 1 (LB) soil-structure model are plotted in Figure 4.11. It is observed that the peak value of FRS is reduced by 22% when the SSI effect is accounted, despite the peak floor acceleration, which represents the structural response, is decreased by only 10%. It means that the SSI effect is more significant on FRS. However, FRS of the soil-structure model are not always lower than those of the fixed-base model. It can be seen that there is a peak emerging on the left of the main peak (around 4 Hz), which leads to a 23% increase in FRS. Furthermore, the

spectral value at the second FRS peak is increased by 13% in contrast to the behaviour at the main peak.

Another observation is made in Figure 4.12, in which FRS at Node 5 for two SSI cases, Case 2 (BE) and Case 3 (UB), are compared. Only slight differences are observed at the FRS peaks, although there is a 30% increase in the soil shear modulus. It implies that FRS is not very sensitive to the underlying soil properties when the soil is sufficiently rigid. Although the differences are small, one can still see that FRS of Case 2 (BE), with relatively soft soil, is higher at the first peak but lower at the second peak, which is consistent with the observation in Figure 4.11. Therefore, it is necessary to identify key parameters that affect the FRS when the SSI effect is taken into account. In the following, FRS of Case 1 (LB) and Case 3 (UB) will be generated through the proposed method and be validated by comparing with the "exact" FRS.

Development of foundation level input response spectra (FLIRS)

Following Step 4 in Section 4.4, a modal analysis is performed for the fixed-base model. Basic modal information, including natural frequencies and mode shapes of the first 25 modes, is extracted. The mass matrix and earthquake influence matrix can be readily determined from the information in Table 4.1. Modal information of significant modes at locations of interest is shown in Table 4.4, and the modal damping ratio of the structure is 5%. The dimensionless transfer matrix of the fixed-base model $\mathbf{S}^{\mathrm{fb}}$ is calculated for different values of ω, varying from 0.2π to 200π with an increment of 0.2π. Each elements in the matrix is complex and can be regarded as a transfer function. The modulus of the elements corresponding to the translational DOF at Nodes 2 to 5 are plotted versus frequency in Figure 4.13. It can be seen that the modulus of the transfer functions peak at the structural frequencies of the significant modes.

The transfer matrix $\boldsymbol{\mathcal{T}}$ defined by equation (4.3.10) is determined frequency by frequency, and the modulus of $\boldsymbol{\mathcal{T}}_{11}$ is shown in Figure 4.14. To distinguish the contributions from the translational and rotational motions of the foundation to FLIRS, the contribution of translational components, which is characterized by the modulus of the first term in equation (4.3.10), is also plotted in Figure 4.14. It can be observed that the rotational

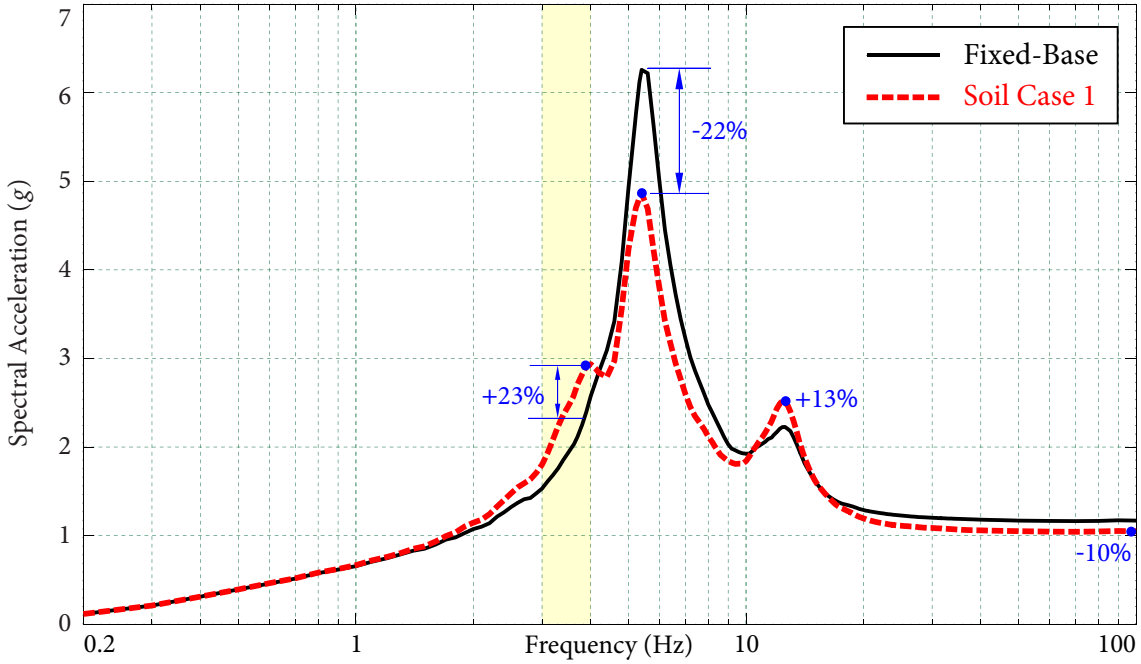

Figure 4.11 Illustration of soil-structure interaction effect on FRS

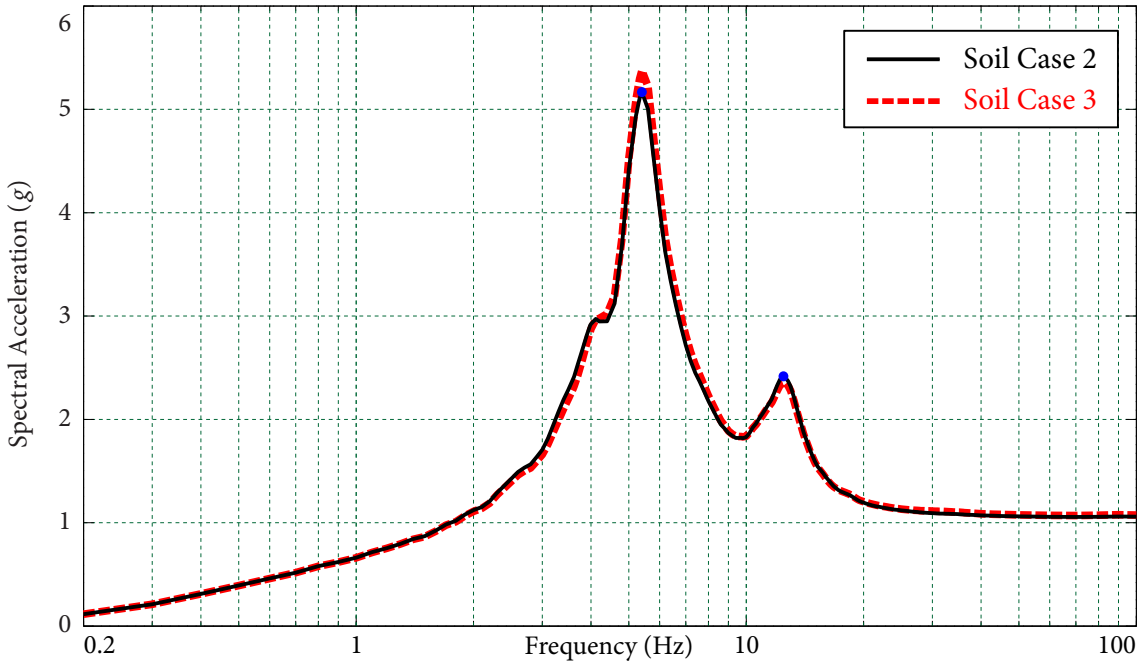

Figure 4.12 Sensitivity analysis of soil properties on FRS

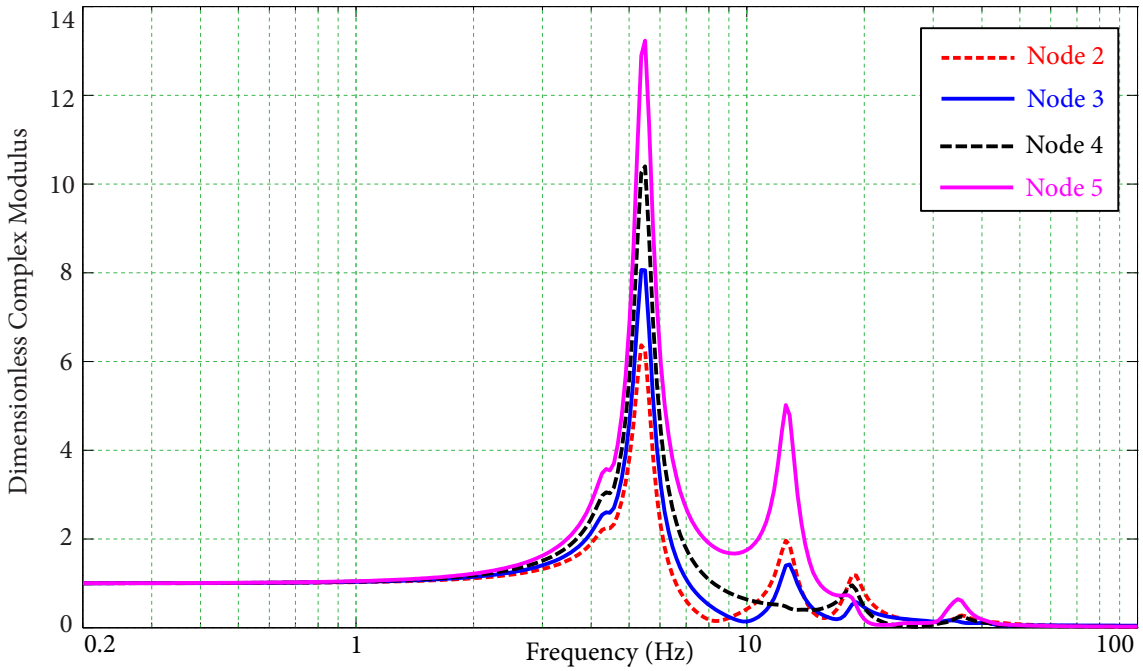

Figure 4.13 Modulus of fixed-base model transfer function for Nodes 2 to 5 in *X*-direction

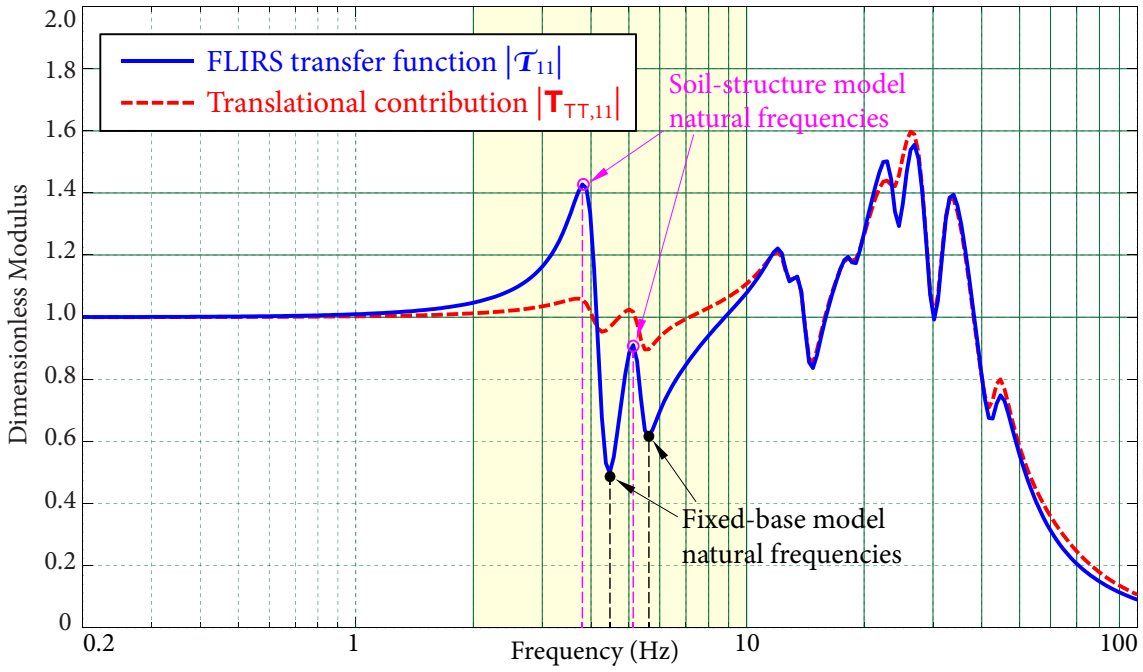

Figure 4.14 Modulus of horizontal component in FLIRS transfer matrix (Case 1)

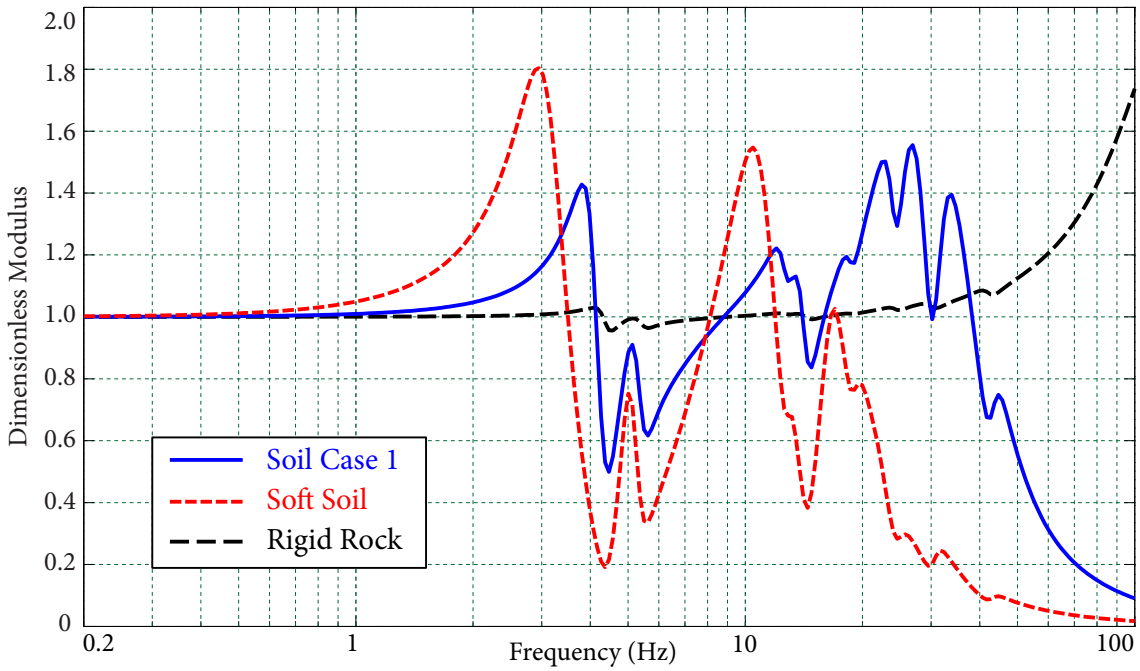

Figure 4.15 Effect of soil properties on modulus of transfer matrix horizontal component

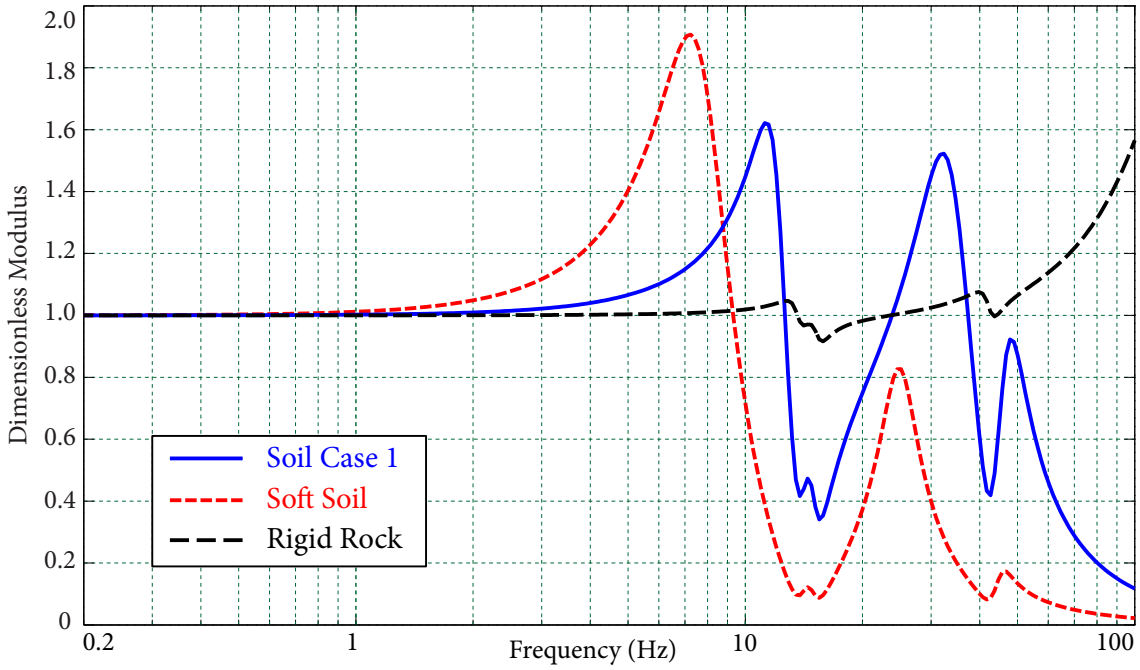

Figure 4.16 Effect of soil properties on modulus of transfer matrix vertical component

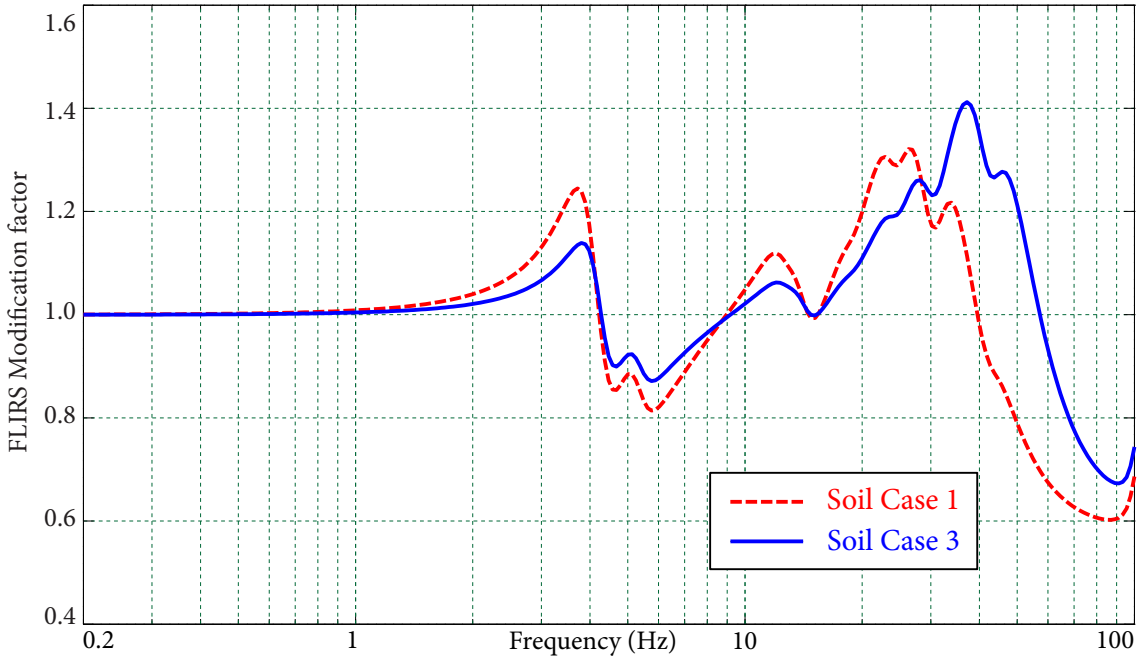

Figure 4.17 Horizontal FLIRS Modification factor

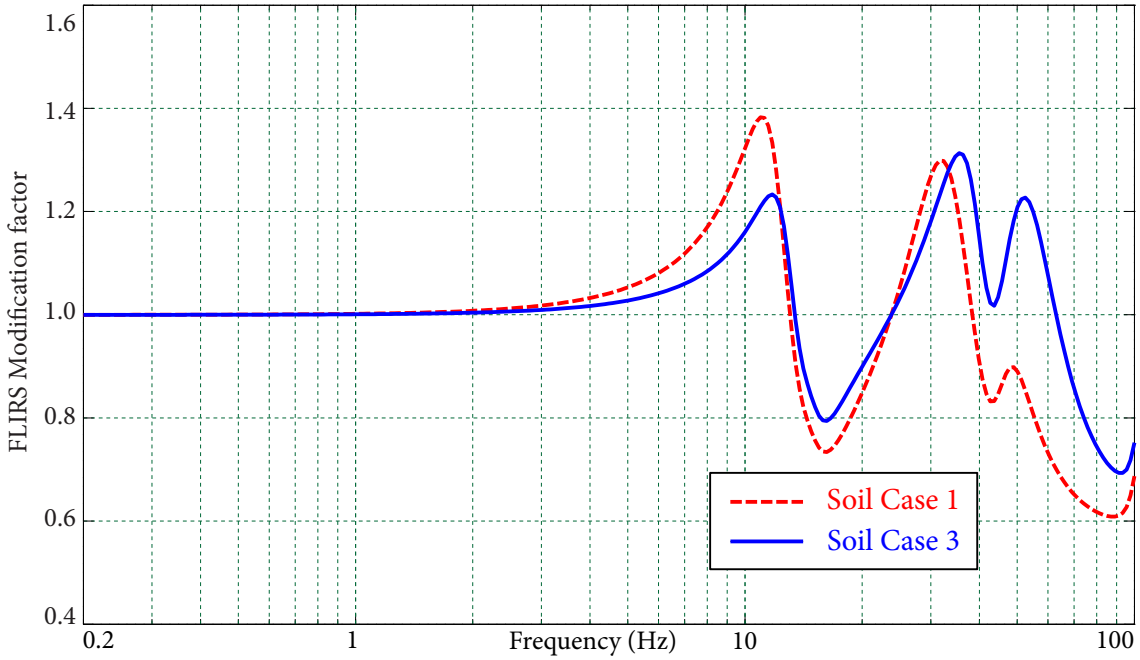

Figure 4.18 Vertical FLIRS Modification factor

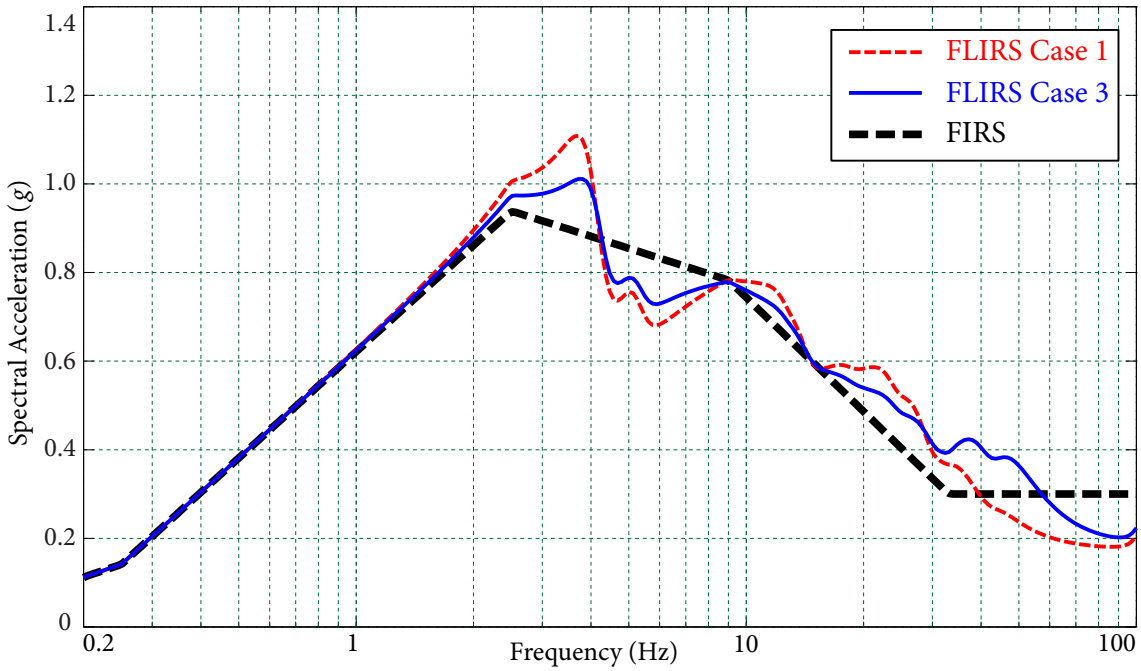

Figure 4.19 Horizontal FLIRS

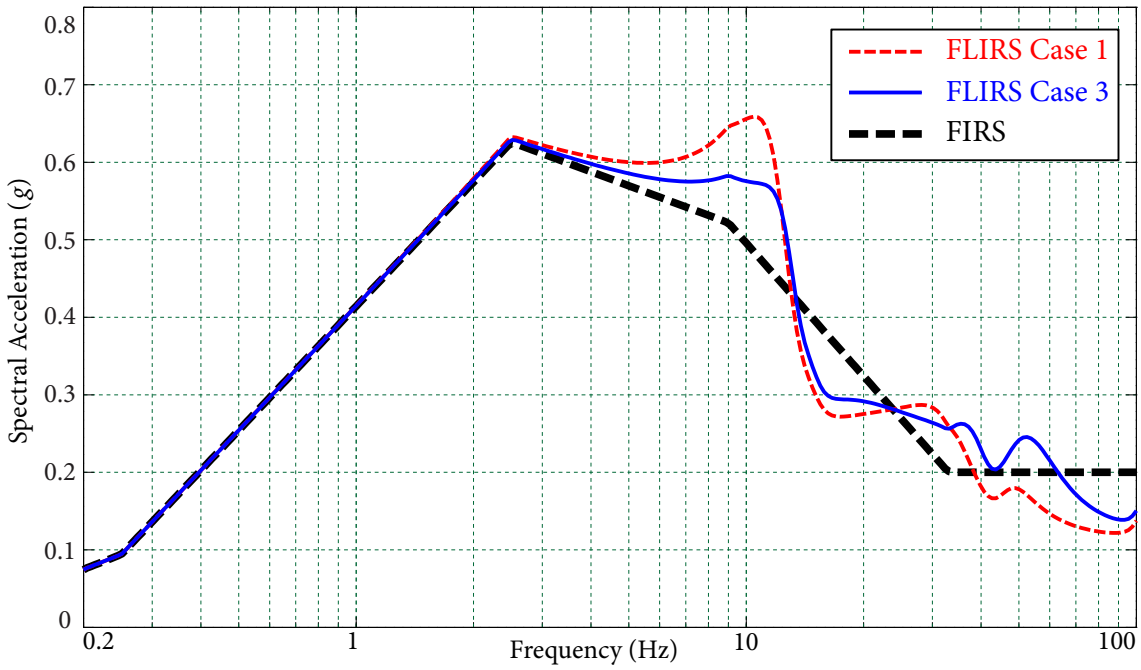

Figure 4.20 Vertical FLIRS

Table 4.4 Modal information of significant modes

Mode	Frequency (Hz)	Participation factor	Modal contribution factor			
			Node 2	Node 3	Node 4	Node 5
2	4.393	1.279	0.04	0.05	0.06	0.08
4	5.449	1.336	0.64	0.82	1.05	1.34
7	12.721	−0.511	0.19	0.14	−0.01	−0.51
12	18.753	0.114	0.11	0.05	−0.10	0.06

components have a pronounced effect on the total equivalent base excitation to the fixed-base model in the frequency range of 2 Hz to 10 Hz, which covers the frequencies of the dominant structural modes. Therefore, the rotational movement of foundation cannot be neglected.

Analogous to the modulus of the transfer matrix of the fixed-base structure shown in Figure 4.13 where peaks emerge at the frequencies of the significant structural modes, the frequencies corresponding to the peaks in Figure 4.14 can be interpreted as the natural frequencies of the soil-structure system (or the equivalent synthesized mass-spring-damper system). For instance, the first two peaks of the soil-structure system, located at 3.8 Hz and 5.1 Hz, can be explained as a result of the frequency shifting of the fixed-base model from 4.4 Hz and 5.4 Hz due to the SSI effect. Meanwhile, the significant modal frequencies of the fixed-base model correspond to the bottom of the valley between the peaks, implying considerable reductions of the responses of the structure.

For further illustration, two special soil cases, a soft soil case given in Table 4.3 and a rigid rock case that the shear modulus is 10 times of that of Case 3 (UB), are added for discussion. The modulus of $\boldsymbol{\mathcal{T}}_{11}$ for these two cases are plotted in Figures 4.15 and 4.16 for comparison. It shows that FLIRS is hardly modified for a structure resting on the surface of rigid rock, thus FIRS can be used as FLIRS directly. For soft soil case, the natural frequency shifting and reduction of responses for a soil-structure system are significant. However, the

locations of the valley do not change for all cases since the frequencies of fixed-base model are not affected by the soil properties.

The FLIRS modification factors $\boldsymbol{\mathcal{R}}(\omega_0, \zeta_0)$ are then used to generate FLIRS from FIRS; FLIRS are used in the direct method for generating FRS from the fixed-base model. Figures 4.17 and 4.18 show the horizontal and vertical components of the FLIRS modification factors for soil Case 1 (LB) and Case 3 (UB). It can be seen that the FLIRS is smoother than the modulus of transfer function $|\boldsymbol{\mathcal{T}}_{11}|$. The FLIRS modification factor in Figure 4.17 can also explain the phenomenon of SSI effect observed in Figure 4.11: FRS decreases at the first peak but increases at the second peak. Therefore, it should be emphasized that FRS may increase when the effect of SSI is taken into account. The resultant FLIRS for soil Case 1 and Case 3 are shown in Figure 4.19 and 4.20.

Validation of the proposed method

The direct spectra-to-spectra method (Jiang *et al.*, 2015; Li *et al.*, 2015) is applied to generate FRS at Nodes 2 to 5 in the internal structure. The resultant FLIRS are used as the input response spectra to the fixed-base model. FRS are calculated at 200 frequencies including the natural frequencies of the structure using the direct spectra-to-spectra method. For soil Case 1 (LB) and Case 3 (UB), the resultant FRS at various nodes are plotted along with the FRS generated by the 30 sets of time history analyses in Figures 4.21 to 4.28. FRS obtained by the direct method and the mean FRS of the time history analyses, which are regarded as the "exact" FRS, are shown in black solid lines and red dash lines, respectively. It is seen that the FRS obtained by the direct method generally agree very well with the "exact" FRS over the entire frequency range, whereas results from time histories analyses exhibit large variability. Particularly, FRS peak values can be overestimated by more than 30% or underestimated by mores than 20%. However, the differences at the FRS peaks between the direct method and the "exact" FRS are generally less than 5%, which are well within the range of acceptable errors.

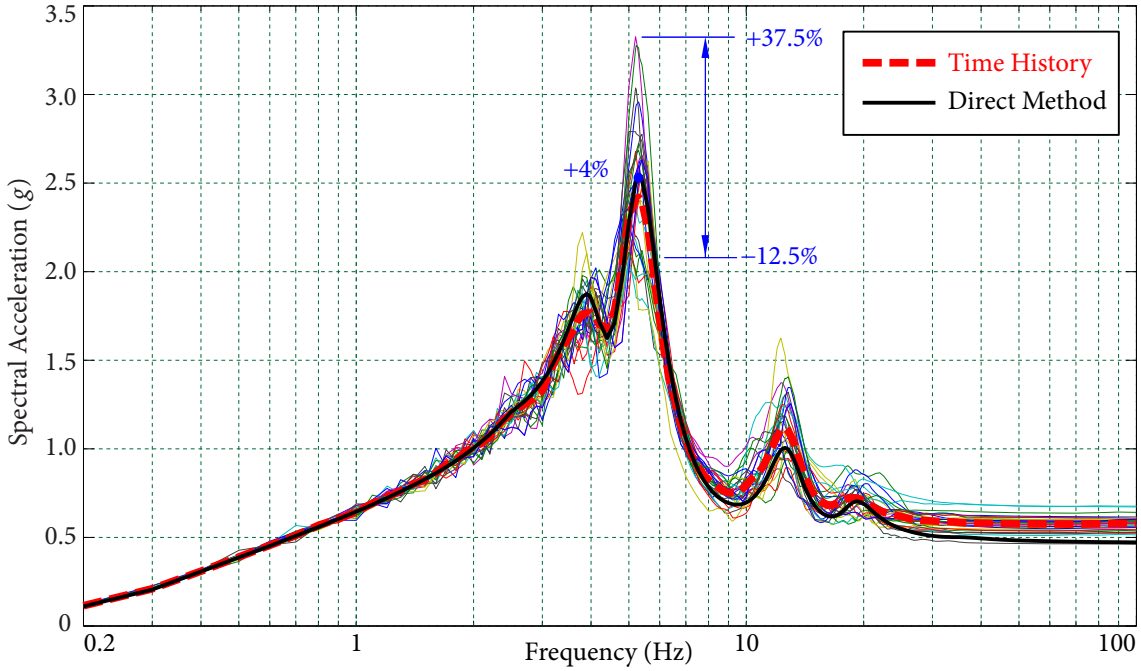

Figure 4.21 Comparison of FRS at Node 2 for soil Case 1 (LB)

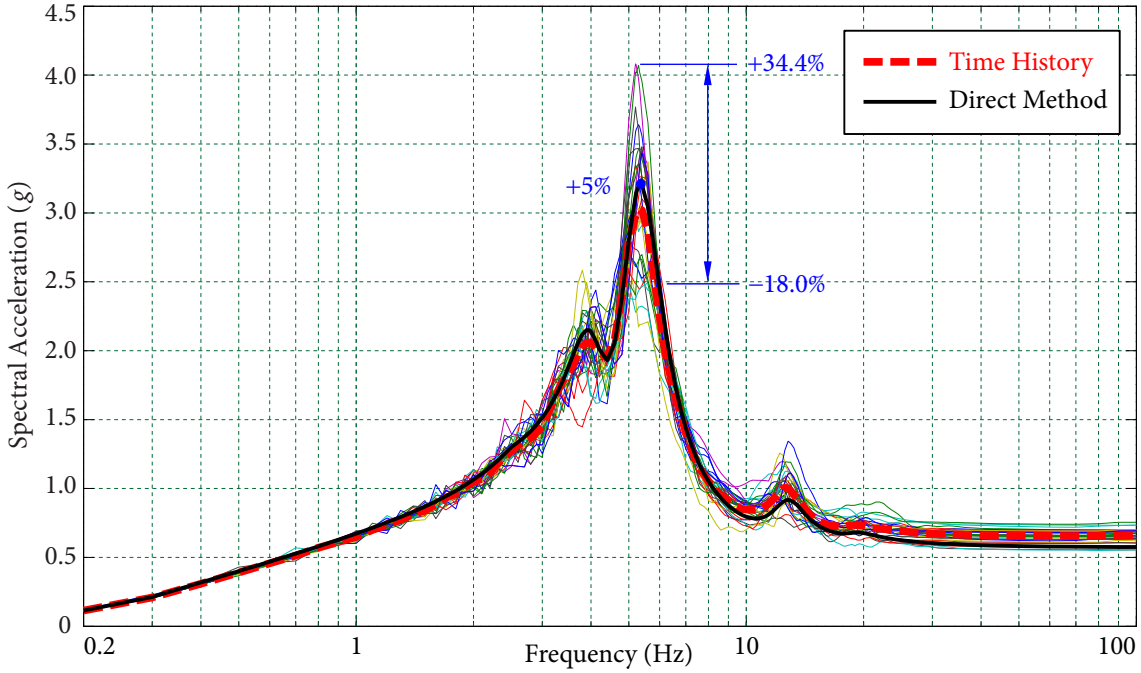

Figure 4.22 Comparison of FRS at Node 3 for soil Case 1 (LB)

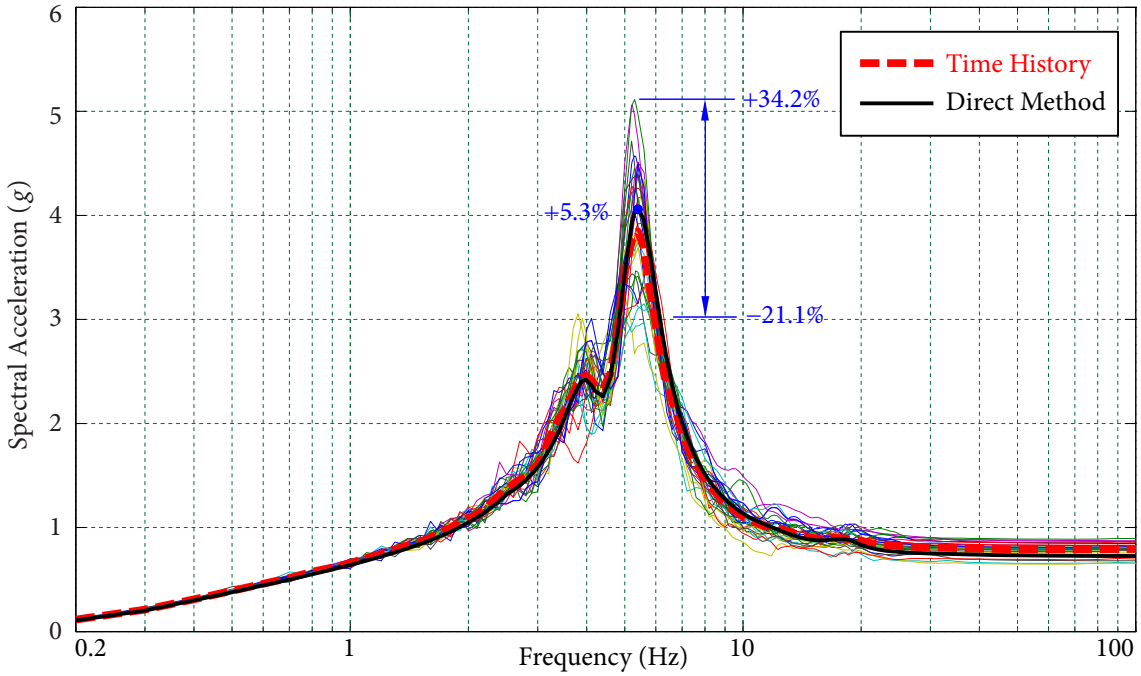

Figure 4.23 Comparison of FRS at Node 4 for soil Case 1 (LB)

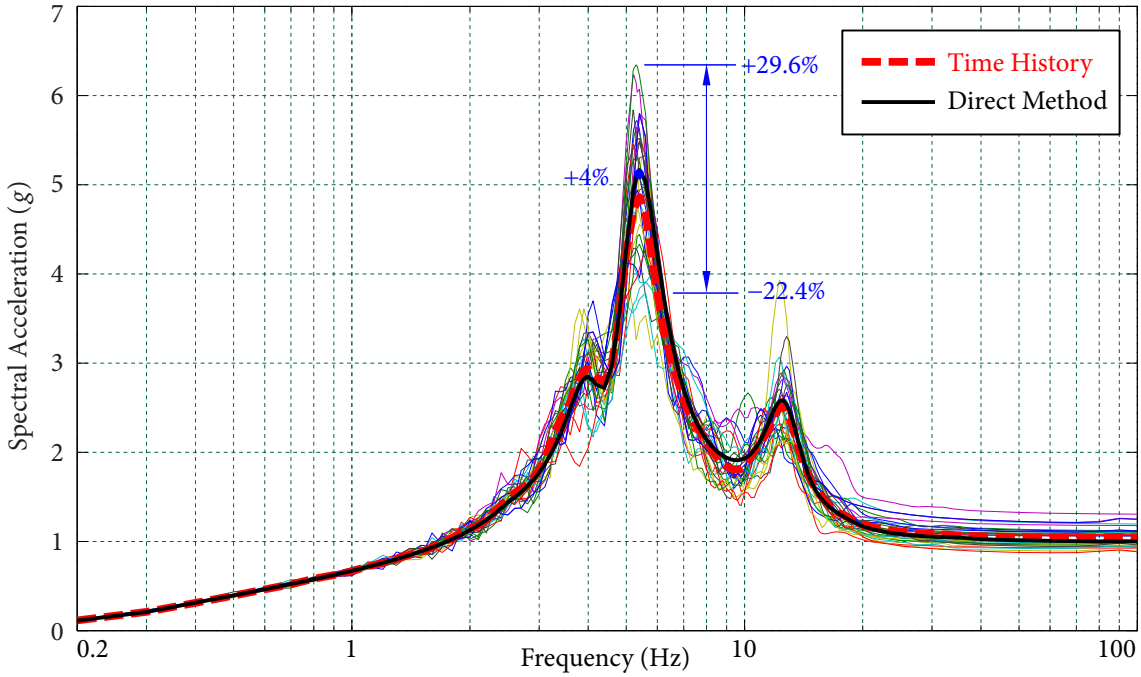

Figure 4.24 Comparison of FRS at Node 5 for soil Case 1 (LB)

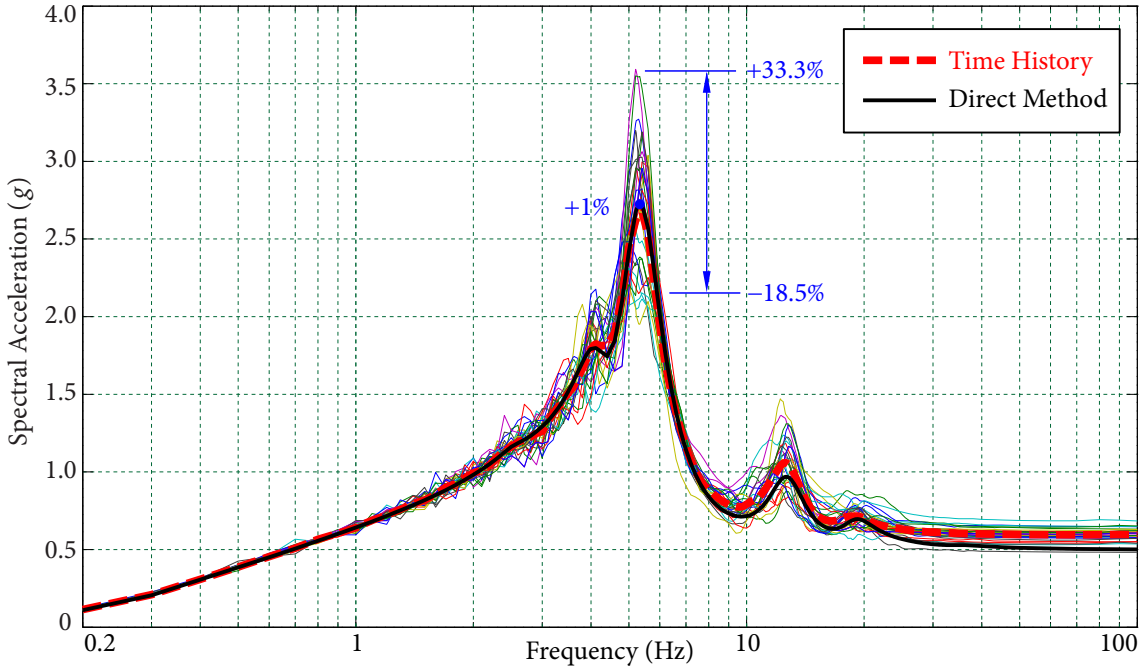

Figure 4.25 Comparison of FRS at Node 2 for soil Case 3 (UB)

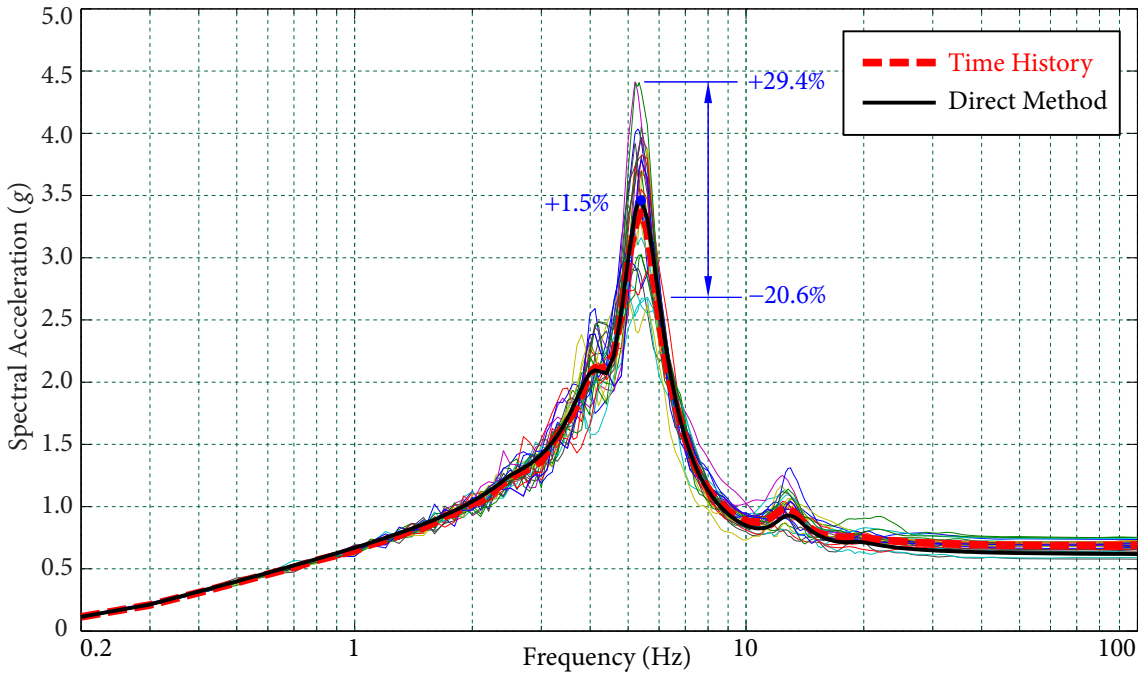

Figure 4.26 Comparison of FRS at Node 3 for soil Case 3 (UB)

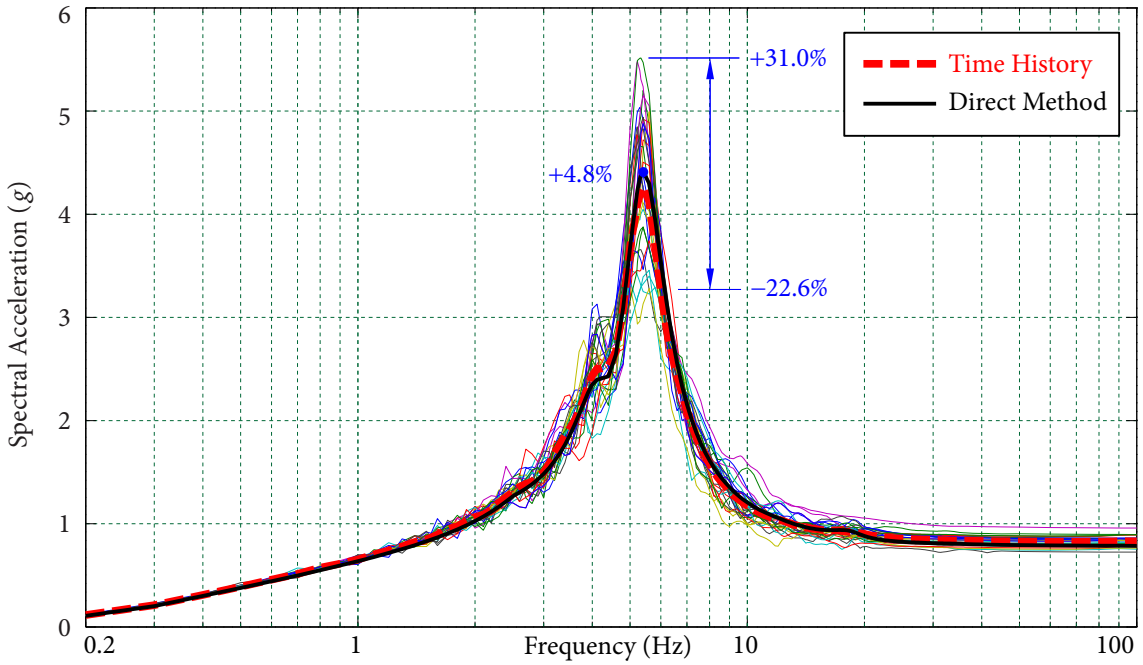

Figure 4.27 Comparison of FRS at Node 4 for soil Case 3 (UB)

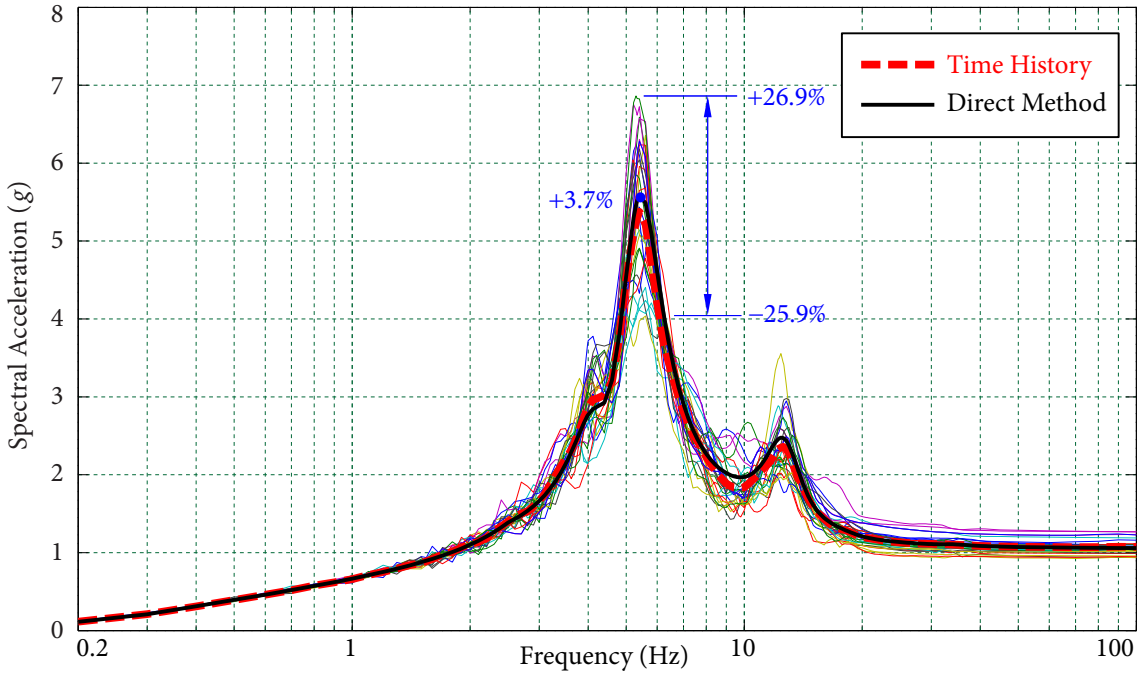

Figure 4.28 Comparison of FRS at Node 5 for soil Case 3 (UB)

4.6 Summary

In this chapter, a method is developed for generating FRS considering SSI based on the substructure technique and the direct spectra-to-spectra method (Jiang *et al.*, 2015; Li *et al.*, 2015). The tri-directional response spectra at the foundation level of the free-field (FIRS) are modified by multiplying a vector of modification factors, which depend on properties of both structure and soil. The modified response spectra, called foundation level input response spectra (FLIRS), are then used as the input to the fixed-base structure to generate FRS using the direct spectra-to-spectra method. The concept of FLIRS has great practical significance in seismic risk assessment.

A numerical example is performed to verify the proposed method. FRS of a typical reactor building with a rigid foundation supported by an elastic homogeneous half-space are generated by 30 sets of time history analyses and the proposed method. Comparison of the resultant FRS shows that the FRS obtained by the proposed method agree very well with the mean FRS of a large number of time history analyses, which is regarded as the "exact" FRS, for all nodes on the internal structure of the reactor building; whereas FRS obtained from time history analyses exhibit large variability at the FRS peaks. The proposed method is efficient and accurate. It is also demonstrated that the effect of soil-structure interaction may increase FRS at certain frequencies, which leads to a higher seismic demand for the equipment in the supporting structure.

C H A P T E R 5

Conclusions and Future Research

Floor Response Spectrum (FRS) is critical in seismic probabilistic risk analysis and design of secondary systems in nuclear power facilities. This study aims at developing an accurate and highly efficient method for the generation of FRS. Some contributions for this purpose have been accomplished in this study, and are summarized as follows.

5.1 Direct Spectra-to-Spectra Method

A direct spectra-to-spectra method is developed to overcome the deficiencies of the time history method. "Direct" means GRS is used as seismic input directly without generating any intermediate input, such as spectrum-compatible time histories. FRS can be determined readily from the input GRS and the basic modal information required in a traditional response spectrum analysis of structure. Some remarkable features and advantages of the proposed direct spectra-to-spectra method are summarized as follows:

- The direct method gives accurate FRS; FRS obtained by this method agree extremely well with the "exact" results obtained from extensive time history analyses. Particularly, values at FRS peaks, which are of main interest to engineers, can be estimated accurately, while the time history method produces large variabilities at the peaks. Apparently, overestimation of FRS peaks results in unnecessary high costs in seismic design and qualification of SSCs; whereas underestimation is strictly impermissible.

- The direct method can give full probabilistic descriptions at FRS peaks, which can satisfy various seismic design and assessment requirements for SSCs with different safety margins.
- The direct method is analytically formulated and it is convenient to implement using a programming language, such as MATLAB, C, or Fortran. Only the specified GRS and basic modal information of the primary structure, which can be readily obtained from a modal analysis, are needed.
- The direct method is highly efficient. FRS can be generated in a few seconds by a computer implementation of the direct method. In contrast, a large number of time history analyses need to be performed in a commercial finite element analysis software to achieve results with similar accuracy. The process of generating spectrum-compatible time histories and performing dynamic analyses is computationally expensive and time-consuming.
- The formulation of the direct method provides physical insight into which vibration modes of the primary structure make significant contributions to the response of the system. For a new build at a different site, the design of the primary structures, including reactor buildings and auxiliary buildings, do not have significant changes. However, the design GRS is dependent on the local site conditions. Using the direct method and the existing modal information, FRS can be quickly estimated using the new design GRS as input, without generating spectrum-compatible time histories. These results can provide guidance for the preliminary design and procurement of SSCs in an early stage.
- Since FRS obtained from a single time history analysis, or even a small number of time history analyses, have rugged spectral shape due to inherent randomness and uncertainty of time histories, the FRS need to be smoothed for practical use. In contrast, the specified GRS having smooth spectral shapes are used as input directly in the direct method, the resulting FRS, which are the amplified GRS, preserve the feature of smooth spectral shapes. Consequently, FRS smoothing can be avoided by using the direct method.

5.2 Scaling of Floor Response Spectra

A scaling method for generating FRS is developed based on the direct spectra-to-spectra method for generating FRS. The analytical formulation of the direct spectra-to-spectra method provides a strong physical insight into FRS, which allows the identification of dynamical information of the significant equivalent modes of the underlying structure from the available GRS-I and FRS-I. Scaling factors are sequently determined in terms of the dynamical information (modal frequencies, damping ratios, and contribution factors) and the input GRS-I and GRS-II. Some remarkable features and advantages of the proposed scaling method are summarized as follows:

- The proposed scaling method allows to obtain accurate FRS by using as much of the available results as possible without performing a complete dynamic analysis, which introduces extra costs and is time consuming.
- A system identification technique is presented to recover the equivalent modal information of significant modes for a complex structure with a large number of degree-of-freedom. FRS or structural responses can be determined with sufficient accuracy by using the equivalent modal information of a few modes.
- FRS with higher equipment damping ratios be can obtained by the scaling method when the interpolation method recommended in standard ASCE (1998) is invalid.
- The scaling FRS can generate accurate FRS even though large variations exist between the spectral shape of GRS-I and GRS-II.
- The scaling factors depends on dynamical characteristics of the structure, damping ratio of the secondary system, and variations in the spectral shape of GRS. It means that scaling of FRS is a complex problem, using a constant scaling factor may result in inaccurate FRS.
- For broadened and smoothed FRS-I which are modified artificially, methods of selecting critical points for performing system identification are presented. Despite there may be bias in selecting the critical points, the equivalent modal information can still provide sufficiently accurate FRS-II after broadening.

5.3 Generating FRS Considering Soil-Structure Interaction

For a structure founded on soil site, the dynamical soil-structure interaction (SSI), which affects the seismic behavior of the structure thus results in different FRS, cannot be neglected. A methodology is developed to generate FRS considering the SSI effect on the basis of the substructure method and the proposed direct spectra-to-spectra method. Some remarkable features and advantages of the proposed method are summarized as follows:

- A method of determining a vector of modification factors for the foundation input response spectra (FIRS), which is obtained from a free-field site response analysis, is developed to incorporate the SSI effect. The modified FIRS, which is called FLIRS, are used as input in the direct spectra-to-spectra method to generate FRS. Additionally, the natural frequencies of the soil-structure system can be identified accurately by the vector of modification factors.
- The proposed method is computationally efficient. A soil-structure system can be physically interpreted as a frequency-dependent synthesized nodal mass with 6 degree-of-freedom supported by generalized soil springs. When the properties of a structure or soil are changed, only the synthesized mass or the stiffnesses of the generalized soil springs need to change; as a result, a reanalysis of the entire system, which is time-consuming, can be avoided. Furthermore, the required computational effort is reduced significantly, since it is needed to evaluate the inverse of a 6×6 matrix rather than a $6N \times 6N$ matrix, which may lead to numerical difficulties for a large-scale system.
- The SSI effect may increase FRS at certain frequencies, which leads to a higher seismic demand for the equipment in the supporting structure.
- The proposed method considering SSI is demonstrated using a structure with rigid foundation supported on soil medium which is modelled as a homogenous half-space. FRS obtained using the proposed method agree well with "exact" results obtained from a large number of time history analyses.

5.4 Future Research

In future research, the direct spectra-to-spectra method and the scaling method will be extended to generate third-level FRS (FRS3) for SSCs mounted on secondary systems. For example, to seismic qualify a component of a large equipment (secondary system), such as a valve of a heat exchanger, mounted on a floor, the excitations to the large equipment are the responses of the floor (FRS) and the excitations to the component are the responses of the large equipment (FRS3). In such situations, the direct method is especially important and useful for the following reasons

- Time histories compatible to the tri-directional FRS are usually not readily available.
- There are very large variabilities in time history analyses in generating FRS from GRS-compatible time histories (Jiang *et al.*, 2015) and further in generating FRS3 from FRS-compatible time histories.

Furthermore, by taking advantage of the accuracy and efficiency of the proposed method for generating FRS considering SSI, the effect of the uncertainties in the properties of structure, secondary system, and underlying soil on the resultant FRS can be investigated systematically.

Bibliography

An, Y., Jiang, Y., and Ly, B., 2013. Direct generation of RRS from FRS. *Proceedings of the 22th International Conference on Structural Mechanics in Reactor Technology*.

ASCE, 1998. *Seismic Analysis of Safety-Related Nuclear Structures and Commentary*, **ASCE 4-98**. American Society of Civil Engineers (ASCE).

ASCE, 2005. *Seismic Design Criteria for Structures, Systems, and Components in Nuclear Facilities*, **ASCE/SEI 43-05**. Structural Engineering Institute, American Society of Civil Engineers (ASCE).

ASCE, 2010. *Minimum Design Loads for Buildings and Other Structures*, **ASCE/SEI 7-10**. American Society of Civil Engineers, Reston, Virginia.

Asfura, A. and Kiureghian, A.D., 1986. Floor response spectrum method for seismic analysis of multiply supported secondary systems. *Earthquake Engineering and Structural Dynamics*, **14**(2): 245–265.

Atkinson, G. M. and Elgohary, M., 2007. Typical uniform hazard spectra for eastern north american sites at low probability levels. *Canadian Journal of Civil Engineering*, **34**(1): 12–18.

Biggs, J.M. and Roesset, J.M., 1970. Seismic analysis of equipment mounted on a massive structure. *Seismic Design for Nuclear Power Plants*, 319–343.

Burdisso, R.A. and Singh, M.P., 1987. Multiply supported secondary systems part i: Response spectrum analysis. *Earthquake Engineering and Structural Dynamics*, **15**(1): 53–72.

Cameron, W.I. and Green, R.A., 2007. Damping correction factors for horizontal ground-motion response spectra. *Bulletin of the Seismological Society of America*, **97**(3): 934–960.

Chaudhuri, S.R. and Villaverde, R., 2008. Effect of building nonlinearity on seismic response of nonstructural components: a parametric study. *Journal of Structural Engineering*, **134**(4): 661–670.

Chen, Y. and Soong, T.T., 1988. Seismic response of secondary systems. *Engineering Structures*, **10**(4): 218–228.

Clough, R.W. and Penzien, J., 2003. *Dynamics of Structures*. Computers & Structures, Inc., third edition.

CSA, 2010. *Design Procedures for Seismic Qualification of Nuclear Power Plants*, **CSA N289.3-10**. Canadian Standard Association (CSA).

Deeks, A.J. and Randolph, M.F., 1994. Axisymmetric time-domain transmitting boundaries. *Journal of Engineering Mechanics*, **120**(1): 25–42.

Der Kiureghian, A., 1981. A response spectrum method for random vibration analysis of mdf systems. *Earthquake Engineering and Structural Dynamics*, **9**: 419–435.

Duff, C.G., 1975. Simplified method for development of earthquake ground and floor response spectra for nuclear power plant design. Technical report, Atomic Energy of Canada Ltd., Ontario.

EPRI, 1991. *A Methodology for Assessment of Nuclear Power Plant Seismic Margin*, **EPRI NP-6041-SL**. Electric Power Research Institute.

EPRI, 1994. *Methodology for Developing Seismic Fragilities*, **EPRI TR-103959**. Electric Power Research Institute.

EPRI, 2002. *Seismic Fragility Application Guide*, **EPRI 1002988**. Electric Power Research Institute.

Ghiocel, D.M., 2015. *ACS SASSI*, **3.0**. GP Technologies, Inc.

Gupta, A.K. and Jaw, J.W., 1986A. Coupled response spectrum analysis of secondary systems using uncoupled modal properties. *Nuclear Engineering and Design*, **92**(1): 61–68.

Gupta, A.K. and Jaw, J.W, 1986B. Seismic response of nonclassically damped systems. *Nuclear Engineering and Design*, **91**(2): 153–159.

Gupta, A.K. and Jaw, J.W, 1986C. A new instructure response spectrum (irs) method for multiply connected secondary systems with coupling effects. *Nuclear Engineering and Design*, **96**(1): 63–80.

Gupta, A.K. and Tembulkar, J.M., 1984. Dynamic decoupling of secondary systems. *Nuclear Engineering and Design*, **81**(3): 359–373.

Gupta, A.K., 1984. Seismic response of multiply connected mdof primary and mdof secondary systems. *Nuclear Engineering and Design*, **81**(3): 385–394.

Gutierrez, J.A. and Chopra, A.K., 1978. A substructure method for earthquake analysis of structures including structure-soil interaction. *Earthquake Engineering and Structural Dynamics*, **6**(1): 51–69.

Hadjian, A. H. and Ellison, B., 1986. Decoupling of secondary systems for seismic analysis. *Journal of Pressure Vessel Technology*, **108**(1): 78–85.

IBC, 2012. *2012 International Building Code*. International Code Council, Washington D.C.

Igusa, T., Kiureghian, A.D., and J.L.Sackman, 1987. Seismic response analysis of structure-equipment systems with non-classical damping effects. *Earthquake Engineering and Structural Dynamics*, **15**(7): 871–888.

Igusa, T. and Kiureghian, A.D., 1985. Dynamic characterization of two-degree-of-freedom equipment-structure systems. *Journal of Engineering Mechanics*, **111**(1): 1–19.

Igusa, T., 1990. Response characteristics of inelastic 2-dof primary-secondary system. *Journal of Engineering Mechanics*, **116**(5): 1160–1174.

Jeanpierre, F. and Livolant, M., 1977. Direct calculation of floor response spectra from the fourier transform of ground movement-application to the superphenix fast reactor project. *Nuclear Engineering and Design*, **41**(1): 45–51.

Jennings, P.C. and Bielak, J., 1973. Dynamics of building-soil interaction. *Bulletin of the Seismological Society of America*, **63**(1): 9–48.

Jiang, W., Li, B., Xie, W-C., and Pandey, M.D., 2015. Generate floor response spectra: Part 1. direct spectra-to-spectra method. *Nuclear Engineering and Design*, **293**: 525–546.

Kapur, K.K. and Shao, L.C., 1970. Generation of seismic floor response spectra for equipment design. *Seismic Design for Nuclear Power Plants*, **1**: 29–71.

Kelly, J.M. and Sackman, J.L., 1978. Response spectra design methods for tuned equipment-structure systems. *Journal of Sound and Vibration*, **59**(2): 171–179.

Kiureghian, A.D., Sackman, J.L., and Nour-Omid, B., 1983. Dynamic analysis of light equipment in structures: Response to stochastic input. *Journal of Engineering Mechanics*, **109**(1): 90–110.

Kiureghian, A.D., 1980. *A Response Spectrum Method for Random Vibrations*, **UCB/EERC-80/15**. Earthquake Engineering Research Center, University of California at Berkeley, California.

Li, B., Jiang, W., Xie, W-C., and Pandey, M.D., 2015. Generate floor response spectra: Part 2. response spectra for equipment-structure resonance. *Nuclear Engineering and Design*, **293**: 547–560.

Li, Z.-X., LI, Z.-C., and Shen, W.-X., 2005. Sensitivity analysis for floor response spectra of nuclear reactor buildings. *Nuclear Power Engineering*, **26**(1): 44–50.

Lysmer, J., , Tabatabaie-Raissi, M., Tajirian, F., Vahdani, S., and Ostadan, F., 1983. *SASSI. System for Analysis of Soil Structure Interaction*. UC Berkeley, Department of Civil Engineering, Berkeley, CA.

Ni, S-H., Xie, W-C., and Pandey, M. D., 2011. Tri-directional spectrum-compatible earthquake time-histories for nuclear energy facilities. *Nuclear Engineering and Design*, **241**(8): 2732–2743.

Ni, S-H., Xie, W-C., and Pandey, M. D., 2013. Generation of spectrum-compatible earthquake ground motions considering intrinsic spectral variability using Hilbert-Huang transform. *Structural Safety*, **42**: 45–53.

PEER, 2010. *Report for the PEER Ground Motion Database Web Application*. Pacific Earthquake Engineering Research Center, Berkeley, California.

Peters, K.A., Schmitz, D., and Wagner, U., 1977. Determination of floor response spectra on the basis of the response spectrum method. *Nuclear Engineering and Design*, **44**(2): 255–262.

Politopoulos, I. and Feau, C., 2007. Some aspects of floor spectra of 1dof nonlinear primary structures. *Earthquake Engineering and Structural Dynamics*, **36**(8): 975–993.

Roesset, J.M., Whitman, R.V., and Dohry, R., 1973. Modal analysis for structures with foundation interaction. *Journal of the Structural Division*, **99**(3): 399–416.

Sackman, J.L. and Kelly, J.M., 1979. Seismic analysis of internal equipment and components in structures. *Engineering Structures*, **1**(4): 179–190.

Sackman, J.L. and Kelly, J.M., 1980. Equipment response spectra for nuclear power plant systems. *Nuclear Engineering and Design*, **57**(2): 277–294.

Sackman, J.L., Kiureghian, A.D., and Nour-Omid, B., 1983. Dynamic analysis of light equipment in structures: Modal properties of the combined system. *Journal of Engineering Mechanics*, **109**(1): 73–89.

Scanlan, R.H., 1974. Earthquake time histories and response spectra. *Journal of the Engineering Mechanics Division*, **100**(4): 635–655.

Sewell, R.T., 1986. Study of factors influencing floor response spectra in nonlinear multi-degree-of-freedom structures. Technical report, John A. Blume Earthquake Engineering Center.

Singh, M.P. and Burdisso, R.A., 1987. Multiply supported secondary systems part ii: Seismic inputs. *Earthquake Engineering and Structural Dynamics*, **15**(1): 73–90.

Singh, M.P. and Sharma, A.M., 1985. Seismic floor spectra by mode acceleration approach. *Journal of Engineering Mechanics*, **111**(11): 1402–1419.

Singh, M.P. and Suarez, L.E., 1986. A perturbation analysis of the eigenproperties of equipment-structure systems. *Nuclear Engineering and Design*, **97**(2): 167–185.

Singh, M.P. and Suarez, L.E., 1987. Seismic response analysis of structure-equipment systems with non-classical damping effects. *Earthquake Engineering and Structural Dynamics*, **15**(7): 871–888.

Singh, M.P., 1975. Generation of seismic floor spectra. *Journal of the Engineering Mechanics Division*, **101**(5): 593–607.

Singh, M.P., 1980. Seismic design input for secondary systems. *Journal of the Structural Division*, **106**(2): 505–517.

Singh, M.P., 1988. Seismic design of secondary systems. *Probabilistic Engineering Mechanics*, **3**(3): 151–158.

Smith, W.D., 1974. A nonreflecting plane boundary for wave propagation problems. *Journal of Computational Physics*, **15**(4): 492–503.

SQUG, 2001. *Generic Implementation Procedure for Seismic Verification of Nuclear Plant Equipment, Revision 3A*. Seismic Qualification Utilities Group.

Suarez, L.E. and Singh, M.P., 1987a. Eigenproperties of non-classically damped primary structure and equipment systems by a perturbation approach. *Earthquake Engineering and Structural Dynamics*, **15**(5): 565–583.

Suarez, L.E. and Singh, M.P., 1987b. Floor response spectra with structure¨cequipment interaction effects by a mode synthesis approach. *Earthquake Engineering and Structural Dynamics*, **15**(2): 141–158.

Suarez, L.E. and Singh, M.P., 1987c. Seismic response of sdf equipment-structure system. *Journal of Engineering Mechanics*, **113**(1): 16–30.

Suarez, L.E. and Singh, M.P., 1989. Floor spectra with equipment-structure-equipment interaction effects. *Journal of Engineering Mechanics*, **115**(2): 247–264.

Tsai, N.C., 1973. Modal damping for soil-structure interaction. *Journal of Engineering Mechanics*, **100**(2): 323–341.

USNRC, 1973. *Design Response Spectra for Seismic Design of Nuclear Power Plants*, **R.G. 1.60**. U.S. Atomic Energy Commission.

USNRC, 1978. *Development of Criteria for Seismic Review of Selected Nuclear Power Plants*, **NUREG CR-0098**. U.S. Nuclear Regulatory Commission.

USNRC, 2012. *Standrad Review Plan*, **NUREG-0800**. U.S. Nuclear Regulatory Commission.

Villaverde, R., 1997. Seismic design of secondary structures: state of the art. *Journal of Structural Engineering*, **123**(8): 1011–1019.

Villaverde, R., 2009. *Fundamental Concept of Earthquake Engineering*. CRC Press, New York.

Viti, G., Olivieri, M., and Travi, S., 1981. Development of non-linear floor response spectra. *Nuclear Engineering and Design*, **64**(1): 33–38.

Wolf, J.P. and Song, C., 1996. *Finite-Element Modelling of Unbounded Media*. Chichester: Wiley.

Wolf, J.P., 1985. *Dynamic Soil Structure Interaction*. Prentice Hall.

Wolf, J.P., 1987. *Soil-Structure-Interaction Analysis in Time Domain*. Structural Mechanics in Reactor Technology.

Wu, W.H. and Smith, H.A., 1995. Efficient modal analysis for structures with soil-structure interaction. *Earthquake Engineering and Structural Dynamics*, **24**(2): 83–99.

Yasui, Y., Yoshihara, J., Takeda, T., and Miyamoto, A., 1993. Direct generation method for floor response spectra. *Proceedings of the 12th International Conference on Structural Mechanics in Reactor Technology*, **13**(4).